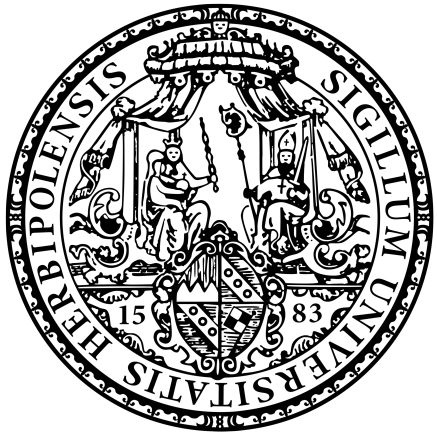

A novel USP11-TCEAL1-mediated mechanism protects transcriptional elongation by RNA Polymerase II

Ein neuer USP11-TCEAL1 vermittelter Mechanismus
schützt die transkriptionelle Elongation der RNA Polymerase II

Doctoral thesis for a doctoral degree
at the Graduate School of Life Sciences,
Julius-Maximilians-Universität Würzburg,
Section Biomedicine

submitted by

Markus Dehmer

from

Albstadt-Ebingen

Würzburg, 2023

Submitted on: 19th of December 2023

Members of the Thesis Committee

Chairperson: Prof. Dr. Christoph Sotriffer

Primary Supervisor:	Prof. Dr. Martin Eilers
Second Supervisor:	Prof. Dr. Caroline Kisker
Third Supervisor:	Travis Stracker, PD
Fourth Supervisor:	Prof. Dr. Gabriele Büchel

Date of Public Defense:

Date of Receipt of Certificates:

We look up. For weeks, for months, that is all we have done. Look up. And there it is-the top of Everest. Only it is different now: so near, so close, only a little more than a thousand feet above us. It is no longer just a dream, a high dream in the sky, but a real and solid thing, a thing of rock and snow, that men can climb. We make ready. We will climb it. This time, with God's help, we will climb on to the end. – Tenzing Norgay

my family

Summary

Deregulated expression of MYC oncoproteins is a driving event in many human cancers. Therefore, understanding and targeting MYC protein-driven mechanisms in tumor biology remain a major challenge.

Oncogenic transcription in MYCN-amplified neuroblastoma leads to the formation of the MYCN-BRCA1-USP11 complex that terminates transcription by evicting stalling RNAPII from chromatin. This reduces cellular stress and allows reinitiation of new rounds of transcription. Basically, tumors with amplified *MYC* genes have a high demand on well orchestration of transcriptional processes-dependent and independent from MYC proteins functions in gene regulation. To date, the cooperation between promoter-proximal termination and transcriptional elongation in cancer cells remains still incomplete in its understanding.

In this study the putative role of the dubiquitinase Ubiquitin Specific Protease 11 (USP11) in transcription regulation was further investigated. First, several USP11 interaction partners involved in transcriptional regulation in neuroblastoma cancer cells were identified. In particular, the transcription elongation factor A like 1 (TCEAL1) protein, which assists USP11 to engage protein-protein interactions in a MYCN-dependent manner, was characterized. The data clearly show that TCEAL1 acts as a pro-transcriptional factor for RNA polymerase II (RNAPII)-mediated transcription. In detail, TCEAL1 controls the transcription factor S-II (TFIIS), a factor that assists RNAPII to escape from paused sites. The findings claim that TCEAL1 outcompetes the transcription elongation factor TFIIS in a non-catalytic manner on chromatin of highly expressed genes. This is reasoned by the need regulating TFIIS function in transcription. TCEAL1 equilibrates excessive backtracking and premature termination of transcription caused by TFIIS.

Collectively, the work shed light on the stoichiometric control of TFIIS demand in transcriptional regulation via the USP11-TCEAL1-USP7 complex. This complex protects RNAPII from TFIIS-mediated termination helping to regulate productive transcription of highly active genes in neuroblastoma.

Zusammenfassung

Die deregulierte Expression von MYC Onkoproteinen ist ein zentrales Event in vielen humanen Krebsarten. Aus diesem Grund sind das Verständnis und die gezielte Bekämpfung MYC-getriebener Mechanismen in der Tumorbiologie nach wie vor eine große Herausforderung.

In MYCN-amplifizierten Neuroblastomen führt eine übermäßig hohe Transkriptionsrate zur stress-bedingten Rekrutierung des MYCN-BRCA1-USP11-Komplexes. Dieser Komplex beendet vorzeitig die Transkription, indem er RNAPII Moleküle vom Chromatin wirft. Durch diesen Mechanismus wird zellulärer Stress reduziert und ermöglicht dadurch einen erneuten Start der Transkription. Grundsätzlich stellen Tumoren mit einer Amplifikation von einem der MYC Proteine hohe Anforderungen an eine feine Abstimmung der einzelnen Schritte in der Transkription. Dies ist sowohl abhängig als auch unabhängig von den bereits beschriebenen Funktionen der MYC-Proteine in der Genregulation. Bis heute ist das Zusammenspiel zwischen promoter-proximaler Termination und transkriptioneller Elongation noch nicht vollständig aufgeklärt.

In dieser Studie wurde eine potenzielle Rolle von USP11 in der Regulation der Transkription weitergehend untersucht. Zunächst wurden mehrere Interaktionspartner von USP11, die an der Regulation der Transkription in Neuroblastom Krebszellen beteiligt sind, identifiziert. Es wurde insbesondere das Transcription Elongation Factor A Like 1 (TCEAL1) Protein charakterisiert. Dieses Protein unterstützt USP11 dabei, Protein-Protein-Interaktionen MYCN-vermittelt einzugehen. Die Daten zeigen, dass TCEAL1 als pro-transkriptioneller Faktor für die RNA-Polymerase II (RNAPII) -vermittelte Transkription fungiert. Genauer, TCEAL1 kontrolliert den Transkriptionsfaktor S-II (TFIIS), einen Faktor, der der RNAPII dabei hilft, die Transkription nach einem kurzen Pausieren („pausing“) fortzusetzen. Die Ergebnisse zeigen, dass TCEAL1 den Elongationsfaktor TFIIS auf nicht-katalytische Weise von dem Chromatin von hochexprimierten Genen verdrängt. Dies ist darin begründet, dass die Funktion von TFIIS bei der Transkription reguliert werden muss. TCEAL1 gleicht übermäßiges Zurückwandern der RNAPII und die vorzeitige Beendigung der Transkription, das durch TFIIS vermittelt wird, aus.

Diese Arbeit gibt Aufschluss über die stöchiometrische Kontrolle des TFIIS-Bedarfs bei der Transkriptionsregulation durch den USP11-TCEAL1-USP7-Komplex. Dieser Komplex schützt die RNAPII vor der TFIIS-vermittelter Termination der Transkription und trägt zur Regulierung einer produktiven Transkription hochaktiver Gene im Neuroblastom bei.

Content

1 Introduction

1.1 Neuroblastoma

Cancer is estimated to have caused 20 million new cases and to be accountable for 10 million deaths in 2020 worldwide. This makes it the second leading cause of death after cardiovascular diseases. Cancer pathogenesis occurs when cells acquire the ability to make their way from normal to neoplastic growth, and further specifically to malignant neoplasms (Hanahan, 2022). Germline mutations, genetic alterations due to errors in cell division, and DNA damage promote cancer development in humans. Cancer progression is influenced by many factors such as age and gender. Further, cancer in adults is associated with lifestyle choices (e.g. smoking, alcohol consumption) and environmental exposures (WHO, 2021).

Childhood cancer is the second leading cause of death among children under the age of 14 years, after accidents, and the fourth leading cause of death among adolescents aged 15 to 19 years in the United States (Siegel et al., 2022). The most common types of cancer in children are leukemia, followed by brain and other CNS tumors, lymphomas, kidney tumors, malignant bone tumors and neuroblastoma (Siegel et al., 2022). The etiology of many childhood cancers is believed to result from mutations in embryonal tissues that lead to uncontrolled abnormal cell division. Hence, preventive measures are not applicable for childhood carcinogenesis (WHO, 2021).

Generally, embryonal cells have an inherent inclination to undergo cell death and spontaneous regression, which are features required for organogenesis (Marshall et al., 2014). Neuroblastoma fail to respond to stimuli that determine neuronal cell fate maturation. Therefore remaining multipotent and prone to neoplastic progression (Huber, 2006). Neuroblastoma are the most common extracranial solid tumors in childhood which account for 15% of all childhood cancer-related deaths (Park et al., 2010). They originate from neural crest sympathoadrenal progenitors, commonly known as neuroblasts, primarily located in the adrenal medulla, paraspinal or periaortic regions (Johnsen et al., 2019). Predominantly they are composed of two differentiation lineages: adrenergic (ADRN) and undifferentiated mesenchymal (MES) cells (van Groningen et al., 2017). These cell types may interconvert into each other (van Groningen et al., 2017), depending on the activity of the transcriptional core regulatory circuitry (CRC) (Boeva et al., 2017; Durbin et al., 2018).The networks of CRCs are regulated by subtype-specific transcription factors (TF), for instance, MES-specific *NFKB2*, *RUNX1* and *RARB* or ADRN-specific *PHOX2B*, *HAND2* and *GATA3* (Gartlgruber et al., 2021).

Genetically, neuroblastomas can present structural or numeric chromosomal alterations such as 1p, 11q, 14q deletions and 17q gain (Matthay et al., 2016). In particular, neuroblastoma tumors can display *MYCN* (Brodeur et al., 1984) and *LIN28B* (Molenaar et al., 2012) amplification, germline or somatic mutations of *ALK* (Mosse et al., 2008) and *PHOX2B* (Bourdeaut et al., 2005; Trochet et al., 2004), or rearrangements at *ATRX* (Pugh et al., 2013) and *TERT* (Valentijn et al., 2015) loci. These genomic alterations have a major impact on the prognosis of neuroblastoma.

For instance, Figure 1 shows that activation of *MYCN* with 4-hydroxytamoxifen (4-OHT) in SH-EP neuroblastoma cells not expressing endogenous MYCN generates expression profiles that discriminate *MYCN*-amplified from non-*MYCN* amplified neuroblastoma (Herold et al., 2019). Interestingly, expression changes caused by *MYCN* amplification is independent of tumor stage.

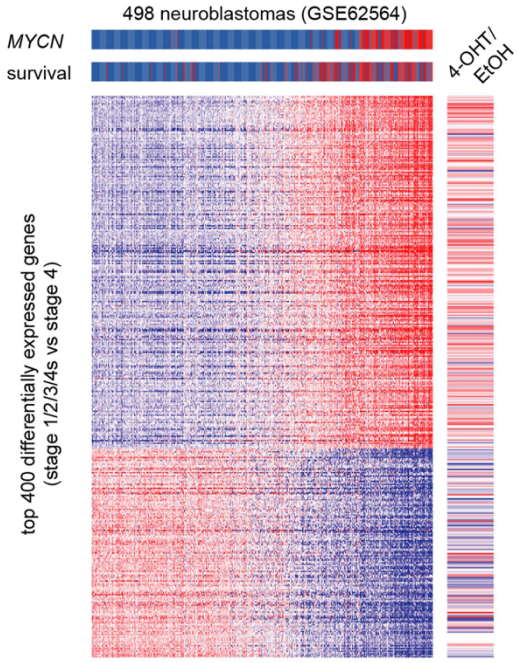

Figure 1: *MYCN* amplification determines gene expression profiles in neuroblastoma.

The heat map shows the 400 most-differentially expressed genes between 498 low- and high-grade neuroblastomas (GSE62564). MYCN amplification status of the tumors and survival of the patients is indicated by the horizontal bars on top. The right panel illustrates gene expression changes after MYCN-ER activation (4-OHT) in SH-EP cells of the same genes. This figure was published in similar form by Herold et al. (2019).

In high-risk patients, *MYCN* amplification, *ATRX* or *TERT* alterations lead to an increase of tumor aggressiveness and worsen prognosis (Ackermann et al., 2018). In addition, neuroblastoma patients whose tumors harbored telomere maintenance mechanisms together with RAS and/or p53 pathway mutations showed the lowest survival rates. It is unclear whether initial genetic aberrations are sufficient to cause the development of neuroblastoma.

While some forms of low-risk neuroblastoma regress spontaneously, others may require multiple treatment strategies. Hence, clinical factors and the aforementioned biological markers stratify for different risks at the time of diagnosis and thus classify neuroblastoma cancer. For the risk stratification the International Neuroblastoma Risk Group Staging System (INRGSS) is used. INRGSS defines four different stages (L1, L2, M, MS) of disease progression based on tumor localization and metastasis (Monclair et al., 2009). The treatment for low-risk (L1) neuroblastoma involves surgery alone with limited use of chemotherapy (Irwin et al., 2021; Strother et al., 2012). In contrast, intermediate (L2) and high-risk (M, MS) neuroblastoma patients receive surgery, radiation and multiple cycles of (high-dose) chemotherapy (Irwin et al., 2021; Twist et al., 2019).

Stem cell transplantation or novel biologic and immune-based therapeutic approaches are also applicable treatment options (Park et al., 2019).

Undesirable long-term consequences can manifest months to years after completion of childhood cancer therapies. Survivors, particularly those treated with intensive multimodal therapy, require lifelong surveillance and risk-based follow-up care to reduce morbidity and mortality (Friedman & Henderson, 2018). Improvements in survival of neuroblastoma have been achieved over the last decades. For children younger than 1 year, the rate increased from 86% to 95%, while for children aged 1 to 14 years, the rate increased from 34% to 68% (Smith et al., 2014). Only modest progress has been made in terms of survival rate for children with high-risk neuroblastoma, especially those with *MYCN* amplification (Huang & Weiss, 2013; Smith & Foster, 2018).

Pediatric oncology still faces challenges in achieving patient-tailored precision medicine approaches for neuroblastoma treatment. Designing new beneficial therapies to address the genetic alterations and improve existing treatment strategies remains necessary (Qiu & Matthay, 2022).

1.2 The oncogenic transcription factor MYC

The *MYC* oncogene family is involved in various aspects of cancer, including its formation, maintenance and progression. Deregulation of MYC proteins can occur due to gene amplification (Beroukhim et al., 2010) or translocation to loci with high transcriptional activity, as reported in Burkitt lymphoma (Dalla-Favera et al., 1982; Taub et al., 1982) or multiple myeloma (Shou et al., 2000), respectively. MYC family protein levels are major driver of tumorigenesis (Chen et al., 2018) and serve as bona fide markers for poor prognosis and unfavorable patient survival (Jung et al., 2017).

1.2.1 MYC family proteins

The MYC family has three different paralogs (MYC, MYCN and MYCL) which serve as transcription factors displaying both shared and unique features (Dang, 2012). MYC proteins are deregulated in the vast majority of human cancers (Schaub et al., 2018). Oncogenic MYC drives a broad spectrum of cancer types like leukemia (Dalla-Favera et al., 1983; Nowell et al., 1983), B-cell lymphomas (Hayward et al., 1981), lung cancer (Little et al., 1983), neuroblastoma (Schwab et al., 1983), and multiple myeloma (Shou et al., 2000). The expression of MYCN in progenitor cells contributes as driver for development of neuroblastoma (Weiss et al., 1997) or medulloblastoma (Swartling et al., 2010) in transgenic mice models. Lastly, MYCL promotes small cell lung cancer (Nau et al., 1985). Interestingly, tolerance for MYC loss could be conferred by compensatory MYCN up-regulation. This suggests, that despite differences between MYC paralogs essential protein functions remain conserved (for details see 1.2.2) (Malynn et al., 2000; Nesbit et al., 1999).

MYC family members belong to the basic helix-loop-helix (bHLH) family of transcription factors which allows DNA binding (Luscher & Larsson, 1999). Moreover, MYC proteins contain leucine zipper (LZ) structural motifs which facilitate heterodimerization with MAX. This dimerization takes place at consensus sequences termed enhancer boxes (E-box: 5'-CAC(G/A)TG-3') (Blackwell et al., 1993; Blackwood & Eisenman, 1991; Ma et al., 1993). E-box occupancy of MYC cannot be solely attributed to its intrinsic DNA specificity, indicating that the transcription machinery and promoter accessibility play a significant role in MYC recruitment (Guo et al., 2014). MYC and MAX proteins operate with larger networks to either promote or repress transcription (Conacci-Sorrell et al., 2014). Heterodimerization of other bHLH-LZ containing proteins (like MXD (MAX-interacting) and MGA) with MAX compete with MYC for E-box binding sites, and therefore induces repression of MYC target genes (Ayer et al., 1995; Hurlin et al., 1999). Competition between MYC and MXD proteins for MAX dimerization is tightly controlled by ubiquitin-mediated degradation (Zhu et al., 2008). Moreover, MYC can recruit MIZ1 (MYC-interacting zinc finger 1) (Peukert et al., 1997; Schneider et al., 1997), which antagonizes MYC-MAX-mediated transcriptional activation resulting in transcriptional repression (Walz et al., 2014).

Besides the homologous bHLH-LZ interface at the C-terminus, MYC slightly differs from MYCN by size (439 vs. 464 amino acids, respectively) and further by low complexity sequence within the N-terminus (Baluapuri et al., 2020; Z. Liu et al., 2020). They have several structural features in common due to partial sequence conservation (Kohl et al., 1986). These conserved amino acid sequences are defined as canonical MYC boxes (MB0, I, II, IIIa, IIIb and IV (Baluapuri et al., 2020). MB0, MBI and MBII comprise the transcriptional activation domain (TAD) at the N-terminus of MYC proteins. The TAD domain recruits co-activators/repressors which regulate chromatin remodeling, transcription and MYC protein stability. MB0 and MBI interact with factors involved in transcription elongation complexes, including GTF2F1, CDC73, WHSC2 and p-TEFb (Kalkat et al., 2018). These complexes impact the travelling of RNAPII (Rahl et al., 2010). Aurora kinase A (AURKA) binds also to MYC within this region and prevents its degradation via the E3 ubiquitin ligase SCF-FBXW7 (Buchel et al., 2017; Dauch et al., 2016; Richards et al., 2016). MBI contains a phosphodegron with the highly conserved phospho-residues Thr58, Ser62 and Ser64 that play essential roles for MYC and MYCN function and stability. ubiquitin E3 ligases like SCF-FBXW7 promote MYC degradation when these sites are "primed" (e.g. via phosphorylation) by a number of kinases (CDK1, ERK, JNK, DYRK2, GSK3) (Beaulieu et al., 2020; Chen et al., 2019). The PIN1 enzyme performs cis-trans isomerization at Pro63. This facilitates dephosphorylation at Ser62 in MYC, thus counteracting MYC degradation (Helander et al., 2015). Ubiquitination of MYC and MYCN at aforementioned degrons are reversed by deubiquitinases e.g. USP28 (Diefenbacher et al., 2015; Popov et al., 2007) or USP7 (Nicklas et al., 2019; Tavana et al., 2016).

MBII contributes to chromatin modification processes and the assembly of the transcriptional machinery (Conacci-Sorrell et al., 2014). This includes TRRAP (transformation-transcription domain-associated protein (McMahon et al., 1998; McMahon et al., 2000)) which acts as a scaffold for the acetyltransferase complex NuA4 and the helicase P400 to dock the chromatin remodeling machinery (Kalkat et al., 2018; Zhang et al., 2014). A PEST domain (enriched for Pro, Glu/Asp, Ser, Thr residues) identified between the subdomains MBIIIa and MBIIIb contributes to the stability of short-lived MYC (Gregory & Hann, 2000). The interaction of MBIIIb with the chromatin regulator WDR5 to enhances the affinity of MYC to chromatin (Thomas et al., 2015). Furthermore, two nuclear localization signals (NLS) for nuclear sequestration were identified in MBIV and the bHLH-LZ interface (Rosales et al., 2013).

Apart from the canonical MYC boxes and the bHLH-LZ domains, MYC proteins display large intrinsically disordered regions (IDRs). These regions only fold when in complex with other proteins, as described for MAX (Nair & Burley, 2003), BIN1 (Pineda-Lucena et al., 2005), WDR5 (Thomas et al., 2015), AURKA (Richards et al., 2016) and TBP (Wei et al., 2019). Together with conserved canonical domains, IDRs enable a dynamic ensemble of structure-function relationships in MYC proteins.

1.2.2 Functions of MYC proteins

The Bishop group characterized MYC as a transcription factor already in the early 90s (Eilers et al., 1991). Since then, MYC proteins have been described as universal regulator of transcription through interaction with many factors and complexes that regulate almost every cellular process. Interestingly, many studies revealed that their function is highly cell context and cell type dependent (Baluapuri et al., 2020). Generally speaking, MYC proteins bind to promoters and intergenic regions of virtually all active genes (Guo et al., 2014; Lorenzin et al., 2016), as well as to multiple enhancers (Sabo et al., 2014). Strikingly, only a small subset of genes is actually expressed proportionally in response to changes in MYC levels at its promoters (Walz et al., 2014). Additionally, distribution of MYC proteins cannot be explained by their DNA binding specificity alone even if binding sites are enriched at E-boxes (Guo et al., 2014; Lorenzin et al., 2016).

Several models have been proposed in the recent years to describe MYC/MYCN function and to solve other apparent inconsistencies. They are briefly outlined in the following paragraphs.

The specific gene regulation model

Consensus E-box binding by the MYC-MAX heterodimer at target promoters leads to activation or repression of specific gene sets (Walz et al., 2014). MYC shows ubiquitous binding at active promoters with an open chromatin structure but only a small discrete subset of genes reacts to changed MYC levels (Perna et al., 2012; Sabo et al., 2014; Tesi et al., 2019).

The global gene activation model

Over the last years a lot of research has been done that supports a model where MYC is delineated as a "global amplifier". This term reflects observations that elevated MYC levels lead to productive global gene expression output (Lin et al., 2012; Nie et al., 2012). In addition, an increase in gene expression not only for active, but also for silent genes upon MYC induction was observed (Lewis et al., 2018). Interestingly, saturated promoters with bound MYC proteins do not increase their gene expression even when MYC expression is elevated (Lorenzin et al., 2016). To act as a "global amplifier", MYC changes transcription factor dynamics by altering dwell times of transcription factors involved in RNAPII complex assembly and productive elongation (Patange et al., 2022). Consistent with this model, studies employing inhibitors of cyclin dependent kinases (CDKs), generally promoting RNAPII activity, showed that tumors driven by MYC proteins strongly rely on post-translationally modified RNAPII enzymes to perform transcription (Chipumuro et al., 2014; Huang et al., 2014).

The gene-specific affinity model

Both aforementioned models predict that at physiological levels, MYC proteins bind to "high-affinity" canonical E-boxes at the promoters of genes involved in growth and proliferation. At oncogenic MYC protein levels, active high-affinity promoters become saturated by MYC and thus non-canonical "low-affinity" E-boxes get also bound, leading to pleiotropic consequences (Lorenzin et al., 2016). Additionally, promoter recognition is dictated by histone marks (Guccione et al., 2006), protein-protein interactions (Guo et al., 2014) or enhancer invasion (Zeid et al., 2018). Moreover, oncogenic MYC binding can lead to gene repression, for example via recruitment of MYC/MIZ1 complexes (Wiese et al., 2013). Taken together, the affinity model can reconcile the opposing observations of gene specific regulation and global gene amplification by MYC proteins (models described above) to explain the perturbed transcriptional landscape of cancer cells driven by MYC proteins.

However, all of these models conceal two shortcomings. The findings supporting the models above heavily rely on data analysis methods chosen and have resulted in debates about technical matters. Second, the marginal effect on gene expression in response to MYC protein level manipulation (Baluapuri et al., 2020) cannot be fully explained by these models. Thus, MYC proteins must also drive mechanisms independent of their role in gene regulation.

Gene regulation-independent concepts

Recent progress towards an emerging perspective on a likely tumorigenesis promoting role of MYC proteins independent of global or relative changes in expression of target genes has been made by several groups in the field. For example, MYC proteins can modulate transcription machineries and thus oncogenic phenotypes (Buchel et al., 2017; Herold et al., 2019). Beside the

comprehensive collection of interactome data of novel interactors of MYC proteins (Baluapuri et al., 2020), more and more work elucidated the effect of MYC involved complexes on RNAPII (see chapter 1.3), for instance regarding resilience to transcription stress (Endres et al., 2021; Herold et al., 2019) or transcription-replication coordination (Buchel et al., 2017; Papadopoulos et al., 2022; Roeschert et al., 2021). A rather new concept of gene-independent transcriptional control is the involvement of MYC in the formation of condensates (Boija et al., 2018), more precisely termed liquid-liquid phase separation (Banani et al., 2017; Shin & Brangwynne, 2017). To date, little is known about how the regulatory processes during transcription are brought about by this phenomenon (Wang et al., 2021). Indeed, new findings substantiate how MYC multimerization supports its oncogenic function. In response to perturbation of transcription elongation, MYC and environmental factors (e.g. SPT5) redistribute from active promoters. This is triggered in a ubiquitylation controlled manner to limit DNA double strand break formation during S phase (Solvie et al., 2022). This can mechanistically explain how resolution of transcription and DNA replication coordination (Herold et al., 2019; Roeschert et al., 2021) or transcription associated DNA break repair (Endres et al., 2021) is exerted by MYC proteins.

The following chapters introduce a biological nexus of MYC and MYCN proteins as well as their complexes involved in transcription regulation and ubiquitin biology. A deeper understanding of transcriptional processes mediated by MYC and MYCN will open new possibilities for the targeted treatment of neuroblastoma.

1.3 Transcription

Transcription is the event by which genetic information on a single strand of DNA is copied into a new molecule of messenger RNA (mRNA) inside the nucleus (Crick, 1970). This process is regulated on multiple levels and involves a complex machinery consisting of RNA polymerases, accessory proteins called transcription factors as well as several auxiliary and regulatory factors. Moreover, *cis*-regulatory elements, proximal and distal from transcription start sites (TSS) (Jeziorska et al., 2009) and methylation status of CpG islands (Lovkvist et al., 2016) are crucial for setting up transcription in mammals.

1.3.1 RNA polymerase II

RNA molecules are produced during transcription, by RNA polymerases (RNAPs). Mammals have numerous forms of RNAPs (Roeder & Rutter, 1969), of which RNAPI, RNAPII and RNAPIII are the most prominent ones. They synthesize ribosomal (Grummt, 1999), messenger (Young, 1991) and transfer (Willis, 1993) RNA, respectively. From a structural perspective RNAPI, RNAPII and RNAPIII consist of 14 (589 kDa), 12 (514 kDa) and 17 (693 kDa) conserved subunits in eukaryotes (Cramer et al., 2008), as illustrated in Figure 2.

Eukaryotes						
RNAPII		RNAPI		RNAPIII		
yeast	human	yeast	human	yeast	human	
Rpb1	RPB1	Rpa190	RPA1	Rpc160	RPC1	
Rpb2	RPB2	Rpa135	RPA2	Rpc128	RPC2	
Rpb6	RPABC2	Rpb6	RPABC2	Rpb6	RPABC2	
Rpb5	RPABC1	Rpb5	RPABC1	Rpb5	RPABC1	
Rpb8	RPABC3	Rpb8	RPABC3	Rpb8	RPABC3	
Rpb10	RPABC5	Rpb10	RPABC5	Rpb10	RPABC5	Assembly platform
Rpb12	RPABC4	Rpb12	RPABC4	Rpb12	RPABC4	
Rpb3	RPB3	Rpc40	RPAC1	Rpc40	RPAC1	
Rpb11	RPB11-a	Rpc19	RPAC2	Rpc19	RPAC2	
Rpb4	RPB4	Rpa14	RPA14(?)	Rpa17	RPC9	Stalk
Rpb7	RPB7	Rpa43	RPA43	Rpc25	RPC8	
Rpb9	RPB9	Rpa12	RPA12	Rpc11	RPC10	
		Rpa49	RPA49	Rpc53	RPC4	TFIIF-like
		Rpa34	RPA34	Rpc37	RPC5	
				Rpc82	RPC3	TFIIE-like
				Rpc34	RPC6	
				Rpc31	RPC7	

Figure 2: Structural composition of eukaryotic RNA polymerases.

Polymerase subunit composition of eukaryotic RNAPs. Some transcription factors are homologous to additional subunits of RNAPs (i.e., TFIIF). This figure was published in similar form by Turowski and Boguta (2021).

The assembly of the RNAPII core starts with the formation of a subassembly by RPB3 together with RPB2 and RPB11 (Kimura et al., 1997) and finalizes by association with RPB1 (Kolodziej & Young, 1991). The other subunits are added to the core enzymes as preassembled polymerase building blocks (Wild & Cramer, 2012). The two large subunits RPB1 and RPB2 form the active center cleft of the RNAPII that exerts its enzymatic activity (Cramer et al., 2000). Recent studies on RNAPII integrity underlined that the subunits RPB1, RPB2, RPB5, RPB6, RPB7 and RPB8 are essential for polymerase functionality, while other subunits, such as RPB3, RPB9, RPB10 and RPB11 are regulators (Li et al., 2022). Metagenes and pausing indices (which is indicative of RNAPII proficiency in elongation) of active genes after depletion of each RNAPII subunit suggest, that RPB1-3, RPB6 and RPB7 are crucial for RNAPII-mediated transcription initiation, even if their role in elongation is different. On the other side RPB8 and RPB10 are thought to play a role in pause release and initiation (see Figure 3).

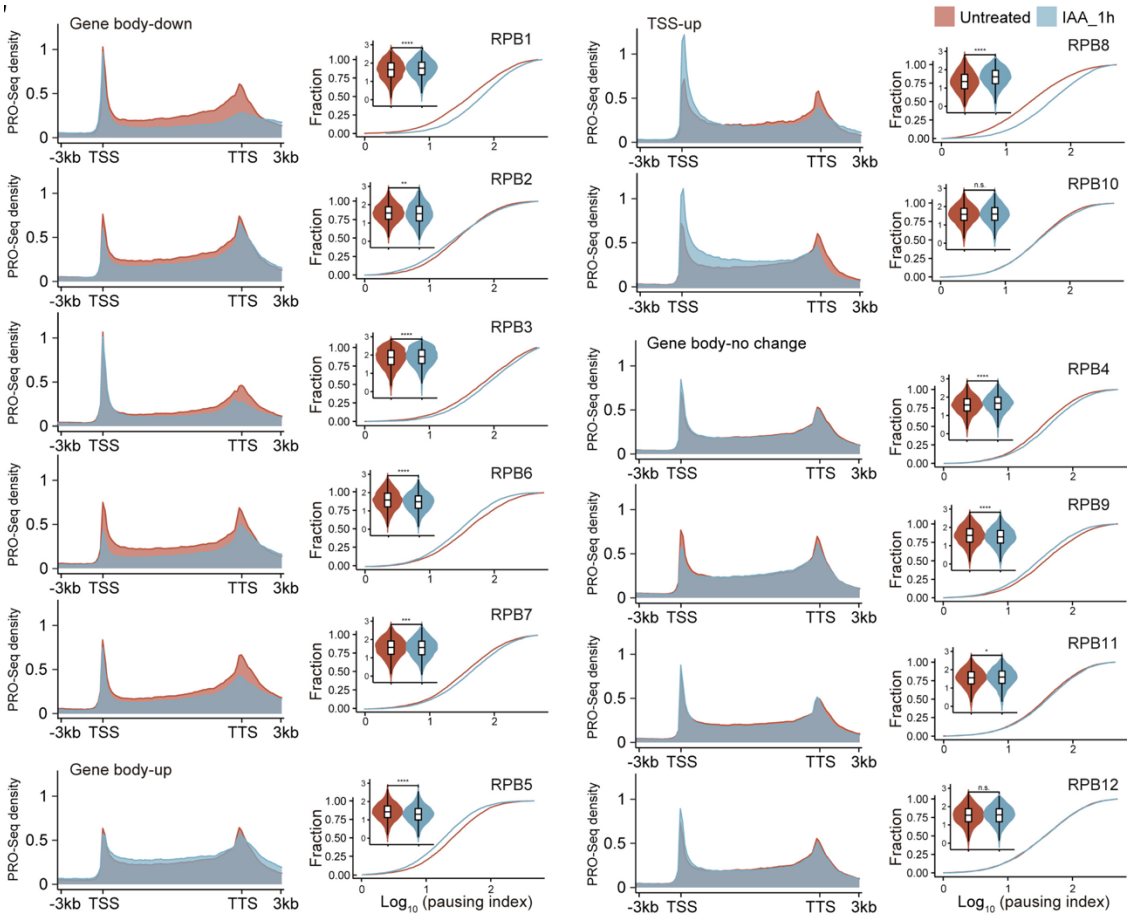

Figure 3: Individual RNAPII subunits influence transcription differently.

Left: PRO-Seq profiles of RNAPII subunits across the entire gene body of 4,668 active genes upon untreated (red) and IAA-treated (blue) RPB degron cell lines (TIR1 inducible expressed mESCs). Right: Pausing index by IAA treatment based on PRO-Seq signals for the indicated RNAPII subunit. This figure was published in similar form by Li et al. (2022).

Collectively, the (dis)assembly, degradation of RNAPs and recycling of their subunits is dependent on many factors and stimuli to ensure functional and processive gene transcription (Wild & Cramer, 2012).

1.3.2 Regulation of the basal transcription cycle

RNAPII-mediated cycles of transcription are regulated by fine-tuned steps. Progression of RNAPII molecules through checkpoints between the steps are reliant on activity of transcriptional cyclin-dependent kinases, phosphatases and interactions with specific (transcription) factors (Cossa et al., 2021; Vervoort et al., 2022). Particular attention is directed to the C-terminal domain (CTD) of RNAPII, which contains (in human) 52 repeats of the heptapeptide Tyr-Ser-Pro-Thr-Ser-Pro-Ser ($Y_1S_2P_3T_4S_5P_6S_7$), that undergoes dynamic phosphorylation through the different steps of the transcription cycle (Buratowski, 2009; Eick & Geyer, 2013).

Basically, periods of active nascent RNA synthesis, are divided in initiation, pausing, elongation, termination and recycling (Rodriguez & Larson, 2020):

Initiation

Nucleosome removal makes chromatin accessible for RNAPII-mediated promoter scanning and recruitment of initiation factors (Lorch & Kornberg, 2015; Lorch et al., 1987). Enhancers aid this process by recruiting cofactors such as the mediator complex (Kim et al., 1994; Seizl et al., 2011) or the histone de-acetyltransferase p300 (Visel et al., 2009). Hence, melted DNA duplexes at promoters facilitate binding of general transcription factors (TFII) which build the preinitiation complex (PIC) together with RNAPII (Esnault et al., 2008; Farnung & Vos, 2022). After PIC assembly the RNAPII is able to initiate transcription at the TSS. When the first few nucleotides of the nascent transcript are synthesized, the RNAPII is released from core promoters and from the whole TFII complex ("promoter escape") due to phosphorylation of Ser5 and Ser7 at the CTD of RNAPII by CDK7, a TFIIH subunit (Akhtar et al., 2009; Czudnochowski et al., 2012; Eick & Geyer, 2013; Glover-Cutter et al., 2009). The Ser5 mark also offers a platform for RNA capping enzymes to regulate 5' end capping of nascent RNA co-transcriptionally (Bentley, 2014).

Pausing

RNAPII distribution throughout the gene body is not uniform. High-resolution methods defined regions of high RNAPII density as RNAPII pausing sites (Churchman & Weissman, 2011; Gajos et al., 2021; Kwak et al., 2013; Nojima et al., 2015; Weber et al., 2014). In early transcription, RNAPII can enter a paused state 50-70 nucleotides downstream of the TSS, where it remains stably associated with the nascent RNA. This phenomenon, known as promoter-proximal pausing, gives metazoans an additional opportunity for maturation of RNAPII before transcription progresses, terminates or reinitiates (Adelman & Lis, 2012; Core & Adelman, 2019). This paused elongation complex (PEC) is stabilized by the elongation factor DSIF, which forms an RNA clamp, and the negative elongation factor (NELF) to prevent binding of the elongation factor PAF1c (Vos, Farnung, Urlaub, et al., 2018; Yamaguchi et al., 1999). Furthermore, NELF also opposes binding of RNA-cleavage stimulatory factor TFIIS, which promotes escape from promoter proximal pause sites (Kettenberger et al., 2003; Palangat et al., 2005; Pokholok et al., 2002).

Elongation

Remarkably, *Steurer and coworkers* found that the resident time of paused RNAPII was on average only 42 seconds and that only 10% of those RNAPII molecules entered into productive elongation (Steurer et al., 2018), remaining paused RNAPII molecules are prematurely terminated (Krebs et al., 2017), a process originally termed abortive elongation. To release paused RNAPII (PEC) into elongation (EC), the positive elongation factor b (P-TEFb), which contains the catalytic unit CDK9, is required (Marshall & Price, 1995). P-TEFb itself is typically found in larger

complexes and its activity can be inhibited by association with the 7SK regulatory small nuclear RNA complex whose release by several cellular stresses and signaling pathways can in turn enable large-scale activation of gene expression (AJ et al., 2016; Zhou et al., 2012). CDK9 then phosphorylates DSIF, NELF and Ser2 of the CTD tail of RNAPII (RPB1 subunit) (Peterlin & Price, 2006; Zhou et al., 2012). This leads to the dissociation of NELF and subsequent transition into active elongation (EC*) where RNAPII is associated to the elongation factor PAF1c (Vos, Farnung, Boehning, et al., 2018; Yu et al., 2015). Other elongation factors which are excluded from EC, can promote allosteric mechanisms to alter RNAPII activity, as reported for RTF1, a subunit of PAF1c (Vos et al., 2020), ELL, elongin and the super elongation complex (Conaway & Conaway, 2019), and NELF (Palangat et al., 2005). In addition, productive transcription elongation is stimulated by histone chaperones like SPT6, which binds the CTD of RNAPII, thus opening the RNA clamp formed by DSIF (Narain et al., 2021; Vos, Farnung, Boehning, et al., 2018). The histone chaperones FACT and CHD1 also engage the EC* (Farnung et al., 2021; Y. Liu et al., 2020) to help uncoiling DNA from nucleosomes (Hsieh et al., 2013) and to reduce histone loss in order to safeguard chromatin during elongation (Goswami et al., 2022).

Termination

The Ser2 phosphorylation signal in the CTD of RNAPII couples transcription with the release and the post-transcriptional processing of the RNA (Ahn et al., 2004). This marks the final event of transcription, termed termination. Termination is initiated as soon as RNAPII encounters a poly-adenylation site (PAS) and engages the cleavage and polyadenylation (CPA) complex (Proudfoot, 2016). Two distinct models were proposed to explain PAS-dependent termination, which are referred to as allosteric/anti-terminator or torpedo model. The allosteric model postulates a RNAPII conformational change promoted by transcription of a PAS. This causes transcriptional slow-down and gradual release of RNAPII from the DNA template (Zhang et al., 2015). The torpedo model postulates that the nascent transcript is still synthesized after recognition and cleavage at the PAS (Connelly & Manley, 1988; Proudfoot, 1989). In detail, the nuclear 5'-3' exonuclease XRN2 (termed "torpedo") is recruited and progressively degrades the transcript in kinetic competition with elongating RNAPII (West et al., 2004). Recently, a combination of the allosteric and the torpedo model was discussed by Eaton and West (2020) as well.

Recycling

To generate robust transcriptional output, the fine-tuned RNAPII machinery produces multiple copies of DNA templates by returning to the promoters (Dieci & Sentenac, 2003). Post-transcriptionally a subset of general transcription factors and co-factors, like mediator proteins, are likely to remain on promoters to facilitate re-initiation under certain circumstances *in vitro* (Yudkovsky et al., 2000). Moreover, a new methodological attempt by using distinguishable templates to

separate multi-round transcription and recycling phases attributes a new role to PAF1 in transcriptional recycling *in vitro* (Chen et al., 2021). To date, factors involved in transcription recycling are predominantly characterized *in vitro* and lack evidences in *in vivo*.

1.3.3 Transcriptional stress response

In response to stress RNAPII molecules can undergo disassembly, dissociation from chromatin or posttranslational modifications. Sophisticated mechanisms are required in cancer cells to sustain the stress of oncogenic transcription (Cruz-Ruiz et al., 2021), and in general to remain highly stress tolerant (Hanahan & Weinberg, 2011). Highly active genes have an efficient stress sensing activity (e.g. repair) upon transcription stress (Lavigne et al., 2017). Finally, obstacles that hamper transcription and related processes (Gaillard & Aguilera, 2016; Lans et al., 2019) can continuously cause genomic instability by generating a transcription memory of stress over mitotic divisions (Vihervaara et al., 2021).

As explained in chapter 1.3.2, elongating RNAPII is controlled by several factors in order to suppress pausing and arrest (Conaway & Conaway, 2019). Sequencing of nascent RNA isolated with RNAPII elongation complexes showed that the majority of detectable pause sites are associated with backtracked polymerases (Churchman & Weissman, 2011). When RNAPII is backtracked and arrested from the paused state due to facing obstacles, TFIIS helps the RNAPII to restart transcription and to escape the pause site by activating the 3'-endonucleolytic activity of the polymerase (Kettenberger et al., 2003). Non-functional TFIIS results in elongation defects, increased DNA-RNA hybrid formation (R-loops), and DNA double-strand breaks (DSBs) (Sheridan et al., 2019; Zatreanu et al., 2019).

If lesion-blocked transcription leads to R-loop formation, it compromises fidelity of gene expression (Crossley et al., 2019; W. Wang et al., 2018). GC rich regions ("skews") form more stable R-loops (Ginno et al., 2013) and increased DNA negative supercoiling promotes R-loop accumulation (Manzo et al., 2018; Promonet et al., 2020; Tuduri et al., 2009). These R-loops in turn hamper the ability of RNAPII to move forward. R-loop resolution at promoter-proximal regions and transcription end sites is promoted by BRCA1 through recruitment of senataxin, an R-loop-specific DNA/RNA helicase (Hatchi et al., 2015; Zhang, Chiang, et al., 2017). Another study showed, that BRCA1 depletion stabilizes senataxin binding to promoter-proximal regions and promotes MYCN-mediated RNAPII accumulation, as evidenced by a decline of nascent transcription at the pause site upstream of the most 5'-located PAS (Herold et al., 2019). Interestingly, although aberrant retention of BRCA1 at transcriptional regions with high R-loop levels after DNA damage was observed, transcription was not suppressed (Gorthi et al., 2018). Conceivably, to relieve R-loop-mediated transcription stress throughout the cell cycle, transcription-coupled nucleotide excision repair factors (e.g. XPF, XPG) may also process R-loops into DSBs followed by HR repair (Shivji et al., 2018; Sollier et al., 2014; Yasuhara et al., 2018). Not only deregulation

of oncogenes but also exposure to environmental genotoxic agents such as ultraviolet light (UV), ionizing radiation and/or from cellular sources (e.g. reactive oxygene species) that eventuate in the formation of bulky DNA lesions and DSBs, can result in transcription blockage (Gregersen & Svejstrup, 2018; Lans et al., 2019; Machour & Ayoub, 2020) as well as replication impediment (Kotsantis et al., 2018).

Fragile genomic regions are particularly prone to collisions between RNAPII or R-loops and chromatin associated protein complexes such as replisomes which lead to impairment of proper gene expression (Gaillard & Aguilera, 2016). Such transcription-replication conflicts (TRCs) occur either co- or head-on-directionally. Head-on collisions are mainly involved in the alteration of chromatin topology including R-loop promotion (Brambati et al., 2018; Chedin & Benham, 2020). DNA damage repair (DDR) mechanisms are activated by DNA damage checkpoints upon encounter of DNA damage (Chao et al., 2017; Shaltiel et al., 2015). Latest findings showed that RNAPII mediated transcription at DSBs results in production of distinct non-coding transcripts which function directly in DDR (Burger et al., 2019; Francia et al., 2016; Michelini et al., 2017). For instance, c-Abl triggers the phosphorylation of Tyr1 in the CTD of RNAPII at DSBs leading to the transcription of damage-responsive RNAs. These RNAs recruit repair factors (e.g. 53BP1, MDC1) to the breaks (Burger et al., 2019). In addition, *Pessina and coworkers* found that the synthesis of aforementioned RNA species at DSBs can directly induce liquid-liquid phase separation of DDR proteins in condensate foci (Pessina et al., 2019). This is underpinned by the observations that the elongation factor PAF1 prevents TRCs (Poli et al., 2016) and couples transcription-induced DSBs with repair (Endres et al., 2021). This is consistent with the observation that TRCs due to deregulation of RNAPII showed a deregulation in BRCA1-mutant cancer cells (Patel et al., 2023). Moreover, processive transcription is restored after DNA damage repair with the help of a number of other factors (Kokic et al., 2021; van den Heuvel et al., 2021). Rapid proliferating tumor cells have several strategies to cope with such stress-induced conflicts throughout the cell cycle (Buchel et al., 2017; Papadopoulos et al., 2022; Roeschert et al., 2021). Accumulating evidence supports a view in which these transcriptional stress responses are orchestrated by phase-separated condensates (Boija et al., 2018; Hnisz et al., 2017). Phase separation changes properties and functional activity on transcription performance (Sharp et al., 2022). For instance, the intrinsic disordered regions of NELF drives stress-induced condensation to downregulate transcription and to ensure cell survival upon stress (Rawat et al., 2021). Several other studies have reported that factors undergo condensate formation to regulate gene transcription (Guo et al., 2020; Lu et al., 2018). Upon distinct stress signals this formation was also shown for the transcription factors YAP and TAZ (Cai et al., 2019; Lu et al., 2020) or RNAPII together with the mediator complex (Cho et al., 2018; Sabari et al., 2018). Moreover, as mentioned in 1.2.2, oncoproteins like MYC can control condensate formation to avoid or resolve TRCs (Solvie et al., 2022).

Taken together, all these response mechanisms enable more efficient gene expression despite stress-induced chromatin topology changes and DNA damage. Factors of such mechanisms rely on dynamic control through posttranslational metabolic modifiers (see chapter 1.4).

1.4 Ubiquitin System

Posttranslational modifications (PTM) alter protein functions, thereby increasing the complexity and functional diversity of the proteome and ensuring that cells are able to respond rapidly and dynamically to intra- and extracellular stimuli (Walsh et al., 2005). In particular, ubiquitylation is of central importance for nearly all aspects of eukaryotic biology, as it controls cellular processes such as protein activity, localization and stability (Clague et al., 2015; Hershko & Ciechanover, 1998). Protein ubiquitylation and the pool of free ubiquitin depend on the balance between "writer" (e.g. E3 ligases) and "eraser" enzymes (e.g. deubiquitinases, DUBs) (Komander et al., 2009; Reyes-Turcu et al., 2009; Reyes-Turcu & Wilkinson, 2009). However, ubiquitylation is often regulated by additional PTMs (Herhaus & Dikic, 2015). In the following sections the main protagonists and the widespread spectrum of functions of the ubiquitin system are introduced, with particular attention to the ubiquitin specific protease 11 (USP11).

1.4.1 Main protagonists and features of the Ubiquitin System

Over the last decades research on the ubiquitin system has led to a broader understanding in protein metabolism. In general, the output of substrate ubiquitylation is defined as "ubiquitin code" (Damgaard, 2021). This code is built by "writers" (E1, E2, E3), edited by "erasers" (DUBs) and decoded by "readers", shown at a glance in Figure 4. The latter are equipped with ubiquitin-binding domains (UBDs) to distinguish ubiquitin linkage types and to link the modified substrate to downstream events (Herhaus & Dikic, 2015). DUBs maintain an adequate pool of free ubiquitin either by recycling of ubiquitin from ubiquitin conjugates or processing of ubiquitin precursors synthesized *de novo* (Grou et al., 2015).

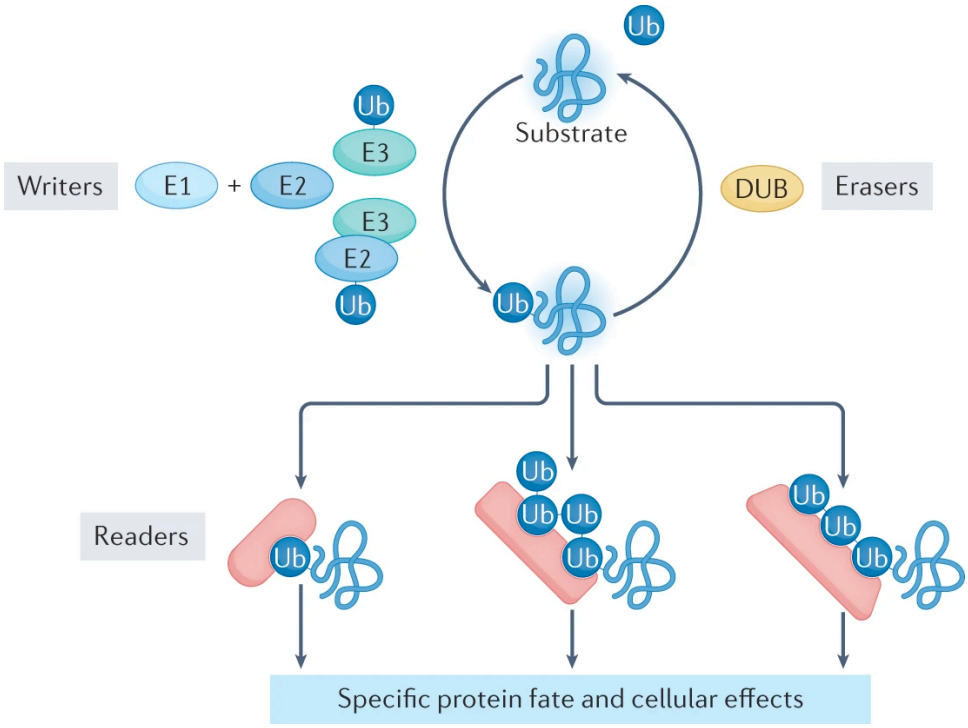

Figure 4: Writers, readers and erasers of the ubiquitin code.

E3 enzymes (together with E1 and E2 enzymes) function as writers of the ubiquitin code by attaching ubiquitin to one or more residues of the substrate. Ubiquitylation can be edited by deubiquitylating enzymes (DUBs) that function as erasers of the ubiquitin code. Ubiquitin chains are decoded by readers equipped with ubiquitin-binding domains that are able to distinguish ubiquitin modifications and link substrates to downstream events. This figure was published in similar form by Dikic and Schulman (2022).

Since the discoveries on the ubiquitin system, a large body of data on the properties of several other ubiquitin-like proteins (UBLs), such as SUMO, NEDD8, ISG15, FAT10, MNSFβ, UFM1, ATG8, ATG12, URM1 and HUB1, has accumulated (Cappadocia & Lima, 2018; Hochstrasser, 2009; van der Veen & Ploegh, 2012). The crystal structure of UBL family proteins and ubiquitin itself share a structural and evolutionary relationship: each family possesses a β-grasp fold (β-GF) composed of five antiparallel β-strands that are partially wrapped around a single helical segment (central helix) (Burroughs et al., 2012). Some UBLs, referred to as ubiquitin-family modifiers (UFMs), are ubiquitin-like not only in their structural similarity to ubiquitin but also in their ability to be attached to other proteins in reactions catalyzed by enzymes that are similar to the enzymes of the ubiquitin system (Varshavsky, 2012).

Ubiquitin mediates selective proteolysis through its enzymatic conjugation to substrates that contain “primary” degradation signals, thereby initialize proteolysis by the 26S proteasome. A majority of proteins are targeted for “primary” degradation signaling by N-degron (Varshavsky, 2011) or C-degron pathways (Chatr-Aryamontri et al., 2018; Koren et al., 2018; Lin et al., 2018). For instance, specific “primary” degrons (degradation signals) are created by N-terminal acetylation of cellular proteins (Hwang et al., 2010). Ubiquitin mediates selective proteolysis as a “second” degron through its enzymatic conjugation to proteins that contain “primary” degradation

signals (Varshavsky, 2019). The aforementioned pathways and other ubiquitin-mediated circuits can selectively degrade subunits of an oligomer without targeting other polypeptides of a complex (Johnson et al., 1990; Schrader et al., 2009).

The "second" degron, ubiquitin, is written by a combination of ligases. The modification is ultimately read by downstream machineries that selectively bind and alter the fates of modified proteins. Moreover, the modification is controlled by deubiquitinating enzymes (DUBs). The following paragraphs briefly outline the role of writers, readers and erasers of the ubiquitin code.

Writing

The enzymatic apparatus for ubiquitin modification is comprised of a signaling cascade of three enzyme types (Hershko & Ciechanover, 1998). First, the ubiquitin activating enzyme (E1) consumes ATP to catalyze the formation of a thioester between the C-terminal carboxyl group of ubiquitin and the single cysteinyl residue on E1 itself (Haas & Rose, 1982). Second, a ubiquitin conjugating enzyme (E2) accepts the thioester-linked ubiquitin from E1 and carries ubiquitin thioester-linked on a cysteinyl E2 residue containing a conserved 140-200 aa UBC region. The loaded E2 enzyme then transfers the ubiquitin moiety to a substrate. This process is catalyzed by E3 enzymes that either promote the interaction between the E2 enzyme and the target (e.g. RING E3 ligase) or , in the case of HECT or RBR E3 enzymes, form an intermediary thioester via one of their cysteine residues (Pickart & Rose, 1985; Stewart et al., 2016). In this final step, the ubiquitin is conjugated to the ε-amino group of a lysine residue in the target, forming an isopeptide bond (Ardley & Robinson, 2005; Pickart, 2001; Tanaka et al., 1998). These E3s are grouped into three protein families: RING, HECT and RBR (Toma-Fukai & Shimizu, 2021). In principle, terminal degron motif recognition by a large number of E3s enables intricate and selective control of protein quality and response to signals (Sherpa et al., 2022). Protein substrates can be modified by either mono- or polyubiquitin moieties, homotypic or heterotypic lysine-linked chains as well as by linear ubiquitin chains where each monomer is linked to the N-methionine of the preceding one (Komander & Rape, 2012; Yau & Rape, 2016).

Importantly, the type of ubiquitin signal determines the fates of ubiquitin-modified proteins (Komander & Rape, 2012; van Wijk et al., 2019) through the specific conformational properties (Berg et al., 2018). Ubiquitin conjugation processes are believed to be highly dynamic (Clague & Urbe, 2010; Pierce et al., 2009). Moreover, there are reports about processes (e.g. transcriptional regulation or cell fate (Vosper et al., 2009)) which involve also ubiquitin modifications of Cys, Ser and/or Thr side chains (Dikic & Schulman, 2022).

Reading

The ubiquitin code is read by downstream effectors that selectively bind and determine the biological effects of modified proteins. In general, UBDs within the readers allow recognition of

either monoubiquitin or particular polyubiquitin chains (Haakonsen & Rape, 2019; Harper & Schulman, 2006; Hurley et al., 2006; Husnjak & Dikic, 2012). The mechanism of recognition can be very diverse (Garcia-Rodriguez et al., 2016; Grumati & Dikic, 2018; Jackson & Durocher, 2013; Oh et al., 2018) and its understanding has recently deepened due to a number of novel methods (Chojnacki et al., 2017; Zhang, Smits, et al., 2017). The most prominent example of a reader is the 26S proteasome which binds polyubiquitylated chains via its ubiquitin receptors. Then, the conserved pore loops of the heterohexameric ring of ATPases translocate the substrates to an internal degradation chamber for proteolytic cleavage while the deubiquitinase Rpn11 removes substrate-attached ubiquitin chains (de la Pena et al., 2018; Dong et al., 2019). Beyond degradation the downstream output includes also re-localization and modified activity of substrates primed by E3 ligase ubiquitylation (Swatek & Komander, 2016). Non-proteasomal pathways are selected by different ubiquitin topologies with distinct functions in e.g. protein trafficking, inflammation, cell cycle or DNA repair (Liao et al., 2022). Additionally, E3 ubiquitin ligases and many other enzymes harbor structural elements that allow them to engage scaffolding roles independently of their catalytic functions, which opens possibilities for new pharmacological approaches (Kim et al., 2022) in addition to conventional therapeutic strategies targeted against members of the ubiquitylation process (Deng et al., 2020).

Erasing

Ubiquitylation levels of proteins and the pool of free ubiquitin are critically controlled by the activities of various linkage-specific deubiquitylating enzymes (DUBs) (Clague et al., 2019; Estavoyer et al., 2022; Snyder & Silva, 2021). The six main functions of DUBs are precursor processing to generate free ubiquitin, preventing the degradation of ubiquitylated target proteins, removal of non-degradative ubiquitin signal from substrate proteins, ubiquitin recycling, processing of *en bloc* disassembled ubiquitin chains and editing of ubiquitin chains to allow exchanging of an ubiquitin signal for another (Komander et al., 2009). Moreover, DUBs exert a positioning specificity, as they can cleave ubiquitin chains distally (exo), internally (endo) or from monoubiquitylated targets (He et al., 2016). DUBs which perform distal trimming of ubiquitin chains, in particular, have to bind to at least two of the very last subunits of a ubiquitin chain to obtain linkage type specificity (Reyes-Turcu & Wilkinson, 2009). Despite positioning and linkage specificity, another feature is substrate selectivity, as DUBs are found associated with substrates directly through binding domains or indirectly via adaptors and scaffolds (Mevissen & Komander, 2017). DUBs can be grouped into five different families: JAB1/MPN/Mov34 metalloenzyme (JAMM) family members belong to Zn-dependent proteases whereas the other four, ovarian tumor domain (OTU), the ubiquitin C-terminal hydrolase (UCH), Machado-Josephin domain (MJD) and ubiquitin-specific proteases (USP) are papain-like Cys-protease superfamily enzymes (Hanzelmann et al., 2012). Papain superfamily enzymes feature an active site cysteine in

proximity of a conserved histidine which activates the cysteine sulfhydryl. This allows a nucleophilic attack onto the carbonyl carbon of the scissile bond and results in the formation of an acyl-enzyme intermediate (Storer & Menard, 1994). A third non-obligatory catalytic residue, typically asparagine or aspartic acid, orientates the histidine side chain (Chapman et al., 1997). The USP family represents the largest DUB class with over 50 members in humans, and displays a conserved architecture despite the absence of extensive sequence homology (Komander et al., 2009). The USP fold almost always consists of three subdomains (as illustrated exemplarily in Figure 5): fingers, palm and thumb, with the catalytic center located between the thumb and palm (Hu et al., 2002). The C-terminus of the ubiquitin molecule is positioned in a cleft between the thumb and palm subdomains. The fingers engulf the core of the ubiquitin all the way to the N-terminus (Hanzelmann et al., 2012).

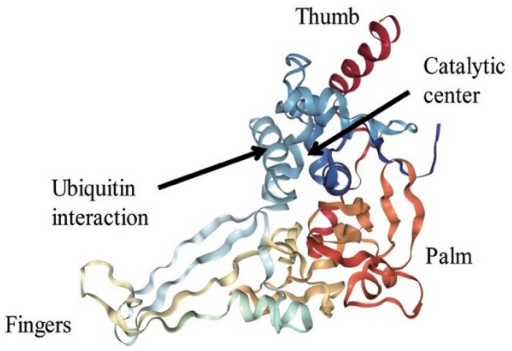

Figure 5: Structure of USP7.
The structure of USP7 (PDB identifier 1NBF). The fingers, thumb, and palm regions of the USP domain are indicated. This figure was published in similar form by Yuan et al. (2018).

DUBs are controlled by various factors, including PTMs, allosteric activation, subcellular localization and transcriptional regulation (Lacoursiere et al., 2022; Wang & Wang, 2021). To date, targeting DUB and their functionality itself are subject of extensive studies. Accordingly, advances in small molecule compound development against DUBs help to understand their role in protein modification processes as well as to highlight their putative therapeutic potential (Magin et al., 2021). Intriguingly, an adaption of the proteolysis targeting chimera (PROTAC) technology to DUBs could employ DUB-targeting chimeras (DUBTACs) to enable stabilization or rescue of proteins that are ubiquitylated and degraded in disease (Henning et al., 2022).

1.4.2 Ubiquitin specific protease 11

Over the last decades, there has been increasing attention to deubiquitinating enzymes that are involved in biochemical processes in human cancers (Dou, 2014). The observations suggest that they serve as tumor suppressors and oncogenes. USP11 is a deubiquitinase is located on the Xp21.2-p11.2 locus (Brandau et al., 1998). Within the USP protein family USP11, USP4 and USP15 are paralogs as evidenced by sequence similarity and structural organization (Vlasschaert

et al., 2015). The structural architecture of the 963 aa long USP11 protein is illustrated in Figure 6. Two domains are involved in catalytic and binding activities of USP11, ubiquitin-specific proteases domain (DUSP) and ubiquitin-like (UBL) domain (together referred to as DU domain) (Harper et al., 2014; Spiliotopoulos et al., 2019). *Harper et al.* propose domains outside the catalytic core domain serve as protein interaction or trafficking modules than having a direct regulatory function of the proteolytic activity. Further, a feature in the interface between DUSP and UBL was suggested to contribute in interacting with other proteins (Harper et al., 2014). Comparisons between USP11 and its paralogs USP4 and USP15 showed variations in the DUSP domain (Elliott et al., 2011). These are consistent with functional differences, since the binding partners of USP11 are more unique, whereas many of the binding partners for USP4 have also been identified for USP15 (Sowa et al., 2009). For instance, a binding pocket-deficient double mutant showed that the non-catalytic UBL region at the N-terminus modulates USP11's function in homologous recombination-mediated DNA repair (Spiliotopoulos et al., 2019). This shows that in USP11 these domains are not directly involved in regulating the enzymatic activity. It is conceivable that its regulatory role is enabled through interacting with other proteins (Faesen et al., 2011; van der Knaap et al., 2005).

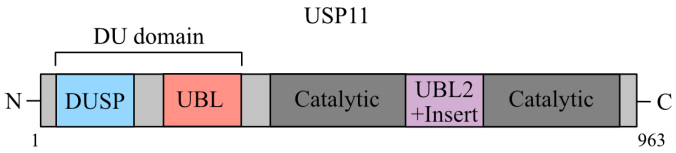

Figure 6: The structure of USP11.

Schematic representation of the USP11 protein (963 aa). DUSP (blue), domain present in ubiquitin-specific proteases. UBL (light red), ubiquitin-like domain. Catalytic domain (dark grey). UBL2+Insert domain (purple).

Ubiquitinating and deubiquitinating enzymes are part of dynamic, transient and precisely regulated processes. USP11 itself is subjected to different modifications at different amino acid residues. For instance, *Choudhary et al.* identified acetylated lysine residues not only in nuclear ubiquitin ligases but also in DUBs like USP11. This modification might modulate or co-regulate its cellular function (Choudhary et al., 2009). It was demonstrated that methylation of USP11 at Arg433 promotes DNA end-resection and repair of DNA DSBs by HR (Sanchez-Bailon et al., 2021). Several phospho-proteomic approaches identified distinct serine sites which putatively regulate the function of USP11 but the identification of the related kinases is still pending (Bian et al., 2014; Dephoure et al., 2008; Olsen et al., 2010; Rigbolt et al., 2011). In this context, it was discovered that S6-kinase dependent phosphorylation of Ser453 reduces USP11's deubiquitinase activity in order to stabilize and promote EIF4B-dependent oncogenic translation (Kapadia et al., 2018).

USP11 is predominantly found in the nucleus (Ideguchi et al., 2002; Schoenfeld et al., 2004) and it typically complexes with other proteins to perform biological functions in proximity to chromatin (Maertens et al., 2010; Ting et al., 2019; Wiltshire et al., 2010). Many biological processes controlled by USP11 have been identified over the last decades (in Table 1).

Table 1: Processes involved by USP11.

Process	Targets
DNA repair	BRCA2 (Schoenfeld et al., 2004), H2AX (Yu et al., 2016), XPC (Shah et al., 2017), H2AK119/H2BK120 (Ting et al., 2019), p21 (Deng et al., 2018), SPRTN (Perry et al., 2021), PRMT1 (Sanchez-Bailon et al., 2021), PALB2 (Orthwein et al., 2015), CENP-A and HJURP (Yilmaz et al., 2021)
R-loop control	SETX (Jurga et al., 2021)
transcription	MYCN (Herold et al., 2019)
cancer promotion	NF90 (Zhang et al., 2020), NONO (Feng et al., 2021), XIAP (Zhou et al., 2017), E2F1 (D. Wang et al., 2018), PPP1CA (Sun et al., 2019)
cancer suppression	PML (Wu et al., 2017), VGLL4 (Zhang et al., 2016), P53 (Ke et al., 2014), ARID1A (Luo et al., 2020)
genome stability	RAE1 (Stockum et al., 2018)

Notably, USP11 heterodimerizes with USP7, another common USP (Sowa et al., 2009), in a relationship that strengthen multiple physiological and pathological effects (Georges et al., 2018; Maertens et al., 2010; Perry et al., 2021).

From a pathophysiological perspective, USP11 is involved in the occurrence and progression of different diseases by deubiquitinating different proteins. Ubiquitin chain cleavage assays revealed a preference of USP11 for Lys63, Lys6, Lys33 and Lys11 linked chains over Lys27, Lys29 and Lys48 linked chains, consistent with its predominant role in DNA repair pathways (Harper et al., 2014). However, examples of deubiquitylation by USP11 in diseases were found for Lys48 as well as Lys63. For instance, ovarian cancer chemoresistance was promoted by removing Lys48 ubiquitin chain of BIP via USP11 (Zhu et al., 2021). In addition, Lys48 chain removal of ALK by USP11 was also identified to amplify TGFβ signaling (Al-Salihi et al., 2012). USP11 removes Lys63 chains from KLF4 to regulate liver diseases (Yang et al., 2021) and of phosphorylated E2F1 which drives gene expression of paternally imprinted *Peg10* thereby promoting cell proliferation (D. Wang et al., 2018).

1.4.3 Involvement in transcription and stress

Ubiquitylation is widely known for its role in protein surveillance. It affects a wide variety of processes including endocytosis, membrane-protein trafficking, cell signaling, transcription and DNA repair (Hochstrasser, 2009).

With reference to transcription, studies with CDK9 or GSK3 inhibitors clearly showed that actively transcribing RNAPII needs to be subjected to ubiquitylation before promoter-bound degradation (Jonkers et al., 2014; Nieto Moreno et al., 2020; Steurer et al., 2022). These results propose a model in which RNAPII stalling in *cis* induces degradation of promoter-bound RPB1 (i.e. RNAPII largest subunit) in *trans*. A growing body of evidence demonstrates that clearance of stalled RNAPII is achieved, in part, by ubiquitylation RPB1 to ensure proper functional and processive gene expression. The subunit RPB1 is ubiquitylated in response to DNA damage, leading to degradation of RPB1 in *S. cerevisiae* (Beaudenon et al., 1999; Huibregtse et al., 1997). Newer data showed that especially the ubiquitylation of K1268 primes RNAPII for degradation, which is required for cells to survive DNA damage (Tufegdzic Vidakovic et al., 2020). In addition, this encourages transcription-coupled nucleotide excision repair (TC-NER) initiated by the stalling of the elongating RNAPII at such DNA lesions (Nakazawa et al., 2020). The ubiquitylation at K1268 is facilitated by ELOF1 which functions as a key signal for the assembly of downstream repair factors like the binding and positioning of CUL4A for optimal RNAPII ubiquitylation (van der Weegen et al., 2021). USP7 facilitates the recruitment of the CUL4A ubiquitin ligase (Ray et al., 2013) and stabilizes the damage recognition factor CSB in TC-NER, while RNAPII is remodeling (Schwertman et al., 2012). In yeast, it has been demonstrated that the degradation associated K48-linked ubiquitin chain is generated by snipping K63-linked ubiquitin chains resulting in mono-ubiquitylation of RNAPII which then prompts generation of K48-linked ubiquitin chains (Harreman et al., 2009). Interestingly, the DUB Ubp3 digests polyubiquitin chains on yeast RPB1 to proofread and rescue RPB1 from degradation (Kvint et al., 2008). Absence of a Bre5-Ubp3 ubiquitin protease complex resulted in impaired co-transcriptional splicing and defect in RNAPII elongation *in vivo* (Milligan et al., 2017). Another example to inhibit transcription was reported for the HECT E3 ubiquitin ligase WWP2. WWP2 associates with components of the DNA-PK and RNAPII complexes at DSBs in RNAPII transcribed genes to mark RPB1 via K48-linked ubiquitylation. This drives proteasome-dependent eviction of RNAPII to promote DSB repair and protection from collision of the NHEJ machinery with the transcription machinery (Caron et al., 2019). Interestingly, *Daulny et al.* found that RNAPII, when phosphorylated at Ser5, gets ubiquitylated by ASR1 which then leads to the ejection of the RPB4/RPB7 heterodimer from the whole polymerase complex and results in inactivation of polymerase function (Daulny et al., 2008). Additionally, it was demonstrated that Elongin A deficient cells suppress ubiquitylation and proteasomal degradation of RPB1, underlined by the observation that Elongin A colocalizes with RPB1 when it is phosphorylated at Ser5 in response to DNA damage (Yasukawa et al., 2008).

The E3 ligases BRCA1-BARD1 (Greenberg et al., 2006) ubiquitylate phosphorylated RPB1 (Krum et al., 2003) to initiate degradation of stalled RPB1 during DNA damage (Kleiman et al., 2005). Interestingly, SETX, stabilized by USP11 (Jurga et al., 2021), and BRCA1 can resolve R-loops at 3' termination sites (Hatchi et al., 2015). Differently to BRCA1, BRCA2 inactivation diminishes PAF1 recruitment and subsequent H2B K120 ubiquitination for chromatin opening, and thus induces R-loop formation and widespread DNA damage at promoter proximal pausing sites via defective RNAPII control (Shivji et al., 2018). Also the small subunit RPB8 of RNAPII is ubiquitylated upon DNA damage via BRCA1, resulting in increased levels of soluble RPB8 (Wu et al., 2007). In addition, a recent report underlines the importance of RPB8 for functional RNAPII molecules in transcription and damage resolution (Li et al., 2022).
Proteasomal degradation of RNAPII as stress response is tightly regulated by both E3 ligases and DUBs as well as auxiliary proteins. The aforementioned mechanisms strengthen the idea that RNAPII ubiquitylation and eviction from chromatin are needed for an orchestrated response to any DNA stress. However, it remains to be clarified which of these factors are involved and how their complex interplay is achieved under physiological conditions as wells as upon stress in transcription.

1.5 Aim of the study

Posttranslational modifications of proteins control many dynamic processes in health and disease. USP11 is a deubiquitinating enzyme that specifically cleaves ubiquitin from ubiquitylated protein substrates. Despite many well-established roles in regulating cell cycle, DNA repair, chromatin remodeling and signaling cascades, little is known about USP11 in transcription.

In this study I investigated the role of USP11 in transcription regulation in detail. First, I identify a putative interaction network of USP11 and validate aspects of protein-protein interactions engaged by USP11. Second, I elaborate the biological relevance of USP11 in transcription regulation. My work aims at finding a putative target for improvement of neuroblastoma cancer treatment.

2 Results

2.1 Analyzing USP11-interacting proteins

The deubiquitinating enzyme USP11 catalyzes removal of ubiquitin from target proteins, thereby editing (poly)ubiquitin moieties to counteract the action of E3 ligases. Deubiquitinases, such as USP11, act as master regulators within the ubiquitin system in a vast variety of cellular processes (introduced in section 1.4.2). Initial evidence that USP11 plays an exceptional role in transcription was reported by *Herold et al.* (2019). Based on those findings we investigated the role of USP11. We intended to understand the interplay with interaction partners of USP11 in an unbiased manner. Therefore, proteins interacting with USP11 were identified by quantitative mass spectrometry (as described in section 5.3.8).

2.1.1 Proteomic approach to define the USP11 interactome

To define the interactome of USP11, cell lysates of SH-EP cells stably overexpressing *USP11* tagged N- or C-terminally with HA-FLAG were immunoprecipitated with antibody against the HA (Figure 7A). Tagging of two different terminal domains was designed and performed to account for potential steric hindrance between USP11 and newly identified interaction partners. In addition, the cells were engineered to overexpress either *MYCN wt* or *MYCN T58A*. The choice for this cell system is based on previous data from *Herold et al.* (2019). They showed that dephosphorylation of MYCN at Thr58 is critical for binding of USP11, and thus MYCN-BRCA1 complexes are stabilized. Before samples were subjected to NanoLC MS/MS mass spectrometry, the expression of tagged USP11 was confirmed by immunoblotting of IP samples (Figure 7B/D). The Coomassie gel staining shows minimal differences in precipitation yield of complexes either containing N- or C-terminal tagged USP11 (Figure 7C/E). Black arrows in Figure 7C and E indicate the protein expression of the HA-tagged USP11 bait.

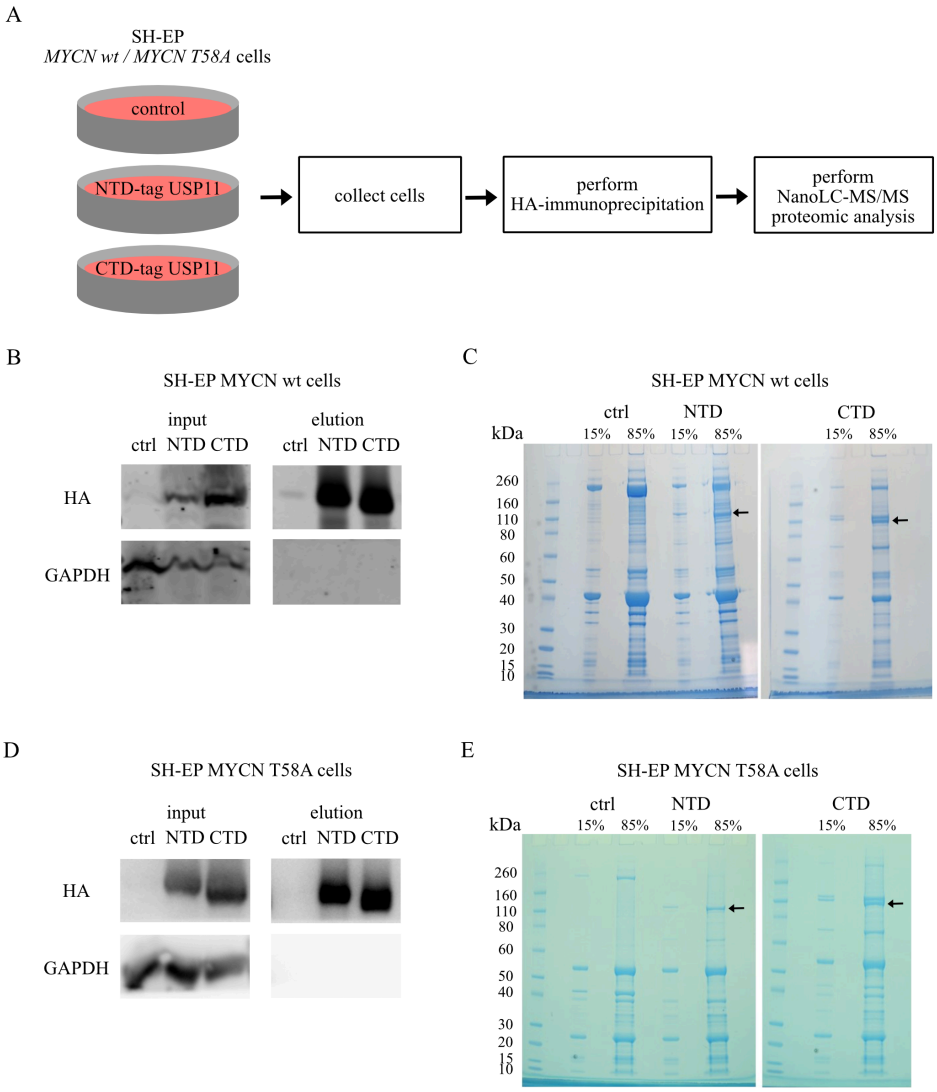

Figure 7: USP11 interactome in SH-EP neuroblastoma cells.

A. *Experimental design for the identification of a USP11 interactome by NanoLC MS/MS mass spectrometry performed in SH-EP cells overexpressing MYCN wt or MYCN T58A and N- or C-terminally HA-FLAG-USP11.* ***B.*** *Western blot analysis of SH-EP cells expressing MYCN wt and N- or C-terminally HA-FLAG-tagged USP11. GAPDH was used as a loading control.* ***C.*** *Coomassie staining showing 15% and 85% of total HA-IP elution of samples from B. Black arrows indicate the size of the HA-tagged USP11 bait.* ***D.*** *Western blot analysis of SH-EP cells expressing MYCN T58A (pWZL) and N- or C-terminally HA-FLAG-tagged USP11 (pLEGO). GAPDH was used as a loading control.* ***E.*** *Coomassie staining showing 15% and 85% of total HA-IP elution of samples from D. Black arrows indicate the size of the HA-tagged USP11 bait.*

2.1.2 Various interaction networks show involvement of USP11

Top hits were identified by overlapping the two datasets of N-terminal and C-terminal tagged USP11 interactomes. Gene ontology (GO) analyses were performed to identify major USP11 interacting networks using the online tool EnrichR (Chen et al., 2013; Kuleshov et al., 2016; Xie et al., 2021). Upon classifying the USP11 interactome in both SH-EP cells used with the KEGG 2019 database three major GO term families were found enriched: metabolism (pyrimidine, purine and glutamate), the ubiquitin-proteasome system and RNA polymerase (Figure 8).

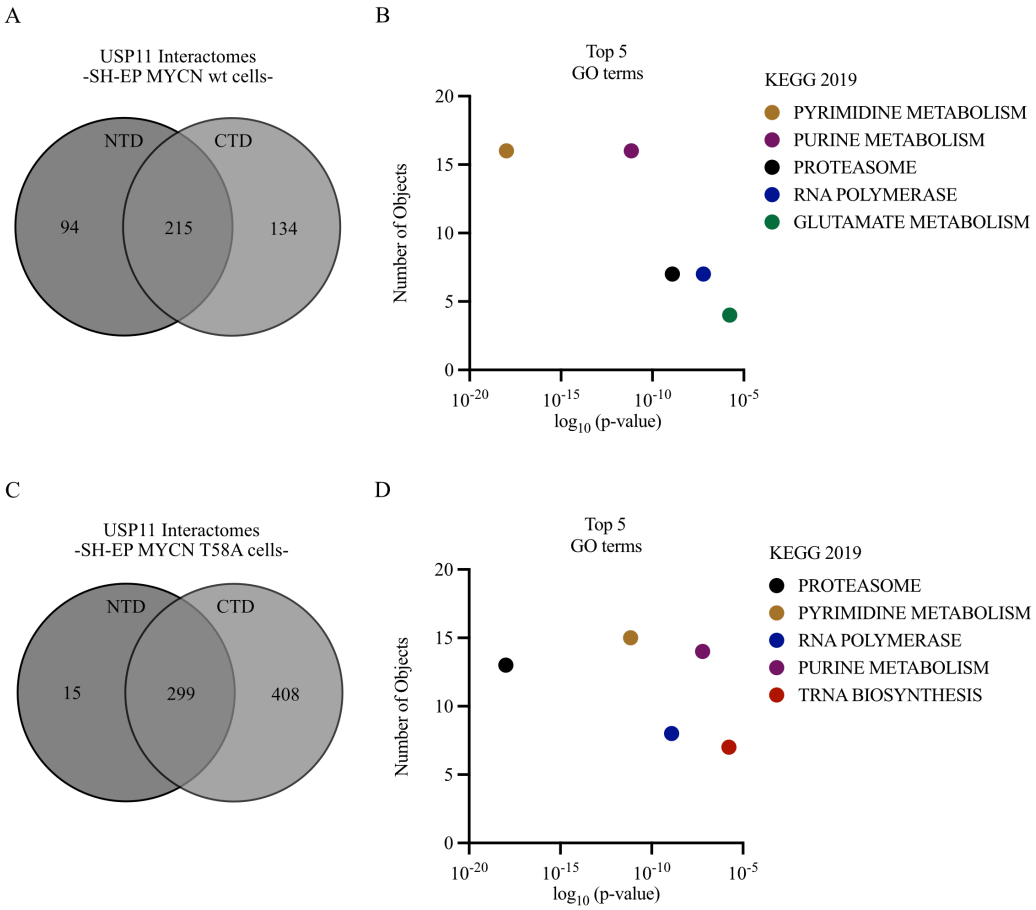

Figure 8: USP11 interactors are enriched in metabolism, ubiquitin-proteasome, and RNAPs.

__A.__ Venn diagram shows overlap of USP11 interactors in SH-EP MYCN wt cells. B. Top 5 GO terms (KEGG 2019) analyzed with EnrichR (see references in text) from overlapping hits found in A. __C.__ Venn diagram shows overlap of USP11 interactors in SH-EP MYCN T58A cells. __D.__ Top 5 GO terms (KEGG 2019) analyzed with EnrichR from overlapping hits found in C. (USP11/Ctrl $log_2FC \geq 2$)

The interactome data from two differently engineered cell lines clearly showed comparable gene ontologies. Moreover, the top hits were found significantly enriched in all four interactome data sets independent of the USP11 tagging strategy. In the following sections the four interactomes were merged for further analysis.

2.1.3 USP11 forms a transcription related complex

The mass spectrometry analysis showed that USP7 is a bona fide interacting protein of USP11 (see Figure 9A). Moreover, based on the GO term analysis, which showed significant enrichment of the RNA polymerase ontology, several RNAPII subunits (e.g. RPB1, RPB2) were identified in the USP11 interactome (Figure 9A). Those were validated by endogenous USP11 immunoprecipitations (IP) (Figure 9B). Interestingly, USP11 significantly interacts with proteins that are found in the context of transcription elongation (e.g. TCERG1, SPT6) or are associated with transcription processes (e.g. TCEAL1), shown in Figure 9. Therefore, we hypothesized a role for USP11 in transcription.

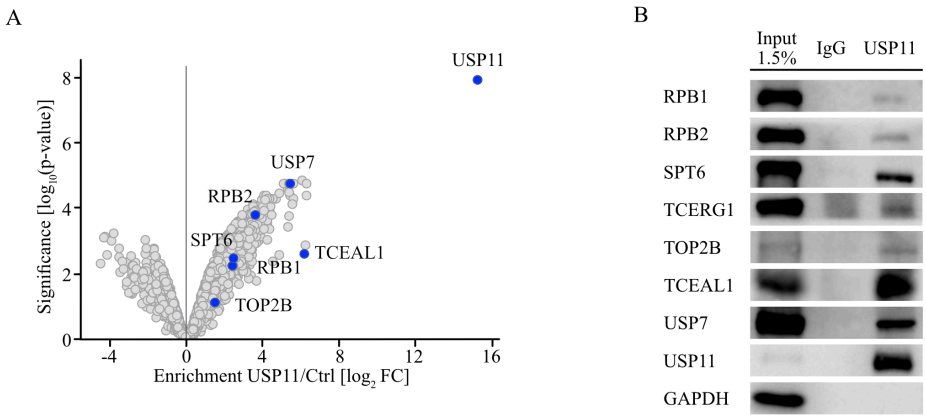

Figure 9: USP11 interacting proteins are related to transcription regulation.

A. *Volcano plot of the USP11 interactome with transcription related proteins marked in blue. The x axis displays the enrichment (log2FC) of proteins co-precipitated by USP11 from exogenous tagged USP11 expressing cells compared to control cells (Ctrl). The y-axis shows the significance (p-value) of enrichment calculated from four biological replicates. (n=4, unless specified otherwise n indicates the number of independent biological replicates)* ***B.*** *Immunoblots of endogenous USP11 immunoprecipitation from SH-EP-MYCN wt cells and co-precipitated proteins highlighted in A. IgG was used as control. (n = 3)*

Consistent with the validation of the USP11 interactome, endogenous immunoprecipitated RPB1 (the largest subunit of RNAPII) and USP7 share interaction partners with USP11 (Figure 10). These assays substantiated that USP11 and USP7 have a putative involvement in transcription networks.

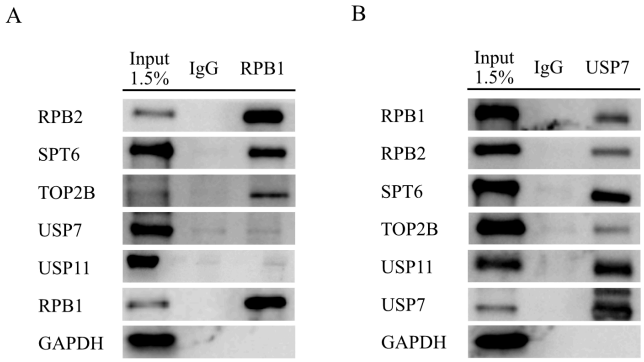

Figure 10: RNAPII and USP7 share interacting partners with USP11.

A./B. *Immunoblots of endogenous RPB1 (**A**) and USP7 (**B**) immunoprecipitations from SH-EP MYCN wt cells. Co-precipitated proteins are indicated. IgG was used as control. (n=3)*

2.1.4 Absence of USP11 impacts the transcription machinery

To investigate the role of USP11 in transcription regulation, first, its chromatin occupancy was assayed by chromatin immunoprecipitation. These assays showed no consistent chromatin binding for USP11. In contrast, heatmaps of Cut&Run sequencing assays revealed that a fraction of USP7, the established interacting protein of USP11 (Maertens et al., 2010), binds to chromatin near the TSS of genes expressed in SH-EP MYCN wt cells (Figure 11). This method also confirmed that the employed USP11 antibody does not allow to identify USP11 on chromatin. The top two panels in Figure 11 refer to the controls H3K4me3 (positive) and IgG (negative).

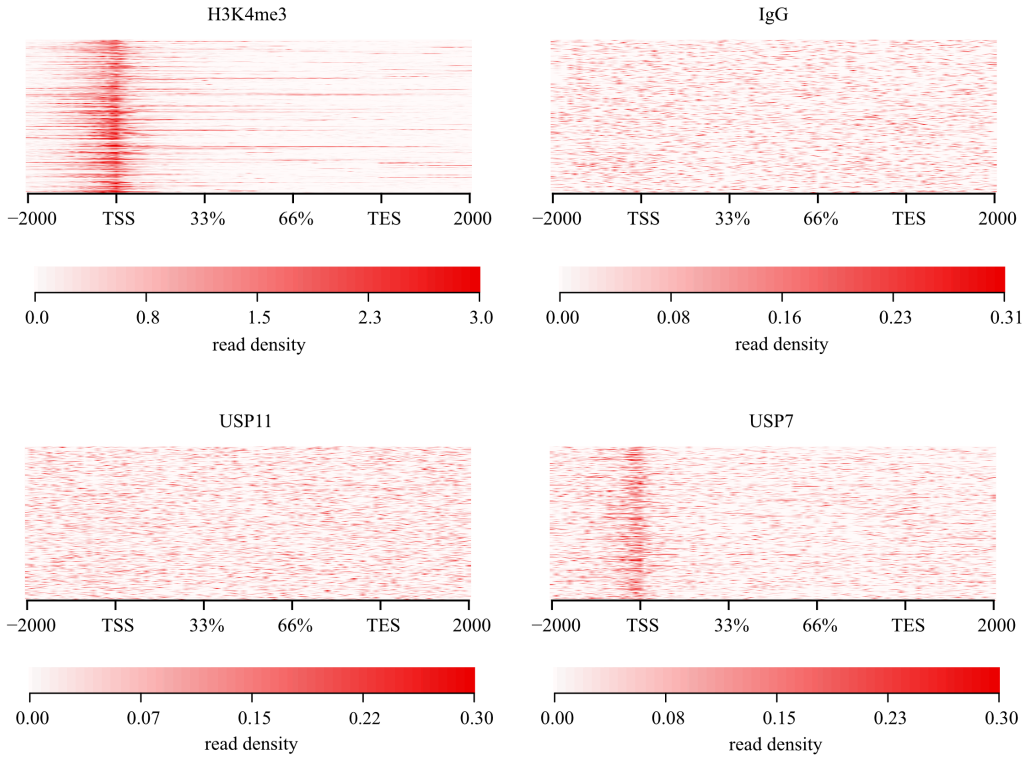

Figure 11: USP11 does not bind chromatin directly.

Heatmaps indicate chromatin occupancy (bars reflect the RPM read density) of H3K4me3 (positive control), IgG (negative control), USP11 and USP7 generated from CUT&RUN sequencing data in SH-EP MYCN wt cells. (n=1)

To explore the presumably indirect role of USP11 in transcription, its impact on RNAPII was studied in greater detail. To do so, SH-EP cells were genetically engineered to manipulate USP11 expression levels using a Doxycycline-inducible shRNA against USP11. These cells were then subjected to RNAPII ChIP-Sequencing. In absence of USP11 (-USP11) the chromatin occupancy of RNAPII is decreased. This effect was observed at TSS (see Figure 12).

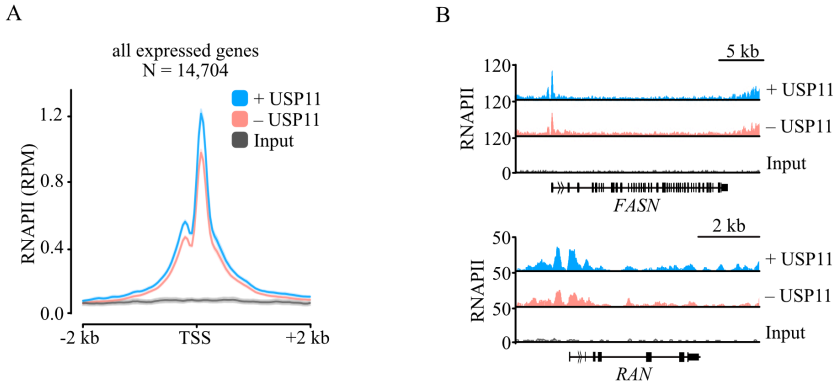

Figure 12: Global RNAPII association is decreased in absence of USP11.

A. *Global average read density of RNAPII ChIP-Rx data in SH-EP MYCN-ER cells in the presence (light blue) or absence (light red) of USP11 and activated MYCN (input: grey; TSS, transcriptional start site). Data show mean ± standard error of the mean (SEM).* ***B.*** *Representative genome browser tracks of the indicated loci of the ChIP experiment described in A. (n=2)*

USP11 regulates chromatin dynamics (Ting et al., 2019), and may therefore affect RNAPII occupancy (Figure 12). Additionally, the absence of USP11 can increase transcription stress by DNA damage in neuroblastoma cells, as it has been previously reported for DNA end-resection and repair (Orthwein et al., 2015; Sanchez-Bailon et al., 2021), thus explaining the decrease in RNAPII chromatin occupancy. To test effects on DNA damage in absence of USP11, damage markers downstream of the ATR/ATM signaling cascades were detected. However, these markers were only induced after 120 h (Figure 13).

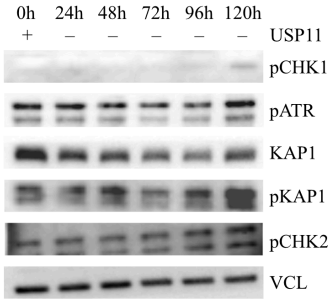

Figure 13: DNA damage markers are not upregulated upon USP11 depletion.

Immunoblot of indicated proteins from SH-EP MYCNER cells upon depletion (-) of USP11 (shUSP11) at different time points (h). Vinculin (VCL) was used as a loading control. (n=2)

To study the role of DSBs in detail, Breaks labeling *in situ* and Sequencing with AsiSI digestion (BLISS8) was performed. The method employs AsiSI, a restriction enzyme that induces double strand breaks (DSB) at a known sequence. Usually, high susceptibility to breakage is detected in regions of open chromatin, meaning that the BLISS signal was expected at its highest directly downstream of the TSS. Therefore, the detected DSBs were visualized by highlighting the promoter regions from 5 kb upstream to 10 kb downstream of the TSS in strongly ("top", n = 3,954) and weakly expressed ("bottom", n = 3,012) genes (Figure 14). USP11 downregulation enriched

the break profile in the “top” genes mildly, indicating that USP11 exerts its effect on transcription stress not predominantly by double strand break induction. However, MYCN activation (4 h) did not further increase susceptibility to breaking in this experimental setting.

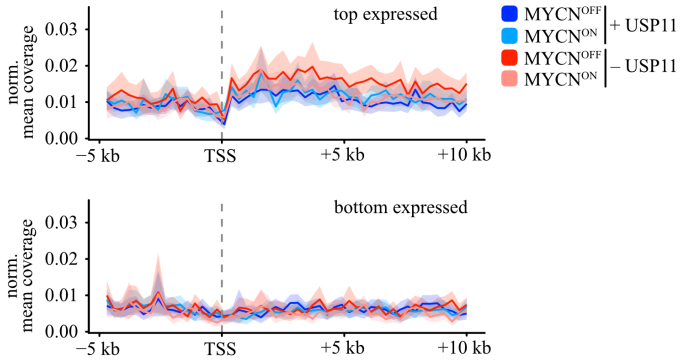

Figure 14: Depletion of USP11 does not enhance accumulation of DSBs.

B. *Average read density (norm. mean coverage) of DNA double-strand breaks sequencing (BLISS8) data in SH-EP MYCNER cells in presence and absence of USP11 when MYCN is inactivated or activated (TSS, transcriptional start site). The data show top (n=3,954) and bottom (n=3,012) expressed genes of SH-EP cells. (n=2)*

Furthermore, transcription stress could be caused by direct control of members of the transcription machinery by USP11. To determine the effect of USP11 on the cellular proteome, the *MYCN*-amplified neuroblastoma cell line IMR-5 containing a doxycycline-inducible shRNA targeting USP11 was used in a proteomic approach (Figure 15A/B). Total proteomics following USP11 knockdown revealed a reduction of RPB8 protein levels (Figure 15C/D). RPB8 is a common subunit of all three RNA polymerases that can be ubiquitinated by BRCA1 (Kwapisz et al., 2008; Wu et al., 2007).

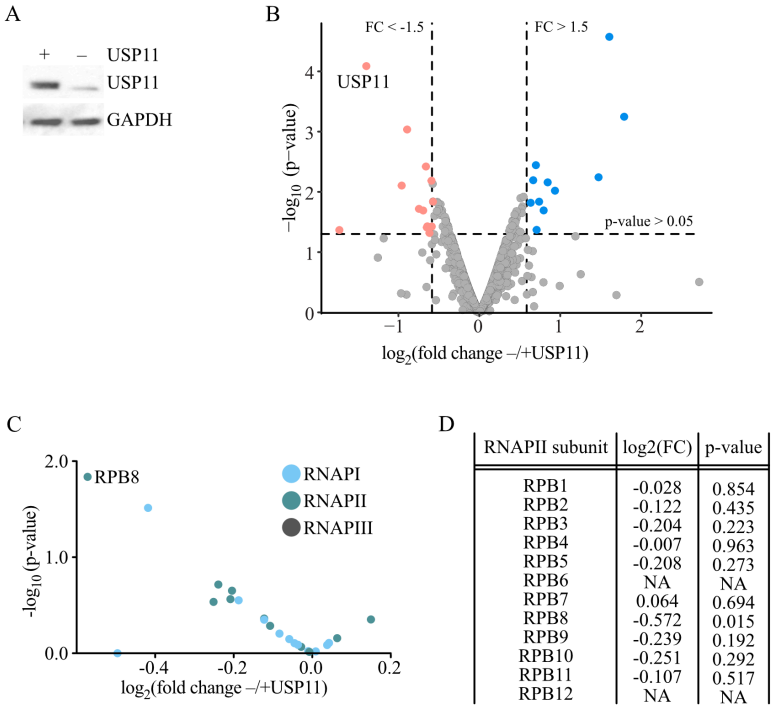

RNAPII subunit	log2(FC)	p-value
RPB1	-0.028	0.854
RPB2	-0.122	0.435
RPB3	-0.204	0.223
RPB4	-0.007	0.963
RPB5	-0.208	0.273
RPB6	NA	NA
RPB7	0.064	0.694
RPB8	-0.572	0.015
RPB9	-0.239	0.192
RPB10	-0.251	0.292
RPB11	-0.107	0.517
RPB12	NA	NA

Figure 15: USP11 stabilizes RPB8.

***A**. Immunoblot from IMR-5 cells in presence and absence of USP11. GAPDH was used as a loading control (n=2). **B**. Volcano plot of total proteomics with cells described in A. The x-axis displays the enrichment (log_2FC) of proteins in cells with presence (+) or absence (-) of USP11. The y-axis shows the significance ($-log_{10}$(p-value)) of enrichment calculated from biological duplicates. (n=2) **C.** Filtered volcano plot from B. highlighting RNAP subunits of RNAPI, RNAPII, and RNAPIII in -/+ USP11 condition. **D.** Table showing enrichment (log_2FC) and significance (p-value) of RNAPII subunits from the proteomics in B.*

Accordingly, depletion of RPB8 (siRPB8) resulted in destabilization of RPB1, the largest subunit of RNAPII (Figure 16A/B). Interestingly, depletion of USP11 led to a significant downregulation of RPB8 (Figure 16C/D). However, impact on RNAPII (RPB1) stability was not detected upon USP11 depletion.

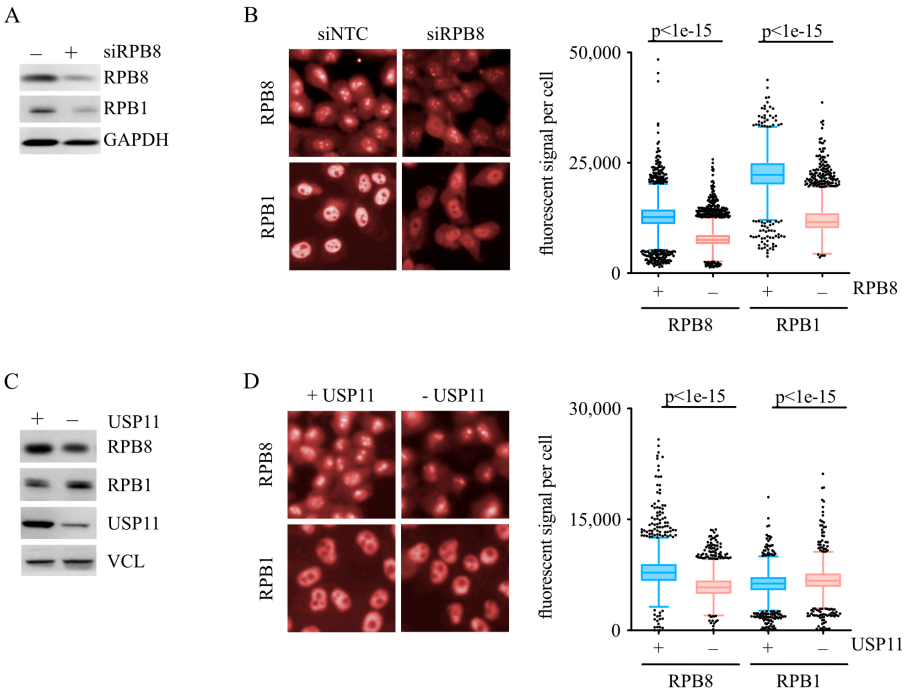

Figure 16: RPB8 is an essential subunit of RNAPII.

A. *Immunoblot of indicated proteins of WCL from SH-EP MYCNER cells in presence (+) or absence (-) of RPB8 using siRNA. GAPDH was used as a loading control. (n=3)* ***B.*** *Images of cells as treated in A and immuno-stained for RPB8 and RPB1 (left panel). Box plots of single cell analysis of one representative experiment (right panel). P-values were calculated using an unpaired t test. (n=3).* ***C.*** *Immunoblot of indicated proteins of WCL from SH-EP-MYCN-ER cells in presence (+) or absence (-) of USP11 using shRNA. VCL was used as a loading control. (n=3)* ***D.*** *Images of cells as treated in C and immuno-stained for RPB8 and RPB1 (left panel). Box plots of single cell analysis of one representative experiment (right panel). P-values were calculated using an unpaired t test. (n=3)*

In addition, a peptide antibody-based affinity approach (Fulzele & Bennett, 2018) has been utilized to enrich for and identify endogenously ubiquitylated proteins upon downregulation of USP11 in IMR-5 cells (overview in Table 28). The assay was performed using a label-swap design (see method section 5.3.9). This ubiquitin remnant profiling showed that USP11 exerts its main effects on the deubiquitylation of proteins predominantly associated with mechanisms linked to transcription regulation and RNA processing (Figure 17).

A

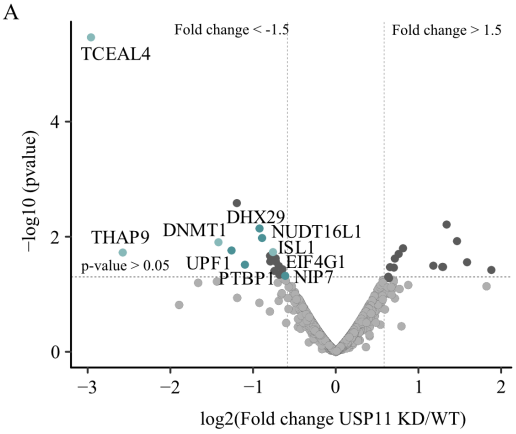

B

Process	Gene	log2FC (USP11 KD/Ctrl)
Transcription regulation	TCEAL4	-2.96
	THAP9	-2.58
	DNMT1	-1.42
RNA processing	ISL1	-0.76
	UPF1	-1.26
	PTBP1	-1.10
	DHX29	-0.92
	NUDT16L1	-0.89
	EIF4G1	-0.79
	NIP7	-0.61

Figure 17: USP11 is involved in deubiquitylation of proteins in transcription and RNA processing.

A. *Volcano plot of diGLY-SILAC-based ubiquitin remnant profiling with IMR-5 cells in presence and absence of USP11. The x-axis displays the enrichment (log_2FC) of ubiquitylation sites of genes identified in cells with presence (+) or absence (-) of USP11. The y-axis shows the significance ($-log_{10}$(p-value)) of the enrichment calculated from biological duplicates.* ***B.*** *table showing log_2FC (USP11 KD/Ctrl) of the indicated genes and the respective biological process found in A. (n=2)*

Overall the results demonstrated that USP11 has a role in transcriptional regulation. USP11 controls the stability of RPB8, one essential subunit of the multi-subunit containing RNAPII holoenzyme. In addition, downregulation of USP11 solely did not make neuroblastoma cells susceptible for DNA breaks in regions of open chromatin and high transcription stress (Figure 13). These findings suggest a more indirect role for USP11 in RNAPII-mediated transcription and/or transcriptional stress response.

2.2 USP11-mediated complex gets involved in transcription

The interactome studies of USP11 in SH-EP MYCN wt cells suggested that this ubiquitous deubiquitinase influences many cellular mechanisms either directly or indirectly. Certainly, the best-known roles of USP11 have been reported in stress resilience and cell cycle progression. On the other hand, there is little knowledge generated about its involvement in the transcription machinery in cancer cells. Due to the fact that USP11 interacts with subunits of the RNAPII holoenzyme and elongation factors (section 2.1), in the following section was aimed for learning more about transcriptional complex(es) involving USP11.

2.2.1 UBL2+Insert domain in USP11 is crucial for protein-protein interaction

To characterize the interaction of USP11 with other partners, first structural information was predicted using the AlphaFold (AF) algorithm on the EBI web server. The output of AF was a 3D ribbon model of USP11 its domain structure and folding (Figure 18).

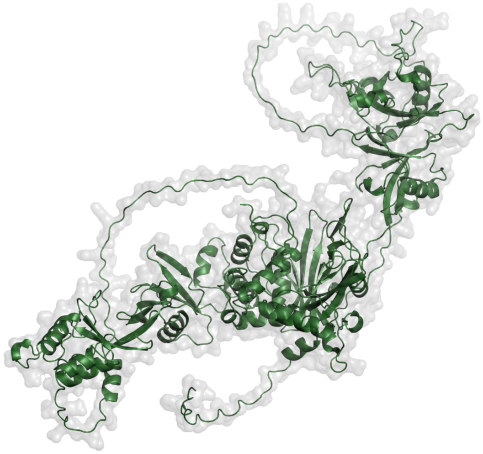

Figure 18: USP11 protein structure.

3D ribbon USP11 protein structure (AF-P51784-F1). Source: AlphaFold Protein Structure Database (Jumper et al., 2021; Varadi et al., 2022). Structure was adapted using the PyMOL software tool.

The AF algorithm gives additionally a per-residue confidence score (pLDDT) as output. Figure 19A illustrates the USP11 model confidence range by color. The contact matrix in Figure 19B indicates the expected position error for each residue in the USP11 sequence (UniProt: P51784). Regions with lowest error (dark grey squares) are expected to represent individual domains (Figure 19B). Domains suggested by AF for USP11 are consistent with available structural information about USP11 from previous reports (Harper et al., 2014; Spiliotopoulos et al., 2019).

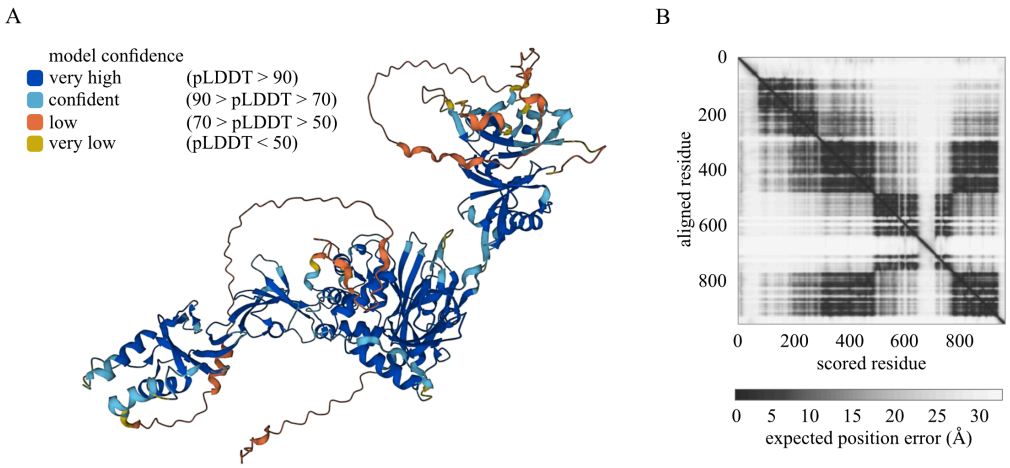

Figure 19: Model confidence of USP11 structure.

***A**. Alphafold structure prediction of USP11 (AF-P51784-F1)(Jumper et al., 2021; Varadi et al., 2022). The AF algorithm produces a per-residue confidence score (pLDDT) between 0 and 100 as indicated by model confidence coloring. **B**. Predicted Aligned Error (PAE) plot indicates the expected distance error in Angströms (Å). The shades of grey correspond to the expected distance error in residue x's position, when the prediction and true structure are aligned on residue y.*

To study the interaction between USP11 and its interaction partners more comprehensively, deletion mutants of recombinant USP11 were designed (scheme illustrated in Figure 20A) to identify the region(s) within the USP11 protein relevant for engaging protein-protein interaction (PPI) (together with F. Sauer, AG Kisker, RVZ, Wuerzburg). These constructs either lack the UBL2+Insert domain within the catalytic domain or the N-terminal domains DUSP and UBL or both (initially described in Figure 6). The Coomassie gel in Figure 20B shows truncated (#1-3) or full-length (#4) recombinant FLAG-tagged USP11 (black arrows) constructs purified from *E. coli* expression system. These constructs were used to study the interaction characteristics between USP11 and proteins identified in the USP11 interactome (see chapter 2.1). First the FLAG tag in the constructs was successfully tested in *in vivo* pulldowns (Figure 20C). Then performing *in vivo* pulldowns with SH-EP MYCN wt cells revealed the UBL2+Insert domain is critical for protein-protein interaction as pointed out for the bona-fide interactor USP7 and TCEAL1 in Figure 20C.

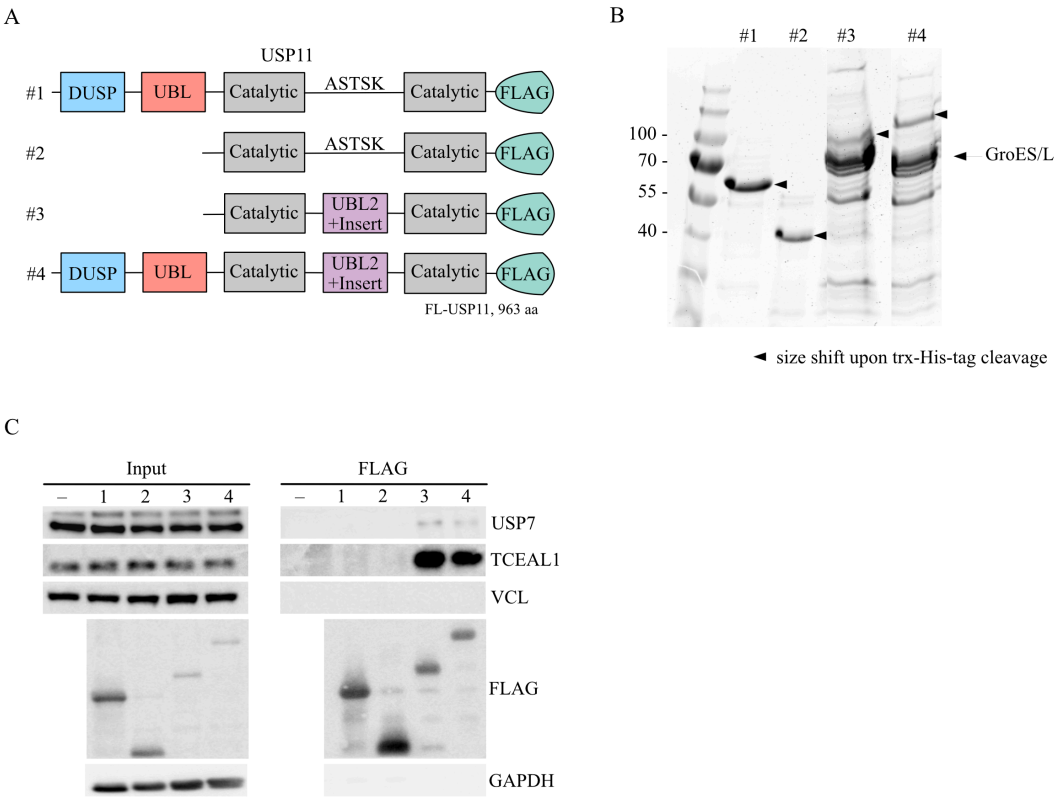

Figure 20: UBL2+Insert domain in USP11 is crucial to engage PPI.

A. *Design of FLAG-tagged recombinant USP11 constructs.* ***B.*** *Coomassie gel of the constructs purified from E. coli expression system based on the design shown in A (from F. Sauer (AG Kisker, RVZ, Wuerzburg). Black arrows indicate the expected size of the respective recombinant protein (#1-#4). GroES/L indicates bacterial contamination from NEB 10-beta cells used for protein expression.* ***C.*** *Immunoblot indicating proteins after in vivo pulldown from lysate from SH-EP MYCN wt cells with added recombinant proteins shown in A. Vinculin (VCL) and GAPDH were used as a loading control. (n=3)*

In addition, structural bioinformatics was applied to underpin the results shown in Figure 20. Such tools use the concept of linking evolutionary information from protein families to machine structure prediction. Recently, Evans et al. (2022) modified the architecture of the AlphaFold tool to predict multimeric complexes with high accuracy. Hereafter, AlphaFold2 Multimer (AF2) was used to predict the USP11-TCEAL1 complex. The 3D ribbon model of the highest ranked multimer out of five is illustrated in Figure 21A. UBL2+Insert domain (purple) within USP11 (green) is highlighted. The model visualizes a potential interaction between TCEAL1 (blue) and the UBL2+Insert domain with USP11. The plots in Figure 21B/C display the predicted LDDT per residue position of the multimers FL-USP11 (in Figure 21B) or USP11 ΔUBL2+Insert (in Figure 21C) and FL-TCEAL1. Strikingly, the per-residue confidence of TCEAL1 (blue) is reduced in the multimer with USP11 lacking UBL2+Insert domain, as revealed in Figure 21C, compared to multimer prediction with FL-USP11.

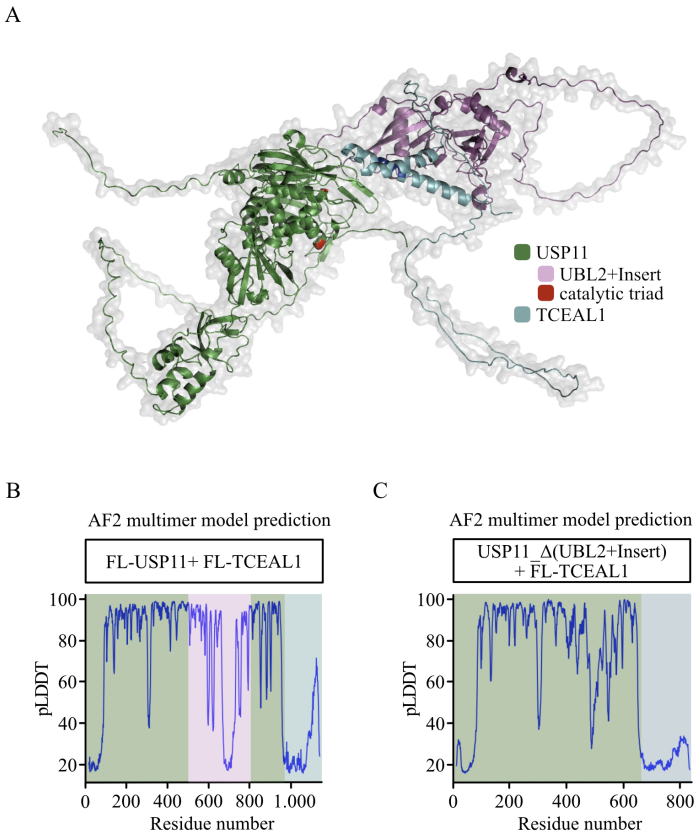

Figure 21: USP11-TCEAL1 multimer model prediction.

A. *3D ribbon model of the USP11-TCEAL1 multimer (FL-USP11, UniProt: P51784; FL-TCEAL1, Uniprot: Q15170) of one representative model predicted by AF2 (AlphaFold2 Multimer tool, v:1.0 (Evans et al., 2022)) and adapted using the PyMOL software tool. Color code: USP11 (green) with UBL2+Insert domain (purple), catalytic triad in USP11 (red), TCEAL1 (blue). n=5.* ***B./C.*** *Model prediction of the 3D structure of USP11 and TCEAL1 multimer from A. The y axis displays the per-residue confidence metric predicted local distance difference test (pLDDT) score (0-100). The x axis displays the residue number of USP11 (green and pink) and TCEAL1 (blue). n=5.* ***B.*** *shows the model prediction of FL-USP11 and FL-TCEAL1.* ***C.*** *shows the model prediction of USP11 ΔUBL2+Insert and FL-TCEAL1. (number of models =5)*

Consistent with *in vivo* pulldown assays (Figure 20), the models (Figure 21) generated by *in silico* multimer structure prediction (AlphaFold2 Multimer Algorithm) indicate that the UBL2+Insert domain within USP11 is critical for the interaction with TCEAL1.

2.2.2 TCEAL1 scaffolds interactions with USP11

Considering the role of USP11 as a DUB, the impact of USP11 on stability of TCEAL1 was investigated. Strikingly, USP11 depletion led to TCEAL1 downregulation, which was rescued by inhibition of the proteasome by MG-132 (see Figure 22). However, downregulation of USP11 showed no effect on protein stability of USP7.

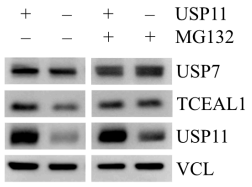

Figure 22: USP11 controls the stability of the TCEAL1 protein.

Immunoblot of indicated proteins from SH-EP MYCNER cells in presence or absence of USP11 and treatment with MG132 (20 μM, 4 h), where indicated. (n=2)

The high yield of co-precipitated TCEAL1 protein in the USP11 immunoprecipitation assays and rather low yield in the reverse experiment (illustrated below in Figure 24) suggested that TCEAL1 has an important role in USP11 biology. To further elucidate the the interplay between USP11 and TCEAL1, the impact of TECAL1 abundance was further investigated. To do so, endogenous USP11 IPs were repeated in SH-EP MYCNER cells containing a doxycycline-inducible shRNA targeting TCEAL1 (Figure 23A). Interestingly, USP11 strongly depends on TCEAL1 to engage protein-protein-interactions (Figure 23) when MYCN is activated. The binding between USP11 and USP7 is strongly diminished. Notably, the binding of USP11 to elongating RNAPII (pS2-RPB1) is more impaired compared to total-RNAPII (RPB1) upon depletion of TCEAL1.

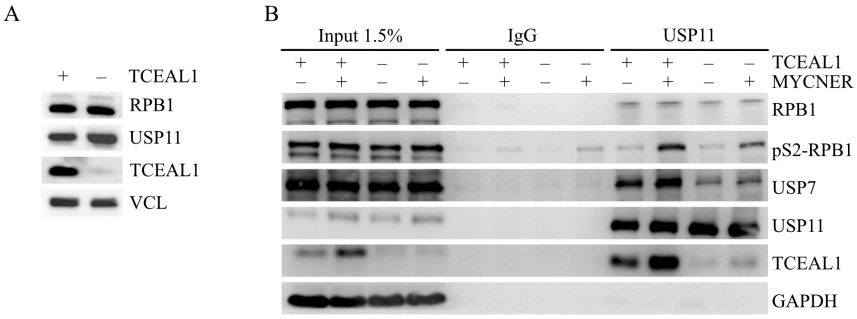

Figure 23: USP11 requires TCEAL1 to engage PPI.

A. *Immunoblot of indicated proteins in presence or absence of TCEAL1.* ***B.*** *Immunoblot of endogenous USP11 IPs from SH-EP-MYCN-ER cells in presence or absence of TCEAL1 and MYCN activation. Co-precipitated proteins are indicated. Beads coupled to non-specific IgG were used as a control. (n=3)*

2.2.3 TCEAL1 plays a role in transcription elongation

After unveiling the relationship between TCEAL1 and USP11, the following section addresses investigations on a putative role of TCEAL1 in transcription regulation. TCEAL1 was found in a transcription complex with USP11, as evidenced by endogenous TCEAL1 immunoprecipitation assays earlier in this thesis (Figure 24). Similar to USP11 (see USP11 Interactome in section 2.1.1), TCEAL1 also interacts with subunits of RNAPII and with USP7.

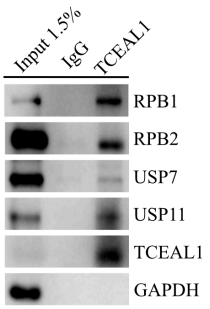

Figure 24: TCEAL1 shares interactions partners with USP11.

Immunoblot of endogenous TCEAL1 IPs from SH-EP-MYCN wt cells. Co-precipitated proteins are indicated. Beads coupled to non-specific IgG were used as a control. (n=3)

To investigate if TCEAL1 is found in transcription complexes, analytical size exclusion chromatography (SEC) was carried out. The elongation complex (EC) or the activated elongation complex (EC*) was assembled from pure components and isolated together with TCEAL1 by SEC. The size exclusion traces in Figure 25A/C show that TCEAL1 co-eluted with elongation complexes (EC, EC*). Also, the gels (see Figure 25B/D) indicate that fractions of TCEAL1 (black arrow) associate with RNAPII.

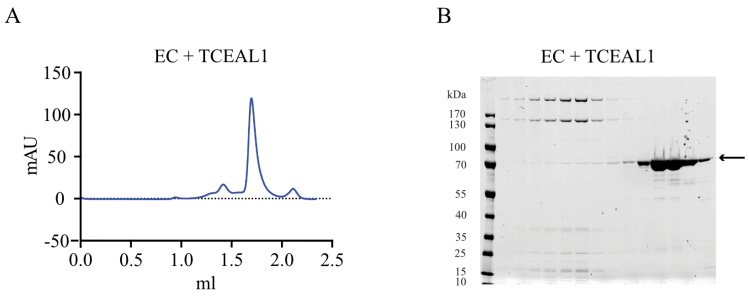

Figure 25: Formation of the EC+TCEAL1 complex.

A. *EC (elongation complex) +TCEAL1 are separated by size exclusion chromatography (dark blue and dark red lines). Curves show absorption at 280 nm milli absorption units (mAU) at specific elution volumes.* ***B.*** *show the respective SDS PAGE gel of A. This data is kindly provided by S. Vos (MIT, Cambridge, USA).*

Moreover, Coomassie staining from size exclusion chromatography runs with USP11, TCEAL1, and USP7 showed that they co-elute with later EC* fractions (Figure 26). This suggests that they form a complex in transcription.

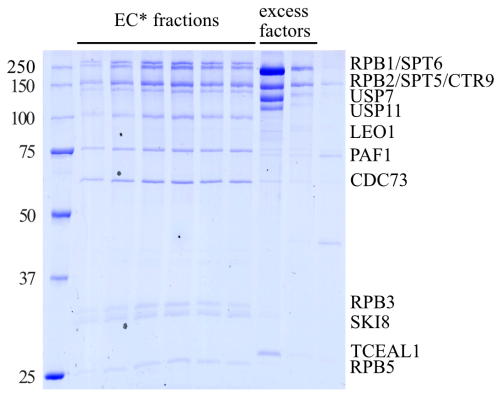

Figure 26: USP11, TCEAL1, and USP7 co-elute with EC*.

Coomassie staining of USP11-TCEAL1-USP7 co-elution with EC (RNAPII-PAF1c-SPT6-DSIF). The fractions are from size exclusion chromatography runs. This data is kindly provided by S. Vos (MIT, Cambridge, USA).*

Based on the test traces in Figure 25, denoted fractions (red box in Figure 27A) of EC+MBP-6His-TCEAL1 were crosslinked and used for a Cryo-EM study. The screening of fraction C5 on gold was fine and so a small test dataset of 1792 images (overnight) was collected (Figure 27B) and pre-processed with WARP (399,208 particles) (Figure 27C). Initial refinement went to 9 Å, however no extra density was observed where TCEAL1 binding was expected (the pore, centered on density images and marked by yellow arrow in initial 3D auto-refine density) or anywhere else (Figure 27D). Moreover, 3D classification to look for sub populations did not reveal any class with extra density as compared to RNAPII alone (Figure 27E-H). Class 4 was further refined since it had the highest estimated resolution to 7 Å (Figure 27I).

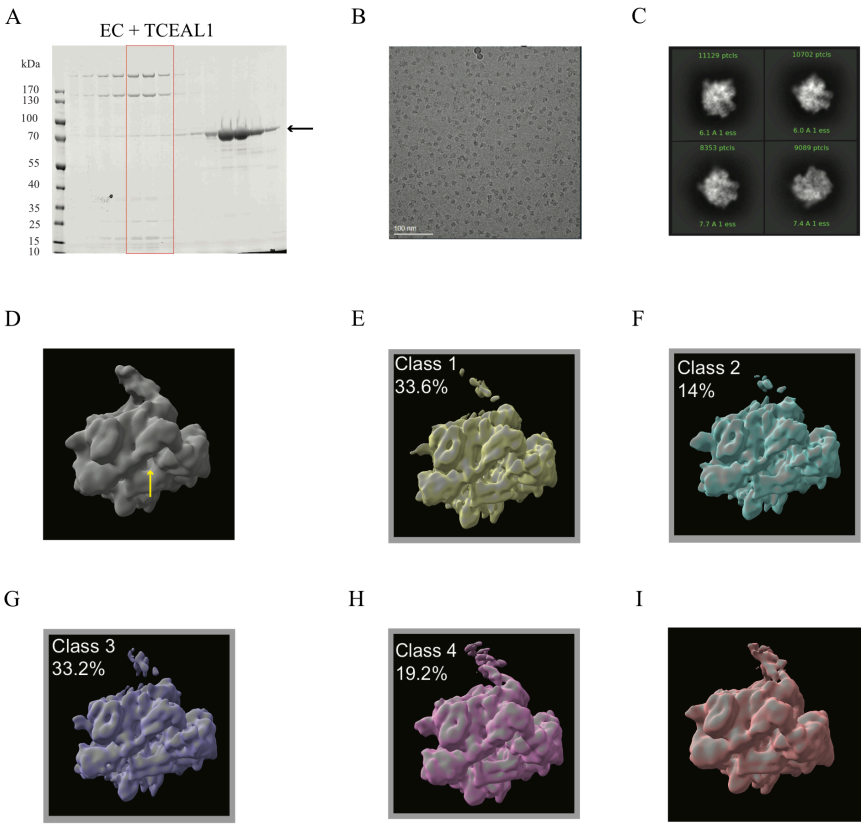

Figure 27: Cryo-EM studies of TCEAL1 and EC.

A.-I. *Cryo-EM study of TCEAL1 and Elongation Complex (EC) from S. Vos (MIT, Cambridge, USA).* ***A.*** *SDS-PAGE of TCEAL1+EC. C1-C11 (snaking fractions, 4.64-5.14 ml, x50 µl). MBP-6HIS-TCEAL1 is highlighted (green arrow). C5-C7 denotes fractions crosslinked and used for Crryo-EM study (red box) in B.-I.* ***B.*** *Representative micrograph of the EC+TCEAL1 (C5 fraction on Au flat 2/2 protogris Arctica, 120k mag, 200 keV).* ***C.*** *Representative 2D classes of EC+TCEAL1 particles (by Cryosparc software).* ***D.*** *Relion 3D auto-refine (all particles). Expected pore of TCEAL1 binding (yellow arrow)* ***E.-H.*** *Relion 3D classification for data processing.* ***I.*** *Relion 3D auto-refinement of Class 4 shown in H, 7Å. This data is kindly provided by S. Vos (MIT, Cambridge, USA).*

In summary, TCEAL1 was co-eluted with RNAPII, although the complex was not resolved in Cryo-EM. It was speculated that TCEAL1 as a monomer is not sufficient and that other complex members (e.g. USP11, USP7) might be required for complex formation.

Although the exact interface between TCEAL1 and RNAPII could not be decoded *in vitro*, its role in transcription regulation was further characterized. To do so, manual ChIPs and ChIP-Rx experiments were conducted in SH-EP MYCNER cells expressing HA-TCEAL1 and activated MYCN (Figure 28). Overexpressed HA-tagged TCEAL1 is enriched at TSS of selected MYCN-bound promoter regions. The pan-CDK inhibitor flavopiridol, that inhibits CDK2, CDK4, CDK6 and CDK9 at nanomolar concentrations, enhanced chromatin binding of TCEAL1 to chromatin (Figure 28A). Interestingly, inhibition of transcription elongation using the specific CDK9 inhibitor NVP-2 (Figure 28B) increased TCEAL1 chromatin occupancy globally and shifted its position towards the pause site (Figure 28C). This effect was especially pronounced for up-regulated genes (Figure 28C, right panel), but not observed using the CDK7 inhibitor THZ1 (Figure

28B/C/D). This provided evidence that TCEAL1 is involved in elongation rather than in transcription initiation. Browser tracks of two selected genes are shown in Figure 28D.

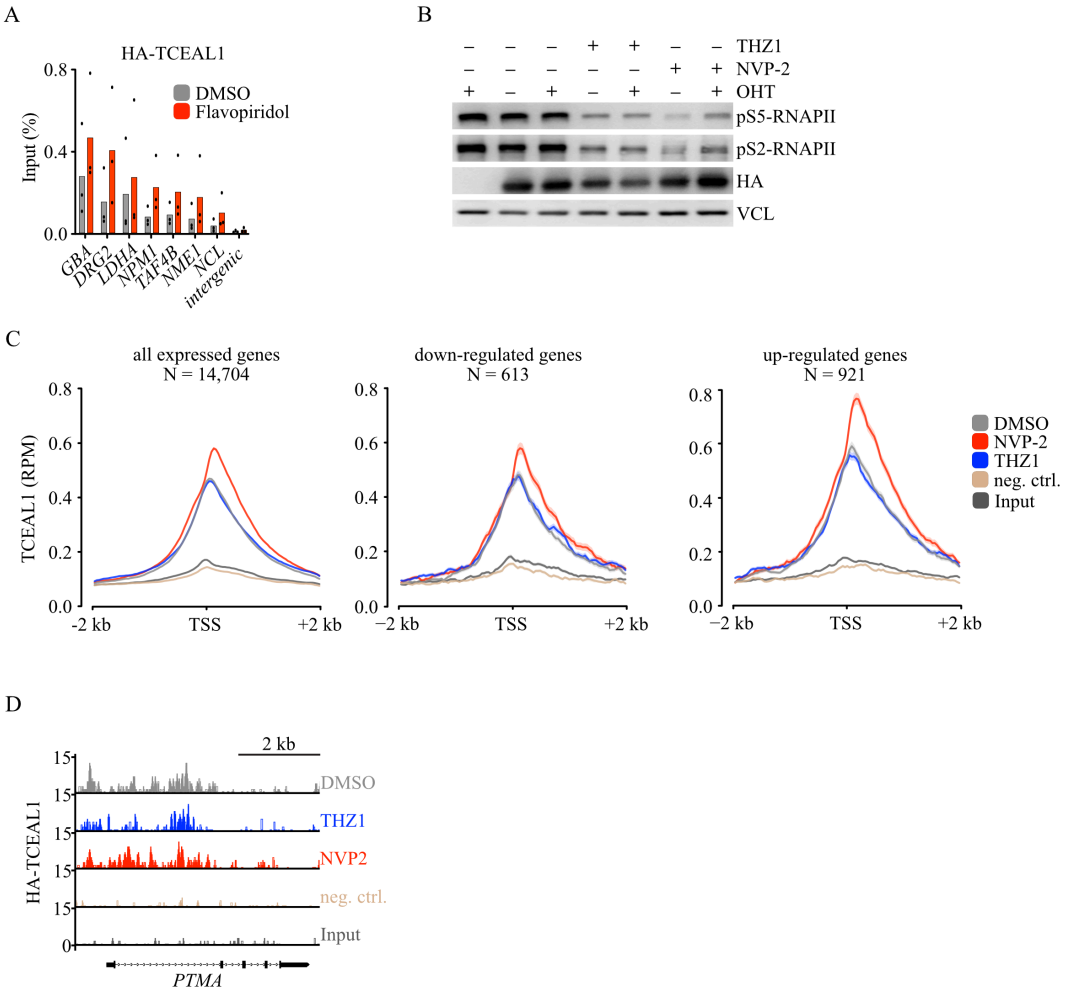

Figure 28: TCEAL1 occupancy is enriched at promoter-proximal pause sites.

A. *HA chromatin immunoprecipitation in SH-EP MYCNER cells treated with flavopiridol (red) or DMSO (grey) at indicated loci. IgG was used as control. Bars show data of technical triplicates. Dots show data of three independent technical triplicates (n=3).* ***B.*** *Immunoblot of indicated proteins of SH-EP MYCN-ER cells with activated MYCN (neg. ctrl.) and these cells expressing HA-tagged TCEAL1 wildtype and treated with NVP-2 (1 µM, 3 h), THZ1 (200 nM, 8 h) or DMSO.* ***C.*** *Global average read density of HA-TCEAL1 ChIP-Rx data from cells as treated in B. Plots represent all expressed (N= 14,704, left panel), down-regulated (N= 613, mid panel) and up-regulated (N= 921, right panel) genes at the TSS. Data are mean* ± SEM. (n = 2). ***D.*** *Representative genome browser tracks of the PTMA locus of the ChIP experiment described in C.*

Immunoprecipitations showed that MYCN enhances the interaction of USP11 with modified RNAPII (pS2, pS5) and that the MYCN-dependent increase is partly dependent on TCEAL1 (Figure 23B). Furthermore, it was demonstrated that TCEAL1 is enriched at promoter-proximal pause sites (Figure 28). Based on these findings the direct influence of TCEAL1 on RNAPII behavior on chromatin was investigated. Intriguingly, ChIP-Sequencing of total-RNAPII as well as its elongating form, pS2-RNAPII, revealed that TCEAL1 depletion dramatically decreased overall RNAPII chromatin association (Figure 29). This implies a novel role of TCEAL1 in global

transcription. The effect of TCEAL1 downregulation on pS2-RNAPII predominantly impaired up-regulated genes (Figure 29B, right panel). Individual genes convincingly reflected the effects seen globally (Figure 29C).

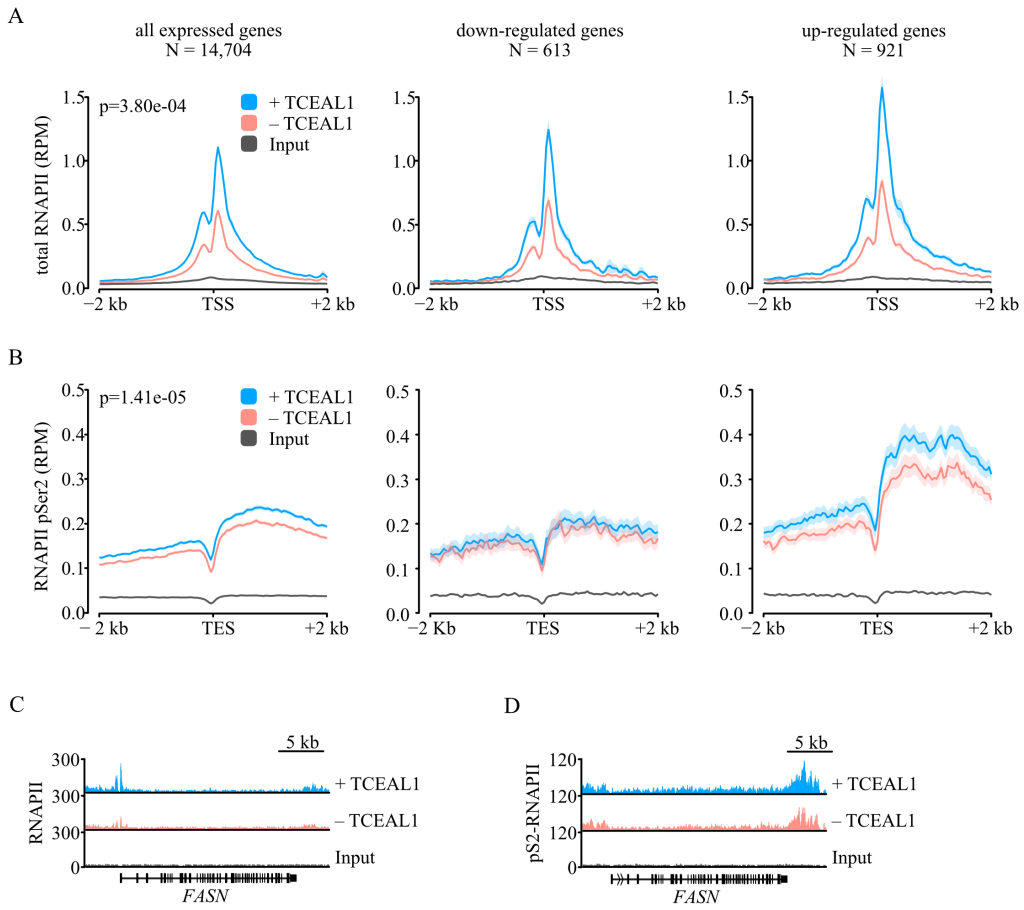

Figure 29: TCEAL1 is important for productive elongation of RNAPII.

A. *Global average read density of total-RNAPII ChIP-Rx data from SH-EP MYCNER cells in presence (+) or absence (-) of TCEAL1. Plots represent all expressed (n= 14,704, left panel) , down-regulated (n= 613, mid panel) and up-regulated (n= 921, right panel) genes at the TSS. Data are mean* ± SEM. (n = 2) **B.** *Global average read density of pS2-RNAPII ChIP-Rx data from cells as treated in A. Plots represent all expressed (N= 14,704, left panel) , down-regulated (N= 613, mid panel) and up-regulated (N= 921, right panel) genes at the TSS. Data are mean* ± SEM. (n = 2) **C.** *Representative genome browser tracks of the FASN locus of the total-RNAPII ChIP- Sequencing experiment described in A.* **D.** *Representative genome browser tracks of the FASN locus of the pS2-RNAPII ChIP-Sequencing experiment described in panel A.*

To understand if TCEAL1 is important for transitioning of the RNAPII from pausing to productive elongation the pausing index was calculated. The pausing index is the ratio of RNAPII signal density near a gene promoter to signal density within the gene body, such that higher pausing indices reflect a greater enrichment of promoter paused RNAPII (Adelman & Lis, 2012). Depletion of TCEAL1 led to reduced pausing (Figure 30).

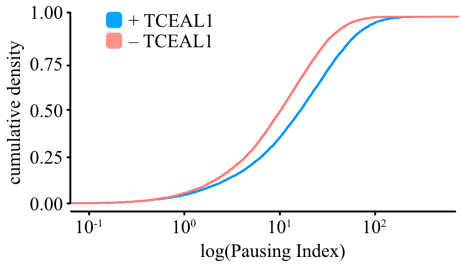

Figure 30: Promoter proximal pausing is decreased in absence of TCEAL1.

Pausing indices of RNAPII signal of 14, 704 genes generated from SH-EP MYCNER cells in presence (+) or absence (-) of TCEAL1.

To address the question if the observation made on RNAPII behavior upon TCEAL1 depletion have effects on transcription output, RNA-Sequencing was performed. RNA-Sequencing showed that TCEAL1 depletion moderately abrogates MYC-dependent gene expression (Figure 31A). Some gene sets are differentially affected by MYCN activation in the presence (+) or absence (-) of TCEAL1 (Figure 31B). hallmark genes found in protein secretion, UV response, and RNA stability suggest a TCEAL1 dependency.

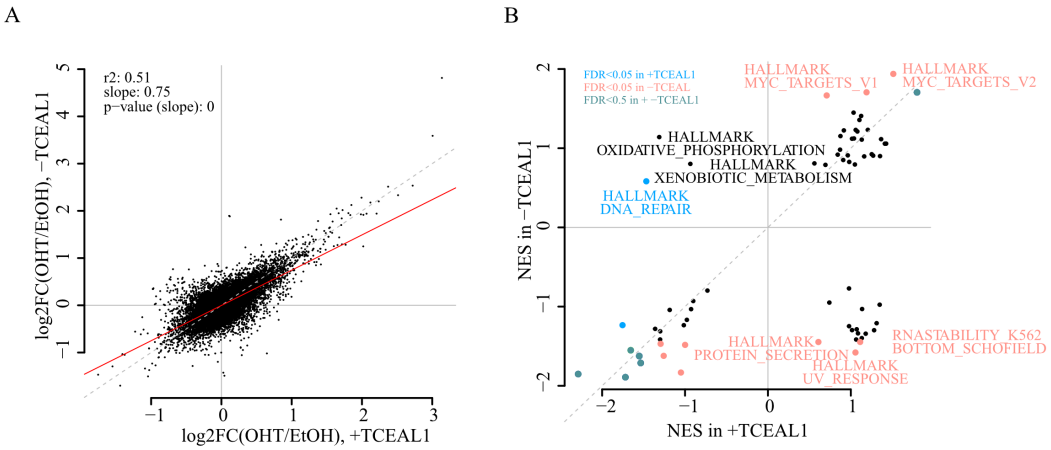

Figure 31: Protein secretion, UV response, and RNA stability genes are TCEAL1-dependent.

A. *Relative gene expression of 16,318 genes (each with logCPM>0) from SH-EP MYCNER cells in presence (+) or absence (-) of TCEAL1 with MYCN activation (4-OHT).* ***B.*** *Hallmark gene sets found in A in absence (-) or presence (+) of TCEAL1 (NES, normalized enrichment score).*

Previous experiments have shown that USP11 is required to recruit BRCA1 in order to terminate transcription of stalled RNAPII (Herold et al., 2019). We hypothesized that TCEAL1 might scaffold this recruitment. Manual BRCA1 ChIP assays in the presence and absence of TCEAL1 demonstrated that TCEAL1 has no effect on BRCA1 recruitment at MYCN promoter regions (Figure 32). Activation of MYCN is crucial for BRCA1 recruitment, as reported elsewhere (Herold et al., 2019). This observation suggests that USP11 molecules that depend on forming a complex with TCEAL1 are unlikely to recruit BRCA1.

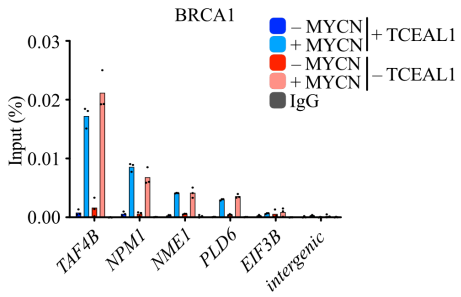

Figure 32: TCEAL1 has no impact on BRCA1 recruitment.

BRCA1 chromatin immunoprecipitation in SH-EP MYCNER cells in presence or absence of TCEAL1 and MYCN activation at indicated loci. IgG was used as control. Dots show data of three independent technical triplicates of one representative experiment. (n=2)

2.3 TCEAL1 antagonizes TFIIS in transcription elongation

TCEAL1's role in transcription elongation remains unclear. It is one of nine members of the transcription factor elongating A-like family (Pillutla et al., 1999). They are nuclear phosphoproteins that are presumably similar to the transcription factor SII (TFIIS, encoded by the *TCEA1*, *TCEA2*, and *TCEA3* genes). It was hypothesized that there is a putative mechanism to counteract the elongation factor TFIIS. In the following section, data is provided to propose a novel "competition" mechanism involving USP11 and TCEAL1 to protect RNAPII molecules from premature TFIIS-mediated termination.

2.3.1 TCEAL1 is a TFIIS-like protein

TCEAL1 consists of three described functional domains: an arginine/serine (RS) domain, a zinc-finger-like (ZnF-L) domain, and a helix-turn-helix (HTH) domain (Pillutla et al., 1999; Yeh & Shatkin, 1994a, 1994b).

The sequence similarity of TCEAL1 with other protein family members as well as TFIIS, as previously reported by *Pillutla et al. (1999*), was proved by a blastp analysis (see in Figure 33). Parts of the motif (EEMIQAADELEEM) in TCEAL1 was also found in TFIIS within its domain II, important for interacting with RNAPII (Agarwal et al., 1991; Kettenberger et al., 2003). Noteworthy, this algorithm did not confirm results of previous sequence similarity analyses regarding a RNAPII binding motif located more upstream (Yeh & Shatkin, 1994b). Additional information on the blastp analysis is provided in Table 29.

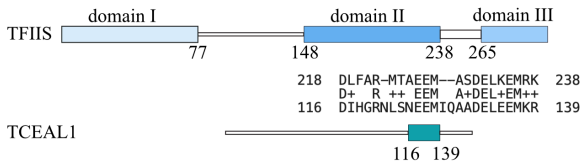

Figure 33: TCEAL1 shows sequence similarity with TFIIS.

Scheme illustrating sequence similarity between TCEAL1 and TFIIS observed by blastp runs.

2.3.2 C-terminal HTH domain in TCEAL1 is crucial for chromatin occupancy

The motif identified in the previous section (2.3.1) is located within the C-terminus of TCEAL1. In Figure 34 the structure of TCEAL1 is predicted and illustrated by AF. The box in Figure 34 zooms in on the amino acid sequence within the HTH which could be relevant for TCEAL1 interaction.

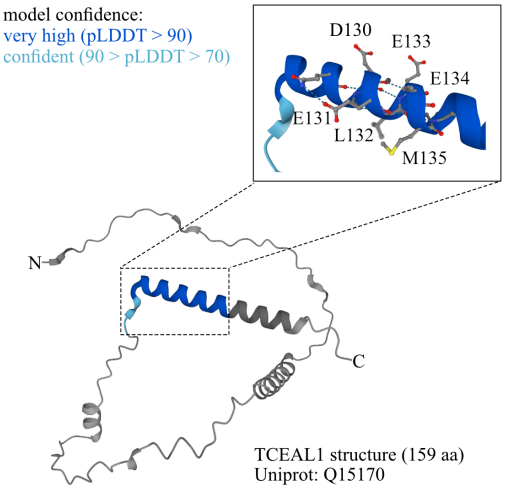

Figure 34: Model confidence of C-terminal helix of TCEAL1.

Predicted TCEAL1 structure adapted from AlphaFold (structure: AF-Q15170-F1). Model confidence of the C-terminal helix domain in TCEAL1 is highlighted by coloring of pLDDT values.

Intrigued by the fact that HTH domains act as a structural motif capable of binding DNA and regulating transcription (Aravind et al., 2005), we challenged the chromatin binding of TCEAL1 by either partial deletion of the sequence or by point mutations of amino acids introduced within the C-terminal domain (see Figure 34, Figure 35). All overexpressed HA-tagged TCEAL1 mutants disrupt the ability to bind chromatin compared to TCEAL1 wildtype (wt) overexpression (see Figure 35A). TCEAL1 mutated at amino acid residues 130-132 disrupted the interaction with USP11 as well as RNAPII in endogenous TCEAL1 immunoprecipitation assays (Figure 35B). This result reinforces the statement made in section 2.2.2, that TCEAL1 must be intact and stable in order to function in transcription.

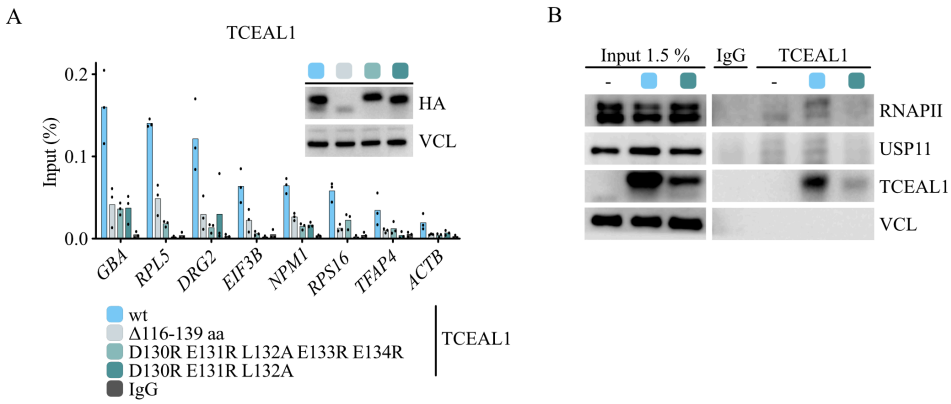

Figure 35: Mutagenesis of the C-terminal domain in TCEAL1 impairs its chromatin occupancy.

A. *HA-TCEAL1 ChIP at indicated loci in SH-EP MYCN wt cells overexpressing HA-tagged TCEAL1 wildtype (light blue) or mutants (turquoise color shades) as indicated. IgG was used as control (dark grey). Dots show data of independent technical triplicates of one representative experiment. (n=3)* ***B.*** *Immunoblot of endogenous TCEAL1 IPs from SH-EP-MYCN-ER cells overexpressing HA-tagged TCEAL1 wildtype (light blue) or mutant (turquoise). Co-precipitated proteins are indicated. Beads coupled to non-specific IgG were used as a control. (n=2)*

2.3.3 TFIIS recruitment on chromatin increases upon TCEAL1 downregulation

Up next, the role of TCEAL1 as an analog of TFIIS was investigated. The domain III (D290, E291) specifically residues of TFIIS are required to stimulate the intrinsic cleavage activity of RNAPII (Kettenberger et al., 2003). This domain is absent in TCEAL1 as shown in Figure 33. However, both, TFIIS (Ghavi-Helm et al., 2008) and TCEAL1 (section 2.2.3) bind to chromatin at the TSS. It was therefore hypothesized that they might compete for binding to chromatin. To test this, TFIIS ChIP experiments with SH-EP cells in the presence or absence of TCEAL1 and after activation of MYCN were performed. While TCEAL1 knockdown had no effect on TFIIS protein abundance (Figure 36A), TFIIS chromatin occupancy at the TSS on individual promoters as well as globally was significantly increased upon TCEAL1 knockdown (Figure 36B-E).

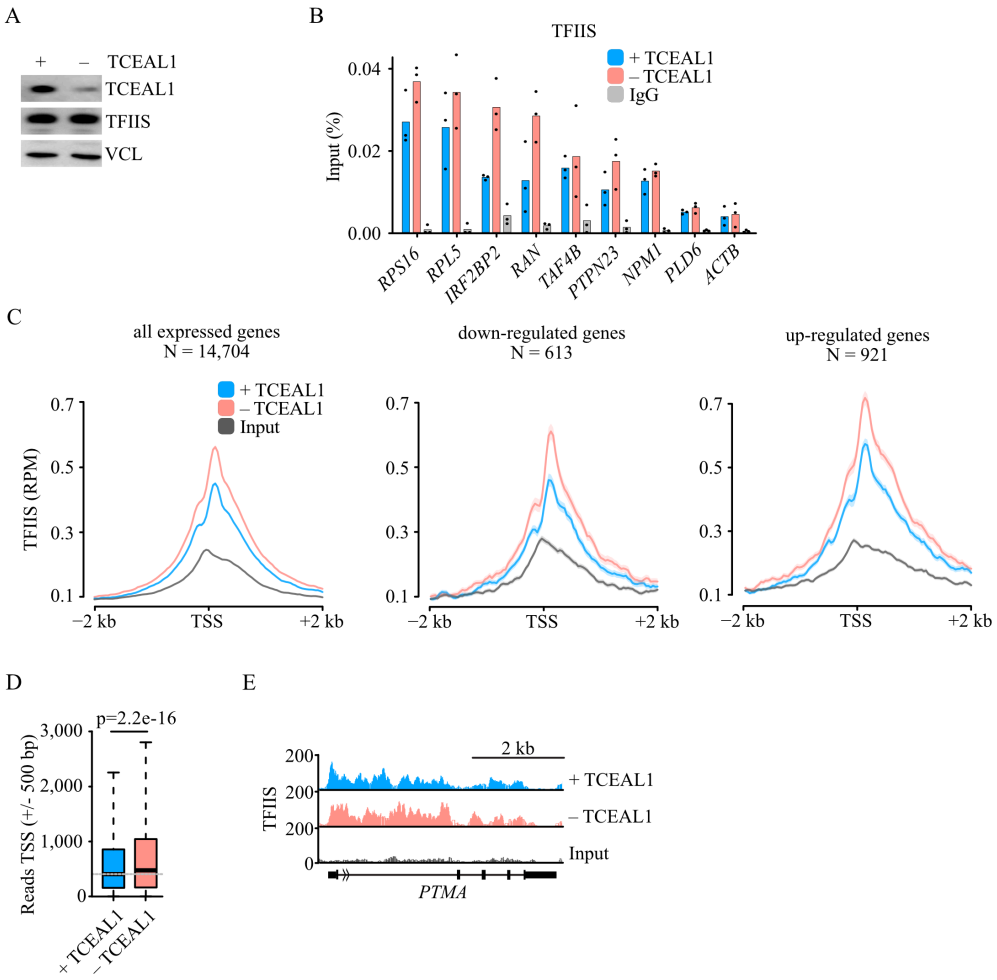

Figure 36: TFIIS is enriched at TSS upon depletion of TCEAL1.

A. *Immunoblot of indicated proteins in presence or absence of TCEAL1.* ***B.*** *TFIIS ChIP at indicated loci in SH-EP MYCN-ER cells in presence (light blue) or absence (light red) of TCEAL1 and activated MYCN. IgG was used as a control. Dots show data of independent technical triplicates of one representative experiment. (n=3)* **C.** *Global average read density of TFIIS ChIP-Rx data in SH-EP-MYCNER cells in presence (light blue) and absence (light red) of TCEAL1 and activated MYCN (input: grey; TSS, transcriptional start site). Plots represent all expressed (N= 14,704, left panel) , down-regulated (N= 613, mid panel) and up-regulated (N= 921, right panel) genes at the TSS. Data show mean ± standard error of the mean (SEM). (n=2).* ***D.*** *Boxplot representing global reads of TFIIS at the TSS from data generated in panel A. p-value was calculated by unpaired t test.* ***E.*** *Representative genome browser tracks of the PTMA locus of the TFIIS ChIP-Sequencing experiment from panel C.*

To investigate which genes show changes in TFIIS binding in presence or absence of TCEAL1 (Figure 36), a gene set enrichment analysis (GSEA) of the TFIIS ChIP-Sequencing data was performed. This analysis revealed that TFIIS binding on highly expressed genes of the MYC targets v2 and E2F targets, among others (Figure 37), is enhanced upon depletion of TCEAL1.

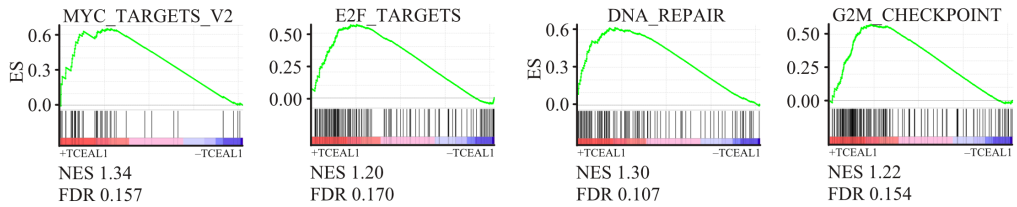

Figure 37: TFIIS accumulates at highly expressed genes in TCEAL1-depleted cells.

Gene sets affected by TCEAL1-depleted effects on TFIIS chromatin enrichment. GSEA was performed on genes ranked for change in TFIIS chromatin enrichment between cells in presence (+) or absence (-) of TECAL1. A positive enrichment score (ES) indicates genes with enhanced TFIIS binding upon TCEAL1 depletion.

Mutations within the C-terminal helix of TCEAL1 led to the loss of chromatin binding (Figure 35). To understand if chromatin binding incompetence of TCEAL1 could phenocopy TCEAL1 downregulation, a TFIIS ChIP was performed (Figure 38). Indeed, overexpression of mutated TCEAL1 proteins enhances TFIIS chromatin binding at selected MYCN-bound promoter regions (Figure 38).

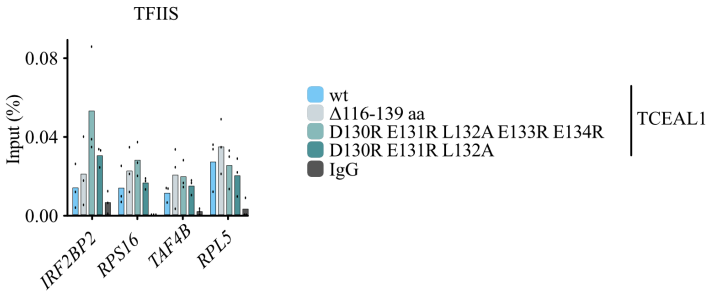

Figure 38: Overexpression of TCEAL1 mutants enhance chromatin occupancy of TFIIS.

TFIIS ChIP at indicated loci in SH-EP MYCN wt cells overexpressing HA-tagged TCEAL1 wildtype (light grey) or mutants (dark red, dark blue, beige) as indicated. IgG was used as control (dark grey). Dots show data of independent technical triplicates of one representative experiment. (n=3)

Additionally, TCEAL1 was overexpressed in SH-EP MYCN wt cells (TCEAL1 OE, see Figure 39A) and TFIIS binding to chromatin compared with cells without overexpression of TCEAL1 was visualized. Global analysis revealed a significant decrease in TFIIS binding in TCEAL1 OE cells (Figure 39A). Moreover, as already shown for individual promoter regions (Figure 38), the overexpression of a TCEAL1 mutant (Figure 39A) impaired in chromatin binding (see Figure 35C) and did not compete with TFIIS and led to an increase of TFIIS binding (Figure 39B). Consistent with TCEAL1 chromatin binding behavior and its abundance impacting TFIIS chromatin

occupancy, TFIIS significantly outcompetes the overexpressed TCEAL1 mutant for chromatin binding significantly (Figure 39C).

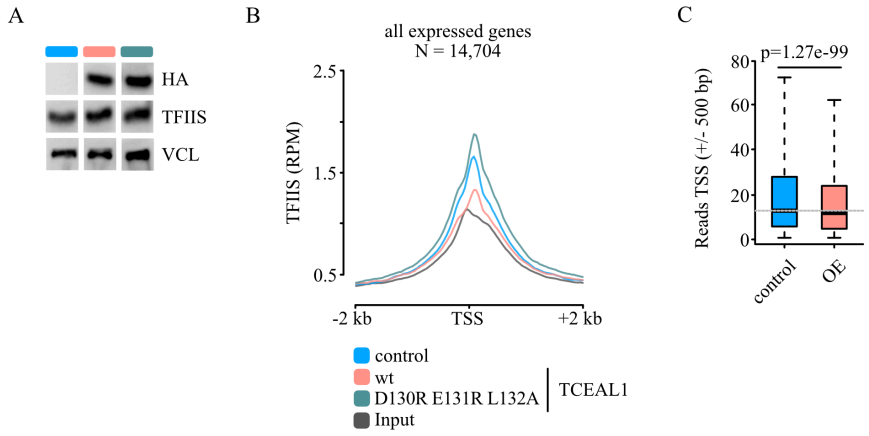

Figure 39: TCEAL1 overexpression impacts TFIIS chromatin occupancy globally.

A. *Immunoblot of indicated proteins of SH-EP MYCN wt cells as a control (light blue) and these cells overexpressing HA-tagged TCEAL1 wildtype (light red) or mutated at 130-132 aa (turquoise).* ***B.*** *Global average density of TFIIS ChIP-Sequencing data from cells in A (Input: grey; TSS, transcriptional start site) (n=2).* ***C.*** *Boxplot representing global reads of TFIIS at the TSS from control cells and cells overexpressing TCEAL1 used in B. P-value was calculated by unpaired t test. (n=1)*

TCEAL1 shares the majority of its bound genes with TFIIS at the TSS. In contrast, TFIIS shares a significant proportion of its bound genes with TCEAL1 at the TSS (Figure 40). The strong correlation (R=0.73) between the chromatin binding of these two proteins is in line with the hypothesis of a competition between the two proteins, although it could also simply imply that these genes require both proteins (Figure 40).

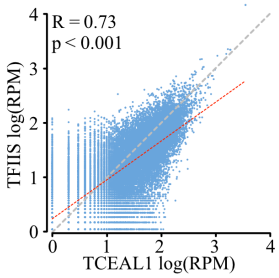

Figure 40: Overlap of TFIIS and TCEAL1 peaks at TSS.

Correlation analysis of TFIIS-bound genes versus TCEAL1-bound genes at the TSS in SH-EP MYCNER cells.

Taken together, the ChIP-Sequencing data indicates that TCEAL1 molecules compete with TFIIS molecules for chromatin binding within the TSS region.

To determine the effect of TCEAL1 on RNA extension in transcription, as previously done for TFIIS (Vos, Farnung, Urlaub, et al., 2018), RNA extension assays were performed (Figure 41; collaboration with Vos Group, MIT, USA). As supposed, TCEAL1 did not show any effect on RNA extension (Figure 41A/B). In contrast, Figure 41C clearly shows that TFIIS causes back-tracking which leads to loss of RNA extension and appearance of -1nt primer band in the gel.

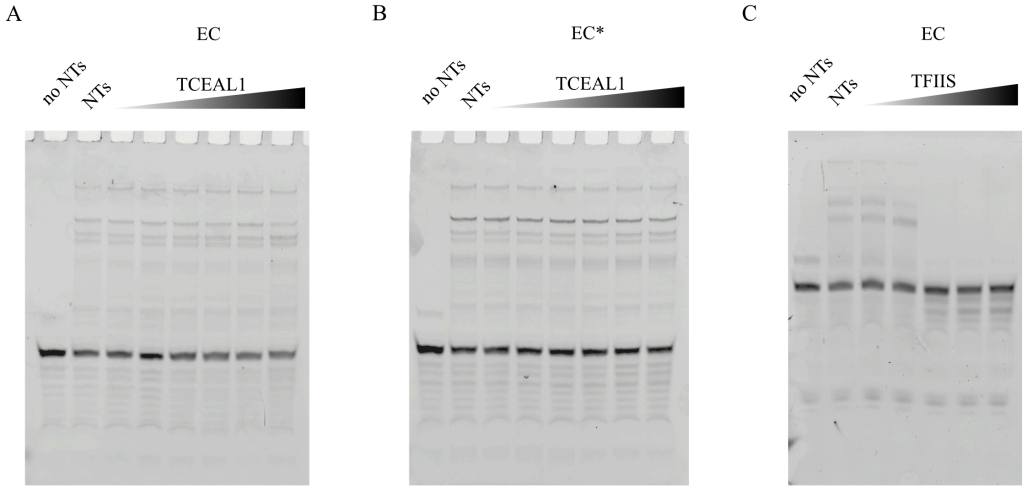

Figure 41: TCEAL1 does not show any effects on RNA extension.

A.-C. *Fluorescence monitored RNA extension on the EC (75 nM RNAPII) and EC*(75 nM RNAPII and 225nM of SPT6, Paf16, DSIF, and P-TEFb) complex.* ***A.*** *and* ***B.*** *are gels with EC and EC*, first lanes are with or without nucleotides (NT), and with nucleotides in the presence of TCEAL1 ranging from 52 nM to 54 μM.* ***C.*** *is a gel with EC, first lanes are with or without nucleotides, and with nucleotides in the presence of TFIIS ranging from 27 nM to 7 μM.*

Moreover, to investigate whether TCEAL1 affects TFIIS in the transcription process, we conducted proximity-ligation assays (PLAs) to capture the proximity of TFIIS with different states of RNAPII in presence or absence of TCEAL1 (see Figure 42). While PLAs between TFIIS and total RNAPII (Figure 42A) showed a mild increase after knockdown of TCEAL1, the proximity to unphosphorylated RNAPII decreased (Figure 42B) and RNAPII phosphorylated at Serine 5, indicating that it is transcriptionally active, increased (Figure 42C). This suggests that TCEAL1 is counteracting the interaction of TFIIS with RNAPII-pSer5 which would lead to enhanced promoter-proximal termination.

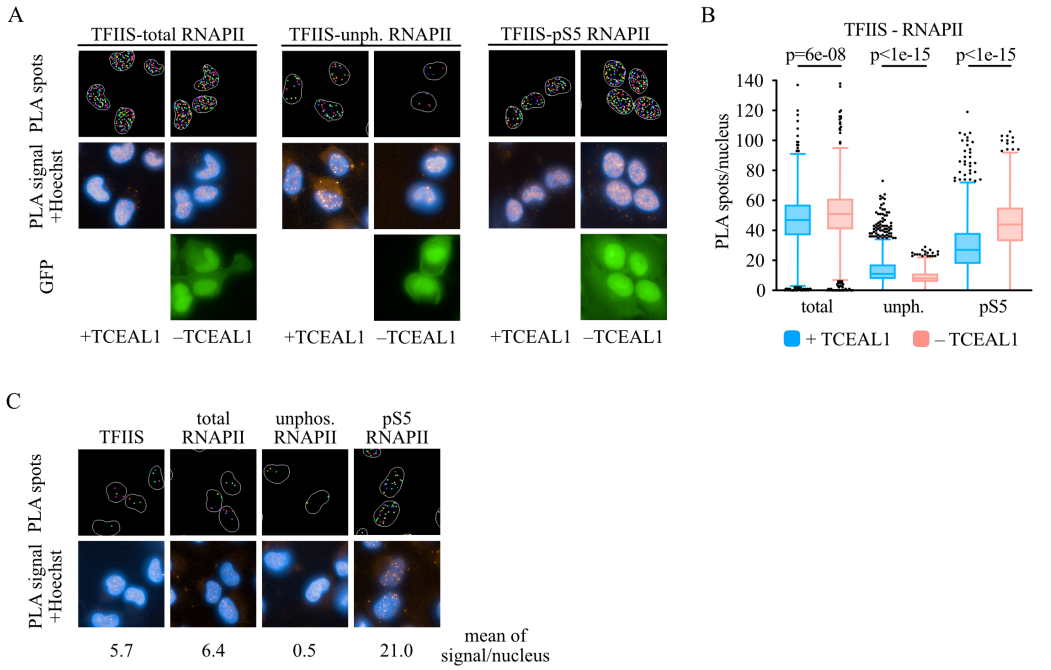

Figure 42: TCEAL1 protects RNAPII pS5 from accumulation with TFIIS.

A. *Representative images of PLAs between TFIIS and differently modified RNAPII showing PLA spots, PLA signal merged with Hoechst 33342 and GFP signal indicating absence of TCEAL1.* ***B.*** *Quantification of the nuclear PLA foci detected in A. Box plots are from single cell analysis of one representative experiment. P-values were calculated using an unpaired t-test.* ***C.*** *Representative images of single antibody control of PLAs shown in A. The numbers indicate the mean of PLA signal per nucleus in these cells. (n=3)*

To confirm that TCEAL1 abundance affects the protein-protein-interaction behavior of TFIIS, immunoprecipitation assays with cells with endogenous TCEAL1 levels, or overexpressing TCEAL1 wildtype, or overexpressing TCEAL1 mutant (D130R E131R L132A) were performed. This mutant only marginally binds chromatin (Figure 35) and is incapable of competing with TFIIS (Figure 39). RNAPII immunoprecipitations showed upon TCEAL1 overexpression, that the interaction between RNAPII and TFIIS was remarkably diminished (Figure 43A). In contrast, the interaction between RNAPII with TFIIS was enhanced when the TCEAL1 mutant instead of TCEAL1 wildtype is overexpressed (Figure 43A). Furthermore, RNAPII interaction with USP11 was enhanced when TCEAL1 was overexpressed and reduced when the TCEAL1 mutant was overexpressed. This supports the idea that TCEAL1 has an important scaffolding function for USP11, as shown earlier (Figure 23B). Similar trends were observed in immunoprecipitations against RNAPII phosphorylated at Serine 5 (Figure 43B).

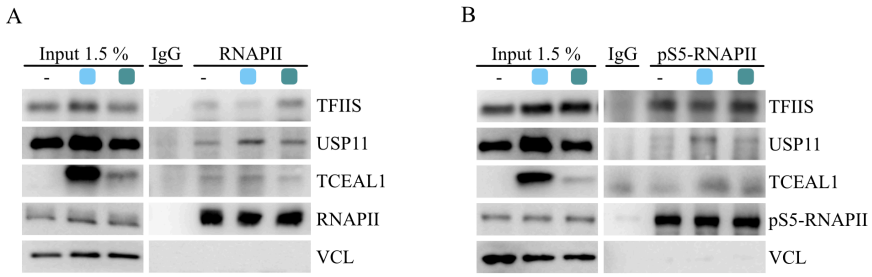

Figure 43: TCEAL1 integrity impacts TFIIS interaction with RNAPII.

A. *Immunoblot of endogenous RNAPII IPs from SH-EP-MYCN-ER cells as control (-) and these cells over-expressing HA-tagged TCEAL1 wildtype (light blue) or mutated at 130-132 aa (turquoise). Co-precipitated proteins are indicated. Beads coupled to non-specific IgG were used as a control (n=2).* ***B.*** *pS5-RNAPII IPs with cells as described in A. Co-precipitated proteins are indicated. Beads coupled to non-specific IgG were used as a control. (n=2)*

Overall, the pro-transcription factor TCEAL1 must be intact at the C-terminus to engage complex formation together with USP11 and the transcription machinery. In this context, the protein levels of TCEAL1 dictate the chromatin occupancy as well as RNAPII binding of TFIIS.

Available databases (e.g. DepMap) indicate that TCEAL1 is non-essential in human cells. To identify the biological context that requires TCEAL1, an unbiased drug screen was performed. Here was inquired whether downregulation of TCEAL1 could make cancer cells sensitive to drugs which induce a certain stress. In addition to downregulation of TCEAL1 and MYCN activation the cells were challenged with incubation of a drug compound library (82 compounds).

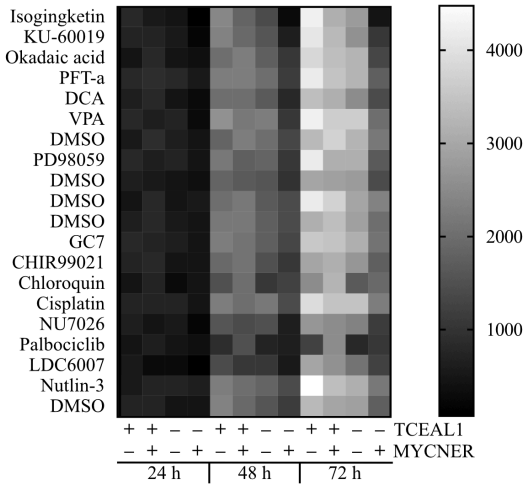

Figure 44: TCEAL1 downregulation does not sensitize cells for selected drugs.

Heatmap of top 20 drug compounds showing most significant changes in cell proliferation upon absence of TCEAL1 when MYCN is active or inactive. Cell number is normalized to cell number measured at T0. Data illustrates cell count from three different time points (t = 24 h, 48 h, 72 h). (n=2)

The selected drugs hardly showed additional effects on cell proliferation in addition to TCEAL1 depletion (Figure 44). The downregulation of TCEAL1 had a very strong effect on cell proliferation, as visualized for the time points 24 h, 48 h, and 72 h. To a certain extent Nutlin-3 and PFT, and to a minor extent PD98059 and Okadaic acid additionally reduced cell proliferation in addition to depletion of TCEAL1.

3 Discussion

3.1 The role of USP11 in transcription regulation

Several recent studies have gathered data about how the oncogenic MYC proteins ease transcription stress in cancer cells (Papadopoulos et al., 2023), in addition to their regulatory function in gene expression (Baluapuri et al., 2020). In particular, significant progress has been made in understanding the mechanisms involving MYCN, one of the three members of the MYC family, which drives many neuroendocrine tumors (Rickman et al., 2018). The specific expression profile of *MYCN*-amplified neuroblastoma tumors (cf. Figure 1) is explained by the equilibrium between the two MYCN-driven processes promoter-proximal termination and transcription elongation. To date, the cooperation between these mechanisms regulated by MYCN remains incompletely understood (Herold et al., 2019).

By building on previous findings from Herold et al. (2019), in this study the role of USP11 was further elucidated, recently identified as a putative player in the aforementioned processes. This thesis strongly indicates a novel mechanistic function of the deubiquitinase USP11 in early transcription.

Basically, MYC proteins function both in physiological and pathological conditions is mainly regulated by a network of bHLH-LZ proteins (e.g. MAX), which can act as either agonists or antagonists of MYC function in transcription (Carroll et al., 2018). To this end the field generated a comprehensive picture of interacting networks of MYC as well as MYCN proteins (Baluapuri et al., 2019; Buchel et al., 2017; Heidelberger et al., 2018; Kalkat et al., 2018). Importantly, MYC and MYCN respond differently to transcription stress (Papadopoulos et al., 2023). In contrast to MYCN, MYC can recruit MIZ1 to repress excessive transcriptional activation (Vo et al., 2016). MYC and MYCN employ different mechanisms to cope with deregulated transcriptional elongation. Extensive studying of such complexes shed light on the understanding of MYC's oncogenic function in gene regulation (see section 1.2.2) and beyond, reviewed by Papadopoulos et al. (2023). In particular, accumulating evidence indicates that MYC is also crucial for improving the resilience to transcription stress in cancer cells by interacting with different protein complexes. Previous work proposed that clearance of stalled RNAPII is a critical step to prevent transcriptional and replicative stress (Herold et al., 2019). They showed that transcription is safeguarded by the MYCN- and USP11-dependent recruitment of BRCA1 in *MYCN*-amplified neuroblastoma cells. BRCA1 recruitment is indirect, as implied by proteomic analysis that showed no interaction between BRCA1 and MYCN (Buchel et al., 2017). The recruitment to chromatin can be induced by USP11 in a cell-cycle-dependent manner (Orthwein et al., 2015). Herold et al. (2019) claimed that the MYCN, BRCA1, and USP11 promote early transcriptional termination by favoring nascent RNA decapping of paused RNAPII (Herold et al., 2019). This allows the release of RNAPII enzymes from pause sites. To date, how USP11 is helping to recruit BRCA1 remained unclear.

The goal of this thesis was to understand the biology of USP11 in transcriptional regulation in greater detail. Turnover of MYC and MYCN is controlled by phosphorylation of two residues, Ser62 and Thr58 (Farrell & Sears, 2014; Li et al., 2017). Selecting two distinctly engineered cells, either expressing MYCN wt or MYCN T58A, to define the USP11 interactome was founded on the idea, that turnover of MYCN limits accumulation of MYCN, BRCA1, and USP11 (Herold et al., 2019) and thus hindering efficient pause release of RNAPII (Jaenicke et al., 2016).

In general, the USP11 interactome (chapter 2.1) yielded 370 proteins ($log_2FC \geq 1.00$, $p<0.05$, n=4) as USP11interacting proteins. From these datasets, 171 interactors were determined to be significantly enriched ($p<0.001$). Enriched proteins were involved in the gene ontologies proteasome, purine/pyrimidine metabolism, and RNA polymerase (cf. 2.1.2).
USP11 interacts with other E3 ligases, deubiquitinases and members of the ubiquitin proteasome system. The bona fide interacting protein USP7 ($log_2FC = 5.49$) was identified as a top hit in the interactome, supporting previous findings that significant amounts of USP11 protein are found in complexes with USP7 (Georges et al., 2018; Hein et al., 2015; Jin et al., 2022; Maertens et al., 2010; Perry et al., 2021; Sowa et al., 2009). DUBs can act cooperatively to stabilize and promote the activity of other proteins (Estavoyer et al., 2022). For example, USP7 and USP11 interact with and stabilize several components of the PRC1 complex (Maertens et al., 2010). Hetero- and homodimerization can add a layer of selectivity for deubiquitylation of substrates and also allows the fine-tuning of signaling events.
The interactome showed that USP11 interacts with distinct glutamine amidotransferases (e.g. PFAS, CAD, PPAT) that catalyze many reactions in purine and pyrimidine nucleotide synthesis. Interestingly, MYCN activates all these enzymes transcriptionally in neuroblastoma cells (T. Wang et al., 2018). This may imply an important role of USP11 together with MYCN in controlling nucleotide demand in rapidly dividing cells.
Finally, USP11 interacts with several subunits of RNA polymerases (RNAPI, RNAPII, RNAPIII) and a number of proteins playing a role in transcription regulation (like SPT6, IKBKAP1 (ELP1), MED16, GTF2F1, s. Table 26). While assaying chromatin binding of USP11 remained unsuccessful (section 2.1.4), immunoprecipitations and *in vitro* assays underpinned that RNAPII, USP7, and USP11 form a complex (cf. Figure 10, Figure 26). In addition, downregulation of USP11 led to a reduction in global chromatin association of RNAPII (cf. Figure 12). This data provide evidence that USP11 triggers a mechanism which impacts RNAPII chromatin occupancy. In general, proteolysis of stalled RNAPII at sites of DNA lesions is tightly controlled by both E3 ligases and DUBs (Fousteri & Mullenders, 2008; Harreman et al., 2009; He et al., 2014; Schwertman et al., 2012; van der Weegen et al., 2020). Reversing ubiquitination of subunits of transcribing RNAPII may regulate elongation rates (Saldi et al., 2016).

Notably, total proteomics in presence or absence of USP11 (cf. Figure 15) revealed a reduction of RPB8 (POLR2H) protein levels, but no significant changes of other polymerase subunits, upon downregulation of USP11. RPB8, an essential poymerase subunit (see Figure 16A-C) of all three RNA polymerases (Kwapisz et al., 2008), was also detected in the USP11 interactome. Interestingly, USP11 may antagonize the activity of the E3 ligase BRCA1, which can ubiquitylate RPB8 of RNAPII in response to DNA damage (Wu et al., 2007). This hypothesis could not be tested, since – apart from the USP11 knockdown- the proteomics were performed under unstressed conditions. This may also explain why downregulation of USP11 alone showed no effects in double strand break profiling (cf. Figure 13B). It could be possible that deubiquitylation of RPB1 is linked to BRE5-UBP3, which are recruited to nascent transcripts following RNA processing events during RNAPII stalling (Milligan et al., 2017). UBP3 can allow resumption of transcription elongation (Kvint et al., 2008).

The observations outlined above shed light on the broad spectrum of networks in which USP11 is involved. The associated mechanisms involving USP11 remain incompletely characterized and understood. As mentioned, there is a growing body of evidence that E3 ligases and DUBs have important roles in transcription surveillance and stress resilience in cancer.

3.2 Elongation factor TCEAL1 as a novel pro-transcriptional regulator

USP11 interacts with proteins that may be involved in transcription regulation. In the USP11 interactome we found the elongation factor TCEAL1, a protein which is so far not well studied but could be involved in transcription.

Validation experiments showed that this protein is strongly bound by USP11 (cf. Figure 9) and that vice versa TCEAL1 binds USP11 and other proteins of the transcription machinery (cf. Figure 24). Furthermore, TCEAL1 protein levels were rescued by MG-132 treatment upon depletion of USP11 (Figure 22).

To further elucidate the binding characteristics of the interplay between USP11 and TCEAL1, we used structural assays and model prediction analysis. Here, we could consistently define the region responsible for TCEAL1 binding within USP11 (cf. Figure 20, Figure 21). For USP11 was previously shown that -in addition to the N-terminal DU domain – the internal UBL2 domain may be involved in trafficking or substrate recruiting to the catalytic domain (Harper et al., 2014). Here we showed that UBL2+Insert domain is essential for interacting with USP7 and TCEAL1 (cf. Figure 20D). This is in accordance with earlier point mutagenesis studies within this domain by Georges et al. (2018). For TCEAL1 only the C-terminal region was predicted with high confidence (cf. Figure 34). Experiments with mutated TCEAL1 within this region showed that a structurally intact C-terminal HTH domain is required for the interaction with USP11 (cf. Figure 35A).

Deubiquitinases receive an additional layer of regulation by interacting partners, that are likely to be critical for their capacity target different substrates (Estavoyer et al., 2022). Indeed, USP11 immunoprecipitations in presence and absence of TCEAL1 convincingly established TCEAL1 as a scaffolding protein connecting USP11 to other proteins (cf. Figure 23B). MYCN activation enhanced these interactions, implying that USP11 mainly engages these interactions under MYCN-mediated stress situations.

TCEAL1 also interacts with USP11, USP7, and RNAPII (cf. Figure 24). *In vitro* assays additionally indicated that USP11, USP7 and TCEAL1 form a complex that includes members of the transcription machinery (cf. Figure 26). Cryo-EM studies failed to solve the transcription complex in detail (Figure 27). In fact, it cannot be ruled out that TCEAL1 requires its complex partners USP11, USP7, and others to form an elongation-related complex. These results hint at a novel complex in transcription regulation.

Basically, TCEAL1 is a member of the transcription factor elongating A-like family (Pillutla et al., 1999). This family comprises nine nuclear phosphoproteins, which share similarities to TFIIS

(Kettenberger et al., 2003). To date, TCEAL1 has not been reported to be involved in chromatin binding complexes. In this work TCEAL1 chromatin enrichment at the TSS, for individual MYCN promoter regions and genome wide (cf. Figure 28A/C), was visualized in neuroblastoma cells. Since the enrichment of TCEAL1 is within the region of the TSS, we wanted to specify in which step TECAL1 is involved in. To do so, the following questions were adressed to characterize TCEAL1 as a novel pro-transcriptional regulator:

i) At which transcription step does TCEAL1 come into play?

To study the chromatin binding behavior of TCEAL1 in transcription in greater detail, cells were treated with different cyclin-dependent kinase (CDK) inhibitors (Parua & Fisher, 2020). Strikingly, CKD9 inhibition led to promoter proximal accumulation of TCEAL1 (cf. Figure 28). Consistently, Olson et al. (2018) showed a comparable NVP-2 signature on RNAPII chromatin occupancy. Increased chromatin occupancy levels of TCEAL1 and RNAPII lacking elongation signals suggest a role for TCEAL1 in a promoter-proximal paused state. When the cells were treated with a CDK7 inhbitor (THZ1), the levels of TCEAL1 chromatin binding remained unchanged in comparison to the DMSO control. In contrast, THZ1 reduces RNAPII occupancy, both at promoters and gene bodies, globally (Kwiatkowski et al., 2014). For the chromatin behavior of RNAPII this is consistent, because CDK7 regulates RNAPII initiation and pausing whereas CDK9 regulates pause release leading to processive elongation (Egloff, 2021; Glover-Cutter et al., 2009; Gressel et al., 2017; Nilson et al., 2015; Sampathi et al., 2019). In comparison to the behavior of RNAPII on chromatin upon CDK7 and CDK9 inhibition, the findings argue for an involvement of TCEAL1 in transcriptional pause release rather than in transcription initiation.

ii) Is TCEAL1 critical for RNAPII-mediated transcription?

The assembly of a highly processive and fast transcriptional machinery is required, to ensure productive elongation (Jonkers & Lis, 2015; Steurer et al., 2018). Elongation factors significantly contribute to the transition from pausing to elongation. The USP11 interactome suggests the existence of an “environment” containing many stimulation factors, like TCEAL1, SPT6 (Narain et al., 2021) and TOP2B (Cowell et al., 2023), for productive transcription. Surprisingly, assaying RNAPII chromatin occupancy in absence of TCEAL1 showed a dramatic decrease on all expressed genes. Similar effects were observed in TFIIS-depleted cells with activated MYCN (Papadopoulos et al., 2022). A decrease of the elongating form of RNAPII was also observed albeit to a lesser extent. Although the RNAPII behavior upon TCEAL1 depletion differs from data after deprivation of elongation factors like SPT5 (Baluapuri et al., 2019) or PAF1c (Endres et al., 2021), the results presented here imply a fundamental role for TCEAL1 in early transcription. RNA-Sequencing upon TECAL1 depletion underpinned that TCEAL1 helps

MYCN to foster its gene signature and that some gene sets are differentially expressed (Figure 31).

iii) Does TCEAL1 participate in transcription termination by evicting stalled RNAPII together with USP11 and BRCA1?

Since USP11 is widely known as a stress resilience factor (see section 1.4.2), TCEAL1's scaffolding function for USP11 (cf. Figure 23) could point to the role of TCEAL1 in early transcription. BRCA1 recruitment to chromatin is USP11-dependent (Herold et al., 2019). In contrast, knockdown of TCEAL1 did not impair BRCA1 recruitment to chromatin in manual ChIP assays (cf. Figure 32), although, both, BRCA1 (Gorthi et al., 2018; Scully et al., 1997) and TCEAL1 (cf. Figure 28) recruitment at the pause site, are enhanced when RNAPII stalls. Interestingly, not all USP11 molecules in cells interact with TCEAL1 but almost all TCEAL1 molecules bind to USP11 in order to form a novel functional complex, mentioned earlier. This means that USP11 molecules which are TCEAL1-independent can recruit BRCA1. Then, BRCA1 will stabilize decapping complexes and suppress R-loop formation in promoter proximal regions (Hatchi et al., 2015; Hernandez et al., 2018). A possible downstream event is that USP11 requires TCEAL1 recruitment later (cf. Figure 23). When TCEAL1 binds chromatin and USP11, it enhances USP11's protein-protein-interactions with transcription complexes. Moreover, TCEAL1 recruitment may help USP11 counteracting or fine-tuning BRCA1 action to stabilize elongation complexes in MYCN-driven neuroblastoma (Herold et al., 2019).

These findings allow the hypothesis that the USP11-TCEAL1-USP7 complex formation could trigger another - not yet described -mechanism different from the coordination of the stress response by BRCA1 (Hatchi et al., 2015; Patel et al., 2023; Zhang, Chiang, et al., 2017) and USP11 (Herold et al., 2019; Jurga et al., 2021).

3.3 Antagonistic mechanisms of premature RNAPII termination

Functional transcription in cancer cells is determined by the fine-tuned regulation of RNAPII dynamics to ensure high levels of basal transcription (Bywater et al., 2013). TCEAL1 is a potential factor in tempering transcription stress in cancer cells - independently of regulating BRCA1 chromatin recruitment, as evidenced in Figure 32. In particular, we hypothesized that TCEAL1 is involved in TFIIS biology. At certain DNA sequences, RNAPII moves backwards and can arrest RNAPII-mediated transcription. RNAPII reactivation is induced by TFIIS, which is important for cell viability (Sigurdsson et al., 2010). This mechanism is involved in transcription through nucleosomes (Kim et al., 2010) and in promoter-proximal gene regulation (Adelman & Lis, 2012; Palangat et al., 2005). TFIIS has two conserved residues at the tip of domain III (D290, E291) that project through the side channel of RNAPII and interact with the polymerase active site that may catalyses the proton transfer during the cleavage reaction (Figure 45) (Cheung & Cramer, 2011).

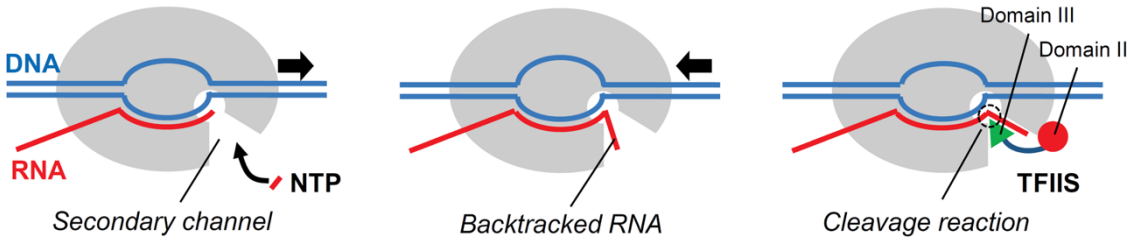

Figure 45: RNAPII elongation complex.

Scheme of the transcribing RNAPII (left panel), backtracked RNAPII (middle panel), and reactivation of RNAPII stimulated by TFIIS (right panel). The arrows (black) indicate the moving direction of RNAPII (grey). This figure was published in similar form by Eun et al. (2014).

TCEAL1 shares a sequence homology with domain II of TFIIS (see Figure 33). This sequence is part of a HTH domain in the C-terminus of TCEAL1 (cf. Figure 34). Indeed, it was possible to identify amino acids within this domain which are critical for chromatin recruitment (Aravind et al., 2005) in ChIP assays (cf. Figure 35A). However, it is likely that TCEAL1's enrichment on chromatin is not direct, but additionally mediated by other proteins. Co-IP assays with overexpressed HA-tagged TCEAL1 mutated in the "DEL" motif (D130-E131-L132) showed a reduced interaction with USP11 as well as RNAPII (cf. Figure 35B). These results argue that the "DEL" motif within the HTH domain is essential for instigating TCEAL1's role in transcription. Both TFIIS (Ghavi-Helm et al., 2008) and TCEAL1 (section 2.2.3) enriches at chromatin at the TSS. Interestingly, TCEAL1 and TFIIS share the majority of their bound promoters (cf. Figure 40). Moreover, our mechanistic studies clearly indicated that TCEAL1 depletion significantly increased TFIIS chromatin occupancy at selected promoter regions and genome-wide (cf. Figure 36). Vice versa overexpression of TCEAL1 resulted in reduced chromatin enrichment of TFIIS. Accordingly, TFIIS occupancy was restored when TCEAL1 mutants were overexpressed (cf.

Figure 38, Figure 39). It turned out that chromatin accumulating TFIIS binds to highly expressed genes of the MYC targets v2 and E2F targets signature, among others, when TCEAL1 levels are downregulated (cf. Figure 37). This may enhance stress at promoter regions in an oncogenic environment. Taken together, these findings strongly indicate that TCEAL1 competes with TFIIS for binding to chromatin.

The balance of TFIIS demand on chromatin is particularly relevant. The absence of intact TFIIS results in poly-ubiquitylation of RNAPII (Zatreanu et al., 2019) and that this fosters stress resolution due to rapid degradation of RNAPII instead of reactivation of backtracked elongation complexes. In this view, this degradation signaling could be controlled by recruitment of USP11 and TCEAL1, leading to RNAPII rapid pause release instead of backtracking. This fits to the emerging concept of preventing accumulation of transcription complexes promoter proximally (Baluapuri et al., 2019; Buchel et al., 2017; Herold et al., 2019). Under physiological conditions RNAPII-mediated transcription is per se a stressful process (Ishida & Kono, 2021). Oncogenic levels of MYC proteins drastically elevate the cellular stress (Murphy et al., 2008) which makes cancer cells dependent on mechansisms to relieve stress in order to maintain their oncogenicity. Finally, the aforementioned mechanisms to control TFIIS demand, may facilitate reinitiation of new transcription cycles and thus ensure productive transcription output.

The homology between TFIIS and TCEAL1 does not apply to the amino acid residues found in TFIIS, that stimulate endonucleolytic cleavage activity of RNAPII when RNAPII molecules backtrack. Consequently, RNA extension was affected by TFIIS but not by TCEAL1 (cf. Figure 41A/B/C). This suggests that TCEAL1 binding displaces TFIIS and thus blocks excessive backtracking while avoiding trapping of RNA (Cheung & Cramer, 2011; Wang et al., 2009). Furthermore, TFIIS association with active RNAPII in absence of TCEAL1 is significantly enhanced (cf. Figure 42), suggesting that TFIIS excessively stimulates the cleavage activity of RNAPII at promoter-proximal pause sites. Accordingly, RNAPII appears to backtrack more rapidly in presence of TFIIS (Galburt et al., 2007). RNAPII can recover from higher backtrack depth only when it is complemented with TFIIS (Lisica et al., 2016). Both, erratic stimulation of backtracking and RNA cleavage, needs to be buffered. Here, TCEAL1 could help balancing TFIIS activity. Intrinsic RNA cleavage generally occurs after backtracking by one position (Wang et al., 2009) and frays the 3'-terminal RNA nucleotide against a gating tyrosine residue (Sydow et al., 2009; Toulokhonov et al., 2007). The gating tyrosine demarcates the active site and delimits the extent of backtracking. TCEAL1 could delimit dwell time of RNAPII on highly transcribed promoters. Moreover, TCEAL1 could antagonize backtracking beyond the gating tyrosine by TFIIS and thus arresting of transcription complexes (Cheung & Cramer, 2011). Notably, other elongation factors, like

SPT5, are also known to be involved in balancing TFIIS activity in transcription (Ehara et al., 2017; Vos, Farnung, Urlaub, et al., 2018).

The data presented in this study revealed four major findings: i) USP11 is involved in transcription regulation, ii) the USP11 interacting protein TCEAL1 is a new pro-transcriptional factor in transcription regulation of MYCN-driven neuroblastoma cells, iii) TCEAL1 competes with TFIIS for chromatin binding and protects RNAPII pS5 from accumulation with TFIIS, and iv) USP11 stabilizes RPB8 and thus contributes to maintaining RNAPII integrity in early transcription. The findings are graphically summarized in Figure 46 (below).

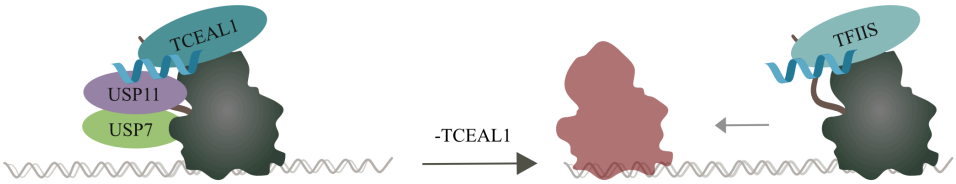

Figure 46: Model summarizing the findings of the study.
Model summarizing findings of the "competition"-mechanism mediated by the USP11-TCEAL1-USP7 complex.

Besides TFIIS, several other factors like CCR4-NOT (Dutta et al., 2015), ELL (Mourgues et al., 2013), DOT1L (Oksenych et al., 2013), and HIRA (Adam et al., 2013) have been identified as specifically engaged in transcription restart mechanisms at lesions or/and promoters. I propose that the ternary complex USP11-TCEAL1-USP7 competes with the restart stimulation mechanism by the elongation factor TFIIS on chromatin. Here, I claim that in early transcription, premature recruitment of TFIIS to promoters has to be controlled by TCEAL1. As a consequence, TCEAL1 most likely provides an alternative for adverse backtrack stimulation by RNAPII (Landick, 2009). In contrast, it is possible that the complex primes backtracked RNAPII for efficient premature termination events (Papadopoulos et al., 2022). Furthermore, TCEAL1, together with USP11, stabilizes the RNAPII subunit RPB8 to enable immediate transcriptional resumption (Li et al., 2022). The latter observation would favor a restart more than a reinitiation mechanism. Taken together, this ternary complex gives MYCN-driven neuroblastoma cells an additional option to reduce transcription stress through the tight control of TFIIS activity (Midha et al., 2023).

3.4 Implications for oncogenic transcription and therapy

The primary function of MYC proteins is most probably not to regulate gene expression but to cope with the threats to genomic integrity that arise from an increased transcription rate. The work presented here proposes a novel mechanism induced by the USP11-TCEAL1-USP7 complex to relieve transcription stress in order to safeguard efficient RNAPII-mediated transcription elongation in cancer cells.

In this study the knockdown of USP11 as well as of TCEAL1 had only a moderate phenotypical effect in neuroblastoma cells. A reason for this observation could be that both proteins are redundant. The USP11 paralogs USP4 and USP15 have a high level of sequence and structure similarity (Vlasschaert et al., 2015). Since proteomic data showed that USP4 also interacts with TCEAL1 (Huttlin et al., 2021), it might be that the USP4-TCEAL1 complex has a similar function. On the other side, the TCEAL protein family comprises nine nuclear phosphoproteins (Pillutla et al., 1999). Blast analysis revealed that TCEAL1 shares sequence similarity with TCEAL7, TCEAL8, and TCEAL9. Therefore, it could be that those proteins have a comparable function.

The work presented here shows that TCEAL1 is an important factor in transcription regulation. Although TCEAL proteins are non-essential in cancer cells (DepMap), they provide a putative target for therapeutic approaches because of their molecular functions in cancers (Sun & Zhao, 2022). To date, there are few studies describing TCEAL family members in cancer. Interestingly, expression analysis from prostate cancer cells lacking androgen stimulus led to a significant increase in the expression of TCEAL gene family members upon downregulation of TFIIS (personal communication, S. Herold, AG Eilers). In absence of TFIIS the MYC signature in prostate cancer cells was decreased. TCEAL proteins could aid MYC-driven disruption of the AR gene expression program (Qiu et al., 2022). Moreover, silencing of TCEAL1 enhanced the response to docetaxel in human prostate cancer cells (Rushworth et al., 2020). The moderate survival benefits in metastatic prostate cancer from using taxanes in chemotherapy could be improved by targeting TCEAL1-mediated mechanism(s) (de Bono et al., 2010; James et al., 2016). Additionally, TCEAL1 could be of peculiar interest, because mitoxantrone, targeting USP11 (Burkhart et al., 2013), improves overall survival of advanced prostate cancer after docetaxel-based therapy (de Bono et al., 2010). Another study in glioblastoma multiforme demonstrated, that TCEAL family proteins possess great potential as therapeutic targets (Aisa et al., 2022). The available data suggest that altered expression of TCEAL genes may be important for cancer cells (cf. Figure 44) and that future studies could help to understand their role in transcription regulation and their therapeutic intervention in disease.

In summary, these findings present a better understanding of how the ternary complex USP11-TCEAL1-USP7 protects processive transcription by RNAPII. TCEAL1 enforce the optimal balance between speed and accuracy achieved by adjusting TFIIS accumulation at pause sites. The findings emphasize an important mechanistic role of USP11 and TCEAL1 in MYCN-amplified neuroblastoma.

4 Materials

4.1 Software

Table 2: Software.

Software	Source
Acrobat Reader	Adobe Inc.
Affinity Designer	Serif
AlphaFold-Multimer tool v1.0	DeepMind
ApE plasmid editor	M. Wayme Davis
bedtools genomecov v2.26.0	Quinlan and Hall (2010)
Bowtie v2.3.5.1	Langmead and Salzberg (2012)
DeepTools v3.5.1	Ramirez et al. (2016)
EndNote v20.6	Clarivate Analytics
EnrichR	Chen et al. (2013); Kuleshov et al. (2016); Xie et al. (2021)
FASTQ v1.0.0	Illumina
FASTQC v0.11.09	Illumina
FileZilla v3.65.0	Tim Kosse
Galaxy	Galaxy
GraphPad Prism v9.0	GraphPad Software Inc.
Harmony High Content Imaging and Analysis Software	Perkin Elmer
ImageJ	By Wayne Rasband
Integrated Genome Browser	Freese et al. (2016), Nicol et al. (2009)
Microsoft Office	Microsoft
Multi Gauge	Fujifilm Global
Multiscan Ascent	Thermo Labsystems
NanoDrop 1000	Thermo Fisher Scientific
ngs.plot.r v2.41.3	Shen et al. (2014)
PyMOLv 2.5.5	DeLano Scientific LLC, Schröder Inc.
R version 3.6.3	The R Foundation
SAMtools v1.9	Danecek et al. (2021)
Sequel Pro	sequelpro.com
StepOne software v6.1.2	Applied Biosystem
TIBCO Spotfire® Analytics	TIBCO Software Inc.
UCSC Genome Bioinformatics	http:/genome.ucsc.edu

4.2 Equipment

Table 3: Equipment.

Equipment	Manufacturer
5200 Fragment Analyzer	Agilent
BBD 6220	Heraeus
BD FACS Aria III	BD Biosciences
C1000 Thermal cycler	Bio-Rad
Casy® cell counter	Innovatis
Digital Sonifier W-250 D	Branson
Dry Bath System	Starlab
Eppendorf 5417R	Eppendorf
Eppendorf 5425	Eppendorf
Eppendorf 5430	Eppendorf
G-25	New Brunswick Scientific
Galaxy MiniStar	VWR
LAS-4000 mini	Fujifilm
M220	Covaris
Mastercycler pro S	Eppendorf
Mini-PROTEAN® Vertical Electrophoresis System	Bio-Rad
Multifuge 1S-R	Heraeus
NanoDrop 1000	Thermo Fisher Scientific
NextSeq 500	Illumina
Operetta CLS High Content Imaging System	Perkin Elmer
Operetta High Content Imaging System	Perkin Elmer
PerfectBlue™ Tank Electro Blotter Web™ S	Peqlab
PowerPac™ HC	Bio-Rad
SP2	Leica
StepOne plus	Applied Biosystem
Ultrospec™ 3100 pro	Amersham Biosciences
Vortex-Genie	Scientific Industries
Water bath	Julabo

4.3 Consumables

Consumables for cell culture and wet lab were purchased from Applied Biosystems, B. Braun, Bemis, Eppendorf, GL Sciences, Greiner, Hartenstein, Merck, Millipore, Nunc, Roth, Sarstedt, Schleicher, Schott, Thermo Scientific and VWR.

4.4 Chemicals

Table 4: Inhibitors.

Inhibitor	Company	Stock	Final
4-Hydroxytamoxifen	Sigma	1 mM in EtOH	200 nM
Doxycycline	Sigma-Aldrich	1 mg/ml	1 µg/ml
Etoposide	Sigma-Aldrich	50 mM in DMSO	25 µM
Flavopiridol	Sigma-Aldrich	1 µM	100 nM
MG-132	Calbiochem/Merck	-	20 µM
NVP-2	Tocris/Bio-Techne	10 mM in DMSO	1 µM
Protease inhibitor cocktail I	Sigma-Aldrich	-	-
Protease inhibitor cocktail II	Sigma-Aldrich	-	-
Protease inhibitor cocktail III	Sigma-Aldrich	-	-
THZ1 Hydrochloride	MedChem	-	200 nM

Table 5: Reagents.

Reagent	Company
Agencourt AMPure XP beads	Beckman Coulter
AsiSI	NEB
Benzonase nuclease purity >99% 25U/µl	Merck Millipore
Blasticidin	Invivogen
CutSmart® Buffer	NEB
Dithiothreitol (DTT)	Invitrogen
DNA marker Gene Ruler 1 kb Plus DNA	Thermo Fisher
Dynabeads Protein A	Thermo Fisher
Dynabeads Protein G	Thermo Fisher
Ethidium Bromide (EtBr)	Roth
GlycoBlue Coprecipitant	Life Technologies
HiMark pre-stained HMW STD	Thermo Fisher
Hoechst 33342	Sigma-Aldrich
Hygromycin B Gold solution	Invivogen
Immbilon Western HRP Substrate	Millipore
InstantBlue™ Safe Coomassie Stain	Sigma-Aldrich
Lipofectamine RNAiMAX Transfeciton Reagent	Thermo Fisher
Opti-MEM	Thermo Fisher
PageRuler™ Prestained Protein Ladder	Thermo Fisher
Penicillin-Streptomycin	Sigma-Aldrich
Phenol/Chlorofrom mixture	Invitrogen
Proteinase K	Roth

Reagent	Company
Puromycin	Invivogen
Quant-iT Pico Green	Thermo Fisher
RNase A	Roth
SPRI select reagent	Beckman Coulter
T4 DNA ligase, concentrated	NEB
T4 RNA ligase 2, truncated	NEB

4.5 Commercial kits

Table 6: Commercial kits.

Kit	Company
Colloidal Blue Staining Kit	Life Technologies
DuoLink In Situ Detection Reagents	Sigma-Aldrich
Duolink In Situ PLA Probe Anti-Mouse MINUS, Affinity purified Donkey anti-Mouse IgG (H+L)	Sigma-Aldrich
Duolink In Situ PLA Probe Anti-Rabbit PLUS, Affinity purified Donkey anti-Rabbit IgG (H+L)	Sigma-Aldrich
DuoLink In Situ Wash Buffers, Fluorescence	Sigma-Aldrich
GeneJET Gel Extraction Kit	Thermo Fisher
MAXIprep	Invitrogen
MEGAscript T7 Transcription Kit	Thermo Fisher
NEBNext Poly (A) mRNA Magnetic Isolation Kit	NEB
NEBNext Poly (A) mRNA Magnetic Isolation Kit	NEB
NEBNext Ultra II DNA Library Prep	NEB
NGS Fragment High Sensitivity Analysis Kit, 1-6,000 bp	Agilent
PowerUp™ SYBR® Green Master Mix	Thermo Fisher
QIAquick® Gel Purification Kit	Qiagen
QIAquick® PCR Purification Kit	Qiagen
Quant-iT™ PicoGreen dsDNA Assay Kit	Thermo Fisher
RNeasy Mini Kit	Qiagen
SuperScript III Reverse Transcriptase kit	Thermo Fisher

4.6 Solutions and buffers

All solutions and buffers were prepared in ddH_2O.

Table 7: Solutions and buffers.

Name	Composition
Ampicillin stock solution	10 g ampicillin (solubilized)/ 100 ml ddH_2O, sterile filtered
BCA buffer A	1% BCA-Na_2
	2% Na_2CO_3 x ddH_2O
BCA buffer B	4% $CuSO_4$ x 5 ddH_2O
	0.16% Na-tartrate
	0.4% NaOH
	0.95% $NaHCO_3$
Bis-Tris (3.5x)	1.25 M Bis-Tris
Bis-Tris separation gel	8-12% (v/v) acrylamide/bisacrylamide
	1X Bis-Tris
	0.03% (v/v) APS
	0.05% (v/v) TEMED
Bis-Tris stacking gel	4% (v/v) acrylamide/bisacrylamide
	1X Bis-Tris
	0.03% (v/v) APS
	0.05% (v/v) TEMED
Blocking solution for PVDF membrane	5% (w/v) milk powder in TBS-T
ChIP elution buffer	1% (v/v) SDS
	0.1 M $NaHCO_3$
	prepared in aqua dest
ChIP lysis buffer I	125 mM PIPES pH 8.0
	85 mM KCl
	0.5% (v/v) NP40
	Protease inhibitor cocktail (1:1000, freshly added)
ChIP lysis buffer II	50 mM HEPES pH 7.9
	140 mM NaCl
	1 mM EDTA
	1% (v/v) Triton X-100
	0.1% (w/v) deoxycholic acid
	sodium salt
	0.1% (v/v) SDS
	Protease inhibitor cocktail (1:1000, freshly added)

Name	Composition
ChIP wash buffer I	20 mM Tris HCl pH 8.1
	150 mM NaCl
	2 mM EDTA
	0.1% (v/v) SDS
	1% (v/v) Triton X-100
ChIP wash buffer II	20 mM Tris HCl pH 8.1
	500 mM NaCl
	2 mM EDTA
	0.1% (v/v) SDS
	1% (v/v) Triton X-100
ChIP wash buffer III	10 mM Tris HCl pH 8.1
	250 mM LiCl
	1 mM EDTA
	1% (v/v) NP-40
	1% (v/v) deoxycholic acid sodium salt
Coomassie destain	20% (v/v) methanol
	10% (v/v) acetic acid
Coomassie solution	50% (v/v) methanol
	10% (v/v) acetic acid
	0.5% Coomassie Brilliant Blue R-250
Crystal violet solution	125 % (w/v) crystal violet
	20% (v/v) ethanol
EDTA	0.5 M EDTA
	adjusted to pH 8.0 using 10 M NaOH
HEPES lysis buffer for benzonase treatment	20 mM HEPES pH 7.9
	150 mM NaCl
	0.2% (v/v) NP-40
	0.5 mM EDTA
	10% (v/v) Glycerol
	2 mM $MgCl_2$
	50 U/ml Benzonase (freshly added)
	Protease inhibitor cocktail (1:1000, freshly added)
Laemmli Buffer 6X	12% (w/v) SDS
	60‰ (w/v) bromphenol blue
	47% (v/v) glycerol
	60 mM Tris/HCl pH 6.8
	9.3% (w/v) DTT
Miniprep lysis buffer	0.2 M NaOH
	1% SDS

Name	Composition
Miniprep precipitation buffer	3 M KOAc, pH 5.2
Miniprep resuspension buffer	TE with Rnase A (1:100, freshly added)
modified RIPA buffer	50 mM HEPES pH 7.5
	150 mM NaCl
	1 mM EDTA
	1% NP-40
	0.1 % Sodium deoxycholate
	Protease inhibitor cocktail (1:1000, freshly added)
MOPS running buffer	1 M MOPS
(20X)	1 M Tris
	20 mM EDTA
	2% SDS
MOPS running buffer	1X MOPS running buffer
(ready to use)	5 mM sodium bisulfite
NuPAGE transfer buffer (20X)	500 mM Bis-Tris
	500 mM Bicine
	20.5 mM EDTA
	0.1 mM chlorobutanol
NuPAGE transfer buffer (ready to use)	1X NuPAGE transfer buffer
	20% MeOH
PBS	137 mM NaCl
	2.7 mM KCl
	10.1 mM Na_2HPO_4
	1.76 mM KH_2PO_4
	autoclaved
Polytethylenimin	0.09% PEI
	6 mM HCl
	sterile filtered
Proteinase K	10 mg/ml in ddH_2O
RIPA lysis buffer	50 mM HEPES pH 7.9
	140 mM NaCl
	1 mM EDTA
	1% Triton X-100
	0.1% Sodium deoxycholate
	0.1% SDS
	Protease inhibitor cocktail (1:1000, freshly added)
RNase A	10 mg/ml in ddH_2O
TBS-T	1X TBS
	0.2% Tween-20

Name	Composition
TE	10 mM Tris pH 7.4
	1 mM EDTA pH 8.0
Trypsin solution	0.25% trypsin
	5 mM EDTA
	22.3 mM Tris pH 7.4
	125 mM NaCl
Washing solution for Dynabeads	5 mg/ml BSA in PBS

4.7 Nucleic acids

RNA interference (RNAi)

In this work were used two types of RNAi applications. For knock down gene expression of genes of interest by small hairpin RNA (shRNA), in Table 8 the target gene sequences are shown (Fellmann et al., 2013).

Table 8: miR-E shRNA targets.

Target gene	shRNA	Target sequence
USP11	#1	TCACCGAGTACTTCCTCAACAA
	#2	GAAGCGTTACTATGACGAGGTA
TCEAL1	#1	ACAGTGGTTGTGTGGTAAGATA
	#2	GAGGCTTTATTTTAGATGTTTA

Moreover, ON-TARGETplus human small interfering RNA (siRNA) SMARTpools (by Dharmacon™) against POLR2H (RPB8) were used for gene silencing by Lipofectamine RNAiMAX transfection (5.1.2).

gBlocks™

For this study gBlocks™ Gene Fragments in tubes were used, which are double-stranded DNA fragments of 500-3000 bps in length ready for cloning (IDT). Usually, the gBlocks™ design was RB-RE1-tag-Linker-cDNA-RE2-RB (RB: random bases, RE: restriction site). The following Table 9 shows an overview about the gBlocks in use.

Table 9: gBlock gene fragment designs.

Product	cDNA (Ensembl database)	Design
gBlock gene fragment	*TCEAL1* (human) *ENSG00000172465*	HA-TCEAL1

Plasmids

Table 10: Plasmids.

Name	Use	Description
pLT3GEPIR	RNAi (shRNA)	pRRL vector backbone expressing Tet-ON miR-E based RNAi
pRRLSin.cPPT.SFFV-IRES-GFP.WPRE	overexpression	Lentiviral expression vector, SFFV promoter, fluorescence marker GFP
pRRLSin.cPPT.SFFV-IRES-Tomato.WPRE	overexpression	Lentiviral expression vector, SFFV promoter, fluorescence marker dTomato
psPAX.2	lentiviral production	plasmid encoding virion packaging system
pMD2G	lentiviral production	plasmid encoding virion envelope

Primer for ChIP qPCR

Table 11: ChIP-qPCR primers.

Gene	Forward	Reverse
GBA	AGCCCTTCCTCAAGTCTCAT	ACTGTGGGAATTCAATCGCC
RPL5	TTTTCTTGCCCGTATGCCAG	CGCACTCAGGCTGTCTACTA
DRG2	CGTGGGCCAGTACAGCAT	CCGGAAGCCAAAGAGAACAG
EIF3B	CTGAACCACTGTGAAAGCCC	TCGCCTACTGACTGAGCAAA
NPM1	TTCACCGGGAAGCATGG	CACGCGAGGTAAGTCTACG
RPS16	CCGAGCGTGGACTAGACAA	GTTAGCCGCAACAGAAGCC
TFAP4	CCGGGCGCTGTTTACTA	CAGGACACGGAGAACTACAG
ACTB	GAGGGGAGAGGGGGTAAA	AGCCATAAAAGGCAACTTTCG
IRF2BP2	GTTCATGAGCGGCACCAG	CCTCGGCTCTGACTTCGG
RAN	CAAGGTGGCTGAAACGGAAA	GTTCATGAGCGGCACCAG
TAF4B	AAGGTCGTCGCTCACAC	GCGTGGCTATATAAACATGGCT
PTPN23	CCAGTCTCCGGTCAGTGATT	CGTATTGTCAAGAGCCGTGG
PLD6	TGTGGGTCCCGGATTAG	CTCCAGAGTCAGAGCCA
NME1	GGGGTGGAGAGAAGAAAGCA	TGGGAGTAGGCAGTCATTCT
Intergenic region_1	TTTTCTCACATTGCCCCTGT	TCAATGCTGTACCAGGCAAA
intergenic region_2	GCAGTTCAACCTACAAGCCAA-TAGAC	CACAAATTAGCGCATTGCCTGA

NEBNext® Multiplex Oligos for Illumina®

The following table shows the list of index primers which were used for producing barcode libraries with NEBNext® Ultra™ II DNA Library Prep Kit for Illumina®:

Table 12: NEBNext® Multiplex Oligos for Illumina®.

Index Primer (cat. number)	Application	Sequence
i501 *(#E7603A)*	barcoding NEBNext library	5′-AATGATACGGCGACCACCGAGATCTACAC-TATAGCCTACACTCTTTCCCTACACGAC-GCTCTTCCGATC*T-3′
i502 *(#E7604A)*	barcoding NEBNext library	5′-AATGATACGGCGACCACCGA-GATCTACACATAGAGGCACAC-TCTTTCCCTACACGACGCTCTTCCGATC*T-3′
i503 *(#E7605A)*	barcoding NEBNext library	5′-AATGATACGGCGACCACCGA-GATCTACACCCTATCCTACACTCTTTCCCTACAC-GACGCTCTTCCGATC*T-3′
i504 *(#E7606A)*	barcoding NEBNext library	5′-AATGATACGGCGACCACCGAGATCTACAC-GGCTCTGAACACTCTTTCCCTACACGAC-GCTCTTCCGATC*T-3′
i505 *(#E7607A)*	barcoding NEBNext library	5′-AATGATACGGCGACCACCGA-GATCTACACAGGCGAAGACAC-TCTTTCCCTACACGACGCTCTTCCGATC*T-3′
i506 *(#E7608A)*	barcoding NEBNext library	5′-AATGATACGGCGACCACCGAGATCTACAC-TAATCTTAACACTCTTTCCCTACACGAC-GCTCTTCCGATC*T-3′
i507 *(#E7609A)*	barcoding NEBNext library	5′-AATGATACGGCGACCACCGAGATCTACAC-CAGGACGTACACTCTTTCCCTACACGAC-GCTCTTCCGATC*T-3′
i508 *(#E7610A)*	barcoding NEBNext library	5′-AATGATACGGCGACCACCGAGATCTACAC-GTACTGACACACTCTTTCCCTACACGAC-GCTCTTCCGATC*T-3′
i701 *(#E7611A)*	barcoding NEBNext library	5′-CAAGCAGAAGACGGCATACGAGATCGAG-TAATGTGACTGGAGTTCAGAC-GTGTGCTCTTCCGATC*T-3′
i702 *(#E7612A)*	barcoding NEBNext library	5′-CAAGCAGAAGACGGCATACGAGATTCTCCG-GAGTGACTGGAGTTCAGAC-GTGTGCTCTTCCGATC*T-3′
i703 *(#E7613A)*	barcoding NEBNext library	5′-CAAGCAGAAGACGGCATACGAGA-TAATGAGCGGTGACTGGAGTTCAGAC-GTGTGCTCTTCCGATC*T-3′
i704 *(#E7614A)*	barcoding NEBNext library	5′-CAAGCAGAAGACGGCATACGA-GATGGAATCTCGTGACTGGAGTTCAGAC-GTGTGCTCTTCCGATC*T-3′

Index Primer (cat. number)	Application	Sequence
i705	barcoding	5´-CAAGCAGAAGACGGCATACGAGAT-
(#E7615A)	NEBNext library	TTCTGAATGTGACTGGAGTTCAGAC-
		GTGTGCTCTTCCGATC*T-3´
i706	barcoding	5´-CAAGCAGAAGACGGCATACGAGATAC-
(#E7616A)	NEBNext library	GAATTCGTGACTGGAGTTCAGAC-
		GTGTGCTCTTCCGATC*T-3´
i707	barcoding	5´-CAAGCAGAAGACGGCATACGAGA-
(#E7617A)	NEBNext library	TAGCTTCAGGTGACTGGAGTTCAGAC-
		GTGTGCTCTTCCGATC*T-3´
i708	barcoding	5´-CAAGCAGAAGACGGCATACGAGATGCG-
(#E7618A)	NEBNext library	CATTAGTGACTGGAGTTCAGAC-
		GTGTGCTCTTCCGATC*T-3´
i709	barcoding	5´-CAAGCAGAAGACGGCATACGA-
(#E7619A)	NEBNext library	GATCATAGCCGGTGACTGGAGTTCAGAC-
		GTGTGCTCTTCCGATC*T-3´
i710	barcoding	5´-CAAGCAGAAGACGGCATACGAGATTTCGCG-
(#E7620A)	NEBNext library	GAGTGACTGGAGTTCAGAC-
		GTGTGCTCTTCCGATC*T-3´
i711	barcoding	5´-CAAGCAGAAGACGGCATACGAGATGCGCGA-
(#E7621A)	NEBNext library	GAGTGACTGGAGTTCAGAC-
		GTGTGCTCTTCCGATC*T-3´
i712	barcoding	5´-CAAGCAGAAGACGGCATACGA-
(#E7622A)	NEBNext library	GATCTATCGCTGTGACTGGAGTTCAGAC-
		GTGTGCTCTTCCGATC*T-3´

4.8 Antibodies

Table 13: Antibodies.

Antibody	Catalogue number	Manufacturer
rabbit polyclonal USP11	Cat# A301-613A, RRID: AB_1211380	Bethyl
rabbit polyclonal USP11	Cat# HPA003103, RRID: AB_10671088	Sigma-Aldrich
rabbit polyclonal USP7	Cat# A300-033A, RRID: AB_203276	Bethyl
mouse monoclonal TCEAL1	Cat# sc-393621, RRID: N/A	Santa Cruz Biotechnology
mouse monoclonal Pol II (8WG16)	Cat# sc-56767, RRID: AB_785522	Santa Cruz Biotechnology
mouse monoclonal Pol II (A-10)	Cat# sc-17798, RRID: AB_677355	Santa Cruz Biotechnology
mouse monoclonal Pol II (F-12)	Cat# sc-55492,	Santa Cruz Biotechnology

Antibody	Catalogue number	Manufacturer
	RRID: AB_630203	
mouse monoclonal pS5 RNAPII	Cat# 904001, RRID: AB_2565036	BioLegend
rabbit polyclonal pS2/9 RNAPII	Cat# ab5095, RRID: AB_304749	Abcam
monoclonal mouse POLR2B (E-12)	Cat# sc-166803, RRID: AB_2167499	Santa Cruz Biotechnology
rabbit polyclonal RPB3	Cat# A303-771A, RRID: N/A	Bethyl
rabbit polyclonal POLR2H	Cat# LS-C346152, RRID: N/A	LS Bio
rabbit polyclonal SPT6	Cat# NB100-2582, RRID: N/A	Novus Biologicals
rabbit monoclonal TCEA1	Cat# ab185947, RRID: N/A	Abcam
rabbit polyclonal BRCA1	Cat# A300-000A, RRID: AB_67367	Bethyl
rabbit polyclonal HA tag	Cat# ab9110, RRID: AB_307019	Abcam
monoclonal mouse FLAG tag (M2)	Cat# F3165, RRID: AB_259529	Merck
mouse monoclonal N-Myc (B8.4.B)	Cat# sc-53993, RRID: AB_831602	Santa Cruz Biotechnology
rabbit monoclonal cMYC (Y69)	Cat# ab32072, RRID: AB_731658	Abcam
monoclonal mouse ß-Actin	Cat# A5441, RRID: AB_476744	Sigma-Aldrich
rabbit monoclonal GAPDH (14C10)	Cat# 2118, RRID: AB_561053	Cell Signaling
mouse monoclonal Vinculin	Cat# V9131, RRID: AB_477629	Sigma-Aldrich
Goat Anti-Rabbit IgG (H+L), Cross-adsorbed Antibody, Alexa Fluor™ 647, Conjugated	Cat# A-21244, RRID: AB_2535812	Thermo Fisher Scientific
Goat Anti-Mouse IgG (H+L), Cross-adsorbed Antibody, Alexa Fluor™ 647, Conjugated	Cat# A-21235, RRID: AB_2535804	Thermo Fisher Scientific
Mouse monoclonal TrueBlot ULTRA:	Cat# 18-8817-31, RRID: AB_2610850,	Rockland
Rabbit monoclonal TrueBlot: Anti-Rabbit	Cat# 18-8816-31, RRID: AB_2610847,	Rockland
Sheep Anti-Mouse IgG - Horseradish	Cat# NA931, RRID: AB_772210,	GE Healthcare
Donkey Anti-Rabbit IgG, Whole Ab ECL	Cat# NA934, RRID: AB_772206,	GE Healthcare
Murine IgG Control Antibody, Unconjugated	Cat# I5381, RRID: AB_1163670	Sigma-Aldrich
Rabbit IgG Control Antibody, Unconjugated	Cat# I5006, RRID: AB_1163659	Sigma-Aldrich

4.9 Cell lines and bacteria strains

Table 14: Eukaryotic cell lines.

Cell line	Species	Disease/origin	Source	Medium
SH-EP	hs	Neuroblastoma cells	Manfred Schwab	RPMI
IMR-5	hs	Neuroblastoma cells, *MYCN*-amplified	Angelika Eggert	RPMI
HEK293T	hs	embryonic kidney cells	ATCC	DMEM
HeLa	hs	cervix carcinoma cells	JHH	DMEM
NIH-3T3	mm	murine embryonic fibroblasts	ATCC	DMEM

hs: homo sapiens; mm: mus musculus

Table 15: Bacterial strain.

Name	Description
XL1 blue	*E. coli*, genotype: recA1, gyrA96, thi-1, hsdR17, supE44, relA1 lac [F´proAB lacIqZΔM15 Tn10 (Tetr)]

4.10 Media and supplements

bacteria strains cultivation

For bacterial cell cultivation was used LB medium (Table 16).

Table 16: Medium for bacterial strain cultivation.

Medium	Composition
Lysogeny broth (LB)	10% (w/v) bacto tryptone, 0.5% (w/v) yeast extract, 1% (w/v) NaCl for agar plates LB medium was supplementend with 1.2% (w/v) bacto-agar (autoclaved)

For selection of successfully transformed bacteria were added antibiotics (100 µg/ml ampicillin or 100 µg/ml carbenicillin) to the medium (Table 16).

mammalian cell culture

For cultivation of eukaryotic cells were used either RPMI or DMEM media with different supplementation (Table 17).

Table 17: mammalian cell culture medium.

Medium	Composition
RPMI-1640 (complete)	RPMI-1640 (Thermo), 10% (v/v) heat-inactivated FCS, 1% (v/v) Penicillin/Streptomycin
SILAC medium, light	RPMI with substituted L-Lysine^{0}/L-Arginine^{0}
SILAC medium, heavy	RPMI with substituted L-Lysine^{8}/L-Arginine^{10}
DMEM (complete)	DMEM 10% (v/v) heat-inactivated FCS, 1% (v/v) Penicillin/Streptomycin
transfection medium	DMEM 2% (v/v) heat-inactivated FCS
OptiMEM	-
Freezing medium	70% RPMI or DMEM (complete) 20 % FCS 10 % DMSO

To passage adherent cells (see 5.1.1), Trypsin/EDTA (0.25% Trypsin, 5 mM EDTA, 22.3 mM Tris (pH 7.4), 125 mM NaCl) was added for cell dissociation. Further, depending on experimental setups inhibitors and supplements, which are listed in chapter 4.4, were added to the mammalian cell culture medium.

5 Methods

5.1 Cell biology methods

5.1.1 Cultivation of eukaryotic cell lines

Cultivation

All eukaryotic cell lines (for further details see chapter 4.9) in use were cultured in standard medium (either RPMI or DMEM) supplemented with 10% FBS and 1% pencillin/streptomycin in a cell incubator (37°C, 5% CO_2, 95% humidity).

Passaging

The adherent eukaryotic cells were passaged by removing the medium, washing once with PBS (RT) and trypsinizing until the cells detached from the plate. The trypsinization was stopped by adding serum containing medium. Hereafter, the cell suspension was centrifuged for 5 min at 1,500 rpm and resuspended again in complete medium to get rid of residual Trypsin/EDTA. The cells were either counted by CASY® cell counter if a specific number of cells was required for distributing and/or split in a new plate for incubation.

Freezing

Upon trypsinzing and centrifuging the cells, they were resuspended in freezing medium (80% medium + 20% FBS+ 10% DMSO). The cell suspension was transferred to cryo tubes which were placed in a Mr. Frosty™ container (freezing 1°C/min) and shortly stored at -80°C. After slow-freezing the cells, they were put into a liquid nitrogen tank for long-term storage.

Thawing

Frozen cell stored in liquid nitrogen were quickly thawed by resuspending in ten times volume of standard medium. To get rid of residual traces of DMSO, the resuspended cells were centrifuged for 5 min at 1,500 rpm at RT and the pellet subsequently resuspended again in fresh medium. Then the cells were subjected to seeding for cultivation.

5.1.2 Cell transfection

Transfection is the process of introducing nucleic acids into eukaryotic cells by non-viral methods. In this work were used chemical methods for gene transfer by using the reagents Lipofectamine 2000 or polyethilenimine (PEI). The cells were seeded with a specific density one day before the transfection started. The medium was exchanged with medium w/o pencillin/streptomycin (usually 5 ml/plate) before the transfection mix was added. First, two reaction tubes were prepared containing 250-500 µl Opti-MEM medium. Second, one tube was mixed dropwise with Lipofectamine RNAiMAX (10 µl) or PEI (≤ 30 µl) and the other tube with appropriate amount of siRNA (20 nM diluted in siRNA buffer) or plasmid DNA (≤ 15 µg). Following this, the two mixes were incubated for 5 min at RT. Third, the two tubes were combined dropwise and incubated for another 20 min at RT. Fourth, the transfection mix was added to the plate dropwise by

turning around the plate in a circle. Between 4h and 12h post-transfection the medium was removed and fresh medium (full) was added.

5.1.3 Lentiviral work

For lentivirus production 5*10^6 HEK 293TN cells were seeded 24 h before PEI transfection of DNA of virus components (as described in 5.1.2). To produce lentivirus there were needed different plasmids: first, 2.8 µg of the packaging vector psPAX2; second, 1.4 µg of the envelope vector pMD2.G and 11.1 µg of a lentiviral expression vector (e.g. pWZL, pLEGO, pRRL, pLT3GEPIR). The medium was changed to 5 ml fresh medium after 8-12 h incubation (S2 cell incubator) upon PEI transfection. The supernatant containing the virus was collected and pooled after 24 h, 48 h and optionally after 72h post-transfection. After the last harvesting time point the virus was filtered with 0.45 µm filter using a syringe and stored in 2 ml aliquots at -80°C until using for infection.

Lentiviral infection was performed with cultivated cells on Ø10 cm plates. Therefore, a mixture of 3 ml full medium, 2 ml filtered lentiviral supernatant and 5 µl polybrene (stock 4µg/ml) was added upon removing culture medium off the plates. 24h after infection, either a second infection of 24 h was performed or the cells were subjected to selection.

The expression vectors in use contained either a fluorescence or an antibiotic resistance marker to select infected cells either by FACS sorting or antibiotic agents. SH-EP dTomato cells were sorted based on dTomato signal with the BD FACS Aria III. To monitor a successful selection, a control plate with uninfected cells was used during selection.

5.1.4 Crystal Violet staining

The crystal violet assay stains cell that are attached to cell culture plates, whereas it relies on the detachment of adherent cells from cell culture plates during cell death. Before the cells were subjected to staining, cells grown in a 6-well format were fixed with 4% PFA and incubated for 10 min at RT on an orbital shaker. Subsequently, the cells were washed with PBS. Cells were stained with 2 ml crystal violet solution (stains “viable” cultured cells) for 30 min at RT on an orbital shaker (Serrano et al., 1997). Afterwards the staining solution was discarded and the plates washed carefully and thoroughly with ddH_2O. The 6-well plate was air-dried overnight at RT. Crystal violet stain was documented by taking images with a camera.

5.2 Molecular biology methods

5.2.1 Nucleic acid isolation

DNA isolation

To deproteinize DNA, extraction with phenol was performed, which efficiently denatures protein and isolates DNA (Kirby, 1957). The DNA was isolated by Phenol-Chloroform purification, where one volume of lysate and one volume of phenol-chloroform-isoamyl alcohol (25:24:1) was mixed thoroughly by vortexing. Hereafter, the sample was centrifuged with full speed for 10 min at RT. The upper aqueous phase containing the DNA was transferred into a new 1.5 ml reaction tube which contains 1 ml 100% EtOH, 50 µl NaAc (3M) and 1.5 µl GlycoBlue. The DNA is precipitated due to mixing the sample thoroughly and incubating for at least 30 min at -20°C, followed by centrifuging with 14000 rpm for 30 min at 4°C. The pellet containing the DNA was washed twice with 500 µl 70% EtOH, air-dried and resuspended in 20 µl ddH_2O. Optional, the DNA concentration was measured either by NanoDrop or PicoGreen (see 5.2.2), and/or the DNA size was observed by running agarose gels.

RNA isolation

To isolate total RNA from adherent cells, medium was discarded and 600 µl TriFAST™ per 10 cm plate was added. The cells were scraped and collected in a 1.5 ml low-binding tube. After incubation for 5 min at RT was added 100 µl Chloroform. The mix was vortexed for 15 s and again incubated for another 5-10 min at RT. Upon centrifugation with full speed for 5 min at 4°C the aqueous phase was transferred to a new low-binding tube. 500 µl Isopropanol and 1 µl GlycoBlue were added and thoroughly mixed. Then, after the incubation for 15 min at -20 C the sample was centrifuged with full speed for 10 min at 4°C. The supernatant was removed and the RNA pellet was washed twice with 1 ml 75% EtOH. The sample was centrifuged at full speed for 10 min at 4°C. The RNA was dissolved in 25 µl RNase-free water and stored at -80°C after RNA concentration measurement by using NanoDrop photometer (see 5.2.2).

5.2.2 Nucleic acid concentration determination

NanoDrop

Nuclei acid concentration was routinely determined by using NanoDrop™ 1000 Spectrophotometer (Thermo). This device measures the absorption at 260 nm. By measuring the optical density at 260 and 280 nm the purity of the nucleic acid solution was determined (OD_{260}/OD_{280}: 2.1 for pure RNA, 1.8 pure DNA).

PicoGreen

Double-stranded DNA (dsDNA) concentration was measured with the Quant-iT™ PicoGreen dsDNA Assay Kit (Thermo Fisher Scientific) to quantify DNA concentrations of input material for library preparations of next generation sequencing (NGS) experiments. PicoGreen is an ultrasensitive fluorescent nucleic acid stain which was measured at a wavelength of 485/535 nm with

Spark® Multimode Microplate Reader (TECAN). All samples including negative controls and standards were prepared according to the manufacturer's protocol.

Fragment Analyzer

The fragment analyzer (FA) system (Agilent) was used to ensure reliable nucleic acid quality and quantity for preparing NGS libraries. This system utilizes a parallel capillary electrophoresis to determine molarity and peak size of nucleic acid fragments. The FA runs were performed according to manufacturer's protocol. Usually were performed smear analysis for sizing DNA fractions of interest for following sequencing approaches.

5.2.3 cDNA synthesis

Total RNA was transcribed reversely into complementary DNA (cDNA) upon RNA isolation. For the synthesis was used 0.2-2 µg RNA and adjusted with ddH_2O to 10 µl. 2 µl random primer (2 mg/ml) was added and incubated for 1 min at 65°C by using a thermocycler. Then 38 µl master mix (see Table 18) was added and continued with the cDNA synthesis program (see Table 19).

Table 18: master mix for cDNA synthesis.

Amount	Reagent
10 µl	first strand buffer (5X)
1.25 µl	dNTPs (10 mM)
0.2 µl	Ribolock
1 µl	M-MLV Reverse Transcriptase (200 U/ml)
adjust to 50 µl	ddH_2O

Table 19: cDNA synthesis program.

Step	Temperature	Duration
1	65°C	1 min
2	25°C	10 min
	37°C	50 min
	70°C	15 min
3	4°C	∞

After the synthesis the cDNA was diluted 1:10 with ddH_2O and stored at -20°C.

5.2.4 Polymerase chain reaction

The Polymerase chain reaction (PCR) technique is based on using the ability of DNA polymerases to synthesize new strands of DNA complementary to an offered DNA template strand (Saiki et al., 1985).

In this thesis were used mainly three PCR-based methods: qPCR for amplification (qPCR), Realtime Quantitative PCR (RT-qPCR) and *in situ* rolling-circle amplification (RCA) of hybridized DNA (the latter is described in 5.3.11).

qPCR for DNA amplification

To amplify DNA for cloning was performed qPCR with a thermo cycler (Bio-Rad, Eppendorf). For the reactions was calculated the master mix as described in Table 20.

Table 20: master mix for DNA amplification.

Amount	Reagent
5 µl	Primer mix (10 µM)
5 µl	DNA template (50-100 ng)
1 µl	dNTPs (10 mM)
1.5 µl	DMSO
10 µl	HF buffer (5X)
1 µl	Phusion Hi-Fi DNA polymerase
Adjust to 50 µl	ddH_2O

The PCR program (Table 21) was calculated and designed according to the melting temperature of primers in use.

Table 21: (Gradient) PCR program for DNA amplification.

Step	Temperature	Duration	Cycles
1	98C	180 s	1 x
2 (optional)	98°C	25 s	10 x (gradient)
	72°C/ 58°C*	30 s	
	72°C	60 s	
3	98°C	25 s	
4	54°C	30 s	25 x
5	72°C	60 s	
6	4 °C	∞	1 x

*optional: 10x step gradient by ramping down **-Δ10°C** for initial amplification

RT-qPCR

To measure expression levels of specific genes or to check enrichment of DNA fragments upon chromatin immunoprecipitation was performed quantitative real-time PCR. For this application in addition to a standard PCR, was used a master mix containing SYBR Green (Table 22), a double-stranded DNA binding dye (Ponchel et al., 2003). During extension phase this fluorescent dye intercalates into double-stranded DNA sequences. This signal was measured at the end of every thermal cycle which will allow to determine the quantity of dsDNA present. The program for RT-qPCR is shown in Table 23.

Table 22: RT-qPCR master mix.

Amount	Reagent
2.5 µl	SYBR Green Mix (Thermo)
1 µl	fwd/rev primer mix (10 µM)
1.5 µl	ddH_2O

Table 23: RT-qPCR program.

Step	Temperature	Duration	Cycles
1	95°C	15 min	1 x
2	95°C	30 s	38 x
	60°C	20 s	
	72°C	15 s	
3	4°C	∞	1 x

To compare levels of a target gene expression between different samples (treatment/control), a housekeeping gene (e.g. β-Microtubulin) was used for normalization. Therefore, the Livak method (Schmittgen & Livak, 2008) was applied to determine the relative expression rate of the target gene. First, the cycle threshold (ct) of the target gene was normalized to the ct of the house-keeping gene (reference), for both the experimental sample (test) and control sample (calibrator), as described in Equation 1. Second, the Δct of the test sample was normalized to the control sample to gain the ΔΔct value (see Equation 2). Finally, the fold change (FC, see Equation 3) value, which reflects the expression ratio, was calculated. For the analysis of the ChIP application, the enrichment (occupancy) was presented as % of input.

Equation 1: Δct value calculation

$$\Delta ct\ (test\ or\ calibrator) = ct\ (target\ gene) - ct(housekeeping\ gene)$$

Equation 2: ΔΔct value calculation

$$\Delta\Delta ct = \Delta ct\ (test) - \Delta ct(calibrator)$$

Equation 3: fold change gene expression ratio

$$FC = 2^{-\Delta\Delta ct}$$

5.2.5 Cloning of nucleic acid fragments

shRNAs

To obtain stable and regulated gene silencing, cells were engineered by using RNA interference (RNAi). The RNAi pathway can be entered when cells are transfected with an inducible small hairpin RNA (shRNA) of choice (Brummelkamp et al., 2002; Paddison et al., 2002). Constructs to generate shRNA targeting the protein of interest were cloned into pLT3GEPIR vector, which harbors a miR-E based backbone based on the design reported initially (Fellmann et al., 2013).

The oligo of choice was used for amplification by PCR with miR-E primer (see Table 20). The PCR program was similar as in Table 21 but without gradient PCR steps. Upon amplification the shRNA was purified (see 5.2.7), eluted in 20 µl TE. Hereafter, the shRNA insert was subjected together with the pLT3GEPIR vector to digestion using EcoRI and XhoI restriction enzymes (see 5.2.6), agarose gel (1%) clean-up purification (see 5.2.7), ligation (see 5.2.8), transformation into competent bacteria (see 5.2.9) and DNA upscale as well as isolation (see 5.2.10). The integrity of the DNA sequences was confirmed by Sanger sequencing (LGC genomics), as described in 5.2.10.

double-stranded DNA fragments (gBlock™)

To generate reliable gene constructs (> 500 bp), gBlock Gene Fragments (IDT) were used which are chemically synthesized double-stranded DNA (gBlock User Guide, IDT). In this work were used gBlocks of USP11, TCEAL1 and RPB8 for cohesive-end cloning. Usually, the gBlocks were designed like this: NNN-RE-ATG-TAG-LINKER-cDNA (N= random base, RE= restriction site). The tube containing the gBlock lyophilizate was centrifuged with 3000 x g for 3-5 s and resuspended with 100 µl TE to have a final concentration of 10 ng/µl. After briefly vortexing and spinning down the tube was incubated for 20 min at 50°C. Again, the tube was vortexed and spun down and stored at -20°C. Cohesive ends of gBlocks were prepared by restriction digest of 800 ng gBlock for 4 h at 37°C (as described in 5.2.6). This was followed by ligation (ratios 3:1 and 5:1) of restricted gBlocks and vector (as described in 5.2.8) and transformation with competent bacteria cells (as described in 5.2.9).

site directed mutagenesis (SDM)

To engineer proteins with loss or gain of function, usually SDM cloning was performed. Here, mutations were generated by PCR using a pair of oligonucleotide primers designed with mismatching nucleotides within the coding codon of interest (by using SnapGene Viewer, ApE plasmid editor and Tm Calculator (source: https://tmcalculator.neb.com/#!/main)). According to the requirements of loci where mutations had to be introduced, one, two or more consecutive PCR runs, agarose gel checkups as well as clean-ups were needed. Further, for this purpose, the PCR was optimized by prefixing a gradient PCR before the standard amplification PCR program started (see Table 21). After the final PCR the newly engineered DNA was eluted in 20 µl ddH_2O.

5.2.6 Restriction digestion of DNA

A restriction enzyme digestion was performed to generate compatible sticky ends capable for ligation. For the hydrolysis of DNA were used restriction enzymes (RE, endonucleases) as instructed by the manufacturer (NEB). The restriction was set up as shown in Table 24.

Table 24: restriction digestion mix

Amount	Reagent

20 µl	DNA
0.5 µl	RE1, high fidelity (NEB)
0.5 µl	RE2, high fidelity (NEB)
2.5 µl	10X CutSmart Buffer (NEB)
1.5 µl	ddH_2O

*RE= restriction endonuclease

The restriction digestion mix was incubated between 2 h and 5 h at 37°C.

5.2.7 DNA separation and extraction

Agarose gel electrophoresis

To determine the size of specific DNA fragments was performed agarose gel electrophoresis. Depending on the expected size of the DNA fragment, 1-3% gels were prepared by dissolving agarose in 1X TAE buffer using a microwave oven. After the solution cooled down it was supplemented with 0.3 µg/ml of the staining chemical ethidium bromide (EtBr). Then, the solution was poured in a gel chamber with a comb. To the sample containing the DNA fragment was added 6X DNA loading buffer. After loading the sample onto the gel, the DNA was separated according to size by applying for 30 to 50 min at 120-180 V. EtBr was able to intercalate with DNA and thus DNA bands were detected with UV light (254/365 nm) with an UV transilluminator. The analysis and documentation were performed by using ImageJ software.

DNA extraction and purification

The extraction of DNA followed upon either cutting out DNA fragments from the agarose gel or using DNA fragments e.g. after restriction digest and the DNA fragment was subjected to purification. This was performed by using the gel extraction kit (GeneJET Gel Extraction Kit) according to manufacturer's protocol. The sample was eluted in 20 µl ddH_2O.

5.2.8 Ligation of cohesive end inserts

The equimolarity for ligation of insert (DNA fragment) and a backbone vector (both restricted digested) was calculated by a ligation calculator (source: https://nebiocalculator.neb.com/#!/ligation). The vector to insert ratio was usually defined 1:3 or 1:5 for cohesive end ligation. The ligation reaction was mixed (as described in Table 25) and incubated overnight at 16°C, followed by heat inactivation for 10 min at 65°C and then subjected to transformation into competent bacteria (see 5.2.9).

Table 25: DNA ligation reaction mix

Amount	Reagent
100 ng	linearized vector
x ng	Insert
2 µl	T4 ligase buffer (10X)

1 µl	T4 Ligase
adjust to 20 µl	ddH_2O

5.2.9 Transformation of bacterial cells

To introduce foreign DNA into a cell (transformation) chemically competent bacteria strains (XL-1 blue bacteria) were used. The bacteria were taken out of -80°C, mixed with either 1 µg or ligation mix (from 5.2.5) and thawed on ice, followed by a heat shock for 45 s at 42°C. After subsequent cool down for 2 min on ice, transformation samples were mixed with 700 µl prewarmed LB medium (w/o antibiotics) and incubated in a thermoshaker (800 rpm) for 60 min at 37°C to allow recovery of cells. Then, the suspension was spun down and the supernatant poured away. Either in the residual supernatant or new 70-80 µl LB medium was added to resuspend the bacteria pellets. The bacteria suspension was plated on LB agar plates (with antibiotics for selection) and incubated overnight at 37°C.

5.2.10 DNA scale up, isolation and sequencing

DNA scale up and isolation (MiniPrep, MaxiPrep)

To isolate plasmid DNA, alkaline lysis was performed. Therefore, 1.5 ml medium (LB medium with antibiotics) was inoculated with bacteria containing the DNA of interest (from 5.2.9) and incubated overnight. Bacteria were pelleted by centrifuging and resuspended in 150 µl Mini buffer I containing 100 µg/ml RNase A. Then, 150 µl mini buffer II was added to lyse the bacteria. Subsequently the tubes were inverted several five times and incubated for 5 min at RT, before the lysis was stopped by adding 150 µl mini buffer III. The sample was inverted again five times and centrifuged for 5 min at 14,000 rpm at RT. The supernatant, was mixed with 500 µl isopropanol in a new reaction tube and incubated for 15 min at RT to precipitate the DNA. The plasmid DNA was pelleted by centrifuging at 14, 000 rpm at 4°C and washed once with 1ml 70%. After air-drying the pellet was resuspended in 20 µl ddH_2O.

For large scale isolation (Maxiprep) the procedure was performed. Here, 200 ml bacteria culture (LB medium with antibiotics) was processed after incubation overnight by using the PureLink™ HiPure Plasmid Maxiprep kit according to manufacturer's protocol. The purified DNA was re-suspended in TE buffer and adjusted to a concentration of 1 mg/ml (see 5.2.2).

Sequencing

All sequences of plasmids were confirmed by Sanger sequencing which was conducted by LGC Genomics (Berlin, Germany). The results were analyzed by using ApE plasmid editor software.

5.3 Biochemical methods

5.3.1 Protein quantification by colorimetric assays

To prepare cells for protein concentration measurement, the plate with adherent cells was washed two times with ice-cold PBS. Then ice-cold PBS containing protease and phosphatase inhibitor cocktail (1:1000) was added to the plate and the cells were scraped and collected in a new tube. Cells were centrifuged at 15000 rpm for 15 min at 4°C. The supernatant was discarded and the pellets were lysed (RIPA lysis buffer). After 10 min incubation on ice the lysates were centrifuged again at 14 000 rpm for 5 min at 4°C to get rid of cell debris. The supernatant containing the lysate was transferred to a new tube and subjected to protein concentration measurement. After cell lysis two different colorimetric methods were used to determine the protein concentration of samples. On the one hand, protein concentration of lysates was determined using Bradford assay (Bradford, 1976). Coomassie-brilliant blue G250-dye binds to unpolar, hydrophobic and cationic side chains of amino acids which shifts the absorbent maxima from 465 nm to 595 nm. The protein concentration was determined by diluting 1 µl cell lysate and 1 ml Bradford reagent in a cuvette, mixed and incubated for 5 min at RT and measured at 595 nm using the Ultrospec™ 3100 pro. On the other hand, protein concentration of lysates was determined using Bicinchoninic acid assay (BCA). The reduction of $Cu^{2+}$to Cu^{+} by protein in an alkaline medium (biuret reaction) is detected by bicinchoninic acid. (Larger) polypeptides will react to produce the light blue-to-violet complex that absorbs light at 562 nM. The intensity of the color produced is proportional to the number of peptide bonds participating in the reaction. The protein concentration was determined by diluting 1.5 µl with 150 µl BCA solution (BCA buffer A and B were mixed in a 50:1 ratio) to a flat bottom 96 well plate. After incubation for up to 15 min at 37°C the 96 well plate was measured with the Multiscan Ascent plate reader at 550 nm. For both methods the protein concentration was calculated using a standard curve, defined by known concentrations of BSA.

5.3.2 Bis-Tris gel electrophoresis

Bis-Tris SDS-PAGE (sodium dodecyl sulfate polyacrylamide gel electrophoresis) was performed to separate proteins according to size (Laemmli, 1970). To run gel electrophoresis, the protein amount of lysates (protein concentration determined in 5.3.1) were mixed with Lämmli Buffer (6X stock) and ddH_2O to reach equal volume as well as protein concentration of samples between 10-20 µg. The samples were boiled to denaturate the protein for 5 min at 95°C. SDS in the buffer helps to linearize (denaturation) the proteins and bring a net negative charge to the proteins irrespective of the initial charge. Further, the buffer contains DTT a redox reagent that reduces and disrupts disulfides. For the electrophoresis were used 8-12% Bis-Tris gels (Acrylamide, 3,5x Bis-Tris, H_2O, APS (10%), TEMED) containing a 4% stacking gel zone. To monitor running and later after the immunoblot determining the size of proteins (see 5.3.4) PageRuler™ Prestained Protein

Ladder (Thermo) or HiMark™ Prestained HMW STD Ladder (Thermo) were used. Protein were run through the gel in the direction of the anode by using 1X MOPS running buffer in a SDS-PAGE chamber (Bio-Rad). The voltage was applied between 80-120 V.

5.3.3 Colorimetric total protein staining

To stain proteins in SDS gels Coomassie Brilliant Blue dye was used (Merril, 1990). SDS gels were stained with Coomassie fixing solution for 1h. Excess stain is then eluted with de-staining solution 4-24 h until the background is clear. Stained gels were digitized by a scanner.

5.3.4 Immunoblot

After proteins were separated by SDS-PAGE (see 5.3.2), immunoblotting onto a nitrocellulose membrane using a transfer blot system is followed (Renart et al., 1979; Towbin et al., 1979). To activate the PVDF nitrocellulose membrane it was incubated for 1 min in 100% methanol at RT and afterwards was put together with gel, sponges and whatman filter papers into 1x NuPAGE transfer buffer for equilibration. The gel was sandwiched on an activated membrane between four Whatman papers soaked in transfer buffer. To remove air bubbles, each sandwich was rolled over with a plastic roller. Hereafter, the transfer was performed with 300 mA electric current for 3h at 4°C using a immunblot transfer chamber and power supply (Bio-Rad). After transfer the membrane was blocked in 5% milk-TBST for 1h at RT to block unspecific binding on orbital shaker. Following blocking the membrane was cut into pieces according to the size of proteins of interest. The pieces were incubated with the respective antibody overnight at 4 °C. To get rid of unspecific bound antibody, the membranes were washed three times with TBST for 5 min at RT on an orbital shaker. Next, the membranes were incubated for 1h with the secondary antibody coupled to a horseradish peroxidase (HRP). For visualizing immunoprecipitation assays (see 5.3.5) were used TrueBlot® HRP-conjugated anti-rabbit or -mouse IgG monoclonal secondary antibody for detection without hindrance by interfering immunoprecipitating immunoglobulin heavy and light chains. Afterwards, the membranes were washed again three times with TBST for 5 min at RT on an orbital shaker. According to the manufacturer's instructions Immobilon Western HRP ECL substrate was used to detect chemiluminescence with LAS-4000 imager (Fujifilm) the antibody labelled proteins. Digitized membranes were subjected for analysis to ImageJ or Affinity Designer.

5.3.5 Co-immunoprecipitation

To characterize proteins and protein-protein interactions we assayed Co-immunoprecipitation, a robust tool in which an antigen is isolated to bind to a specific antibody (Bonifacino et al., 2006). The method described hereafter was established in the Wolf and Eilers lab (Dr. Julia Hofstetter

& Dr. Dimitros Papadopoulos, personal communication, 2018). For immunoprecipitation were used 2-3 cell culture plates (Ø 15 cm) per IP of 70-80% confluent adherent cells. In advance to the protein immunoprecipitation, 20 µl Dynabeads protein A/G mix (1:1, Thermo) were washed three times with BSA-PBS (5 mg/ml) and then pre-incubated with 2 µg of antibody against the protein of interest overnight at 4°C circulating on a rotating wheel. Upon harvest with 1ml PBS (containing proteinase and phosphatase inhibitor cocktail, 1:1000) per plate, cell pellet of 2-3 plates was resuspended in 1 ml HEPES buffer for Benzonase treatment (incl. proteinase and phosphatase inhibitor cocktail, 1:1000). Lysate was sonified (4x5 s pulse interval, 10s pause, 20% amplitude), supplemented with 50 U/ml Benzonase (Sigma) and incubated for 1h at 4°C on a rotating wheel. Next, the lysate was cleared by centrifugation with full speed for 5 min at 4°C. This step was repeated as many times as there is no visible pellet in the reaction tube left. The protein concentration of the lysate was determined as described in 5.3.1. After the supernatant of the bead-antibody mix was carefully removed with a magnetic rack, were added 1-3 mg protein lysate per IP. 1.5-2% Input per IP was reserved for western blotting. The sample was incubated for 6h at 4°C on a rotating wheel. Afterwards, beads were collected with a magnetic rack and the supernatant discarded. Beads were washed 5-6 times with HEPES buffer with a magnetic rack. Finally, the IP beads were resuspended with 1X Lämmli buffer and the input was resuspended with 3X Lämmli buffer. The sample and its input were boiled for 5 min at 95°C and analyzed by immunoblotting as described in 5.3.2 and 5.3.4.

5.3.6 Chromatin Immunoprecipitation

Chromatin Immunoprecipitation is the main tool for assaying protein-DNA binding (Gilmour & Lis, 1985). For running chromatin immunoprecipitation, four plates (Ø 15 cm) per IP at confluency of 70-80% were needed. To crosslink proteins with DNA 1% Paraformaldehyde (Solomon et al., 1988) was added to the medium for 5 min at RT on an orbital shaker. To stop the reaction, 2.5 ml of 1 M Glycine was added and again incubated for 5 min at RT on an orbital shaker. Subsequently, the medium was removed and cell were washed twice with ice-cold PBS. Cells were scraped in 1 ml ice-cold PBS containing protease- and phosphatase inhibitor cocktail (1:1000) and collected in falcon tubes. After centrifugation with 1500 rpm for 15 min at 4°C the supernatant was discarded and the pellet was lysed in 2 ml ChIP Lysis Buffer I containing protease- and phosphatase inhibitor cocktail (1:1000). Upon incubation for 20 min on ice the lysate was centrifuged again at 1500 rpm for 5 min at 4°C. The supernatant was discarded again and the nuclei were resuspended in 1 ml ChIP Lysis Bufer II containing protease- and phosphatase inhibitor cocktail (1:1000). After cell lysis the DNA was fragmented using the Covaris M220 (Peak Power = 75.0, Cycles/Burst = 200, Duty Factor = 10.0, Duration = 3000s per 1 ml cell lysate, < $30*10^6$cells/ml) by keeping samples constantly on ice. To check the fragment size after

sonication, 25 µl of sonicated samples were incubated with 475 µl TE, 16.87 µl NaCl (5 M) and 2 µl Rnase A (10 mg/ml) using the following program of a thermomixer (Eppendorf): 1 h at 37°C to degrade RNA, followed by shaking (900 rpm) overnight at 65°C to revert the crooslink. Next, 2 µl Proteinase K (10 mg/ml) and 5 µl EDTA (0.5 M) was added and again mixed for 2 h at 45°C by shaking (900 rpm) to degrade all the protein. To isolate the DNA this is followed by phenol-chloroform purification (see 5.2.1); the pellet was resuspended in 20 µl ddH_2O. Then, the fragment size was analyzed by separating the DNA on a 2% agarose gel (see 5.2.10). Fragmented DNA should have a size about 250 bp. Afterwards, the chromatin was centrifuged with full speed for 15 min at 4°C and the supernatant containing the soluble chromatin was transferred to a fresh 1.5 ml reaction tube and stored till further proceeding at 4°C. In parallel, 30 µl Dynabeads protein A/G mix (1:1, Thermo) was washed three times with BSA-PBS (5 mg/ml). Then for the immunoprecipitation 3µg antibody of interest and IgG as a control were added each to beads and incubated overnight at 4°C on a rotating wheel. Following this, the antibody-beads were washed again three times with BSA-PBS (5 mg/ml). After the last washing step 900 µl lysate was distributed to the antibody-beads mixtures and again incubated for 6 h at 4°C on a rotating wheel as well as 1% Input was kept as control reference. After incubation the sample was washed three times each with 1 ml ChIP washing buffer I, ChIP washing buffer II, ChIP washing buffer III and twice with TE. The DNA was eluted by adding 150 µl ChIP elution buffer and incubating 15 min on the rotating wheel at RT. The elution step was performed twice, and the eluates were merged into on 1.5 ml reaction tube. Also 300 µl elution buffer was added to the input sample. Following this, chromatin decrosslinking was performed for all samples as described above. The DNA was purified using phenol-chloroform purification (see 5.2.1); the pellet was resuspended in 500 µl ddH_2O. Hereafter with the samples were performed qPCR (see 5.2.4).

5.3.7 In vivo pulldown

To investigate protein protein interaction characteristics, *in vivo* pulldowns with recombinant purified USP11 protein were performed. The method was performed as described in 5.3.5 beside some minor optimizations. Directly upon cell lysis of samples was added 20 µg recombinant purified USP11 protein per 1 ml cell lysate. FLAG-tagged recombinant protein of full length and deletion mutants of USP11 were designed, produced and purified by F. Sauer (AG Kisker, RVZ, Wuerzburg). Samples were incubated overnight at 4°C on a rotating wheel. Next, procedure is followed as in 5.3.5. Then 20 µl/IP FLAG-M2 magnetic beads (Sigma) were washed three times with BSA-PBS (5 mg/ml) and added to the pulldown samples. As a control reference 1% input per lysate used for pulldown was kept. FLAG pulldown samples were incubated for 6h at 4 °C circulating on a rotating wheel. After incubation beads were washed 5-6 times with HEPES buffer. Samples were eluted and subjected to western blotting as described 5.3.5.

5.3.8 NanoLC-MS/MS proteomic analysis

To define the interactome of the USP11 protein 200 million SH-EP MYCNwt or SH-EP MYCN T58A cells stably expressing either N-terminal or C-terminal tagged HA-FLAG-USP11 were harvested at 60-70% confluency. Cell pellets were resuspended with 4 ml lysis buffer (HEPES lysis buffer for benzonase treatment) containing protease and phosphatase inhibitor cocktail (1:1000) and were homogenized 10x times with a pre-cold glass homogenizer. Each milliliter of cell lysate was sheared by sonicating four times 10 s with 45 s pausing (20% amplitude). After combining the lysates, they were supplemented with 100 U Benzonase (stock: 25 U/µl) and incubated for 40 min at 4°C on a rotating wheel. Samples were distributed into three 1.5 ml centrifuge tubes (Beckman Coulter) and were centrifuged (Beckman JA25.50 rotor) at 18 000 rpm for 30 min at 4°C by using pre-cold adaptors. The soluble fraction was used in IP with 80 µl HA-coupled beads (Pierce™ Thermo Fisher Scientific, #88836) resuspended in lysis buffer. For the check-up on western blot, 60 µl supernatant was left aside. Again, the samples were supplemented with 150 U Benzonase and incubated for 3h at 4°C on a rotating wheel. The beads were washed four times with 1 ml lysis buffer supplemented with 0.1% Triton-X-100 and two times with 1 ml lysis buffer w/o Triton-X-100. In the 1st elution step was added 100 µl 1X LDS sample buffer (NuPAGE™ Thermo Fisher Scientific, #NP0007) and incubated for 30 min at 37°C with 400 rpm shaking. To the supernatant was added DTT to a final concentration of 50 mM and boiled for 5 min at 95°C. In the 2nd elution was added 100 µl LDS buffer to the beads and boiled for 7 min at 95°C. To this supernatant was added DTT to a final concentration of 50 mM, boiled again for 5 min at 95°C and later on tested in western blotting assays. To reduce sample volumes of the 1st elution protein precipitation was performed overnight at -20°C with fourfold volume of ice-cold acetone. After centrifugation at 2,000 g for 15 min, pellets were washed with acetone at -20°C. Precipitated proteins were dissolved in LDS samples buffer (NuPAGE™ Thermo Fisher Scientific, #NP0007), reduced with 50mM DTT for 10 min at 70°C and alkylated with 120 mM Iodoacetamide for 20 min at room temperature. Separation was performed on NuPAGE® Novex® 4-12% Bis-Tris gels (Life Technologies) with MOPS buffer according to manufacturer's instructions. Gels were washed three times for 5 min with water and stained for 1h with Simpley Blue™ Safe Stain (Life Technologies). After washing with water 1h, each gel lane was cut into 15 slices. The excised gel bands were destained with 30% acetonitrile in 0.1 M NH_4HCO_3 (pH 8), shrunk with 100% acetonitrile, and dried in a vacuum concentrator (Concentrator 5301, Eppendorf, Germany). Digests were performed with 0.1 µg trypsin (Trypsin Gold, Mass Spectrometry Grade, Promega) per gel band overnight at 37°C in 0.1 M NH_4CO_3 (pH 8). After removing the supernatant, peptides were extracted from the gel slices with 5% formic acid, and extracted peptides were pooled with the supernatant. NanoLC-MS/MS analysis were performed on an Orbitrap Fusion (Thermo Scientific) equipped with a PicoView Ion Source (New Objective) and coupled to an EASY-nLC 1000

(Thermo Scientific). Peptides were loaded on capillary columns (PicoFrit, 30 cm x 150 μM ID, New Objective) self-packed with ReproSil-Pur 120 C18-AQ, 1.9 μM (Dr. Maisch) and separated with a 30 min linear gradient from 3% to 30% acetonitrile and 0.1% formic acid and a flow rate of 500nl/min. Both MS and MS/MS scans were acquired in the Orbitrap analyzer with a resolution of 60,000 for MS scans and 15, 000 for MS/MS scancs. HCD fragmentation with 35% normalized collision energy was applied. A top speed data-dependent MS/MS method with a fixed cycle time of 3s was used. Dynamic exclusion was applied with a repeat count of 1 and an exclusion duration of 30s, singly charged precursors were excluded from selection. Minimum signal threshold for precursor selection was set to 50,000. Predictive AGC was used with a target value of 2e5 for MS scans and 5e4 for MS/MS scans. To add confidence to protein quantification results EASY-IC for internal calibration was used.

The samples from the 1st elution were subjected to NanoLC-MS/MS spectrometry performed and analyzed (section 5.5) by AG Schlosser (Rudolf-Virchow-Center, Wuerzburg).

5.3.9 SILAC-based ubiquitin remnant profiling

The ubiquitin-modified proteome was identified and quantified by conducting Ubiquitin diGLY SILAC-based proteomics and full proteomics as described initially (Fulzele & Bennett, 2018). For the SILAC experiments, IMR5 cells harboring a shRNA against USP11 were cultured at least four to five passages for population doubling in either containing L-Lysine^{0}/L-Arginine^{0} (light) or L-Lysine^{8}/L-Arginine^{10} (heavy) SILAC-medium. The setup of the proteomic assay was designed as a label-swap experiment, to have light or heavy labeled cells either with or without downregulation of USP11. During expansion a confluent 15 cm plate was trypsinized, resuspended in SILAC medium and pelleted for incorporation testing. Cell pellets were snap-frozen, stored at -80°C and analyzed by AG Beli (IMB Mainz). The cell population was expanded to reach a final protein amount per sample of 15-25 mg. After washing cells twice with ice-cold PBS cells each plate was scraped upon adding 500 μl PBS containing protease and phosphatase inhibitor cocktail. Cells were collected in 50 ml falcon tubes by centrifugation for 20 min at 4°C with 1500 rpm. Cell pellets were lysed by adding modified RIPA buffer (500 μl per plate). Lysate was incubated for 15 min on ice. Further, 1/10 volume of NaCl (5M) was added to the lysate and mixed thoroughly. Each milliliter of cell lysate was sheared by sonicating four times 30 s with 30 s pausing on ice (20% amplitude) until the solution became transparent and of low viscosity. The lysate was centrifuged for 15 min at 4°C with 14 000 rpm. Supernatants belonging to the same condition after centrifugation were combined into a new 15 ml falcon tube. To check if the treatment worked to a 50 μl aliquot of lysate of each sample were added LDS buffer and DTT (end conc.: 2X LDS, 1mM DTT), boiled for 10 min at 70°C and stored at -20°C until testing by western blotting. The protein concentration of the supernatant of each condition was measured by using

Bradford. Lysates of the same conditions were combined 1:1 to aim for a combined mass of 30-50 mg. Protein concentration of the combined treatment condition was measured again. To prepare the samples for the diGLY SILAC proteomics proteins of the supernatant were precipitated in fourfold excess of ice-cold acetone overnight at -20°C and re-dissolved in denaturation buffer. Cysteines were reduced with 1 mM DTT and alkylated with 5.5 mM CAA. Proteins were digested with endoproteinase Lys-C (Wako Chemicals) and sequencing grade modified trypsin (Sigma). Protease digestion was stopped by addition of TFA to 0.5%, and precipitates were removed by centrifugation. Peptides were purified using reversed-phase Sep-Pak C18 cartridges (Waters) and eluted in 50% acetonitrile. For ubiquitin remnant peptide enrichment, peptides were re-dissolved in immunoprecipitation buffer and precipitates were removed by centrifugation. Modified peptide were enriched using PTMScan Ubiquitin Remnant Motif beads (Cell Signaling Technology, 5562). Peptides were incubated with the beads for 4h at 4°C on a rotation wheel. Supernatants were recovered and subjected to a second round of enrichment with fresh beads. The beads were washed three times in ice-cold immunoprecipitation buffer followed by three washes in water. The enriched peptides were eluted with 0.15% TFA in H_2O, fractionated in six fractions using micro-column-based stron-cation exchange chromatography (SCX) (Weinert et al., 2013), and desalted on reversed-phase C18 StageTips (Rappsilber et al., 2007). For proteome analysis 50 µg of protein from each SILAC condition was pooled and separated by SDS-PAGE. To the combined samples were added NuPAGE® LDS Sample Buffer (Life Technologies) supplemented with DTT (end conc.: 2X LDS, 1mM DTT) and boiled for 10 min at 70°C. After the samples have cooled down, they were alkylated by adding CAA to a final concentration of 5 mM and loaded onto 4-12% gradient Bis-Tris gels. Proteins were stained using the Colloidal Blue Staining Kit (Life Technologies) and in-gel digested using trypsin. Peptides were extracted from gel and de-salted on reversed-phase C18 StageTips (Rappsilber et al., 2007). Peptides were analyzed on a quadrupole Orbitrap mass spectrometer (Exploris 480, Thermo Scientific) equipped with a UHPLC system (EASY-nLC 1200, Thermo Scientific) as described (Bekker-Jensen et al., 2020; Kelstrup et al., 2012). The mass spectrometer was operated in data-dependent mode, automatically switching between MS and MS2 acquisition. Survey full scan MS spectra (m/z 300-1,700) were acquired in the Orbitrap. The 15 most intense ions were sequentially isolated and fragmented by higher energy C-trap dissociation (HCD) (Olsen et al., 2007). An ion selection threshold of 5,000 was used. Peptides with unassigned charge states, as well as with charge states < +2, were excluded from fragmentation. Fragment spectra were acquired in the Orbitrap mass analyzer.
The LC-MS/MS and analysis (section 5.5) of diGLY-SILAC proteomics and full proteomics was performed by AG Beli (IMB Mainz).

5.3.10 Immunofluorescence

Immunofluorescence (IF) is a technique to localize protein in cells. Thereby antibodies for a specific target molecule are exposed to the cell and detected by incubating the samples with a secondary antibody specific for immunoglobulin molecules and conjugated to a fluorophore. Cells were seeded on 96-well plates and incubated for a desired time (e.g. shRNA induction and/or inhibitor treatment). After washing the cells twice with PBS were added 100 µl/well of 3.7 % Paraformaldehyde (PFA) and incubated for 10 min at RT to fix the cells. Fixed cells were washed again one time with 100 µl/well PBS and permeabilized by adding 100 µl/well 0.3% Triton X-100 for 10 min at RT. After removing Triton X-100, cells were blocked for 30 min with BSA-PBS (5%) for 30 min at RT to reduce unspecific binding of primary antibodies. To stain the protein of interest, the primary antibody was diluted to the desired concentration (1:100-1:3000) in BSA-PBS (5%) and 50 µl/well was added to the sample. After incubation overnight at 4°C the sample was washed two times with PBS and incubated with 50 µl/well of fluorophore-conjugated secondary antibody (1:400) in BSA-PBS (5%) protected from the light for 1h at RT. Directly afterwards nuclei were counterstained with 50 µl/well Hoechst 33342 (1:2000 from 5 mg/ml stock) protected from the light for 5 min at RT. The samples were washed two times 100 µl/well with PBS to remove residual unspecific bound secondary antibody and Hoechst 33342. The 96-well plate was measured and analyzed with the Operetta® High-Content Imaging System.

5.3.11 Proximity Ligation Assay

The *in situ* proximity ligation assay (PLA) is a highly selective and sensitive method for detecting proteins in proximity (see https://reedd.people.uic.edu/ReedLabPLA.pdf). The protocol was adapted for 384 well plates (Leuchowius et al., 2010). Cells were seeded in a 384-well plate and incubated for a desired time (e.g. shRNA induction and/or inhibitors treatment). For pulsed 5-ethynyl-2'-deoxyuridine (EdU) incorporation, cells were incubated for 30 min in medium containing 10 µM EdU before fixation of cells. Cells were washed with 100 µl/well PBS and incubated with 20 µl/well 3.7 % PFA for 10 min at RT to fix the cells. After washing three times with 100 µl/well PBS the cells were permeabilized with 0.3 % Triton-X 100 for 20 min at RT. After removing Triton X-100, cells were blocked for 60 min with 50 µl/well BSA-PBS (5%) for 60 min at RT to reduce unspecific binding of primary antibodies. The Click-iT™ EdU Alexa Fluor 647 Imaging Kit was used according to manufacturer`s protocol for EdU detection (Click-iT cocktail: 856 µl Tris pH 8.5, 40 µl $CuSO_4$, 4 µl AFDye 647 Azide, 100 µl L-Asorbic Acid). After 30 min incubation protected from the light at RT the samples were washed two times with 100 µl/well PBS. To stain the protein of interest, the primary antibody was diluted to the desired concentration (1:100-1:3000) in BSA-PBS (5%) and 20 µl/well was added to the sample. After incubation overnight at 4°C the sample were processed in *in situ* proximity ligation assays as per manufacturer`s instructions.

Cells were washed four times with 100 µl/well TBST and treated for 60 min at 37°C with plus and minus probes directed at rabbit and mouse antibodies, respectively. After washing four times with 100 µl/well Wash Buffer A the probes were ligated for 30 min at 37°C to form a closed, circle DNA template if PLA probes in close proximity. Next, after washing again four times with 100 µl/well Wash Buffer A *in situ* "rolling-circle" PCR amplification (RCA) was done with Alexa 568 or Alexa 488-conjugated oligonucleotides for 120 min at 37°C. RCA generates concatemeric sequences which allows up to 1000-fold amplified signal for localization. Labeled oligos hybridize to the complementary sequences within the amplicon which are then visualized as spots (PLA signals). In addition, directly after the PCR reaction nuclei were counterstained with 20 µl/well Hoechst 33342 (1:2000 from 5 mg/ml stock) protected from the light for 10 min at RT. After washing the sample again two times with 100 µl/well Wash Buffer B and one time with 100 µl/well 1% Wash Buffer B was added 50 µl/well PBS and stored protected from the day light at 4°C. The 384-well plate was measured with the Operetta® High-Content Imaging System for spot visualization and quantification.

5.4 Next generation sequencing based methods

5.4.1 ChIP-Sequencing

In chromatin immunoprecipitation followed by sequencing (ChIP-Seq) are precisely mapped protein-binding sites of DNA fragments of interest genome-wide (Johnson et al., 2007). The ChIP part of ChIP-Seq was followed as described in 5.3.6. For the assay were used $30*10^6$ cells per IP with 10 % of mouse NIH3T3 cells spike-in. When an exogenous reference genome is used for normalization, it is also termed as ChIP-Rx (Orlando et al., 2014). For the immunoprecipitation were used 100 µl Dynabeads protein A/G mix (1:1, Thermo) and 15 µg antibody against the protein of interest. The DNA pellet (from 5.2.1) was solubilized with 30 µl ddH_2O. To test efficiency of the ChIP, 3 µl of DNA was mixed with 127 µl ddH_2O and tested via RT-qPCR (see 5.2.4). Further, 1 µl was used to determine the dsDNA yield of the IP by PicoGreen measurement (see 5.2.2). Between 3-5 ng input DNA was used for the library prep. The DNA libara preparation was performed using the NEBNext Ultra II DNA Library Prep Kit (NEB) following manufacturer's instructions. The quality, quanitity and size of the the PCR-amplified DNA fragments of the prepared libraries were determined by the Fragment Analyzer (Agilent) using the NGS Fragment High Sensitivity Analysis Kit (1-6,000 bp; Agilent). Finally, libraries were subjected to cluster generation and base calling for 75 cycles paired end on Illumina NextSeq500 platform.

5.4.2 CUT&RUN-Sequencing

Alternatively to ChIP, Cleavage Under Targets & Release Using Nuclease (CUT&RUN) method was used to run *in situ* genome-wide target profiling on chromatin (Skene & Henikoff, 2017). For each assay $5*10^5$ cells (SH-EP cells) were collected in low binding falcons upon Accutase detachment. Hereafter, it was proceeded as described in the protocol "CUT&RUN: Targeted in situ genome-wide profiling with high efficiency for low cell numbers V.3" (source: https://www.protocols.io/view/cut-amp-run-targeted-in-situ-genome-wide-profiling-14egnr4ql5dy/v3) by Janssens, D. from the Henikoff lab in 2019. The input material for the library preparation for sequencing was 6 ng per CUT&RUN DNA sample. CUT&RUN libraries were prepared according to the protocol from Liu, N. 2019 (source: https://www.protocols.io/view/library-prep-for-cut-amp-run-with-nebnext-ultra-ii-kxygxm7pkl8j/v1?version_warning=no) using the NEBNext® Ultra™ II DNA Library Prep Kit for Illumina® (E7645).

5.4.3 BLISS8

Global DNA damage site profiling was observed by running breaks labeling *in situ* and sequencing with AsiSI digestion for double strand break normalization (BLISS8) (Iannelli et al., 2017; Yan et al., 2017). The original protocol from *Yan et al* (2017) was adapted and performed as the modified version which was reported recently (Endres et al., 2021). For the BLISS8 assay were

seeded 5,000 SH-EP MYCNER shUSP11 cells/well in a 24-well plate format. After 120 h Doxycycline (Doxycycline-inducible shRNA against USP11) incubation time (incl. 25 µM Etoposide sample (3h), as a positive control) a 80% cell confluency was aimed for. In general, the following steps were performed: cell fixation, permeabilization, lysis *in situ* AsiSI digestion, *in situ* DSB blunting, *in situ* DSB ligation, DNA purification, fragmentation and concentration, *in vitro* transcription (IVT), and RNA clean up by two-sided size selection.

Samples were then subjected to the library preparation. The library was prepared by ligating the RA3 adapter to the samples with a T4 RNA Ligase 2 (NEB) supplemented with recombinant ribonuclease inhibitor (Thermo Fisher Scientific). The samples were reverse transcribed using SuperScript III Reverse Transcriptase kit (Thermo Fisher Scientific) and library indexing and amplification performed using NEBNext HF 2X PCR Master Mix (NEB) with RP1- and desired RP1-primer. Finally, the libraries were cleaned up using Ampure XP Beads (Beckman Coulter). The quality, quantity and fragment size were assessed by the Fragment Analyzer (Agilent) using the NGS Fragment High Sensitivity Analysis Kit (1-6,000 bp; Agilent). The libraries were subjected to cluster generation and base calling for 75 cycles on the Illumina NextSeq500 platform.

5.4.4 RNA-Sequencing

RNA-sequencing was performed by extracting RNA with RNeasy Mini Kit (Qiagen) according to manufacturer's instructions. On-column DNase I digestion was performed followed by mRNA isolation with the NEBNext Poly (A) mRNA Magnetic Isolation Kit (NEB).

Library preparation was done with the Ultra II Directional RNA Library Prep for Illumina following the manufacturer's manual. Size selection of the library was done by using SPRIselect Beads (Beckman Coulter) after amplification with 9 PCR cycles. After the final purification, the concentration and size distribution of the library was checked with the Fragment Analyzer (Agilent) using the NGS Fragment High Sensitivity Analysis Kit (1-6,000 bp; Agilent). Finally, the libraries were subjected to cluster generation and base calling for 100 cycles paired end on Illumina NextSeq 2000 platform.

5.5 Bioinformatics

ChIP-Sequencing, CUT&RUN Sequencing, RNA-Sequencing analysis

All sequencing libraries were subjected to Ilumina NextSeq 500 sequencing according to the manufacturer's instructions. After base calling with Illumina's FASTQ Generation software (v1.0.0, NextSeq 500 Sequencing), high quality PF-clusters were selected for further analysis and sequencing quality was ascertained using FastQC software (v0.11.09; available online at: http://www.bioinformatics.babraham.ac.uk/projects/fastqc/). ChIP-Sequencing samples were mapped separately to the human hg19 and to the murine mm10 genome using Bowtie2 (v2.3.5.1;

(Langmead & Salzberg, 2012)) using the preset parameter "very-sensitive-local". Further, ChIP samples were normalized to the number of mapped reads in the smallest samples. For ChIP spike-in (NIH-3T3 cells) normalized reads were calculated by dividing the number of mapped reads mapped to hg19 by the number of reads mapped to mm10 for each sample and multiplying this ratio with the smallest number of reads mapped to mm10 for any sample. Alternatively: Human ChIP-seq samples were either normalized relative to the spiked-in mouse reads, or to the same number of human reads (read-normalized samples). The normalized bam files were sorted using SAMtools (v1.9, (Danecek et al., 2021)) and converted to bedgraphs using bedtools genomecov (v2.26.0; (Quinlan & Hall, 2010)) and the Integrated Genome Browser (Nicol et al., 2009) was used to visualize these density files. Metagene and density plots were generated with ngs.plot.r v2.41.3 (Shen et al., 2014) or DeepTools v3.5.1 (Ramirez et al., 2016) using a bin size of 10 bp. Plots labeled with "all expressed genes" refer to the 14,704 genes annotated for hg19/GRCh37.p13 by Ensembl v75 (Feb 2014). The bioinformatic analysis was done either by Peter Gallant, Raphael Vidal, or me.

BLISS8-Sequencing analysis

Demultiplexing of BLISS8 samples was based on the condition-specific barcodes using UMI tools (Smith et al., 2017), allowing 1 mismatch in the barcode. The samples were separately mapped to hg19 using Bowtie2 as described above (Langmead & Salzberg, 2012). Biological replicates were merged and collectively processed. Then the samples were filtered against an ENCODE Blacklist file to remove regions of high variance in mappability (Amemiya et al., 2019) using bedtools intersect (Quinlan & Hall, 2010). This allows absolute quantification of double-strand breaks and remove PCR-introduced artifacts. Proximal reads with identical UMI were grouped and deduplicated with UMItools (Smith et al., 2017). Deduplicated reads were normalized by counting the *in situ* AsiSI restriction sites using countBAMInGRange from the R package exomeCopy. Restriction sites (AsiSI) from the 1,123 predicted sites without mapped reads across all conditions in the experiment were dropped. The smallest read number of specific AsiSI reads in a sample was divided by the number of respective reads from each sample. This ratio was then multiplied by the total amount of deduplicated reads. This was followed by randomly subsampling to the calculated number of deduplicated reads. Read density profiles were generated using the R package metagene2 with the assay parameter 'ChIPseq', 150 bp read extension and 50 bins to smoothen the curve. Genes sets were generated from RNA sequencing data using RPKM (top n= 3,954, bottom n= 3,012 expressed genes of SH-EP cells). BLISS8 data was visualized by R studio scripts. The bioinformatic analysis was done by Daniel Solvie.

NanoLC-MS/MS proteomic analysis

Raw MS data files were analyzed with MaxQuant version 1.6.2.2 (Cox & Mann, 2008). Data base search was performed with Andromeda (Cox et al., 2011), which is integrated in the utilized version of MaxQuant. The search was performed against the UniProt human database (June 27, 2018, UP000005640, 73099 entries). Additionally, a database containing common contaminants was used. The search was performed with tryptic cleavage specificity with three allowed miscleavages. Protein identification was under control of the false-discovery rate (FDR; <1% FDR on protein and PSM level). In addition to MaxQuant default settings, the search was performed against following variable modifications: protein n-terminal acetylation, Gln to pyro-Glu formation (n-term. Gln) and oxidation (Met). Carbamidomethyl (Cys) was set as fixed modification. Further data analysis was performed using R script developed in-house. Missing LFQ intensities in the control samples were imputed with values close to the baseline. Data imputation was performed with values from a standard normal distribution with a mean of the 5% quantile of the combined log_{10}-transformed LFQ intensities and a standard deviation of 0.1. For the identification of significantly enriched proteins, median log_2 transformed protein ratio were calculated from the two replicate experiments and boxplot outliers were identified in intensity bins of at least 300 proteins. Log_2 transformed protein ratios of sample versus control with values outside a 1.5x (significance 1) or 3x (significance 2) interquartile range (IQR), respectively, were considered as significantly enriched.

SILAC-based ubiquitin remnant profiling analysis

Raw data files were analyzed using MaxQuant (development version 1.5.2.8) (Cox & Mann, 2008). Parent ion and MS2 spectra were searched against a database containing 96,817 human protein sequences obtained from the UniProtKB (February 2020 release) using Andromeda seach engine (Cox et al., 2011). Spectra were searched with a mass tolerance of 6 ppm in MS mode, 20 ppm in HCD MS2 mode, strict trypsin specificity and allowing up to two miscleavages. Cysteine carbamidomethylation was set as a fixed modification. N-terminal acetylation, oxidation, and N-ethylmaleimide (NEM) were set as variable modifications. For ubiquitylome data analysis, glycine-glycine (GlyGly) modification of lysine was additionally set as a variable modification. Site localization probabilities were determined by MaxQuant using the PTM scoring algorithm as described previously(Cox & Mann, 2008). The dataset was filtered based on posterior error probability (PEP) to arrive at a FDR < 1% estimated using a target-decoy approach (Elias & Gygi, 2007). Di-glycine lysine-modified peptides with a minimum score of 40 and delta score of 6 are reported and used for analysis. Processed data from MaxQuant was analyzed in Rstudio (version 4.1). Proteins or peptided flagged as “reverse”, “only identified by site” or “potential contaminant” were excluded from downstream analysis. Only proteins identified by no less than two peptides and at least one unique peptide were used considered for downstream analysis. Statistical significance was assessed using LIMMA (Smyth, 2004).

Structure prediction using AlphaFold

For 3D structure modelling of USP11 (UniProt: P51784) and TCEAL1 (Uniprot: Q15170) was used the AlphaFold Protein Structure Database (DeepMind, EMBL-EBI). Further, to highlight specificity of complexes in detail the COSMIC[2] web platform was used. Here, fasta files from UniProt entries were taken to run the AlphaFold-Multimer tool (v: 1.0; (Evans et al., 2022)) to predict 3D protein-protein complexes (Jumper et al., 2021; Varadi et al., 2022). For the multimer computations the default pretrained AlphaFold2 algorithm was used. The lowest predicted local distance difference test (pLDDT) scores to indicate prediction accuracy was used. Finally, the highest ranked AlphaFold Multimer prediction of five structures of the input set, sampled from five different model checkpoints, was evaluated using PyMOL (v: 2.5.5).

6 References

Ackermann, S., Cartolano, M., Hero, B., Welte, A., Kahlert, Y., Roderwieser, A., Bartenhagen, C., Walter, E., Gecht, J., Kerschke, L., Volland, R., Menon, R., Heuckmann, J. M., Gartlgruber, M., Hartlieb, S., Henrich, K. O., Okonechnikov, K., Altmuller, J., Nurnberg, P., Lefever, S., de Wilde, B., Sand, F., Ikram, F., Rosswog, C., Fischer, J., Theissen, J., Hertwig, F., Singhi, A. D., Simon, T., Vogel, W., Perner, S., Krug, B., Schmidt, M., Rahmann, S., Achter, V., Lang, U., Vokuhl, C., Ortmann, M., Buttner, R., Eggert, A., Speleman, F., O'Sullivan, R. J., Thomas, R. K., Berthold, F., Vandesompele, J., Schramm, A., Westermann, F., Schulte, J. H., Peifer, M., & Fischer, M. (2018). A mechanistic classification of clinical phenotypes in neuroblastoma. *Science*, *362*(6419), 1165-1170.

Adam, S., Polo, S. E., & Almouzni, G. (2013). Transcription recovery after DNA damage requires chromatin priming by the H3.3 histone chaperone HIRA. *Cell*, *155*(1), 94-106.

Adelman, K., & Lis, J. T. (2012). Promoter-proximal pausing of RNA polymerase II: emerging roles in metazoans. *Nat Rev Genet*, *13*(10), 720-731.

Agarwal, K., Baek, K. H., Jeon, C. J., Miyamoto, K., Ueno, A., & Yoon, H. S. (1991). Stimulation of transcript elongation requires both the zinc finger and RNA polymerase II binding domains of human TFIIS. *Biochemistry*, *30*(31), 7842-7851.

Ahn, S. H., Kim, M., & Buratowski, S. (2004). Phosphorylation of serine 2 within the RNA polymerase II C-terminal domain couples transcription and 3' end processing. *Mol Cell*, *13*(1), 67-76.

Aisa, A., Tan, Y., Li, X., Zhang, D., Shi, Y., & Yuan, Y. (2022). Comprehensive Analysis of the Brain-Expressed X-Link Protein Family in Glioblastoma Multiforme. *Front Oncol*, *12*, 911942.

AJ, C. Q., Bugai, A., & Barboric, M. (2016). Cracking the control of RNA polymerase II elongation by 7SK snRNP and P-TEFb. *Nucleic Acids Res*, *44*(16), 7527-7539.

Akhtar, M. S., Heidemann, M., Tietjen, J. R., Zhang, D. W., Chapman, R. D., Eick, D., & Ansari, A. Z. (2009). TFIIH kinase places bivalent marks on the carboxy-terminal domain of RNA polymerase II. *Mol Cell*, *34*(3), 387-393.

Al-Salihi, M. A., Herhaus, L., Macartney, T., & Sapkota, G. P. (2012). USP11 augments TGFbeta signalling by deubiquitylating ALK5. *Open Biol*, *2*(6), 120063.

Amemiya, H. M., Kundaje, A., & Boyle, A. P. (2019). The ENCODE Blacklist: Identification of Problematic Regions of the Genome. *Sci Rep*, *9*(1), 9354.

Aravind, L., Anantharaman, V., Balaji, S., Babu, M. M., & Iyer, L. M. (2005). The many faces of the helix-turn-helix domain: transcription regulation and beyond. *FEMS Microbiol Rev*, *29*(2), 231-262.

Ardley, H. C., & Robinson, P. A. (2005). E3 ubiquitin ligases. *Essays Biochem*, *41*, 15-30.

Ayer, D. E., Lawrence, Q. A., & Eisenman, R. N. (1995). Mad-Max transcriptional repression is mediated by ternary complex formation with mammalian homologs of yeast repressor Sin3. *Cell*, *80*(5), 767-776.

Baluapuri, A., Hofstetter, J., Dudvarski Stankovic, N., Endres, T., Bhandare, P., Vos, S. M., Adhikari, B., Schwarz, J. D., Narain, A., Vogt, M., Wang, S. Y., Duster, R., Jung, L. A., Vanselow, J. T., Wiegering, A., Geyer, M., Maric, H. M., Gallant, P., Walz, S., Schlosser, A., Cramer, P., Eilers, M., & Wolf, E. (2019). MYC Recruits SPT5 to RNA Polymerase II to Promote Processive Transcription Elongation. *Mol Cell*, *74*(4), 674-687 e611.

Baluapuri, A., Wolf, E., & Eilers, M. (2020). Target gene-independent functions of MYC oncoproteins. *Nat Rev Mol Cell Biol*, *21*(5), 255-267.

Banani, S. F., Lee, H. O., Hyman, A. A., & Rosen, M. K. (2017). Biomolecular condensates: organizers of cellular biochemistry. *Nat Rev Mol Cell Biol*, *18*(5), 285-298.

Beaudenon, S. L., Huacani, M. R., Wang, G., McDonnell, D. P., & Huibregtse, J. M. (1999). Rsp5 ubiquitin-protein ligase mediates DNA damage-induced degradation of the large subunit of RNA polymerase II in Saccharomyces cerevisiae. *Mol Cell Biol*, *19*(10), 6972-6979.

Beaulieu, M. E., Castillo, F., & Soucek, L. (2020). Structural and Biophysical Insights into the Function of the Intrinsically Disordered Myc Oncoprotein. *Cells*, *9*(4).

Bekker-Jensen, D. B., Martinez-Val, A., Steigerwald, S., Ruther, P., Fort, K. L., Arrey, T. N., Harder, A., Makarov, A., & Olsen, J. V. (2020). A Compact Quadrupole-Orbitrap Mass Spectrometer with FAIMS Interface Improves Proteome Coverage in Short LC Gradients. *Mol Cell Proteomics*, *19*(4), 716-729.

Bentley, D. L. (2014). Coupling mRNA processing with transcription in time and space. *Nat Rev Genet*, *15*(3), 163-175.

Berg, A., Kukharenko, O., Scheffner, M., & Peter, C. (2018). Towards a molecular basis of ubiquitin signaling: A dual-scale simulation study of ubiquitin dimers. *PLoS Comput Biol*, *14*(11), e1006589.

Beroukhim, R., Mermel, C. H., Porter, D., Wei, G., Raychaudhuri, S., Donovan, J., Barretina, J., Boehm, J. S., Dobson, J., Urashima, M., Mc Henry, K. T., Pinchback, R. M., Ligon, A. H., Cho, Y. J., Haery, L., Greulich, H., Reich, M., Winckler, W., Lawrence, M. S., Weir, B. A., Tanaka, K. E., Chiang, D. Y., Bass, A. J., Loo, A., Hoffman, C., Prensner, J., Liefeld, T., Gao, Q., Yecies, D., Signoretti, S., Maher, E., Kaye, F. J., Sasaki, H., Tepper, J. E., Fletcher, J. A., Tabernero, J., Baselga, J., Tsao, M. S., Demichelis, F., Rubin, M. A., Janne, P. A., Daly, M. J., Nucera, C., Levine, R. L., Ebert, B. L., Gabriel, S., Rustgi, A. K., Antonescu, C. R., Ladanyi, M., Letai, A., Garraway, L. A., Loda, M., Beer, D. G., True, L. D., Okamoto, A., Pomeroy, S. L., Singer, S., Golub, T. R., Lander, E. S., Getz, G., Sellers, W. R., & Meyerson, M. (2010). The landscape of somatic copy-number alteration across human cancers. *Nature*, *463*(7283), 899-905.

Bian, Y., Song, C., Cheng, K., Dong, M., Wang, F., Huang, J., Sun, D., Wang, L., Ye, M., & Zou, H. (2014). An enzyme assisted RP-RPLC approach for in-depth analysis of human liver phosphoproteome. *J Proteomics*, *96*, 253-262.

Blackwell, T. K., Huang, J., Ma, A., Kretzner, L., Alt, F. W., Eisenman, R. N., & Weintraub, H. (1993). Binding of myc proteins to canonical and noncanonical DNA sequences. *Mol Cell Biol*, *13*(9), 5216-5224.

Blackwood, E. M., & Eisenman, R. N. (1991). Max: a helix-loop-helix zipper protein that forms a sequence-specific DNA-binding complex with Myc. *Science*, *251*(4998), 1211-1217.

Boeva, V., Louis-Brennetot, C., Peltier, A., Durand, S., Pierre-Eugene, C., Raynal, V., Etchevers, H. C., Thomas, S., Lermine, A., Daudigeos-Dubus, E., Geoerger, B., Orth, M. F., Grunewald, T. G. P., Diaz, E., Ducos, B., Surdez, D., Carcaboso, A. M., Medvedeva, I., Deller, T., Combaret, V., Lapouble, E., Pierron, G., Grossetete-Lalami, S., Baulande, S., Schleiermacher, G., Barillot, E., Rohrer, H., Delattre, O., & Janoueix-Lerosey, I. (2017). Heterogeneity of neuroblastoma cell identity defined by transcriptional circuitries. *Nat Genet*, *49*(9), 1408-1413.

Boija, A., Klein, I. A., Sabari, B. R., Dall'Agnese, A., Coffey, E. L., Zamudio, A. V., Li, C. H., Shrinivas, K., Manteiga, J. C., Hannett, N. M., Abraham, B. J., Afeyan, L. K., Guo, Y. E., Rimel, J. K., Fant, C. B., Schuijers, J., Lee, T. I., Taatjes, D. J., & Young, R. A. (2018). Transcription Factors Activate Genes through the Phase-Separation Capacity of Their Activation Domains. *Cell*, *175*(7), 1842-1855 e1816.

Bonifacino, J. S., Dell'Angelica, E. C., & Springer, T. A. (2006). Immunoprecipitation. *Curr Protoc Neurosci*, *Chapter 5*, Unit 5 24.

Bourdeaut, F., Trochet, D., Janoueix-Lerosey, I., Ribeiro, A., Deville, A., Coz, C., Michiels, J. F., Lyonnet, S., Amiel, J., & Delattre, O. (2005). Germline mutations of the paired-like homeobox 2B (PHOX2B) gene in neuroblastoma. *Cancer Lett*, *228*(1-2), 51-58.

Bradford, M. M. (1976). A rapid and sensitive method for the quantitation of microgram quantities of protein utilizing the principle of protein-dye binding. *Anal Biochem*, *72*, 248-254.

Brambati, A., Zardoni, L., Achar, Y. J., Piccini, D., Galanti, L., Colosio, A., Foiani, M., & Liberi, G. (2018). Dormant origins and fork protection mechanisms rescue sister forks arrested by transcription. *Nucleic Acids Res*, *46*(3), 1227-1239.

Brandau, O., Nyakatura, G., Jedele, K. B., Platzer, M., Achatz, H., Ross, M., Murken, J., Rosenthal, A., & Meindl, A. (1998). UHX1 and PCTK1: precise characterisation and localisation within a gene-rich region in Xp11.23 and evaluation as candidate genes for retinal diseases mapped to Xp21.1-p11.2. *Eur J Hum Genet*, *6*(5), 459-466.

Brodeur, G. M., Seeger, R. C., Schwab, M., Varmus, H. E., & Bishop, J. M. (1984). Amplification of N-myc in untreated human neuroblastomas correlates with advanced disease stage. *Science*, *224*(4653), 1121-1124.

Brummelkamp, T. R., Bernards, R., & Agami, R. (2002). A system for stable expression of short interfering RNAs in mammalian cells. *Science*, *296*(5567), 550-553.

Buchel, G., Carstensen, A., Mak, K. Y., Roeschert, I., Leen, E., Sumara, O., Hofstetter, J., Herold, S., Kalb, J., Baluapuri, A., Poon, E., Kwok, C., Chesler, L., Maric, H. M., Rickman, D. S., Wolf, E., Bayliss, R., Walz, S., & Eilers, M. (2017). Association with Aurora-A Controls N-MYC-Dependent Promoter Escape and Pause Release of RNA Polymerase II during the Cell Cycle. *Cell Rep*, *21*(12), 3483-3497.

Buratowski, S. (2009). Progression through the RNA polymerase II CTD cycle. *Mol Cell*, *36*(4), 541-546.

Burger, K., Schlackow, M., & Gullerova, M. (2019). Tyrosine kinase c-Abl couples RNA polymerase II transcription to DNA double-strand breaks. *Nucleic Acids Res*, *47*(7), 3467-3484.

Burkhart, R. A., Peng, Y., Norris, Z. A., Tholey, R. M., Talbott, V. A., Liang, Q., Ai, Y., Miller, K., Lal, S., Cozzitorto, J. A., Witkiewicz, A. K., Yeo, C. J., Gehrmann, M., Napper, A., Winter, J. M., Sawicki, J. A., Zhuang, Z., & Brody, J. R. (2013). Mitoxantrone targets human ubiquitin-specific

peptidase 11 (USP11) and is a potent inhibitor of pancreatic cancer cell survival. *Mol Cancer Res*, *11*(8), 901-911.
Burroughs, A. M., Iyer, L. M., & Aravind, L. (2012). Structure and evolution of ubiquitin and ubiquitin-related domains. *Methods Mol Biol*, *832*, 15-63.
Bywater, M. J., Pearson, R. B., McArthur, G. A., & Hannan, R. D. (2013). Dysregulation of the basal RNA polymerase transcription apparatus in cancer. *Nat Rev Cancer*, *13*(5), 299-314.
Cai, D., Feliciano, D., Dong, P., Flores, E., Gruebele, M., Porat-Shliom, N., Sukenik, S., Liu, Z., & Lippincott-Schwartz, J. (2019). Phase separation of YAP reorganizes genome topology for long-term YAP target gene expression. *Nat Cell Biol*, *21*(12), 1578-1589.
Cappadocia, L., & Lima, C. D. (2018). Ubiquitin-like Protein Conjugation: Structures, Chemistry, and Mechanism. *Chem Rev*, *118*(3), 889-918.
Caron, P., Pankotai, T., Wiegant, W. W., Tollenaere, M. A. X., Furst, A., Bonhomme, C., Helfricht, A., de Groot, A., Pastink, A., Vertegaal, A. C. O., Luijsterburg, M. S., Soutoglou, E., & van Attikum, H. (2019). WWP2 ubiquitylates RNA polymerase II for DNA-PK-dependent transcription arrest and repair at DNA breaks. *Genes Dev*, *33*(11-12), 684-704.
Carroll, P. A., Freie, B. W., Mathsyaraja, H., & Eisenman, R. N. (2018). The MYC transcription factor network: balancing metabolism, proliferation and oncogenesis. *Front Med*, *12*(4), 412-425.
Chao, H. X., Poovey, C. E., Privette, A. A., Grant, G. D., Chao, H. Y., Cook, J. G., & Purvis, J. E. (2017). Orchestration of DNA Damage Checkpoint Dynamics across the Human Cell Cycle. *Cell Syst*, *5*(5), 445-459 e445.
Chapman, H. A., Riese, R. J., & Shi, G. P. (1997). Emerging roles for cysteine proteases in human biology. *Annu Rev Physiol*, *59*, 63-88.
Chatr-Aryamontri, A., van der Sloot, A., & Tyers, M. (2018). At Long Last, a C-Terminal Bookend for the Ubiquitin Code. *Mol Cell*, *70*(4), 568-571.
Chedin, F., & Benham, C. J. (2020). Emerging roles for R-loop structures in the management of topological stress. *J Biol Chem*, *295*(14), 4684-4695.
Chen, E. Y., Tan, C. M., Kou, Y., Duan, Q., Wang, Z., Meirelles, G. V., Clark, N. R., & Ma'ayan, A. (2013). Enrichr: interactive and collaborative HTML5 gene list enrichment analysis tool. *BMC Bioinformatics*, *14*, 128.
Chen, H., Liu, H., & Qing, G. (2018). Targeting oncogenic Myc as a strategy for cancer treatment. *Signal Transduct Target Ther*, *3*, 5.
Chen, Y., Sun, X. X., Sears, R. C., & Dai, M. S. (2019). Writing and erasing MYC ubiquitination and SUMOylation. *Genes Dis*, *6*(4), 359-371.
Chen, Z., Hankey, W., Zhao, Y., Groth, J., Huang, F., Wang, H., Campos, A. R., Huang, J., Roeder, R. G., & Wang, Q. (2021). Transcription recycling assays identify PAF1 as a driver for RNA Pol II recycling. *Nat Commun*, *12*(1), 6318.
Cheung, A. C., & Cramer, P. (2011). Structural basis of RNA polymerase II backtracking, arrest and reactivation. *Nature*, *471*(7337), 249-253.
Chipumuro, E., Marco, E., Christensen, C. L., Kwiatkowski, N., Zhang, T., Hatheway, C. M., Abraham, B. J., Sharma, B., Yeung, C., Altabef, A., Perez-Atayde, A., Wong, K. K., Yuan, G. C., Gray, N. S., Young, R. A., & George, R. E. (2014). CDK7 inhibition suppresses super-enhancer-linked oncogenic transcription in MYCN-driven cancer. *Cell*, *159*(5), 1126-1139.
Cho, W. K., Spille, J. H., Hecht, M., Lee, C., Li, C., Grube, V., & Cisse, II. (2018). Mediator and RNA polymerase II clusters associate in transcription-dependent condensates. *Science*, *361*(6400), 412-415.
Chojnacki, M., Mansour, W., Hameed, D. S., Singh, R. K., El Oualid, F., Rosenzweig, R., Nakasone, M. A., Yu, Z., Glaser, F., Kay, L. E., Fushman, D., Ovaa, H., & Glickman, M. H. (2017). Polyubiquitin-Photoactivatable Crosslinking Reagents for Mapping Ubiquitin Interactome Identify Rpn1 as a Proteasome Ubiquitin-Associating Subunit. *Cell Chem Biol*, *24*(4), 443-457 e446.
Choudhary, C., Kumar, C., Gnad, F., Nielsen, M. L., Rehman, M., Walther, T. C., Olsen, J. V., & Mann, M. (2009). Lysine acetylation targets protein complexes and co-regulates major cellular functions. *Science*, *325*(5942), 834-840.
Churchman, L. S., & Weissman, J. S. (2011). Nascent transcript sequencing visualizes transcription at nucleotide resolution. *Nature*, *469*(7330), 368-373.
Clague, M. J., Heride, C., & Urbe, S. (2015). The demographics of the ubiquitin system. *Trends Cell Biol*, *25*(7), 417-426.
Clague, M. J., & Urbe, S. (2010). Ubiquitin: same molecule, different degradation pathways. *Cell*, *143*(5), 682-685.

Clague, M. J., Urbe, S., & Komander, D. (2019). Breaking the chains: deubiquitylating enzyme specificity begets function. *Nat Rev Mol Cell Biol*, *20*(6), 338-352.
Conacci-Sorrell, M., McFerrin, L., & Eisenman, R. N. (2014). An overview of MYC and its interactome. *Cold Spring Harb Perspect Med*, *4*(1), a014357.
Conaway, R. C., & Conaway, J. W. (2019). The hunt for RNA polymerase II elongation factors: a historical perspective. *Nat Struct Mol Biol*, *26*(9), 771-776.
Connelly, S., & Manley, J. L. (1988). A functional mRNA polyadenylation signal is required for transcription termination by RNA polymerase II. *Genes Dev*, *2*(4), 440-452.
Core, L., & Adelman, K. (2019). Promoter-proximal pausing of RNA polymerase II: a nexus of gene regulation. *Genes Dev*, *33*(15-16), 960-982.
Cossa, G., Parua, P. K., Eilers, M., & Fisher, R. P. (2021). Protein phosphatases in the RNAPII transcription cycle: erasers, sculptors, gatekeepers, and potential drug targets. *Genes Dev*, *35*(9-10), 658-676.
Cowell, I. G., Casement, J. W., & Austin, C. A. (2023). To Break or Not to Break: The Role of TOP2B in Transcription. *Int J Mol Sci*, *24*(19).
Cox, J., & Mann, M. (2008). MaxQuant enables high peptide identification rates, individualized p.p.b.-range mass accuracies and proteome-wide protein quantification. *Nat Biotechnol*, *26*(12), 1367-1372.
Cox, J., Neuhauser, N., Michalski, A., Scheltema, R. A., Olsen, J. V., & Mann, M. (2011). Andromeda: a peptide search engine integrated into the MaxQuant environment. *J Proteome Res*, *10*(4), 1794-1805.
Cramer, P., Armache, K. J., Baumli, S., Benkert, S., Brueckner, F., Buchen, C., Damsma, G. E., Dengl, S., Geiger, S. R., Jasiak, A. J., Jawhari, A., Jennebach, S., Kamenski, T., Kettenberger, H., Kuhn, C. D., Lehmann, E., Leike, K., Sydow, J. F., & Vannini, A. (2008). Structure of eukaryotic RNA polymerases. *Annu Rev Biophys*, *37*, 337-352.
Cramer, P., Bushnell, D. A., Fu, J., Gnatt, A. L., Maier-Davis, B., Thompson, N. E., Burgess, R. R., Edwards, A. M., David, P. R., & Kornberg, R. D. (2000). Architecture of RNA polymerase II and implications for the transcription mechanism. *Science*, *288*(5466), 640-649.
Crick, F. (1970). Central dogma of molecular biology. *Nature*, *227*(5258), 561-563.
Crossley, M. P., Bocek, M., & Cimprich, K. A. (2019). R-Loops as Cellular Regulators and Genomic Threats. *Mol Cell*, *73*(3), 398-411.
Cruz-Ruiz, S., Uriostegui-Arcos, M., & Zurita, M. (2021). The transcriptional stress response and its implications in cancer treatment. *Biochim Biophys Acta Rev Cancer*, *1876*(2), 188620.
Czudnochowski, N., Bosken, C. A., & Geyer, M. (2012). Serine-7 but not serine-5 phosphorylation primes RNA polymerase II CTD for P-TEFb recognition. *Nat Commun*, *3*, 842.
Dalla-Favera, R., Bregni, M., Erikson, J., Patterson, D., Gallo, R. C., & Croce, C. M. (1982). Human c-myc onc gene is located on the region of chromosome 8 that is translocated in Burkitt lymphoma cells. *Proc Natl Acad Sci U S A*, *79*(24), 7824-7827.
Dalla-Favera, R., Westin, E., Gelmann, E. P., Martinotti, S., Bregni, M., Wong-Staal, F., & Gallo, R. C. (1983). The human onc gene c-myc: structure, expression, and amplification in the human promyelocytic leukemia cell line HL-60. *Haematol Blood Transfus*, *28*, 247-254.
Damgaard, R. B. (2021). The ubiquitin system: from cell signalling to disease biology and new therapeutic opportunities. *Cell Death Differ*, *28*(2), 423-426.
Danecek, P., Bonfield, J. K., Liddle, J., Marshall, J., Ohan, V., Pollard, M. O., Whitwham, A., Keane, T., McCarthy, S. A., Davies, R. M., & Li, H. (2021). Twelve years of SAMtools and BCFtools. *Gigascience*, *10*(2).
Dang, C. V. (2012). MYC on the path to cancer. *Cell*, *149*(1), 22-35.
Dauch, D., Rudalska, R., Cossa, G., Nault, J. C., Kang, T. W., Wuestefeld, T., Hohmeyer, A., Imbeaud, S., Yevsa, T., Hoenicke, L., Pantsar, T., Bozko, P., Malek, N. P., Longerich, T., Laufer, S., Poso, A., Zucman-Rossi, J., Eilers, M., & Zender, L. (2016). A MYC-aurora kinase A protein complex represents an actionable drug target in p53-altered liver cancer. *Nat Med*, *22*(7), 744-753.
Daulny, A., Geng, F., Muratani, M., Geisinger, J. M., Salghetti, S. E., & Tansey, W. P. (2008). Modulation of RNA polymerase II subunit composition by ubiquitylation. *Proc Natl Acad Sci U S A*, *105*(50), 19649-19654.
de Bono, J. S., Oudard, S., Ozguroglu, M., Hansen, S., Machiels, J. P., Kocak, I., Gravis, G., Bodrogi, I., Mackenzie, M. J., Shen, L., Roessner, M., Gupta, S., Sartor, A. O., & Investigators, T. (2010). Prednisone plus cabazitaxel or mitoxantrone for metastatic castration-resistant prostate cancer progressing after docetaxel treatment: a randomised open-label trial. *Lancet*, *376*(9747), 1147-1154.

de la Pena, A. H., Goodall, E. A., Gates, S. N., Lander, G. C., & Martin, A. (2018). Substrate-engaged 26S proteasome structures reveal mechanisms for ATP-hydrolysis-driven translocation. *Science*, *362*(6418).

Deng, L., Meng, T., Chen, L., Wei, W., & Wang, P. (2020). The role of ubiquitination in tumorigenesis and targeted drug discovery. *Signal Transduct Target Ther*, *5*(1), 11.

Deng, T., Yan, G., Song, X., Xie, L., Zhou, Y., Li, J., Hu, X., Li, Z., Hu, J., Zhang, Y., Zhang, H., Sun, Y., Feng, P., Wei, D., Hu, B., Liu, J., Tan, W., & Ye, M. (2018). Deubiquitylation and stabilization of p21 by USP11 is critical for cell-cycle progression and DNA damage responses. *Proc Natl Acad Sci U S A*, *115*(18), 4678-4683.

Dephoure, N., Zhou, C., Villen, J., Beausoleil, S. A., Bakalarski, C. E., Elledge, S. J., & Gygi, S. P. (2008). A quantitative atlas of mitotic phosphorylation. *Proc Natl Acad Sci U S A*, *105*(31), 10762-10767.

Dieci, G., & Sentenac, A. (2003). Detours and shortcuts to transcription reinitiation. *Trends Biochem Sci*, *28*(4), 202-209.

Diefenbacher, M. E., Chakraborty, A., Blake, S. M., Mitter, R., Popov, N., Eilers, M., & Behrens, A. (2015). Usp28 counteracts Fbw7 in intestinal homeostasis and cancer. *Cancer Res*, *75*(7), 1181-1186.

Dikic, I., & Schulman, B. A. (2022). An expanded lexicon for the ubiquitin code. *Nat Rev Mol Cell Biol*.

Dong, Y., Zhang, S., Wu, Z., Li, X., Wang, W. L., Zhu, Y., Stoilova-McPhie, S., Lu, Y., Finley, D., & Mao, Y. (2019). Cryo-EM structures and dynamics of substrate-engaged human 26S proteasome. *Nature*, *565*(7737), 49-55.

Dou, Q. P. (2014). *Resistance to Proteasome Inhibitors in Cancer : Molecular Mechanisms and Strategies to Overcome Resistance* (1st ed.). Springer International Publishing : Imprint: Springer,.

Durbin, A. D., Zimmerman, M. W., Dharia, N. V., Abraham, B. J., Iniguez, A. B., Weichert-Leahey, N., He, S., Krill-Burger, J. M., Root, D. E., Vazquez, F., Tsherniak, A., Hahn, W. C., Golub, T. R., Young, R. A., Look, A. T., & Stegmaier, K. (2018). Selective gene dependencies in MYCN-amplified neuroblastoma include the core transcriptional regulatory circuitry. *Nat Genet*, *50*(9), 1240-1246.

Dutta, A., Babbarwal, V., Fu, J., Brunke-Reese, D., Libert, D. M., Willis, J., & Reese, J. C. (2015). Ccr4-Not and TFIIS Function Cooperatively To Rescue Arrested RNA Polymerase II. *Mol Cell Biol*, *35*(11), 1915-1925.

Eaton, J. D., & West, S. (2020). Termination of Transcription by RNA Polymerase II: BOOM! *Trends Genet*, *36*(9), 664-675.

Egloff, S. (2021). CDK9 keeps RNA polymerase II on track. *Cell Mol Life Sci*, *78*(14), 5543-5567.

Ehara, H., Yokoyama, T., Shigematsu, H., Yokoyama, S., Shirouzu, M., & Sekine, S. I. (2017). Structure of the complete elongation complex of RNA polymerase II with basal factors. *Science*, *357*(6354), 921-924.

Eick, D., & Geyer, M. (2013). The RNA polymerase II carboxy-terminal domain (CTD) code. *Chem Rev*, *113*(11), 8456-8490.

Eilers, M., Schirm, S., & Bishop, J. M. (1991). The MYC protein activates transcription of the alpha-prothymosin gene. *EMBO J*, *10*(1), 133-141.

Elias, J. E., & Gygi, S. P. (2007). Target-decoy search strategy for increased confidence in large-scale protein identifications by mass spectrometry. *Nat Methods*, *4*(3), 207-214.

Elliott, P. R., Liu, H., Pastok, M. W., Grossmann, G. J., Rigden, D. J., Clague, M. J., Urbe, S., & Barsukov, I. L. (2011). Structural variability of the ubiquitin specific protease DUSP-UBL double domains. *FEBS Lett*, *585*(21), 3385-3390.

Endres, T., Solvie, D., Heidelberger, J. B., Andrioletti, V., Baluapuri, A., Ade, C. P., Muhar, M., Eilers, U., Vos, S. M., Cramer, P., Zuber, J., Beli, P., Popov, N., Wolf, E., Gallant, P., & Eilers, M. (2021). Ubiquitylation of MYC couples transcription elongation with double-strand break repair at active promoters. *Mol Cell*, *81*(4), 830-844 e813.

Esnault, C., Ghavi-Helm, Y., Brun, S., Soutourina, J., Van Berkum, N., Boschiero, C., Holstege, F., & Werner, M. (2008). Mediator-dependent recruitment of TFIIH modules in preinitiation complex. *Mol Cell*, *31*(3), 337-346.

Estavoyer, B., Messmer, C., Echbicheb, M., Rudd, C. E., Milot, E., & Affar, E. B. (2022). Mechanisms orchestrating the enzymatic activity and cellular functions of deubiquitinases. *J Biol Chem*, *298*(8), 102198.

Eun, C., Ortiz-Sanchez, J. M., Da, L., Wang, D., & McCammon, J. A. (2014). Molecular dynamics simulation study of conformational changes of transcription factor TFIIS during RNA polymerase II transcriptional arrest and reactivation. *PLoS One*, *9*(5), e97975.

Evans, R., O'Neill, M., Pritzel, A., Antropova, N., Senior, A., Green, T., Žídek, A., Bates, R., Blackwell, S., Yim, J., Ronneberger, O., Bodenstein, S., Zielinski, M., Bridgland, A., Potapenko, A., Cowie,

A., Tunyasuvunakool, K., Jain, R., Clancy, E., Kohli, P., Jumper, J., & Hassabis, D. (2022). Protein complex prediction with AlphaFold-Multimer. *bioRxiv*, 2021.2010.2004.463034.
Faesen, A. C., Luna-Vargas, M. P., Geurink, P. P., Clerici, M., Merkx, R., van Dijk, W. J., Hameed, D. S., El Oualid, F., Ovaa, H., & Sixma, T. K. (2011). The differential modulation of USP activity by internal regulatory domains, interactors and eight ubiquitin chain types. *Chem Biol*, *18*(12), 1550-1561.
Farnung, L., Ochmann, M., Engeholm, M., & Cramer, P. (2021). Structural basis of nucleosome transcription mediated by Chd1 and FACT. *Nat Struct Mol Biol*, *28*(4), 382-387.
Farnung, L., & Vos, S. M. (2022). Assembly of RNA polymerase II transcription initiation complexes. *Curr Opin Struct Biol*, *73*, 102335.
Farrell, A. S., & Sears, R. C. (2014). MYC degradation. *Cold Spring Harb Perspect Med*, *4*(3).
Fellmann, C., Hoffmann, T., Sridhar, V., Hopfgartner, B., Muhar, M., Roth, M., Lai, D. Y., Barbosa, I. A., Kwon, J. S., Guan, Y., Sinha, N., & Zuber, J. (2013). An optimized microRNA backbone for effective single-copy RNAi. *Cell Rep*, *5*(6), 1704-1713.
Feng, P., Li, L., Dai, J., Zhou, L., Liu, J., Zhao, J., Li, X., Ling, N., Qiu, S., Zhang, L., Xie, T., Chen, Y., Donovan, M. J., Peng, T., Song, J., & Ye, M. (2021). The regulation of NONO by USP11 via deubiquitination is linked to the proliferation of melanoma cells. *J Cell Mol Med*, *25*(3), 1507-1517.
Fousteri, M., & Mullenders, L. H. (2008). Transcription-coupled nucleotide excision repair in mammalian cells: molecular mechanisms and biological effects. *Cell Res*, *18*(1), 73-84.
Francia, S., Cabrini, M., Matti, V., Oldani, A., & d'Adda di Fagagna, F. (2016). DICER, DROSHA and DNA damage response RNAs are necessary for the secondary recruitment of DNA damage response factors. *J Cell Sci*, *129*(7), 1468-1476.
Freese, N. H., Norris, D. C., & Loraine, A. E. (2016). Integrated genome browser: visual analytics platform for genomics. *Bioinformatics*, *32*(14), 2089-2095.
Friedman, D. N., & Henderson, T. O. (2018). Late Effects and Survivorship Issues in Patients with Neuroblastoma. *Children (Basel)*, *5*(8).
Fulzele, A., & Bennett, E. J. (2018). Ubiquitin diGLY Proteomics as an Approach to Identify and Quantify the Ubiquitin-Modified Proteome. *Methods Mol Biol*, *1844*, 363-384.
Gaillard, H., & Aguilera, A. (2016). Transcription as a Threat to Genome Integrity. *Annu Rev Biochem*, *85*, 291-317.
Gajos, M., Jasnovidova, O., van Bommel, A., Freier, S., Vingron, M., & Mayer, A. (2021). Conserved DNA sequence features underlie pervasive RNA polymerase pausing. *Nucleic Acids Res*, *49*(8), 4402-4420.
Galburt, E. A., Grill, S. W., Wiedmann, A., Lubkowska, L., Choy, J., Nogales, E., Kashlev, M., & Bustamante, C. (2007). Backtracking determines the force sensitivity of RNAP II in a factor-dependent manner. *Nature*, *446*(7137), 820-823.
Garcia-Rodriguez, N., Wong, R. P., & Ulrich, H. D. (2016). Functions of Ubiquitin and SUMO in DNA Replication and Replication Stress. *Front Genet*, *7*, 87.
Gartlgruber, M., Sharma, A. K., Quintero, A., Dreidax, D., Jansky, S., Park, Y. G., Kreth, S., Meder, J., Doncevic, D., Saary, P., Toprak, U. H., Ishaque, N., Afanasyeva, E., Wecht, E., Koster, J., Versteeg, R., Grunewald, T. G. P., Jones, D. T. W., Pfister, S. M., Henrich, K. O., van Nes, J., Herrmann, C., & Westermann, F. (2021). Super enhancers define regulatory subtypes and cell identity in neuroblastoma. *Nat Cancer*, *2*(1), 114-128.
Georges, A., Marcon, E., Greenblatt, J., & Frappier, L. (2018). Identification and Characterization of USP7 Targets in Cancer Cells. *Sci Rep*, *8*(1), 15833.
Ghavi-Helm, Y., Michaut, M., Acker, J., Aude, J. C., Thuriaux, P., Werner, M., & Soutourina, J. (2008). Genome-wide location analysis reveals a role of TFIIS in RNA polymerase III transcription. *Genes Dev*, *22*(14), 1934-1947.
Gilmour, D. S., & Lis, J. T. (1985). In vivo interactions of RNA polymerase II with genes of Drosophila melanogaster. *Mol Cell Biol*, *5*(8), 2009-2018.
Ginno, P. A., Lim, Y. W., Lott, P. L., Korf, I., & Chedin, F. (2013). GC skew at the 5' and 3' ends of human genes links R-loop formation to epigenetic regulation and transcription termination. *Genome Res*, *23*(10), 1590-1600.
Glover-Cutter, K., Larochelle, S., Erickson, B., Zhang, C., Shokat, K., Fisher, R. P., & Bentley, D. L. (2009). TFIIH-associated Cdk7 kinase functions in phosphorylation of C-terminal domain Ser7 residues, promoter-proximal pausing, and termination by RNA polymerase II. *Mol Cell Biol*, *29*(20), 5455-5464.
Gorthi, A., Romero, J. C., Loranc, E., Cao, L., Lawrence, L. A., Goodale, E., Iniguez, A. B., Bernard, X., Masamsetti, V. P., Roston, S., Lawlor, E. R., Toretsky, J. A., Stegmaier, K., Lessnick, S. L., Chen,

Y., & Bishop, A. J. R. (2018). EWS-FLI1 increases transcription to cause R-loops and block BRCA1 repair in Ewing sarcoma. *Nature*, *555*(7696), 387-391.
Goswami, I., Sandlesh, P., Stablewski, A., Toshkov, I., Safina, A. F., Magnitov, M., Wang, J., & Gurova, K. (2022). FACT maintains nucleosomes during transcription and stem cell viability in adult mice. *EMBO Rep*, *23*(4), e53684.
Greenberg, R. A., Sobhian, B., Pathania, S., Cantor, S. B., Nakatani, Y., & Livingston, D. M. (2006). Multifactorial contributions to an acute DNA damage response by BRCA1/BARD1-containing complexes. *Genes Dev*, *20*(1), 34-46.
Gregersen, L. H., & Svejstrup, J. Q. (2018). The Cellular Response to Transcription-Blocking DNA Damage. *Trends Biochem Sci*, *43*(5), 327-341.
Gregory, M. A., & Hann, S. R. (2000). c-Myc proteolysis by the ubiquitin-proteasome pathway: stabilization of c-Myc in Burkitt's lymphoma cells. *Mol Cell Biol*, *20*(7), 2423-2435.
Gressel, S., Schwalb, B., Decker, T. M., Qin, W., Leonhardt, H., Eick, D., & Cramer, P. (2017). CDK9-dependent RNA polymerase II pausing controls transcription initiation. *Elife*, *6*.
Grou, C. P., Pinto, M. P., Mendes, A. V., Domingues, P., & Azevedo, J. E. (2015). The de novo synthesis of ubiquitin: identification of deubiquitinases acting on ubiquitin precursors. *Sci Rep*, *5*, 12836.
Grumati, P., & Dikic, I. (2018). Ubiquitin signaling and autophagy. *J Biol Chem*, *293*(15), 5404-5413.
Grummt, I. (1999). Regulation of mammalian ribosomal gene transcription by RNA polymerase I. *Prog Nucleic Acid Res Mol Biol*, *62*, 109-154.
Guccione, E., Martinato, F., Finocchiaro, G., Luzi, L., Tizzoni, L., Dall' Olio, V., Zardo, G., Nervi, C., Bernard, L., & Amati, B. (2006). Myc-binding-site recognition in the human genome is determined by chromatin context. *Nat Cell Biol*, *8*(7), 764-770.
Guo, C., Che, Z., Yue, J., Xie, P., Hao, S., Xie, W., Luo, Z., & Lin, C. (2020). ENL initiates multivalent phase separation of the super elongation complex (SEC) in controlling rapid transcriptional activation. *Sci Adv*, *6*(14), eaay4858.
Guo, J., Li, T., Schipper, J., Nilson, K. A., Fordjour, F. K., Cooper, J. J., Gordan, R., & Price, D. H. (2014). Sequence specificity incompletely defines the genome-wide occupancy of Myc. *Genome Biol*, *15*(10), 482.
Haakonsen, D. L., & Rape, M. (2019). Branching Out: Improved Signaling by Heterotypic Ubiquitin Chains. *Trends Cell Biol*, *29*(9), 704-716.
Haas, A. L., & Rose, I. A. (1982). The mechanism of ubiquitin activating enzyme. A kinetic and equilibrium analysis. *J Biol Chem*, *257*(17), 10329-10337.
Hanahan, D. (2022). Hallmarks of Cancer: New Dimensions. *Cancer Discov*, *12*(1), 31-46.
Hanahan, D., & Weinberg, R. A. (2011). Hallmarks of cancer: the next generation. *Cell*, *144*(5), 646-674.
Hanzelmann, P., Schafer, A., Voller, D., & Schindelin, H. (2012). Structural insights into functional modes of proteins involved in ubiquitin family pathways. *Methods Mol Biol*, *832*, 547-576.
Harper, J. W., & Schulman, B. A. (2006). Structural complexity in ubiquitin recognition. *Cell*, *124*(6), 1133-1136.
Harper, S., Gratton, H. E., Cornaciu, I., Oberer, M., Scott, D. J., Emsley, J., & Dreveny, I. (2014). Structure and catalytic regulatory function of ubiquitin specific protease 11 N-terminal and ubiquitin-like domains. *Biochemistry*, *53*(18), 2966-2978.
Harreman, M., Taschner, M., Sigurdsson, S., Anindya, R., Reid, J., Somesh, B., Kong, S. E., Banks, C. A., Conaway, R. C., Conaway, J. W., & Svejstrup, J. Q. (2009). Distinct ubiquitin ligases act sequentially for RNA polymerase II polyubiquitylation. *Proc Natl Acad Sci U S A*, *106*(49), 20705-20710.
Hatchi, E., Skourti-Stathaki, K., Ventz, S., Pinello, L., Yen, A., Kamieniarz-Gdula, K., Dimitrov, S., Pathania, S., McKinney, K. M., Eaton, M. L., Kellis, M., Hill, S. J., Parmigiani, G., Proudfoot, N. J., & Livingston, D. M. (2015). BRCA1 recruitment to transcriptional pause sites is required for R-loop-driven DNA damage repair. *Mol Cell*, *57*(4), 636-647.
Hayward, W. S., Neel, B. G., & Astrin, S. M. (1981). Activation of a cellular onc gene by promoter insertion in ALV-induced lymphoid leukosis. *Nature*, *290*(5806), 475-480.
He, J., Zhu, Q., Wani, G., Sharma, N., Han, C., Qian, J., Pentz, K., Wang, Q. E., & Wani, A. A. (2014). Ubiquitin-specific protease 7 regulates nucleotide excision repair through deubiquitinating XPC protein and preventing XPC protein from undergoing ultraviolet light-induced and VCP/p97 protein-regulated proteolysis. *J Biol Chem*, *289*(39), 27278-27289.
He, M., Zhou, Z., Shah, A. A., Zou, H., Tao, J., Chen, Q., & Wan, Y. (2016). The emerging role of deubiquitinating enzymes in genomic integrity, diseases, and therapeutics. *Cell Biosci*, *6*, 62.
Heidelberger, J. B., Voigt, A., Borisova, M. E., Petrosino, G., Ruf, S., Wagner, S. A., & Beli, P. (2018). Proteomic profiling of VCP substrates links VCP to K6-linked ubiquitylation and c-Myc function. *EMBO Rep*, *19*(4).

Hein, M. Y., Hubner, N. C., Poser, I., Cox, J., Nagaraj, N., Toyoda, Y., Gak, I. A., Weisswange, I., Mansfeld, J., Buchholz, F., Hyman, A. A., & Mann, M. (2015). A human interactome in three quantitative dimensions organized by stoichiometries and abundances. *Cell*, *163*(3), 712-723.

Helander, S., Montecchio, M., Pilstal, R., Su, Y., Kuruvilla, J., Elven, M., Ziauddin, J. M. E., Anandapadamanaban, M., Cristobal, S., Lundstrom, P., Sears, R. C., Wallner, B., & Sunnerhagen, M. (2015). Pre-Anchoring of Pin1 to Unphosphorylated c-Myc in a Fuzzy Complex Regulates c-Myc Activity. *Structure*, *23*(12), 2267-2279.

Henning, N. J., Boike, L., Spradlin, J. N., Ward, C. C., Liu, G., Zhang, E., Belcher, B. P., Brittain, S. M., Hesse, M. J., Dovala, D., McGregor, L. M., Valdez Misiolek, R., Plasschaert, L. W., Rowlands, D. J., Wang, F., Frank, A. O., Fuller, D., Estes, A. R., Randal, K. L., Panidapu, A., McKenna, J. M., Tallarico, J. A., Schirle, M., & Nomura, D. K. (2022). Deubiquitinase-targeting chimeras for targeted protein stabilization. *Nat Chem Biol*, *18*(4), 412-421.

Herhaus, L., & Dikic, I. (2015). Expanding the ubiquitin code through post-translational modification. *EMBO Rep*, *16*(9), 1071-1083.

Hernandez, G., Ramirez, M. J., Minguillon, J., Quiles, P., Ruiz de Garibay, G., Aza-Carmona, M., Bogliolo, M., Pujol, R., Prados-Carvajal, R., Fernandez, J., Garcia, N., Lopez, A., Gutierrez-Enriquez, S., Diez, O., Benitez, J., Salinas, M., Teule, A., Brunet, J., Radice, P., Peterlongo, P., Schindler, D., Huertas, P., Puente, X. S., Lazaro, C., Pujana, M. A., & Surralles, J. (2018). Decapping protein EDC4 regulates DNA repair and phenocopies BRCA1. *Nat Commun*, *9*(1), 967.

Herold, S., Kalb, J., Buchel, G., Ade, C. P., Baluapuri, A., Xu, J., Koster, J., Solvie, D., Carstensen, A., Klotz, C., Rodewald, S., Schulein-Volk, C., Dobbelstein, M., Wolf, E., Molenaar, J., Versteeg, R., Walz, S., & Eilers, M. (2019). Recruitment of BRCA1 limits MYCN-driven accumulation of stalled RNA polymerase. *Nature*, *567*(7749), 545-549.

Hershko, A., & Ciechanover, A. (1998). The ubiquitin system. *Annu Rev Biochem*, *67*, 425-479.

Hnisz, D., Shrinivas, K., Young, R. A., Chakraborty, A. K., & Sharp, P. A. (2017). A Phase Separation Model for Transcriptional Control. *Cell*, *169*(1), 13-23.

Hochstrasser, M. (2009). Origin and function of ubiquitin-like proteins. *Nature*, *458*(7237), 422-429.

Hsieh, F. K., Kulaeva, O. I., Patel, S. S., Dyer, P. N., Luger, K., Reinberg, D., & Studitsky, V. M. (2013). Histone chaperone FACT action during transcription through chromatin by RNA polymerase II. *Proc Natl Acad Sci U S A*, *110*(19), 7654-7659.

Hu, M., Li, P., Li, M., Li, W., Yao, T., Wu, J. W., Gu, W., Cohen, R. E., & Shi, Y. (2002). Crystal structure of a UBP-family deubiquitinating enzyme in isolation and in complex with ubiquitin aldehyde. *Cell*, *111*(7), 1041-1054.

Huang, C. H., Lujambio, A., Zuber, J., Tschaharganeh, D. F., Doran, M. G., Evans, M. J., Kitzing, T., Zhu, N., de Stanchina, E., Sawyers, C. L., Armstrong, S. A., Lewis, J. S., Sherr, C. J., & Lowe, S. W. (2014). CDK9-mediated transcription elongation is required for MYC addiction in hepatocellular carcinoma. *Genes Dev*, *28*(16), 1800-1814.

Huang, M., & Weiss, W. A. (2013). Neuroblastoma and MYCN. *Cold Spring Harb Perspect Med*, *3*(10), a014415.

Huber, K. (2006). The sympathoadrenal cell lineage: specification, diversification, and new perspectives. *Dev Biol*, *298*(2), 335-343.

Huibregtse, J. M., Yang, J. C., & Beaudenon, S. L. (1997). The large subunit of RNA polymerase II is a substrate of the Rsp5 ubiquitin-protein ligase. *Proc Natl Acad Sci U S A*, *94*(8), 3656-3661.

Hurley, J. H., Lee, S., & Prag, G. (2006). Ubiquitin-binding domains. *Biochem J*, *399*(3), 361-372.

Hurlin, P. J., Steingrimsson, E., Copeland, N. G., Jenkins, N. A., & Eisenman, R. N. (1999). Mga, a dual-specificity transcription factor that interacts with Max and contains a T-domain DNA-binding motif. *EMBO J*, *18*(24), 7019-7028.

Husnjak, K., & Dikic, I. (2012). Ubiquitin-binding proteins: decoders of ubiquitin-mediated cellular functions. *Annu Rev Biochem*, *81*, 291-322.

Huttlin, E. L., Bruckner, R. J., Navarrete-Perea, J., Cannon, J. R., Baltier, K., Gebreab, F., Gygi, M. P., Thornock, A., Zarraga, G., Tam, S., Szpyt, J., Gassaway, B. M., Panov, A., Parzen, H., Fu, S., Golbazi, A., Maenpaa, E., Stricker, K., Guha Thakurta, S., Zhang, T., Rad, R., Pan, J., Nusinow, D. P., Paulo, J. A., Schweppe, D. K., Vaites, L. P., Harper, J. W., & Gygi, S. P. (2021). Dual proteome-scale networks reveal cell-specific remodeling of the human interactome. *Cell*, *184*(11), 3022-3040 e3028.

Hwang, C. S., Shemorry, A., & Varshavsky, A. (2010). N-terminal acetylation of cellular proteins creates specific degradation signals. *Science*, *327*(5968), 973-977.

Iannelli, F., Galbiati, A., Capozzo, I., Nguyen, Q., Magnuson, B., Michelini, F., D'Alessandro, G., Cabrini, M., Roncador, M., Francia, S., Crosetto, N., Ljungman, M., Carninci, P., & d'Adda di Fagagna, F.

(2017). A damaged genome's transcriptional landscape through multilayered expression profiling around in situ-mapped DNA double-strand breaks. *Nat Commun*, *8*, 15656.

Ideguchi, H., Ueda, A., Tanaka, M., Yang, J., Tsuji, T., Ohno, S., Hagiwara, E., Aoki, A., & Ishigatsubo, Y. (2002). Structural and functional characterization of the USP11 deubiquitinating enzyme, which interacts with the RanGTP-associated protein RanBPM. *Biochem J*, *367*(Pt 1), 87-95.

Irwin, M. S., Naranjo, A., Zhang, F. F., Cohn, S. L., London, W. B., Gastier-Foster, J. M., Ramirez, N. C., Pfau, R., Reshmi, S., Wagner, E., Nuchtern, J., Asgharzadeh, S., Shimada, H., Maris, J. M., Bagatell, R., Park, J. R., & Hogarty, M. D. (2021). Revised Neuroblastoma Risk Classification System: A Report From the Children's Oncology Group. *J Clin Oncol*, *39*(29), 3229-3241.

Ishida, H., & Kono, H. (2021). Torsional stress can regulate the unwrapping of two outer half superhelical turns of nucleosomal DNA. *Proc Natl Acad Sci U S A*, *118*(7).

Jackson, S. P., & Durocher, D. (2013). Regulation of DNA damage responses by ubiquitin and SUMO. *Mol Cell*, *49*(5), 795-807.

Jaenicke, L. A., von Eyss, B., Carstensen, A., Wolf, E., Xu, W., Greifenberg, A. K., Geyer, M., Eilers, M., & Popov, N. (2016). Ubiquitin-Dependent Turnover of MYC Antagonizes MYC/PAF1C Complex Accumulation to Drive Transcriptional Elongation. *Mol Cell*, *61*(1), 54-67.

James, N. D., Sydes, M. R., Clarke, N. W., Mason, M. D., Dearnaley, D. P., Spears, M. R., Ritchie, A. W., Parker, C. C., Russell, J. M., Attard, G., de Bono, J., Cross, W., Jones, R. J., Thalmann, G., Amos, C., Matheson, D., Millman, R., Alzouebi, M., Beesley, S., Birtle, A. J., Brock, S., Cathomas, R., Chakraborti, P., Chowdhury, S., Cook, A., Elliott, T., Gale, J., Gibbs, S., Graham, J. D., Hetherington, J., Hughes, R., Laing, R., McKinna, F., McLaren, D. B., O'Sullivan, J. M., Parikh, O., Peedell, C., Protheroe, A., Robinson, A. J., Srihari, N., Srinivasan, R., Staffurth, J., Sundar, S., Tolan, S., Tsang, D., Wagstaff, J., Parmar, M. K., & investigators, S. (2016). Addition of docetaxel, zoledronic acid, or both to first-line long-term hormone therapy in prostate cancer (STAMPEDE): survival results from an adaptive, multiarm, multistage, platform randomised controlled trial. *Lancet*, *387*(10024), 1163-1177.

Jeziorska, D. M., Jordan, K. W., & Vance, K. W. (2009). A systems biology approach to understanding cis-regulatory module function. *Semin Cell Dev Biol*, *20*(7), 856-862.

Jin, Q., Gutierrez Diaz, B., Pieters, T., Zhou, Y., Narang, S., Fijalkwoski, I., Borin, C., Van Laere, J., Payton, M., Cho, B. K., Han, C., Sun, L., Serafin, V., Yacu, G., Von Loocke, W., Basso, G., Veltri, G., Dreveny, I., Ben-Sahra, I., Goo, Y. A., Safgren, S. L., Tsai, Y. C., Bornhauser, B., Suraneni, P. K., Gaspar-Maia, A., Kandela, I., Van Vlierberghe, P., Crispino, J. D., Tsirigos, A., & Ntziachristos, P. (2022). Oncogenic deubiquitination controls tyrosine kinase signaling and therapy response in acute lymphoblastic leukemia. *Sci Adv*, *8*(49), eabq8437.

Johnsen, J. I., Dyberg, C., & Wickstrom, M. (2019). Neuroblastoma-A Neural Crest Derived Embryonal Malignancy. *Front Mol Neurosci*, *12*, 9.

Johnson, D. S., Mortazavi, A., Myers, R. M., & Wold, B. (2007). Genome-wide mapping of in vivo protein-DNA interactions. *Science*, *316*(5830), 1497-1502.

Johnson, E. S., Gonda, D. K., & Varshavsky, A. (1990). cis-trans recognition and subunit-specific degradation of short-lived proteins. *Nature*, *346*(6281), 287-291.

Jonkers, I., Kwak, H., & Lis, J. T. (2014). Genome-wide dynamics of Pol II elongation and its interplay with promoter proximal pausing, chromatin, and exons. *Elife*, *3*, e02407.

Jonkers, I., & Lis, J. T. (2015). Getting up to speed with transcription elongation by RNA polymerase II. *Nat Rev Mol Cell Biol*, *16*(3), 167-177.

Jumper, J., Evans, R., Pritzel, A., Green, T., Figurnov, M., Ronneberger, O., Tunyasuvunakool, K., Bates, R., Zidek, A., Potapenko, A., Bridgland, A., Meyer, C., Kohl, S. A. A., Ballard, A. J., Cowie, A., Romera-Paredes, B., Nikolov, S., Jain, R., Adler, J., Back, T., Petersen, S., Reiman, D., Clancy, E., Zielinski, M., Steinegger, M., Pacholska, M., Berghammer, T., Bodenstein, S., Silver, D., Vinyals, O., Senior, A. W., Kavukcuoglu, K., Kohli, P., & Hassabis, D. (2021). Highly accurate protein structure prediction with AlphaFold. *Nature*, *596*(7873), 583-589.

Jung, M., Russell, A. J., Liu, B., George, J., Liu, P. Y., Liu, T., DeFazio, A., Bowtell, D. D., Oberthuer, A., London, W. B., Fletcher, J. I., Haber, M., Norris, M. D., & Henderson, M. J. (2017). A Myc Activity Signature Predicts Poor Clinical Outcomes in Myc-Associated Cancers. *Cancer Res*, *77*(4), 971-981.

Jurga, M., Abugable, A. A., Goldman, A. S. H., & El-Khamisy, S. F. (2021). USP11 controls R-loops by regulating senataxin proteostasis. *Nat Commun*, *12*(1), 5156.

Kalkat, M., Resetca, D., Lourenco, C., Chan, P. K., Wei, Y., Shiah, Y. J., Vitkin, N., Tong, Y., Sunnerhagen, M., Done, S. J., Boutros, P. C., Raught, B., & Penn, L. Z. (2018). MYC Protein Interactome Profiling Reveals Functionally Distinct Regions that Cooperate to Drive Tumorigenesis. *Mol Cell*, *72*(5), 836-848 e837.

Kapadia, B., Nanaji, N. M., Bhalla, K., Bhandary, B., Lapidus, R., Beheshti, A., Evens, A. M., & Gartenhaus, R. B. (2018). Fatty Acid Synthase induced S6Kinase facilitates USP11-eIF4B complex formation for sustained oncogenic translation in DLBCL. *Nat Commun*, *9*(1), 829.

Ke, J. Y., Dai, C. J., Wu, W. L., Gao, J. H., Xia, A. J., Liu, G. P., Lv, K. S., & Wu, C. L. (2014). USP11 regulates p53 stability by deubiquitinating p53. *J Zhejiang Univ Sci B*, *15*(12), 1032-1038.

Kelstrup, C. D., Young, C., Lavallee, R., Nielsen, M. L., & Olsen, J. V. (2012). Optimized fast and sensitive acquisition methods for shotgun proteomics on a quadrupole orbitrap mass spectrometer. *J Proteome Res*, *11*(6), 3487-3497.

Kettenberger, H., Armache, K. J., & Cramer, P. (2003). Architecture of the RNA polymerase II-TFIIS complex and implications for mRNA cleavage. *Cell*, *114*(3), 347-357.

Kim, C., Wang, X. D., Liu, Z., Zha, S., & Yu, Y. (2022). Targeting Scaffolding Functions of Enzymes Using PROTAC Approaches. *Biochemistry*.

Kim, J., Guermah, M., & Roeder, R. G. (2010). The human PAF1 complex acts in chromatin transcription elongation both independently and cooperatively with SII/TFIIS. *Cell*, *140*(4), 491-503.

Kim, Y. J., Bjorklund, S., Li, Y., Sayre, M. H., & Kornberg, R. D. (1994). A multiprotein mediator of transcriptional activation and its interaction with the C-terminal repeat domain of RNA polymerase II. *Cell*, *77*(4), 599-608.

Kimura, M., Ishiguro, A., & Ishihama, A. (1997). RNA polymerase II subunits 2, 3, and 11 form a core subassembly with DNA binding activity. *J Biol Chem*, *272*(41), 25851-25855.

Kirby, K. S. (1957). A new method for the isolation of deoxyribonucleic acids; evidence on the nature of bonds between deoxyribonucleic acid and protein. *Biochem J*, *66*(3), 495-504.

Kleiman, F. E., Wu-Baer, F., Fonseca, D., Kaneko, S., Baer, R., & Manley, J. L. (2005). BRCA1/BARD1 inhibition of mRNA 3' processing involves targeted degradation of RNA polymerase II. *Genes Dev*, *19*(10), 1227-1237.

Kohl, N. E., Legouy, E., DePinho, R. A., Nisen, P. D., Smith, R. K., Gee, C. E., & Alt, F. W. (1986). Human N-myc is closely related in organization and nucleotide sequence to c-myc. *Nature*, *319*(6048), 73-77.

Kokic, G., Wagner, F. R., Chernev, A., Urlaub, H., & Cramer, P. (2021). Structural basis of human transcription-DNA repair coupling. *Nature*, *598*(7880), 368-372.

Kolodziej, P. A., & Young, R. A. (1991). Mutations in the three largest subunits of yeast RNA polymerase II that affect enzyme assembly. *Mol Cell Biol*, *11*(9), 4669-4678.

Komander, D., Clague, M. J., & Urbe, S. (2009). Breaking the chains: structure and function of the deubiquitinases. *Nat Rev Mol Cell Biol*, *10*(8), 550-563.

Komander, D., & Rape, M. (2012). The ubiquitin code. *Annu Rev Biochem*, *81*, 203-229.

Koren, I., Timms, R. T., Kula, T., Xu, Q., Li, M. Z., & Elledge, S. J. (2018). The Eukaryotic Proteome Is Shaped by E3 Ubiquitin Ligases Targeting C-Terminal Degrons. *Cell*, *173*(7), 1622-1635 e1614.

Kotsantis, P., Petermann, E., & Boulton, S. J. (2018). Mechanisms of Oncogene-Induced Replication Stress: Jigsaw Falling into Place. *Cancer Discov*, *8*(5), 537-555.

Krebs, A. R., Imanci, D., Hoerner, L., Gaidatzis, D., Burger, L., & Schubeler, D. (2017). Genome-wide Single-Molecule Footprinting Reveals High RNA Polymerase II Turnover at Paused Promoters. *Mol Cell*, *67*(3), 411-422 e414.

Krum, S. A., Miranda, G. A., Lin, C., & Lane, T. F. (2003). BRCA1 associates with processive RNA polymerase II. *J Biol Chem*, *278*(52), 52012-52020.

Kuleshov, M. V., Jones, M. R., Rouillard, A. D., Fernandez, N. F., Duan, Q., Wang, Z., Koplev, S., Jenkins, S. L., Jagodnik, K. M., Lachmann, A., McDermott, M. G., Monteiro, C. D., Gundersen, G. W., & Ma'ayan, A. (2016). Enrichr: a comprehensive gene set enrichment analysis web server 2016 update. *Nucleic Acids Res*, *44*(W1), W90-97.

Kvint, K., Uhler, J. P., Taschner, M. J., Sigurdsson, S., Erdjument-Bromage, H., Tempst, P., & Svejstrup, J. Q. (2008). Reversal of RNA polymerase II ubiquitylation by the ubiquitin protease Ubp3. *Mol Cell*, *30*(4), 498-506.

Kwak, H., Fuda, N. J., Core, L. J., & Lis, J. T. (2013). Precise maps of RNA polymerase reveal how promoters direct initiation and pausing. *Science*, *339*(6122), 950-953.

Kwapisz, M., Beckouet, F., & Thuriaux, P. (2008). Early evolution of eukaryotic DNA-dependent RNA polymerases. *Trends Genet*, *24*(5), 211-215.

Kwiatkowski, N., Zhang, T., Rahl, P. B., Abraham, B. J., Reddy, J., Ficarro, S. B., Dastur, A., Amzallag, A., Ramaswamy, S., Tesar, B., Jenkins, C. E., Hannett, N. M., McMillin, D., Sanda, T., Sim, T., Kim, N. D., Look, T., Mitsiades, C. S., Weng, A. P., Brown, J. R., Benes, C. H., Marto, J. A., Young, R. A., & Gray, N. S. (2014). Targeting transcription regulation in cancer with a covalent CDK7 inhibitor. *Nature*, *511*(7511), 616-620.

Lacoursiere, R. E., Hadi, D., & Shaw, G. S. (2022). Acetylation, Phosphorylation, Ubiquitination (Oh My!): Following Post-Translational Modifications on the Ubiquitin Road. *Biomolecules*, *12*(3).

Laemmli, U. K. (1970). Cleavage of structural proteins during the assembly of the head of bacteriophage T4. *Nature*, *227*(5259), 680-685.

Landick, R. (2009). Transcriptional pausing without backtracking. *Proc Natl Acad Sci U S A*, *106*(22), 8797-8798.

Langmead, B., & Salzberg, S. L. (2012). Fast gapped-read alignment with Bowtie 2. *Nat Methods*, *9*(4), 357-359.

Lans, H., Hoeijmakers, J. H. J., Vermeulen, W., & Marteijn, J. A. (2019). The DNA damage response to transcription stress. *Nat Rev Mol Cell Biol*, *20*(12), 766-784.

Lavigne, M. D., Konstantopoulos, D., Ntakou-Zamplara, K. Z., Liakos, A., & Fousteri, M. (2017). Global unleashing of transcription elongation waves in response to genotoxic stress restricts somatic mutation rate. *Nat Commun*, *8*(1), 2076.

Leuchowius, K. J., Jarvius, M., Wickstrom, M., Rickardson, L., Landegren, U., Larsson, R., Soderberg, O., Fryknas, M., & Jarvius, J. (2010). High content screening for inhibitors of protein interactions and post-translational modifications in primary cells by proximity ligation. *Mol Cell Proteomics*, *9*(1), 178-183.

Lewis, L. M., Edwards, M. C., Meyers, Z. R., Talbot, C. C., Jr., Hao, H., Blum, D., & Reproducibility Project: Cancer, B. (2018). Replication Study: Transcriptional amplification in tumor cells with elevated c-Myc. *Elife*, *7*.

Li, J., Rodriguez, Y., Cheng, C., Zeng, L., Wong, E. Y. M., Xu, C. Y., Zhou, M. M., & Xu, P. X. (2017). EYA1's Conformation Specificity in Dephosphorylating Phosphothreonine in Myc and Its Activity on Myc Stabilization in Breast Cancer. *Mol Cell Biol*, *37*(1).

Li, Y., Huang, J., Zhu, J., Bao, L., Wang, H., Jiang, Y., Tian, K., Wang, R., Zheng, H., Duan, W., Lai, W., Yi, X., Zhu, Y., Guo, T., & Ji, X. (2022). Targeted protein degradation reveals RNA Pol II heterogeneity and functional diversity. *Mol Cell*, *82*(20), 3943-3959 e3911.

Liao, Y., Sumara, I., & Pangou, E. (2022). Non-proteolytic ubiquitylation in cellular signaling and human disease. *Commun Biol*, *5*(1), 114.

Lin, C. Y., Loven, J., Rahl, P. B., Paranal, R. M., Burge, C. B., Bradner, J. E., Lee, T. I., & Young, R. A. (2012). Transcriptional amplification in tumor cells with elevated c-Myc. *Cell*, *151*(1), 56-67.

Lin, H. C., Yeh, C. W., Chen, Y. F., Lee, T. T., Hsieh, P. Y., Rusnac, D. V., Lin, S. Y., Elledge, S. J., Zheng, N., & Yen, H. S. (2018). C-Terminal End-Directed Protein Elimination by CRL2 Ubiquitin Ligases. *Mol Cell*, *70*(4), 602-613 e603.

Lisica, A., Engel, C., Jahnel, M., Roldan, E., Galburt, E. A., Cramer, P., & Grill, S. W. (2016). Mechanisms of backtrack recovery by RNA polymerases I and II. *Proc Natl Acad Sci U S A*, *113*(11), 2946-2951.

Little, C. D., Nau, M. M., Carney, D. N., Gazdar, A. F., & Minna, J. D. (1983). Amplification and expression of the c-myc oncogene in human lung cancer cell lines. *Nature*, *306*(5939), 194-196.

Liu, Y., Zhou, K., Zhang, N., Wei, H., Tan, Y. Z., Zhang, Z., Carragher, B., Potter, C. S., D'Arcy, S., & Luger, K. (2020). FACT caught in the act of manipulating the nucleosome. *Nature*, *577*(7790), 426-431.

Liu, Z., Chen, S. S., Clarke, S., Veschi, V., & Thiele, C. J. (2020). Targeting MYCN in Pediatric and Adult Cancers. *Front Oncol*, *10*, 623679.

Lorch, Y., & Kornberg, R. D. (2015). Chromatin-remodeling and the initiation of transcription. *Q Rev Biophys*, *48*(4), 465-470.

Lorch, Y., LaPointe, J. W., & Kornberg, R. D. (1987). Nucleosomes inhibit the initiation of transcription but allow chain elongation with the displacement of histones. *Cell*, *49*(2), 203-210.

Lorenzin, F., Benary, U., Baluapuri, A., Walz, S., Jung, L. A., von Eyss, B., Kisker, C., Wolf, J., Eilers, M., & Wolf, E. (2016). Different promoter affinities account for specificity in MYC-dependent gene regulation. *Elife*, *5*.

Lovkvist, C., Dodd, I. B., Sneppen, K., & Haerter, J. O. (2016). DNA methylation in human epigenomes depends on local topology of CpG sites. *Nucleic Acids Res*, *44*(11), 5123-5132.

Lu, H., Yu, D., Hansen, A. S., Ganguly, S., Liu, R., Heckert, A., Darzacq, X., & Zhou, Q. (2018). Phase-separation mechanism for C-terminal hyperphosphorylation of RNA polymerase II. *Nature*, *558*(7709), 318-323.

Lu, Y., Wu, T., Gutman, O., Lu, H., Zhou, Q., Henis, Y. I., & Luo, K. (2020). Phase separation of TAZ compartmentalizes the transcription machinery to promote gene expression. *Nat Cell Biol*, *22*(4), 453-464.

Luo, Q., Wu, X., Nan, Y., Chang, W., Zhao, P., Zhang, Y., Su, D., & Liu, Z. (2020). TRIM32/USP11 Balances ARID1A Stability and the Oncogenic/Tumor-Suppressive Status of Squamous Cell Carcinoma. *Cell Rep*, *30*(1), 98-111 e115.

Luscher, B., & Larsson, L. G. (1999). The basic region/helix-loop-helix/leucine zipper domain of Myc proto-oncoproteins: function and regulation. *Oncogene*, *18*(19), 2955-2966.

Ma, A., Moroy, T., Collum, R., Weintraub, H., Alt, F. W., & Blackwell, T. K. (1993). DNA binding by N- and L-Myc proteins. *Oncogene*, *8*(4), 1093-1098.

Machour, F. E., & Ayoub, N. (2020). Transcriptional Regulation at DSBs: Mechanisms and Consequences. *Trends Genet*, *36*(12), 981-997.

Maertens, G. N., El Messaoudi-Aubert, S., Elderkin, S., Hiom, K., & Peters, G. (2010). Ubiquitin-specific proteases 7 and 11 modulate Polycomb regulation of the INK4a tumour suppressor. *EMBO J*, *29*(15), 2553-2565.

Magin, R. S., Liu, X., Felix, A., Bratt, A. S., Chan, W. C., & Buhrlage, S. J. (2021). Small molecules as tools for functional assessment of deubiquitinating enzyme function. *Cell Chem Biol*, *28*(7), 1090-1100.

Malynn, B. A., de Alboran, I. M., O'Hagan, R. C., Bronson, R., Davidson, L., DePinho, R. A., & Alt, F. W. (2000). N-myc can functionally replace c-myc in murine development, cellular growth, and differentiation. *Genes Dev*, *14*(11), 1390-1399.

Manzo, S. G., Hartono, S. R., Sanz, L. A., Marinello, J., De Biasi, S., Cossarizza, A., Capranico, G., & Chedin, F. (2018). DNA Topoisomerase I differentially modulates R-loops across the human genome. *Genome Biol*, *19*(1), 100.

Marshall, G. M., Carter, D. R., Cheung, B. B., Liu, T., Mateos, M. K., Meyerowitz, J. G., & Weiss, W. A. (2014). The prenatal origins of cancer. *Nat Rev Cancer*, *14*(4), 277-289.

Marshall, N. F., & Price, D. H. (1995). Purification of P-TEFb, a transcription factor required for the transition into productive elongation. *J Biol Chem*, *270*(21), 12335-12338.

Matthay, K. K., Maris, J. M., Schleiermacher, G., Nakagawara, A., Mackall, C. L., Diller, L., & Weiss, W. A. (2016). Neuroblastoma. *Nat Rev Dis Primers*, *2*, 16078.

McMahon, S. B., Van Buskirk, H. A., Dugan, K. A., Copeland, T. D., & Cole, M. D. (1998). The novel ATM-related protein TRRAP is an essential cofactor for the c-Myc and E2F oncoproteins. *Cell*, *94*(3), 363-374.

McMahon, S. B., Wood, M. A., & Cole, M. D. (2000). The essential cofactor TRRAP recruits the histone acetyltransferase hGCN5 to c-Myc. *Mol Cell Biol*, *20*(2), 556-562.

Merril, C. R. (1990). Gel-staining techniques. *Methods Enzymol*, *182*, 477-488.

Mevissen, T. E. T., & Komander, D. (2017). Mechanisms of Deubiquitinase Specificity and Regulation. *Annu Rev Biochem*, *86*, 159-192.

Michelini, F., Pitchiaya, S., Vitelli, V., Sharma, S., Gioia, U., Pessina, F., Cabrini, M., Wang, Y., Capozzo, I., Iannelli, F., Matti, V., Francia, S., Shivashankar, G. V., Walter, N. G., & d'Adda di Fagagna, F. (2017). Damage-induced lncRNAs control the DNA damage response through interaction with DDRNAs at individual double-strand breaks. *Nat Cell Biol*, *19*(12), 1400-1411.

Midha, T., Mallory, J. D., Kolomeisky, A. B., & Igoshin, O. A. (2023). Synergy among Pausing, Intrinsic Proofreading, and Accessory Proteins Results in Optimal Transcription Speed and Tolerable Accuracy. *J Phys Chem Lett*, *14*(14), 3422-3429.

Milligan, L., Sayou, C., Tuck, A., Auchynnikava, T., Reid, J. E., Alexander, R., Alves, F. L., Allshire, R., Spanos, C., Rappsilber, J., Beggs, J. D., Kudla, G., & Tollervey, D. (2017). RNA polymerase II stalling at pre-mRNA splice sites is enforced by ubiquitination of the catalytic subunit. *Elife*, *6*.

Molenaar, J. J., Domingo-Fernandez, R., Ebus, M. E., Lindner, S., Koster, J., Drabek, K., Mestdagh, P., van Sluis, P., Valentijn, L. J., van Nes, J., Broekmans, M., Haneveld, F., Volckmann, R., Bray, I., Heukamp, L., Sprussel, A., Thor, T., Kieckbusch, K., Klein-Hitpass, L., Fischer, M., Vandesompele, J., Schramm, A., van Noesel, M. M., Varesio, L., Speleman, F., Eggert, A., Stallings, R. L., Caron, H. N., Versteeg, R., & Schulte, J. H. (2012). LIN28B induces neuroblastoma and enhances MYCN levels via let-7 suppression. *Nat Genet*, *44*(11), 1199-1206.

Monclair, T., Brodeur, G. M., Ambros, P. F., Brisse, H. J., Cecchetto, G., Holmes, K., Kaneko, M., London, W. B., Matthay, K. K., Nuchtern, J. G., von Schweinitz, D., Simon, T., Cohn, S. L., Pearson, A. D., & Force, I. T. (2009). The International Neuroblastoma Risk Group (INRG) staging system: an INRG Task Force report. *J Clin Oncol*, *27*(2), 298-303.

Mosse, Y. P., Laudenslager, M., Longo, L., Cole, K. A., Wood, A., Attiyeh, E. F., Laquaglia, M. J., Sennett, R., Lynch, J. E., Perri, P., Laureys, G., Speleman, F., Kim, C., Hou, C., Hakonarson, H., Torkamani, A., Schork, N. J., Brodeur, G. M., Tonini, G. P., Rappaport, E., Devoto, M., & Maris, J. M. (2008). Identification of ALK as a major familial neuroblastoma predisposition gene. *Nature*, *455*(7215), 930-935.

Mourgues, S., Gautier, V., Lagarou, A., Bordier, C., Mourcet, A., Slingerland, J., Kaddoum, L., Coin, F., Vermeulen, W., Gonzales de Peredo, A., Monsarrat, B., Mari, P. O., & Giglia-Mari, G. (2013). ELL, a novel TFIIH partner, is involved in transcription restart after DNA repair. *Proc Natl Acad Sci U S A*, *110*(44), 17927-17932.

Murphy, D. J., Junttila, M. R., Pouyet, L., Karnezis, A., Shchors, K., Bui, D. A., Brown-Swigart, L., Johnson, L., & Evan, G. I. (2008). Distinct thresholds govern Myc's biological output in vivo. *Cancer Cell*, *14*(6), 447-457.

Nair, S. K., & Burley, S. K. (2003). X-ray structures of Myc-Max and Mad-Max recognizing DNA. Molecular bases of regulation by proto-oncogenic transcription factors. *Cell*, *112*(2), 193-205.

Nakazawa, Y., Hara, Y., Oka, Y., Komine, O., van den Heuvel, D., Guo, C., Daigaku, Y., Isono, M., He, Y., Shimada, M., Kato, K., Jia, N., Hashimoto, S., Kotani, Y., Miyoshi, Y., Tanaka, M., Sobue, A., Mitsutake, N., Suganami, T., Masuda, A., Ohno, K., Nakada, S., Mashimo, T., Yamanaka, K., Luijsterburg, M. S., & Ogi, T. (2020). Ubiquitination of DNA Damage-Stalled RNAPII Promotes Transcription-Coupled Repair. *Cell*, *180*(6), 1228-1244 e1224.

Narain, A., Bhandare, P., Adhikari, B., Backes, S., Eilers, M., Dolken, L., Schlosser, A., Erhard, F., Baluapuri, A., & Wolf, E. (2021). Targeted protein degradation reveals a direct role of SPT6 in RNAPII elongation and termination. *Mol Cell*, *81*(15), 3110-3127 e3114.

Nau, M. M., Brooks, B. J., Battey, J., Sausville, E., Gazdar, A. F., Kirsch, I. R., McBride, O. W., Bertness, V., Hollis, G. F., & Minna, J. D. (1985). L-myc, a new myc-related gene amplified and expressed in human small cell lung cancer. *Nature*, *318*(6041), 69-73.

Nesbit, C. E., Tersak, J. M., & Prochownik, E. V. (1999). MYC oncogenes and human neoplastic disease. *Oncogene*, *18*(19), 3004-3016.

Nicklas, S., Hillje, A. L., Okawa, S., Rudolph, I. M., Collmann, F. M., van Wuellen, T., Del Sol, A., & Schwamborn, J. C. (2019). A complex of the ubiquitin ligase TRIM32 and the deubiquitinase USP7 balances the level of c-Myc ubiquitination and thereby determines neural stem cell fate specification. *Cell Death Differ*, *26*(4), 728-740.

Nicol, J. W., Helt, G. A., Blanchard, S. G., Jr., Raja, A., & Loraine, A. E. (2009). The Integrated Genome Browser: free software for distribution and exploration of genome-scale datasets. *Bioinformatics*, *25*(20), 2730-2731.

Nie, Z., Hu, G., Wei, G., Cui, K., Yamane, A., Resch, W., Wang, R., Green, D. R., Tessarollo, L., Casellas, R., Zhao, K., & Levens, D. (2012). c-Myc is a universal amplifier of expressed genes in lymphocytes and embryonic stem cells. *Cell*, *151*(1), 68-79.

Nieto Moreno, N., Villafanez, F., Giono, L. E., Cuenca, C., Soria, G., Munoz, M. J., & Kornblihtt, A. R. (2020). GSK-3 is an RNA polymerase II phospho-CTD kinase. *Nucleic Acids Res*, *48*(11), 6068-6080.

Nilson, K. A., Guo, J., Turek, M. E., Brogie, J. E., Delaney, E., Luse, D. S., & Price, D. H. (2015). THZ1 Reveals Roles for Cdk7 in Co-transcriptional Capping and Pausing. *Mol Cell*, *59*(4), 576-587.

Nojima, T., Gomes, T., Grosso, A. R. F., Kimura, H., Dye, M. J., Dhir, S., Carmo-Fonseca, M., & Proudfoot, N. J. (2015). Mammalian NET-Seq Reveals Genome-wide Nascent Transcription Coupled to RNA Processing. *Cell*, *161*(3), 526-540.

Nowell, P., Finan, J., Dalla-Favera, R., Gallo, R. C., ar-Rushdi, A., Romanczuk, H., Selden, J. R., Emanuel, B. S., Rovera, G., & Croce, C. M. (1983). Association of amplified oncogene c-myc with an abnormally banded chromosome 8 in a human leukaemia cell line. *Nature*, *306*(5942), 494-497.

Oh, E., Akopian, D., & Rape, M. (2018). Principles of Ubiquitin-Dependent Signaling. *Annu Rev Cell Dev Biol*, *34*, 137-162.

Oksenych, V., Zhovmer, A., Ziani, S., Mari, P. O., Eberova, J., Nardo, T., Stefanini, M., Giglia-Mari, G., Egly, J. M., & Coin, F. (2013). Histone methyltransferase DOT1L drives recovery of gene expression after a genotoxic attack. *PLoS Genet*, *9*(7), e1003611.

Olsen, J. V., Macek, B., Lange, O., Makarov, A., Horning, S., & Mann, M. (2007). Higher-energy C-trap dissociation for peptide modification analysis. *Nat Methods*, *4*(9), 709-712.

Olsen, J. V., Vermeulen, M., Santamaria, A., Kumar, C., Miller, M. L., Jensen, L. J., Gnad, F., Cox, J., Jensen, T. S., Nigg, E. A., Brunak, S., & Mann, M. (2010). Quantitative phosphoproteomics reveals widespread full phosphorylation site occupancy during mitosis. *Sci Signal*, *3*(104), ra3.

Olson, C. M., Jiang, B., Erb, M. A., Liang, Y., Doctor, Z. M., Zhang, Z., Zhang, T., Kwiatkowski, N., Boukhali, M., Green, J. L., Haas, W., Nomanbhoy, T., Fischer, E. S., Young, R. A., Bradner, J. E., Winter, G. E., & Gray, N. S. (2018). Pharmacological perturbation of CDK9 using selective CDK9 inhibition or degradation. *Nat Chem Biol*, *14*(2), 163-170.

Orlando, D. A., Chen, M. W., Brown, V. E., Solanki, S., Choi, Y. J., Olson, E. R., Fritz, C. C., Bradner, J. E., & Guenther, M. G. (2014). Quantitative ChIP-Seq normalization reveals global modulation of the epigenome. *Cell Rep*, *9*(3), 1163-1170.

Orthwein, A., Noordermeer, S. M., Wilson, M. D., Landry, S., Enchev, R. I., Sherker, A., Munro, M., Pinder, J., Salsman, J., Dellaire, G., Xia, B., Peter, M., & Durocher, D. (2015). A mechanism for the suppression of homologous recombination in G1 cells. *Nature*, *528*(7582), 422-426.

Paddison, P. J., Caudy, A. A., & Hannon, G. J. (2002). Stable suppression of gene expression by RNAi in mammalian cells. *Proc Natl Acad Sci U S A*, *99*(3), 1443-1448.

Palangat, M., Renner, D. B., Price, D. H., & Landick, R. (2005). A negative elongation factor for human RNA polymerase II inhibits the anti-arrest transcript-cleavage factor TFIIS. *Proc Natl Acad Sci U S A*, *102*(42), 15036-15041.

Papadopoulos, D., Solvie, D., Baluapuri, A., Endres, T., Ha, S. A., Herold, S., Kalb, J., Giansanti, C., Schulein-Volk, C., Ade, C. P., Schneider, C., Gaballa, A., Vos, S., Fischer, U., Dobbelstein, M., Wolf, E., & Eilers, M. (2022). MYCN recruits the nuclear exosome complex to RNA polymerase II to prevent transcription-replication conflicts. *Mol Cell*, *82*(1), 159-176 e112.

Papadopoulos, D., Uhl, L., Ha, S. A., & Eilers, M. (2023). Beyond gene expression: how MYC relieves transcription stress. *Trends Cancer*, *9*(10), 805-816.

Park, J. R., Eggert, A., & Caron, H. (2010). Neuroblastoma: biology, prognosis, and treatment. *Hematol Oncol Clin North Am*, *24*(1), 65-86.

Park, J. R., Kreissman, S. G., London, W. B., Naranjo, A., Cohn, S. L., Hogarty, M. D., Tenney, S. C., Haas-Kogan, D., Shaw, P. J., Kraveka, J. M., Roberts, S. S., Geiger, J. D., Doski, J. J., Voss, S. D., Maris, J. M., Grupp, S. A., & Diller, L. (2019). Effect of Tandem Autologous Stem Cell Transplant vs Single Transplant on Event-Free Survival in Patients With High-Risk Neuroblastoma: A Randomized Clinical Trial. *JAMA*, *322*(8), 746-755.

Parua, P. K., & Fisher, R. P. (2020). Dissecting the Pol II transcription cycle and derailing cancer with CDK inhibitors. *Nat Chem Biol*, *16*(7), 716-724.

Patange, S., Ball, D. A., Wan, Y., Karpova, T. S., Girvan, M., Levens, D., & Larson, D. R. (2022). MYC amplifies gene expression through global changes in transcription factor dynamics. *Cell Rep*, *38*(4), 110292.

Patel, P. S., Algouneh, A., Krishnan, R., Reynolds, J. J., Nixon, K. C. J., Hao, J., Lee, J., Feng, Y., Fozil, C., Stanic, M., Yerlici, T., Su, P., Soares, F., Liedtke, E., Prive, G., Baider, G. D., Pujana, M. A., Mekhail, K., He, H. H., Hakem, A., Stewart, G. S., & Hakem, R. (2023). Excessive transcription-replication conflicts are a vulnerability of BRCA1-mutant cancers. *Nucleic Acids Res*, *51*(9), 4341-4362.

Perna, D., Faga, G., Verrecchia, A., Gorski, M. M., Barozzi, I., Narang, V., Khng, J., Lim, K. C., Sung, W. K., Sanges, R., Stupka, E., Oskarsson, T., Trumpp, A., Wei, C. L., Muller, H., & Amati, B. (2012). Genome-wide mapping of Myc binding and gene regulation in serum-stimulated fibroblasts. *Oncogene*, *31*(13), 1695-1709.

Perry, M., Biegert, M., Kollala, S. S., Mallard, H., Su, G., Kodavati, M., Kreiling, N., Holbrook, A., & Ghosal, G. (2021). USP11 mediates repair of DNA-protein cross-links by deubiquitinating SPRTN metalloprotease. *J Biol Chem*, *296*, 100396.

Pessina, F., Giavazzi, F., Yin, Y., Gioia, U., Vitelli, V., Galbiati, A., Barozzi, S., Garre, M., Oldani, A., Flaus, A., Cerbino, R., Parazzoli, D., Rothenberg, E., & d'Adda di Fagagna, F. (2019). Functional transcription promoters at DNA double-strand breaks mediate RNA-driven phase separation of damage-response factors. *Nat Cell Biol*, *21*(10), 1286-1299.

Peterlin, B. M., & Price, D. H. (2006). Controlling the elongation phase of transcription with P-TEFb. *Mol Cell*, *23*(3), 297-305.

Peukert, K., Staller, P., Schneider, A., Carmichael, G., Hanel, F., & Eilers, M. (1997). An alternative pathway for gene regulation by Myc. *EMBO J*, *16*(18), 5672-5686.

Pickart, C. M. (2001). Mechanisms underlying ubiquitination. *Annu Rev Biochem*, *70*, 503-533.

Pickart, C. M., & Rose, I. A. (1985). Functional heterogeneity of ubiquitin carrier proteins. *J Biol Chem*, *260*(3), 1573-1581.

Pierce, N. W., Kleiger, G., Shan, S. O., & Deshaies, R. J. (2009). Detection of sequential polyubiquitylation on a millisecond timescale. *Nature*, *462*(7273), 615-619.

Pillutla, R. C., Shimamoto, A., Furuichi, Y., & Shatkin, A. J. (1999). Genomic structure and chromosomal localization of TCEAL1, a human gene encoding the nuclear phosphoprotein p21/SIIR. *Genomics*, *56*(2), 217-220.

Pineda-Lucena, A., Ho, C. S., Mao, D. Y., Sheng, Y., Laister, R. C., Muhandiram, R., Lu, Y., Seet, B. T., Katz, S., Szyperski, T., Penn, L. Z., & Arrowsmith, C. H. (2005). A structure-based model of the c-Myc/Bin1 protein interaction shows alternative splicing of Bin1 and c-Myc phosphorylation are key binding determinants. *J Mol Biol*, *351*(1), 182-194.

Pokholok, D. K., Hannett, N. M., & Young, R. A. (2002). Exchange of RNA polymerase II initiation and elongation factors during gene expression in vivo. *Mol Cell*, *9*(4), 799-809.

Poli, J., Gerhold, C. B., Tosi, A., Hustedt, N., Seeber, A., Sack, R., Herzog, F., Pasero, P., Shimada, K., Hopfner, K. P., & Gasser, S. M. (2016). Mec1, INO80, and the PAF1 complex cooperate to limit transcription replication conflicts through RNAPII removal during replication stress. *Genes Dev*, *30*(3), 337-354.

Ponchel, F., Toomes, C., Bransfield, K., Leong, F. T., Douglas, S. H., Field, S. L., Bell, S. M., Combaret, V., Puisieux, A., Mighell, A. J., Robinson, P. A., Inglehearn, C. F., Isaacs, J. D., & Markham, A. F. (2003). Real-time PCR based on SYBR-Green I fluorescence: an alternative to the TaqMan assay for a relative quantification of gene rearrangements, gene amplifications and micro gene deletions. *BMC Biotechnol*, *3*, 18.

Popov, N., Wanzel, M., Madiredjo, M., Zhang, D., Beijersbergen, R., Bernards, R., Moll, R., Elledge, S. J., & Eilers, M. (2007). The ubiquitin-specific protease USP28 is required for MYC stability. *Nat Cell Biol*, *9*(7), 765-774.

Promonet, A., Padioleau, I., Liu, Y., Sanz, L., Biernacka, A., Schmitz, A. L., Skrzypczak, M., Sarrazin, A., Mettling, C., Rowicka, M., Ginalski, K., Chedin, F., Chen, C. L., Lin, Y. L., & Pasero, P. (2020). Topoisomerase 1 prevents replication stress at R-loop-enriched transcription termination sites. *Nat Commun*, *11*(1), 3940.

Proudfoot, N. J. (1989). How RNA polymerase II terminates transcription in higher eukaryotes. *Trends Biochem Sci*, *14*(3), 105-110.

Proudfoot, N. J. (2016). Transcriptional termination in mammals: Stopping the RNA polymerase II juggernaut. *Science*, *352*(6291), aad9926.

Pugh, T. J., Morozova, O., Attiyeh, E. F., Asgharzadeh, S., Wei, J. S., Auclair, D., Carter, S. L., Cibulskis, K., Hanna, M., Kiezun, A., Kim, J., Lawrence, M. S., Lichenstein, L., McKenna, A., Pedamallu, C. S., Ramos, A. H., Shefler, E., Sivachenko, A., Sougnez, C., Stewart, C., Ally, A., Birol, I., Chiu, R., Corbett, R. D., Hirst, M., Jackman, S. D., Kamoh, B., Khodabakshi, A. H., Krzywinski, M., Lo, A., Moore, R. A., Mungall, K. L., Qian, J., Tam, A., Thiessen, N., Zhao, Y., Cole, K. A., Diamond, M., Diskin, S. J., Mosse, Y. P., Wood, A. C., Ji, L., Sposto, R., Badgett, T., London, W. B., Moyer, Y., Gastier-Foster, J. M., Smith, M. A., Guidry Auvil, J. M., Gerhard, D. S., Hogarty, M. D., Jones, S. J., Lander, E. S., Gabriel, S. B., Getz, G., Seeger, R. C., Khan, J., Marra, M. A., Meyerson, M., & Maris, J. M. (2013). The genetic landscape of high-risk neuroblastoma. *Nat Genet*, *45*(3), 279-284.

Qiu, B., & Matthay, K. K. (2022). Advancing therapy for neuroblastoma. *Nat Rev Clin Oncol*, *19*(8), 515-533.

Qiu, X., Boufaied, N., Hallal, T., Feit, A., de Polo, A., Luoma, A. M., Alahmadi, W., Larocque, J., Zadra, G., Xie, Y., Gu, S., Tang, Q., Zhang, Y., Syamala, S., Seo, J. H., Bell, C., O'Connor, E., Liu, Y., Schaeffer, E. M., Jeffrey Karnes, R., Weinmann, S., Davicioni, E., Morrissey, C., Cejas, P., Ellis, L., Loda, M., Wucherpfennig, K. W., Pomerantz, M. M., Spratt, D. E., Corey, E., Freedman, M. L., Shirley Liu, X., Brown, M., Long, H. W., & Labbe, D. P. (2022). MYC drives aggressive prostate cancer by disrupting transcriptional pause release at androgen receptor targets. *Nat Commun*, *13*(1), 2559.

Quinlan, A. R., & Hall, I. M. (2010). BEDTools: a flexible suite of utilities for comparing genomic features. *Bioinformatics*, *26*(6), 841-842.

Rahl, P. B., Lin, C. Y., Seila, A. C., Flynn, R. A., McCuine, S., Burge, C. B., Sharp, P. A., & Young, R. A. (2010). c-Myc regulates transcriptional pause release. *Cell*, *141*(3), 432-445.

Ramirez, F., Ryan, D. P., Gruning, B., Bhardwaj, V., Kilpert, F., Richter, A. S., Heyne, S., Dundar, F., & Manke, T. (2016). deepTools2: a next generation web server for deep-sequencing data analysis. *Nucleic Acids Res*, *44*(W1), W160-165.

Rappsilber, J., Mann, M., & Ishihama, Y. (2007). Protocol for micro-purification, enrichment, pre-fractionation and storage of peptides for proteomics using StageTips. *Nat Protoc*, *2*(8), 1896-1906.

Rawat, P., Boehning, M., Hummel, B., Aprile-Garcia, F., Pandit, A. S., Eisenhardt, N., Khavaran, A., Niskanen, E., Vos, S. M., Palvimo, J. J., Pichler, A., Cramer, P., & Sawarkar, R. (2021). Stress-induced nuclear condensation of NELF drives transcriptional downregulation. *Mol Cell*, *81*(5), 1013-1026 e1011.

Ray, A., Milum, K., Battu, A., Wani, G., & Wani, A. A. (2013). NER initiation factors, DDB2 and XPC, regulate UV radiation response by recruiting ATR and ATM kinases to DNA damage sites. *DNA Repair (Amst)*, *12*(4), 273-283.

Renart, J., Reiser, J., & Stark, G. R. (1979). Transfer of proteins from gels to diazobenzyloxymethyl-paper and detection with antisera: a method for studying antibody specificity and antigen structure. *Proc Natl Acad Sci U S A*, *76*(7), 3116-3120.

Reyes-Turcu, F. E., Ventii, K. H., & Wilkinson, K. D. (2009). Regulation and cellular roles of ubiquitin-specific deubiquitinating enzymes. *Annu Rev Biochem*, *78*, 363-397.

Reyes-Turcu, F. E., & Wilkinson, K. D. (2009). Polyubiquitin binding and disassembly by deubiquitinating enzymes. *Chem Rev*, *109*(4), 1495-1508.
Richards, M. W., Burgess, S. G., Poon, E., Carstensen, A., Eilers, M., Chesler, L., & Bayliss, R. (2016). Structural basis of N-Myc binding by Aurora-A and its destabilization by kinase inhibitors. *Proc Natl Acad Sci U S A*, *113*(48), 13726-13731.
Rickman, D. S., Schulte, J. H., & Eilers, M. (2018). The Expanding World of N-MYC-Driven Tumors. *Cancer Discov*, *8*(2), 150-163.
Rigbolt, K. T., Prokhorova, T. A., Akimov, V., Henningsen, J., Johansen, P. T., Kratchmarova, I., Kassem, M., Mann, M., Olsen, J. V., & Blagoev, B. (2011). System-wide temporal characterization of the proteome and phosphoproteome of human embryonic stem cell differentiation. *Sci Signal*, *4*(164), rs3.
Rodriguez, J., & Larson, D. R. (2020). Transcription in Living Cells: Molecular Mechanisms of Bursting. *Annu Rev Biochem*, *89*, 189-212.
Roeder, R. G., & Rutter, W. J. (1969). Multiple forms of DNA-dependent RNA polymerase in eukaryotic organisms. *Nature*, *224*(5216), 234-237.
Roeschert, I., Poon, E., Henssen, A. G., Garcia, H. D., Gatti, M., Giansanti, C., Jamin, Y., Ade, C. P., Gallant, P., Schulein-Volk, C., Beli, P., Richards, M., Rosenfeldt, M., Altmeyer, M., Anderson, J., Eggert, A., Dobbelstein, M., Bayliss, R., Chesler, L., Buchel, G., & Eilers, M. (2021). Combined inhibition of Aurora-A and ATR kinase results in regression of MYCN-amplified neuroblastoma. *Nat Cancer*, *2*(3), 312-326.
Rosales, T., Nie, Z., Kapoor, V., Casellas, R., Jr., Knutson, J. R., & Levens, D. (2013). Partition of Myc into immobile vs. mobile complexes within nuclei. *Sci Rep*, *3*, 1953.
Rushworth, L. K., Harle, V., Repiscak, P., Clark, W., Shaw, R., Hall, H., Bushell, M., Leung, H. Y., & Patel, R. (2020). In vivo CRISPR/Cas9 knockout screen: TCEAL1 silencing enhances docetaxel efficacy in prostate cancer. *Life Sci Alliance*, *3*(12).
Sabari, B. R., Dall'Agnese, A., Boija, A., Klein, I. A., Coffey, E. L., Shrinivas, K., Abraham, B. J., Hannett, N. M., Zamudio, A. V., Manteiga, J. C., Li, C. H., Guo, Y. E., Day, D. S., Schuijers, J., Vasile, E., Malik, S., Hnisz, D., Lee, T. I., Cisse, II, Roeder, R. G., Sharp, P. A., Chakraborty, A. K., & Young, R. A. (2018). Coactivator condensation at super-enhancers links phase separation and gene control. *Science*, *361*(6400).
Sabo, A., Kress, T. R., Pelizzola, M., de Pretis, S., Gorski, M. M., Tesi, A., Morelli, M. J., Bora, P., Doni, M., Verrecchia, A., Tonelli, C., Faga, G., Bianchi, V., Ronchi, A., Low, D., Muller, H., Guccione, E., Campaner, S., & Amati, B. (2014). Selective transcriptional regulation by Myc in cellular growth control and lymphomagenesis. *Nature*, *511*(7510), 488-492.
Saiki, R. K., Scharf, S., Faloona, F., Mullis, K. B., Horn, G. T., Erlich, H. A., & Arnheim, N. (1985). Enzymatic amplification of beta-globin genomic sequences and restriction site analysis for diagnosis of sickle cell anemia. *Science*, *230*(4732), 1350-1354.
Saldi, T., Cortazar, M. A., Sheridan, R. M., & Bentley, D. L. (2016). Coupling of RNA Polymerase II Transcription Elongation with Pre-mRNA Splicing. *J Mol Biol*, *428*(12), 2623-2635.
Sampathi, S., Acharya, P., Zhao, Y., Wang, J., Stengel, K. R., Liu, Q., Savona, M. R., & Hiebert, S. W. (2019). The CDK7 inhibitor THZ1 alters RNA polymerase dynamics at the 5' and 3' ends of genes. *Nucleic Acids Res*, *47*(8), 3921-3936.
Sanchez-Bailon, M. P., Choi, S. Y., Dufficy, E. R., Sharma, K., McNee, G. S., Gunnell, E., Chiang, K., Sahay, D., Maslen, S., Stewart, G. S., Skehel, J. M., Dreveny, I., & Davies, C. C. (2021). Arginine methylation and ubiquitylation crosstalk controls DNA end-resection and homologous recombination repair. *Nat Commun*, *12*(1), 6313.
Schaub, F. X., Dhankani, V., Berger, A. C., Trivedi, M., Richardson, A. B., Shaw, R., Zhao, W., Zhang, X., Ventura, A., Liu, Y., Ayer, D. E., Hurlin, P. J., Cherniack, A. D., Eisenman, R. N., Bernard, B., Grandori, C., & Cancer Genome Atlas, N. (2018). Pan-cancer Alterations of the MYC Oncogene and Its Proximal Network across the Cancer Genome Atlas. *Cell Syst*, *6*(3), 282-300 e282.
Schmittgen, T. D., & Livak, K. J. (2008). Analyzing real-time PCR data by the comparative C(T) method. *Nat Protoc*, *3*(6), 1101-1108.
Schneider, A., Peukert, K., Eilers, M., & Hanel, F. (1997). Association of Myc with the zinc-finger protein Miz-1 defines a novel pathway for gene regulation by Myc. *Curr Top Microbiol Immunol*, *224*, 137-146.
Schoenfeld, A. R., Apgar, S., Dolios, G., Wang, R., & Aaronson, S. A. (2004). BRCA2 is ubiquitinated in vivo and interacts with USP11, a deubiquitinating enzyme that exhibits prosurvival function in the cellular response to DNA damage. *Mol Cell Biol*, *24*(17), 7444-7455.

Schrader, E. K., Harstad, K. G., & Matouschek, A. (2009). Targeting proteins for degradation. *Nat Chem Biol*, *5*(11), 815-822.

Schwab, M., Alitalo, K., Klempnauer, K. H., Varmus, H. E., Bishop, J. M., Gilbert, F., Brodeur, G., Goldstein, M., & Trent, J. (1983). Amplified DNA with limited homology to myc cellular oncogene is shared by human neuroblastoma cell lines and a neuroblastoma tumour. *Nature*, *305*(5931), 245-248.

Schwertman, P., Lagarou, A., Dekkers, D. H., Raams, A., van der Hoek, A. C., Laffeber, C., Hoeijmakers, J. H., Demmers, J. A., Fousteri, M., Vermeulen, W., & Marteijn, J. A. (2012). UV-sensitive syndrome protein UVSSA recruits USP7 to regulate transcription-coupled repair. *Nat Genet*, *44*(5), 598-602.

Scully, R., Anderson, S. F., Chao, D. M., Wei, W., Ye, L., Young, R. A., Livingston, D. M., & Parvin, J. D. (1997). BRCA1 is a component of the RNA polymerase II holoenzyme. *Proc Natl Acad Sci U S A*, *94*(11), 5605-5610.

Seizl, M., Lariviere, L., Pfaffeneder, T., Wenzeck, L., & Cramer, P. (2011). Mediator head subcomplex Med11/22 contains a common helix bundle building block with a specific function in transcription initiation complex stabilization. *Nucleic Acids Res*, *39*(14), 6291-6304.

Serrano, M., Lin, A. W., McCurrach, M. E., Beach, D., & Lowe, S. W. (1997). Oncogenic ras provokes premature cell senescence associated with accumulation of p53 and p16INK4a. *Cell*, *88*(5), 593-602.

Shah, P., Qiang, L., Yang, S., Soltani, K., & He, Y. Y. (2017). Regulation of XPC deubiquitination by USP11 in repair of UV-induced DNA damage. *Oncotarget*, *8*(57), 96522-96535.

Shaltiel, I. A., Krenning, L., Bruinsma, W., & Medema, R. H. (2015). The same, only different - DNA damage checkpoints and their reversal throughout the cell cycle. *J Cell Sci*, *128*(4), 607-620.

Sharp, P. A., Chakraborty, A. K., Henninger, J. E., & Young, R. A. (2022). RNA in formation and regulation of transcriptional condensates. *RNA*, *28*(1), 52-57.

Shen, L., Shao, N., Liu, X., & Nestler, E. (2014). ngs.plot: Quick mining and visualization of next-generation sequencing data by integrating genomic databases. *BMC Genomics*, *15*, 284.

Sheridan, R. M., Fong, N., D'Alessandro, A., & Bentley, D. L. (2019). Widespread Backtracking by RNA Pol II Is a Major Effector of Gene Activation, 5' Pause Release, Termination, and Transcription Elongation Rate. *Mol Cell*, *73*(1), 107-118 e104.

Sherpa, D., Chrustowicz, J., & Schulman, B. A. (2022). How the ends signal the end: Regulation by E3 ubiquitin ligases recognizing protein termini. *Mol Cell*, *82*(8), 1424-1438.

Shin, Y., & Brangwynne, C. P. (2017). Liquid phase condensation in cell physiology and disease. *Science*, *357*(6357).

Shivji, M. K. K., Renaudin, X., Williams, C. H., & Venkitaraman, A. R. (2018). BRCA2 Regulates Transcription Elongation by RNA Polymerase II to Prevent R-Loop Accumulation. *Cell Rep*, *22*(4), 1031-1039.

Shou, Y., Martelli, M. L., Gabrea, A., Qi, Y., Brents, L. A., Roschke, A., Dewald, G., Kirsch, I. R., Bergsagel, P. L., & Kuehl, W. M. (2000). Diverse karyotypic abnormalities of the c-myc locus associated with c-myc dysregulation and tumor progression in multiple myeloma. *Proc Natl Acad Sci U S A*, *97*(1), 228-233.

Siegel, R. L., Miller, K. D., Fuchs, H. E., & Jemal, A. (2022). Cancer statistics, 2022. *CA Cancer J Clin*, *72*(1), 7-33.

Sigurdsson, S., Dirac-Svejstrup, A. B., & Svejstrup, J. Q. (2010). Evidence that transcript cleavage is essential for RNA polymerase II transcription and cell viability. *Mol Cell*, *38*(2), 202-210.

Skene, P. J., & Henikoff, S. (2017). An efficient targeted nuclease strategy for high-resolution mapping of DNA binding sites. *Elife*, *6*.

Smith, M. A., Altekruse, S. F., Adamson, P. C., Reaman, G. H., & Seibel, N. L. (2014). Declining childhood and adolescent cancer mortality. *Cancer*, *120*(16), 2497-2506.

Smith, T., Heger, A., & Sudbery, I. (2017). UMI-tools: modeling sequencing errors in Unique Molecular Identifiers to improve quantification accuracy. *Genome Res*, *27*(3), 491-499.

Smith, V., & Foster, J. (2018). High-Risk Neuroblastoma Treatment Review. *Children (Basel)*, *5*(9).

Smyth, G. K. (2004). Linear models and empirical bayes methods for assessing differential expression in microarray experiments. *Stat Appl Genet Mol Biol*, *3*, Article3.

Snyder, N. A., & Silva, G. M. (2021). Deubiquitinating enzymes (DUBs): Regulation, homeostasis, and oxidative stress response. *J Biol Chem*, *297*(3), 101077.

Sollier, J., Stork, C. T., Garcia-Rubio, M. L., Paulsen, R. D., Aguilera, A., & Cimprich, K. A. (2014). Transcription-coupled nucleotide excision repair factors promote R-loop-induced genome instability. *Mol Cell*, *56*(6), 777-785.

Solvie, D., Baluapuri, A., Uhl, L., Fleischhauer, D., Endres, T., Papadopoulos, D., Aziba, A., Gaballa, A., Mikicic, I., Isaakova, E., Giansanti, C., Jansen, J., Jungblut, M., Klein, T., Schulein-Volk, C., Maric, H., Doose, S., Sauer, M., Beli, P., Rosenwald, A., Dobbelstein, M., Wolf, E., & Eilers, M. (2022). MYC multimers shield stalled replication forks from RNA polymerase. *Nature*.

Sowa, M. E., Bennett, E. J., Gygi, S. P., & Harper, J. W. (2009). Defining the human deubiquitinating enzyme interaction landscape. *Cell*, *138*(2), 389-403.

Spiliotopoulos, A., Blokpoel Ferreras, L., Densham, R. M., Caulton, S. G., Maddison, B. C., Morris, J. R., Dixon, J. E., Gough, K. C., & Dreveny, I. (2019). Discovery of peptide ligands targeting a specific ubiquitin-like domain-binding site in the deubiquitinase USP11. *J Biol Chem*, *294*(2), 424-436.

Steurer, B., Janssens, R. C., Geijer, M. E., Aprile-Garcia, F., Geverts, B., Theil, A. F., Hummel, B., van Royen, M. E., Evers, B., Bernards, R., Houtsmuller, A. B., Sawarkar, R., & Marteijn, J. (2022). DNA damage-induced transcription stress triggers the genome-wide degradation of promoter-bound Pol II. *Nat Commun*, *13*(1), 3624.

Steurer, B., Janssens, R. C., Geverts, B., Geijer, M. E., Wienholz, F., Theil, A. F., Chang, J., Dealy, S., Pothof, J., van Cappellen, W. A., Houtsmuller, A. B., & Marteijn, J. A. (2018). Live-cell analysis of endogenous GFP-RPB1 uncovers rapid turnover of initiating and promoter-paused RNA Polymerase II. *Proc Natl Acad Sci U S A*, *115*(19), E4368-E4376.

Stewart, M. D., Ritterhoff, T., Klevit, R. E., & Brzovic, P. S. (2016). E2 enzymes: more than just middle men. *Cell Res*, *26*(4), 423-440.

Stockum, A., Snijders, A. P., & Maertens, G. N. (2018). USP11 deubiquitinates RAE1 and plays a key role in bipolar spindle formation. *PLoS One*, *13*(1), e0190513.

Storer, A. C., & Menard, R. (1994). Catalytic mechanism in papain family of cysteine peptidases. *Methods Enzymol*, *244*, 486-500.

Strother, D. R., London, W. B., Schmidt, M. L., Brodeur, G. M., Shimada, H., Thorner, P., Collins, M. H., Tagge, E., Adkins, S., Reynolds, C. P., Murray, K., Lavey, R. S., Matthay, K. K., Castleberry, R., Maris, J. M., & Cohn, S. L. (2012). Outcome after surgery alone or with restricted use of chemotherapy for patients with low-risk neuroblastoma: results of Children's Oncology Group study P9641. *J Clin Oncol*, *30*(15), 1842-1848.

Sun, H., Ou, B., Zhao, S., Liu, X., Song, L., Liu, X., Wang, R., & Peng, Z. (2019). USP11 promotes growth and metastasis of colorectal cancer via PPP1CA-mediated activation of ERK/MAPK signaling pathway. *EBioMedicine*, *48*, 236-247.

Sun, Y., & Zhao, J. (2022). Transcription Elongation Factor A (SII)-Like (TCEAL) Gene Family Member-TCEAL2: A Novel Prognostic Marker in Pan-Cancer. *Cancer Inform*, *21*, 11769351221126285.

Swartling, F. J., Grimmer, M. R., Hackett, C. S., Northcott, P. A., Fan, Q. W., Goldenberg, D. D., Lau, J., Masic, S., Nguyen, K., Yakovenko, S., Zhe, X. N., Gilmer, H. C., Collins, R., Nagaoka, M., Phillips, J. J., Jenkins, R. B., Tihan, T., Vandenberg, S. R., James, C. D., Tanaka, K., Taylor, M. D., Weiss, W. A., & Chesler, L. (2010). Pleiotropic role for MYCN in medulloblastoma. *Genes Dev*, *24*(10), 1059-1072.

Swatek, K. N., & Komander, D. (2016). Ubiquitin modifications. *Cell Res*, *26*(4), 399-422.

Sydow, J. F., Brueckner, F., Cheung, A. C., Damsma, G. E., Dengl, S., Lehmann, E., Vassylyev, D., & Cramer, P. (2009). Structural basis of transcription: mismatch-specific fidelity mechanisms and paused RNA polymerase II with frayed RNA. *Mol Cell*, *34*(6), 710-721.

Tanaka, K., Suzuki, T., & Chiba, T. (1998). The ligation systems for ubiquitin and ubiquitin-like proteins. *Mol Cells*, *8*(5), 503-512.

Taub, R., Kirsch, I., Morton, C., Lenoir, G., Swan, D., Tronick, S., Aaronson, S., & Leder, P. (1982). Translocation of the c-myc gene into the immunoglobulin heavy chain locus in human Burkitt lymphoma and murine plasmacytoma cells. *Proc Natl Acad Sci U S A*, *79*(24), 7837-7841.

Tavana, O., Li, D., Dai, C., Lopez, G., Banerjee, D., Kon, N., Chen, C., Califano, A., Yamashiro, D. J., Sun, H., & Gu, W. (2016). HAUSP deubiquitinates and stabilizes N-Myc in neuroblastoma. *Nat Med*, *22*(10), 1180-1186.

Tesi, A., de Pretis, S., Furlan, M., Filipuzzi, M., Morelli, M. J., Andronache, A., Doni, M., Verrecchia, A., Pelizzola, M., Amati, B., & Sabo, A. (2019). An early Myc-dependent transcriptional program orchestrates cell growth during B-cell activation. *EMBO Rep*, *20*(9), e47987.

Thomas, L. R., Wang, Q., Grieb, B. C., Phan, J., Foshage, A. M., Sun, Q., Olejniczak, E. T., Clark, T., Dey, S., Lorey, S., Alicie, B., Howard, G. C., Cawthon, B., Ess, K. C., Eischen, C. M., Zhao, Z., Fesik, S. W., & Tansey, W. P. (2015). Interaction with WDR5 promotes target gene recognition and tumorigenesis by MYC. *Mol Cell*, *58*(3), 440-452.

Ting, X., Xia, L., Yang, J., He, L., Si, W., Shang, Y., & Sun, L. (2019). USP11 acts as a histone deubiquitinase functioning in chromatin reorganization during DNA repair. *Nucleic Acids Res*, *47*(18), 9721-9740.

Toma-Fukai, S., & Shimizu, T. (2021). Structural Diversity of Ubiquitin E3 Ligase. *Molecules*, *26*(21).
Toulokhonov, I., Zhang, J., Palangat, M., & Landick, R. (2007). A central role of the RNA polymerase trigger loop in active-site rearrangement during transcriptional pausing. *Mol Cell*, *27*(3), 406-419.
Towbin, H., Staehelin, T., & Gordon, J. (1979). Electrophoretic transfer of proteins from polyacrylamide gels to nitrocellulose sheets: procedure and some applications. *Proc Natl Acad Sci U S A*, *76*(9), 4350-4354.
Trochet, D., Bourdeaut, F., Janoueix-Lerosey, I., Deville, A., de Pontual, L., Schleiermacher, G., Coze, C., Philip, N., Frebourg, T., Munnich, A., Lyonnet, S., Delattre, O., & Amiel, J. (2004). Germline mutations of the paired-like homeobox 2B (PHOX2B) gene in neuroblastoma. *Am J Hum Genet*, *74*(4), 761-764.
Tuduri, S., Crabbe, L., Conti, C., Tourriere, H., Holtgreve-Grez, H., Jauch, A., Pantesco, V., De Vos, J., Thomas, A., Theillet, C., Pommier, Y., Tazi, J., Coquelle, A., & Pasero, P. (2009). Topoisomerase I suppresses genomic instability by preventing interference between replication and transcription. *Nat Cell Biol*, *11*(11), 1315-1324.
Tufegdzic Vidakovic, A., Mitter, R., Kelly, G. P., Neumann, M., Harreman, M., Rodriguez-Martinez, M., Herlihy, A., Weems, J. C., Boeing, S., Encheva, V., Gaul, L., Milligan, L., Tollervey, D., Conaway, R. C., Conaway, J. W., Snijders, A. P., Stewart, A., & Svejstrup, J. Q. (2020). Regulation of the RNAPII Pool Is Integral to the DNA Damage Response. *Cell*, *180*(6), 1245-1261 e1221.
Turowski, T. W., & Boguta, M. (2021). Specific Features of RNA Polymerases I and III: Structure and Assembly. *Front Mol Biosci*, *8*, 680090.
Twist, C. J., Schmidt, M. L., Naranjo, A., London, W. B., Tenney, S. C., Marachelian, A., Shimada, H., Collins, M. H., Esiashvili, N., Adkins, E. S., Mattei, P., Handler, M., Katzenstein, H., Attiyeh, E., Hogarty, M. D., Gastier-Foster, J., Wagner, E., Matthay, K. K., Park, J. R., Maris, J. M., & Cohn, S. L. (2019). Maintaining Outstanding Outcomes Using Response- and Biology-Based Therapy for Intermediate-Risk Neuroblastoma: A Report From the Children's Oncology Group Study ANBL0531. *J Clin Oncol*, *37*(34), 3243-3255.
Valentijn, L. J., Koster, J., Zwijnenburg, D. A., Hasselt, N. E., van Sluis, P., Volckmann, R., van Noesel, M. M., George, R. E., Tytgat, G. A., Molenaar, J. J., & Versteeg, R. (2015). TERT rearrangements are frequent in neuroblastoma and identify aggressive tumors. *Nat Genet*, *47*(12), 1411-1414.
van den Heuvel, D., Spruijt, C. G., Gonzalez-Prieto, R., Kragten, A., Paulsen, M. T., Zhou, D., Wu, H., Apelt, K., van der Weegen, Y., Yang, K., Dijk, M., Daxinger, L., Marteijn, J. A., Vertegaal, A. C. O., Ljungman, M., Vermeulen, M., & Luijsterburg, M. S. (2021). A CSB-PAF1C axis restores processive transcription elongation after DNA damage repair. *Nat Commun*, *12*(1), 1342.
van der Knaap, J. A., Kumar, B. R., Moshkin, Y. M., Langenberg, K., Krijgsveld, J., Heck, A. J., Karch, F., & Verrijzer, C. P. (2005). GMP synthetase stimulates histone H2B deubiquitylation by the epigenetic silencer USP7. *Mol Cell*, *17*(5), 695-707.
van der Veen, A. G., & Ploegh, H. L. (2012). Ubiquitin-like proteins. *Annu Rev Biochem*, *81*, 323-357.
van der Weegen, Y., de Lint, K., van den Heuvel, D., Nakazawa, Y., Mevissen, T. E. T., van Schie, J. J. M., San Martin Alonso, M., Boer, D. E. C., Gonzalez-Prieto, R., Narayanan, I. V., Klaassen, N. H. M., Wondergem, A. P., Roohollahi, K., Dorsman, J. C., Hara, Y., Vertegaal, A. C. O., de Lange, J., Walter, J. C., Noordermeer, S. M., Ljungman, M., Ogi, T., Wolthuis, R. M. F., & Luijsterburg, M. S. (2021). ELOF1 is a transcription-coupled DNA repair factor that directs RNA polymerase II ubiquitylation. *Nat Cell Biol*, *23*(6), 595-607.
van der Weegen, Y., Golan-Berman, H., Mevissen, T. E. T., Apelt, K., Gonzalez-Prieto, R., Goedhart, J., Heilbrun, E. E., Vertegaal, A. C. O., van den Heuvel, D., Walter, J. C., Adar, S., & Luijsterburg, M. S. (2020). The cooperative action of CSB, CSA, and UVSSA target TFIIH to DNA damage-stalled RNA polymerase II. *Nat Commun*, *11*(1), 2104.
van Groningen, T., Koster, J., Valentijn, L. J., Zwijnenburg, D. A., Akogul, N., Hasselt, N. E., Broekmans, M., Haneveld, F., Nowakowska, N. E., Bras, J., van Noesel, C. J. M., Jongejan, A., van Kampen, A. H., Koster, L., Baas, F., van Dijk-Kerkhoven, L., Huizer-Smit, M., Lecca, M. C., Chan, A., Lakeman, A., Molenaar, P., Volckmann, R., Westerhout, E. M., Hamdi, M., van Sluis, P. G., Ebus, M. E., Molenaar, J. J., Tytgat, G. A., Westerman, B. A., van Nes, J., & Versteeg, R. (2017). Neuroblastoma is composed of two super-enhancer-associated differentiation states. *Nat Genet*, *49*(8), 1261-1266.
van Wijk, S. J., Fulda, S., Dikic, I., & Heilemann, M. (2019). Visualizing ubiquitination in mammalian cells. *EMBO Rep*, *20*(2).
Varadi, M., Anyango, S., Deshpande, M., Nair, S., Natassia, C., Yordanova, G., Yuan, D., Stroe, O., Wood, G., Laydon, A., Zidek, A., Green, T., Tunyasuvunakool, K., Petersen, S., Jumper, J., Clancy, E., Green, R., Vora, A., Lutfi, M., Figurnov, M., Cowie, A., Hobbs, N., Kohli, P., Kleywegt, G.,

Birney, E., Hassabis, D., & Velankar, S. (2022). AlphaFold Protein Structure Database: massively expanding the structural coverage of protein-sequence space with high-accuracy models. *Nucleic Acids Res*, *50*(D1), D439-D444.
Varshavsky, A. (2011). The N-end rule pathway and regulation by proteolysis. *Protein Sci*, *20*(8), 1298-1345.
Varshavsky, A. (2012). Three decades of studies to understand the functions of the ubiquitin family. *Methods Mol Biol*, *832*, 1-11.
Varshavsky, A. (2019). N-degron and C-degron pathways of protein degradation. *Proc Natl Acad Sci U S A*, *116*(2), 358-366.
Vervoort, S. J., Devlin, J. R., Kwiatkowski, N., Teng, M., Gray, N. S., & Johnstone, R. W. (2022). Targeting transcription cycles in cancer. *Nat Rev Cancer*, *22*(1), 5-24.
Vihervaara, A., Mahat, D. B., Himanen, S. V., Blom, M. A. H., Lis, J. T., & Sistonen, L. (2021). Stress-induced transcriptional memory accelerates promoter-proximal pause release and decelerates termination over mitotic divisions. *Mol Cell*, *81*(8), 1715-1731 e1716.
Visel, A., Blow, M. J., Li, Z., Zhang, T., Akiyama, J. A., Holt, A., Plajzer-Frick, I., Shoukry, M., Wright, C., Chen, F., Afzal, V., Ren, B., Rubin, E. M., & Pennacchio, L. A. (2009). ChIP-seq accurately predicts tissue-specific activity of enhancers. *Nature*, *457*(7231), 854-858.
Vlasschaert, C., Xia, X., Coulombe, J., & Gray, D. A. (2015). Evolution of the highly networked deubiquitinating enzymes USP4, USP15, and USP11. *BMC Evol Biol*, *15*, 230.
Vo, B. T., Wolf, E., Kawauchi, D., Gebhardt, A., Rehg, J. E., Finkelstein, D., Walz, S., Murphy, B. L., Youn, Y. H., Han, Y. G., Eilers, M., & Roussel, M. F. (2016). The Interaction of Myc with Miz1 Defines Medulloblastoma Subgroup Identity. *Cancer Cell*, *29*(1), 5-16.
Vos, S. M., Farnung, L., Boehning, M., Wigge, C., Linden, A., Urlaub, H., & Cramer, P. (2018). Structure of activated transcription complex Pol II-DSIF-PAF-SPT6. *Nature*, *560*(7720), 607-612.
Vos, S. M., Farnung, L., Linden, A., Urlaub, H., & Cramer, P. (2020). Structure of complete Pol II-DSIF-PAF-SPT6 transcription complex reveals RTF1 allosteric activation. *Nat Struct Mol Biol*, *27*(7), 668-677.
Vos, S. M., Farnung, L., Urlaub, H., & Cramer, P. (2018). Structure of paused transcription complex Pol II-DSIF-NELF. *Nature*, *560*(7720), 601-606.
Vosper, J. M., McDowell, G. S., Hindley, C. J., Fiore-Heriche, C. S., Kucerova, R., Horan, I., & Philpott, A. (2009). Ubiquitylation on canonical and non-canonical sites targets the transcription factor neurogenin for ubiquitin-mediated proteolysis. *J Biol Chem*, *284*(23), 15458-15468.
Walsh, C. T., Garneau-Tsodikova, S., & Gatto, G. J., Jr. (2005). Protein posttranslational modifications: the chemistry of proteome diversifications. *Angew Chem Int Ed Engl*, *44*(45), 7342-7372.
Walz, S., Lorenzin, F., Morton, J., Wiese, K. E., von Eyss, B., Herold, S., Rycak, L., Dumay-Odelot, H., Karim, S., Bartkuhn, M., Roels, F., Wustefeld, T., Fischer, M., Teichmann, M., Zender, L., Wei, C. L., Sansom, O., Wolf, E., & Eilers, M. (2014). Activation and repression by oncogenic MYC shape tumour-specific gene expression profiles. *Nature*, *511*(7510), 483-487.
Wang, B., Zhang, L., Dai, T., Qin, Z., Lu, H., Zhang, L., & Zhou, F. (2021). Liquid-liquid phase separation in human health and diseases. *Signal Transduct Target Ther*, *6*(1), 290.
Wang, D., Bushnell, D. A., Huang, X., Westover, K. D., Levitt, M., & Kornberg, R. D. (2009). Structural basis of transcription: backtracked RNA polymerase II at 3.4 angstrom resolution. *Science*, *324*(5931), 1203-1206.
Wang, D., Zhao, J., Li, S., Wei, J., Nan, L., Mallampalli, R. K., Weathington, N. M., Ma, H., & Zhao, Y. (2018). Phosphorylated E2F1 is stabilized by nuclear USP11 to drive Peg10 gene expression and activate lung epithelial cells. *J Mol Cell Biol*, *10*(1), 60-73.
Wang, T., Liu, L., Chen, X., Shen, Y., Lian, G., Shah, N., Davidoff, A. M., Yang, J., & Wang, R. (2018). MYCN drives glutaminolysis in neuroblastoma and confers sensitivity to an ROS augmenting agent. *Cell Death Dis*, *9*(2), 220.
Wang, W., Xu, J., Chong, J., & Wang, D. (2018). Structural basis of DNA lesion recognition for eukaryotic transcription-coupled nucleotide excision repair. *DNA Repair (Amst)*, *71*, 43-55.
Wang, Y., & Wang, F. (2021). Post-Translational Modifications of Deubiquitinating Enzymes: Expanding the Ubiquitin Code. *Front Pharmacol*, *12*, 685011.
Weber, C. M., Ramachandran, S., & Henikoff, S. (2014). Nucleosomes are context-specific, H2A.Z-modulated barriers to RNA polymerase. *Mol Cell*, *53*(5), 819-830.
Wei, Y., Resetca, D., Li, Z., Johansson-Akhe, I., Ahlner, A., Helander, S., Wallenhammar, A., Morad, V., Raught, B., Wallner, B., Kokubo, T., Tong, Y., Penn, L. Z., & Sunnerhagen, M. (2019). Multiple direct interactions of TBP with the MYC oncoprotein. *Nat Struct Mol Biol*, *26*(11), 1035-1043.

Weinert, B. T., Scholz, C., Wagner, S. A., Iesmantavicius, V., Su, D., Daniel, J. A., & Choudhary, C. (2013). Lysine succinylation is a frequently occurring modification in prokaryotes and eukaryotes and extensively overlaps with acetylation. *Cell Rep*, *4*(4), 842-851.

Weiss, W. A., Aldape, K., Mohapatra, G., Feuerstein, B. G., & Bishop, J. M. (1997). Targeted expression of MYCN causes neuroblastoma in transgenic mice. *EMBO J*, *16*(11), 2985-2995.

West, S., Gromak, N., & Proudfoot, N. J. (2004). Human 5' --> 3' exonuclease Xrn2 promotes transcription termination at co-transcriptional cleavage sites. *Nature*, *432*(7016), 522-525.

Wiese, K. E., Walz, S., von Eyss, B., Wolf, E., Athineos, D., Sansom, O., & Eilers, M. (2013). The role of MIZ-1 in MYC-dependent tumorigenesis. *Cold Spring Harb Perspect Med*, *3*(12), a014290.

Wild, T., & Cramer, P. (2012). Biogenesis of multisubunit RNA polymerases. *Trends Biochem Sci*, *37*(3), 99-105.

Willis, I. M. (1993). RNA polymerase III. Genes, factors and transcriptional specificity. *Eur J Biochem*, *212*(1), 1-11.

Wiltshire, T. D., Lovejoy, C. A., Wang, T., Xia, F., O'Connor, M. J., & Cortez, D. (2010). Sensitivity to poly(ADP-ribose) polymerase (PARP) inhibition identifies ubiquitin-specific peptidase 11 (USP11) as a regulator of DNA double-strand break repair. *J Biol Chem*, *285*(19), 14565-14571.

Wu, H. C., Lin, Y. C., Liu, C. H., Chung, H. C., Wang, Y. T., Lin, Y. W., Ma, H. I., Tu, P. H., Lawler, S. E., & Chen, R. H. (2017). Erratum: USP11 regulates PML stability to control Notch-induced malignancy in brain tumours. *Nat Commun*, *8*, 16167.

Wu, W., Nishikawa, H., Hayami, R., Sato, K., Honda, A., Aratani, S., Nakajima, T., Fukuda, M., & Ohta, T. (2007). BRCA1 ubiquitinates RPB8 in response to DNA damage. *Cancer Res*, *67*(3), 951-958.

Xie, Z., Bailey, A., Kuleshov, M. V., Clarke, D. J. B., Evangelista, J. E., Jenkins, S. L., Lachmann, A., Wojciechowicz, M. L., Kropiwnicki, E., Jagodnik, K. M., Jeon, M., & Ma'ayan, A. (2021). Gene Set Knowledge Discovery with Enrichr. *Curr Protoc*, *1*(3), e90.

Yamaguchi, Y., Takagi, T., Wada, T., Yano, K., Furuya, A., Sugimoto, S., Hasegawa, J., & Handa, H. (1999). NELF, a multisubunit complex containing RD, cooperates with DSIF to repress RNA polymerase II elongation. *Cell*, *97*(1), 41-51.

Yan, W. X., Mirzazadeh, R., Garnerone, S., Scott, D., Schneider, M. W., Kallas, T., Custodio, J., Wernersson, E., Li, Y., Gao, L., Federova, Y., Zetsche, B., Zhang, F., Bienko, M., & Crosetto, N. (2017). BLISS is a versatile and quantitative method for genome-wide profiling of DNA double-strand breaks. *Nat Commun*, *8*, 15058.

Yang, H., Park, D., Ryu, J., & Park, T. (2021). USP11 degrades KLF4 via its deubiquitinase activity in liver diseases. *J Cell Mol Med*, *25*(14), 6976-6987.

Yasuhara, T., Kato, R., Hagiwara, Y., Shiotani, B., Yamauchi, M., Nakada, S., Shibata, A., & Miyagawa, K. (2018). Human Rad52 Promotes XPG-Mediated R-loop Processing to Initiate Transcription-Associated Homologous Recombination Repair. *Cell*, *175*(2), 558-570 e511.

Yasukawa, T., Kamura, T., Kitajima, S., Conaway, R. C., Conaway, J. W., & Aso, T. (2008). Mammalian Elongin A complex mediates DNA-damage-induced ubiquitylation and degradation of Rpb1. *EMBO J*, *27*(24), 3256-3266.

Yau, R., & Rape, M. (2016). The increasing complexity of the ubiquitin code. *Nat Cell Biol*, *18*(6), 579-586.

Yeh, C. H., & Shatkin, A. J. (1994a). Down-regulation of Rous sarcoma virus long terminal repeat promoter activity by a HeLa cell basic protein. *Proc Natl Acad Sci U S A*, *91*(23), 11002-11006.

Yeh, C. H., & Shatkin, A. J. (1994b). A HeLa-cell-encoded p21 is homologous to transcription elongation factor SII. *Gene*, *143*(2), 285-287.

Yilmaz, D., Furst, A., Meaburn, K., Lezaja, A., Wen, Y., Altmeyer, M., Reina-San-Martin, B., & Soutoglou, E. (2021). Activation of homologous recombination in G1 preserves centromeric integrity. *Nature*, *600*(7890), 748-753.

Young, R. A. (1991). RNA polymerase II. *Annu Rev Biochem*, *60*, 689-715.

Yu, M., Liu, K., Mao, Z., Luo, J., Gu, W., & Zhao, W. (2016). USP11 Is a Negative Regulator to gammaH2AX Ubiquitylation by RNF8/RNF168. *J Biol Chem*, *291*(2), 959-967.

Yu, M., Yang, W., Ni, T., Tang, Z., Nakadai, T., Zhu, J., & Roeder, R. G. (2015). RNA polymerase II-associated factor 1 regulates the release and phosphorylation of paused RNA polymerase II. *Science*, *350*(6266), 1383-1386.

Yuan, T., Yan, F., Ying, M., Cao, J., He, Q., Zhu, H., & Yang, B. (2018). Inhibition of Ubiquitin-Specific Proteases as a Novel Anticancer Therapeutic Strategy. *Front Pharmacol*, *9*, 1080.

Yudkovsky, N., Ranish, J. A., & Hahn, S. (2000). A transcription reinitiation intermediate that is stabilized by activator. *Nature*, *408*(6809), 225-229.

Zatreanu, D., Han, Z., Mitter, R., Tumini, E., Williams, H., Gregersen, L., Dirac-Svejstrup, A. B., Roma, S., Stewart, A., Aguilera, A., & Svejstrup, J. Q. (2019). Elongation Factor TFIIS Prevents

Transcription Stress and R-Loop Accumulation to Maintain Genome Stability. *Mol Cell*, *76*(1), 57-69 e59.

Zeid, R., Lawlor, M. A., Poon, E., Reyes, J. M., Fulciniti, M., Lopez, M. A., Scott, T. G., Nabet, B., Erb, M. A., Winter, G. E., Jacobson, Z., Polaski, D. R., Karlin, K. L., Hirsch, R. A., Munshi, N. P., Westbrook, T. F., Chesler, L., Lin, C. Y., & Bradner, J. E. (2018). Enhancer invasion shapes MYCN-dependent transcriptional amplification in neuroblastoma. *Nat Genet*, *50*(4), 515-523.

Zhang, C., Xie, C., Wang, X., Huang, Y., Gao, S., Lu, J., Lu, Y., & Zhang, S. (2020). Aberrant USP11 expression regulates NF90 to promote proliferation and metastasis in hepatocellular carcinoma. *Am J Cancer Res*, *10*(5), 1416-1428.

Zhang, E., Shen, B., Mu, X., Qin, Y., Zhang, F., Liu, Y., Xiao, J., Zhang, P., Wang, C., Tan, M., & Fan, Y. (2016). Ubiquitin-specific protease 11 (USP11) functions as a tumor suppressor through deubiquitinating and stabilizing VGLL4 protein. *Am J Cancer Res*, *6*(12), 2901-2909.

Zhang, H., Rigo, F., & Martinson, H. G. (2015). Poly(A) Signal-Dependent Transcription Termination Occurs through a Conformational Change Mechanism that Does Not Require Cleavage at the Poly(A) Site. *Mol Cell*, *59*(3), 437-448.

Zhang, N., Ichikawa, W., Faiola, F., Lo, S. Y., Liu, X., & Martinez, E. (2014). MYC interacts with the human STAGA coactivator complex via multivalent contacts with the GCN5 and TRRAP subunits. *Biochim Biophys Acta*, *1839*(5), 395-405.

Zhang, X., Chiang, H. C., Wang, Y., Zhang, C., Smith, S., Zhao, X., Nair, S. J., Michalek, J., Jatoi, I., Lautner, M., Oliver, B., Wang, H., Petit, A., Soler, T., Brunet, J., Mateo, F., Angel Pujana, M., Poggi, E., Chaldekas, K., Isaacs, C., Peshkin, B. N., Ochoa, O., Chedin, F., Theoharis, C., Sun, L. Z., Curiel, T. J., Elledge, R., Jin, V. X., Hu, Y., & Li, R. (2017). Attenuation of RNA polymerase II pausing mitigates BRCA1-associated R-loop accumulation and tumorigenesis. *Nat Commun*, *8*, 15908.

Zhang, X., Smits, A. H., van Tilburg, G. B., Jansen, P. W., Makowski, M. M., Ovaa, H., & Vermeulen, M. (2017). An Interaction Landscape of Ubiquitin Signaling. *Mol Cell*, *65*(5), 941-955 e948.

Zhou, Q., Li, T., & Price, D. H. (2012). RNA polymerase II elongation control. *Annu Rev Biochem*, *81*, 119-143.

Zhou, Z., Luo, A., Shrivastava, I., He, M., Huang, Y., Bahar, I., Liu, Z., & Wan, Y. (2017). Regulation of XIAP Turnover Reveals a Role for USP11 in Promotion of Tumorigenesis. *EBioMedicine*, *15*, 48-61.

Zhu, J., Blenis, J., & Yuan, J. (2008). Activation of PI3K/Akt and MAPK pathways regulates Myc-mediated transcription by phosphorylating and promoting the degradation of Mad1. *Proc Natl Acad Sci U S A*, *105*(18), 6584-6589.

Zhu, X., Zhang, Y., Luo, Q., Wu, X., Huang, F., Shu, T., Wan, Y., Chen, H., & Liu, Z. (2021). The deubiquitinase USP11 promotes ovarian cancer chemoresistance by stabilizing BIP. *Signal Transduct Target Ther*, *6*(1), 264.

7 Appendix

Supplementary data

i. qMS data – corresponding to section 2.1

Values of the USP11 interactome corresponding to the volcano plot presented in Figure 9.

Table 26: qMS data table

The table displays the enrichment of proteins in HA-USP11 expressing cells compared to control cells (mean of tetraplicates, $log_2FC \geq 1.00$) and their significance indicated shown as adjusted p-values (for p<0.05 ** for p<0.01, *** for p<0.001, ns: not significant).*

Gene name	log_2FC	Significance
USP11	15.39	***
HAUS5	6.36	***
CUL7	6.32	***
BAG2	6.26	**
TCEAL1	6.24	**
NPEPPS	6.14	***
CTAG2	5.67	***
PML	5.62	***
STIP1	5.57	***
USP7	5.49	***
PFKM	5.49	***
ZNHIT2	5.45	***
TCEAL4	5.44	***
POLR1B	5.44	***
POLR1A	5.36	***
DENND3	5.34	***
PFAS	5.21	***
DNA2	5.18	***
HAUS3	5.15	***
MYCBP2	4.92	**
CAD	4.90	***
ILK	4.71	***
HAUS6	4.57	***
BAG5	4.55	**
HGH1	4.50	***
PPAT	4.45	***
TARS	4.37	***
HPS6	4.36	***
POLR1C	4.35	***
AMBRA1	4.29	***
IQGAP3	4.25	***
TNS2	4.24	***
NME1-NME2;NME2;NME1	4.24	***
AHCTF1	4.20	***
PFDN2	4.14	***
POLD1	4.11	***
RAB3GAP2	4.11	***
PFDN1	4.10	***
MTR	4.09	***
HSPA1B;HSPA1A	4.08	***
PNPLA6	4.07	***
DNAJC7	4.04	***
DPP9	4.00	***
FKBP8	3.99	***

CCAR2	3.99	***
PSMA1	3.92	***
CCT2	3.90	***
HSPH1	3.90	***
IKBKAP	3.88	***
HAUS1	3.87	***
RHOBTB3	3.83	***
PSMD11	3.82	***
MCM4	3.81	***
VPS16	3.78	***
SEC16A	3.77	***
CCT5	3.75	***
CCT8	3.72	***
ASCC3	3.70	***
PSMA7	3.69	***
RSU1	3.67	***
UBR5	3.67	*
HAUS4	3.66	***
POLR2B	3.64	***
MED16	3.62	***
TKT	3.61	***
PSMD14	3.59	***
HUWE1	3.58	**
TCAF1	3.56	***
HSPBP1	3.56	***
RRM1	3.55	***
RAF1	3.54	***
DNAJB12	3.54	***
VPS33A	3.53	***
ACSL3	3.53	***
DCAF7	3.51	***
CUL4A	3.50	***
XRCC3	3.48	**
ARHGAP23	3.48	***
RIN1	3.47	***
CCT6A	3.46	**
PSMD13	3.45	***
UBR4	3.44	**
VPS18	3.44	***
CNP	3.42	***
VPS13A	3.42	**
CCZ1;CCZ1B	3.40	***
CTAG1B	3.40	**
AIMP1	3.38	***
TARS2	3.35	***
GNPAT	3.34	***
USP22	3.33	***
GTF2F1	3.33	**
FAM208A	3.32	***
PSMC1	3.31	**
MAGED1	3.31	***
CUL1	3.30	***
PITRM1	3.29	***
PSMD1	3.27	**
PSMC4	3.26	*
NPRL3	3.25	***
DCAF10	3.24	***
HSPA8	3.23	***

UNC119B	3.23	**
CCT4	3.22	**
ELP3	3.22	**
SLC25A1	3.19	***
DNAJC10	3.18	**
MYO9B	3.18	**
SQSTM1	3.18	**
DYNC2H1	3.13	**
CPSF1	3.12	**
DPYD	3.11	***
VBP1	3.06	**
WDR33	3.05	***
MYOF	3.03	***
DARS	3.02	***
PSMC2	3.01	***
PFDN5	3.01	***
COPS2	3.01	**
RAD50	2.99	**
POLR1D	2.99	***
DNAJA2	2.97	***
ESYT1	2.96	***
CBFB	2.96	**
AFG3L2	2.94	***
BAT3;BAG6	2.93	***
NUDC	2.93	***
LIMS1	2.92	***
CDKAL1	2.92	***
USP9X	2.92	**
HELZ2	2.91	**
MRPL37	2.90	**
CCT7	2.89	**
CCT3	2.89	**
TTC31	2.88	***
SAP30	2.88	***
POM121C	2.85	***
PYGL	2.84	***
ARAP3	2.84	**
RNGTT	2.80	***
LDHA	2.79	***
HECTD1	2.79	**
AP3M1	2.78	***
VWA8	2.77	***
PFKP	2.76	**
SLC25A13	2.76	*
TRMT1	2.75	***
PFDN6	2.75	**
BRD9	2.75	**
ACAD9	2.74	***
HSP90AB2P	2.73	**
MTHFD1	2.73	*
MCM3AP	2.73	***
NQO1	2.72	***
POLR2C	2.71	***
CBWD1	2.70	**
PSMA2	2.70	*
XRN1	2.70	***
DNAJA1	2.70	***
VPS13B	2.69	**

NDUFS2	2.69	***
GART	2.69	**
ETFA	2.69	**
SOGA1	2.69	***
LLGL1	2.68	***
PHB2	2.67	**
FAM46A	2.65	***
ARHGEF40	2.65	***
GFPT2	2.65	*
MAEA	2.65	***
PSMA6	2.64	**
IRAK1	2.64	***
NR0B1	2.63	*
TUBA1C	2.62	**
WDR6	2.62	***
EPHA2	2.61	**
RICTOR	2.60	**
KIF11	2.60	**
SMCHD1	2.60	**
NCAPG2	2.59	***
MAPK1	2.59	**
CISD3	2.59	**
CDC42BPB	2.59	**
G6PD	2.58	**
EPRS	2.58	**
PRKDC	2.57	***
PI4KA	2.56	***
TRABD	2.56	***
MB21D2	2.55	**
MRPS36	2.54	*
TCP1	2.54	**
TGFB1	2.53	***
ACACA	2.52	**
VPS45	2.52	**
CKAP5	2.51	**
PUS1	2.51	**
GANAB	2.51	**
DYNLRB1;DYNLRB2	2.51	**
CDK5RAP1	2.50	**
XRCC5	2.50	***
TRRAP	2.49	***
MDN1	2.48	**
CDC123	2.48	***
SMC2	2.48	**
PSMC6	2.47	***
IGF2R	2.47	***
TUBB	2.47	***
NDUFS1	2.47	***
SUPT6H	2.46	**
RFC3	2.46	**
DNAJB14	2.45	**
PSMA3	2.44	***
FASN	2.44	***
USP54	2.44	**
WDR35	2.44	**
DNAJA3	2.44	**
SACS	2.44	***
POLR2A	2.43	**

NT5DC2	2.43	**
TUBA1A	2.43	***
PSMA4	2.43	***
BSG	2.43	**
PRIM1	2.42	***
SLC25A22	2.40	***
DNAJB1	2.40	**
CC2D2A	2.39	**
PANK4	2.39	***
PCOLCE	2.38	***
EXOC8	2.38	**
RPTOR	2.38	**
PSMD2	2.37	***
AAR2	2.37	**
MRPL30	2.36	*
PEX6	2.36	***
HELZ	2.35	**
NDUFAF3	2.35	**
TUBA1B	2.34	***
POLR3B	2.34	**
CBLL1	2.33	**
ANAPC1	2.32	**
CTAG2	2.31	**
HCFC1	2.31	**
ELP2	2.31	***
GLUD1	2.31	***
CYFIP1	2.30	***
MAGEC1	2.29	**
HERC1	2.29	**
RPAP1	2.27	***
S100A9	2.27	*
CHPF	2.27	**
QARS	2.27	***
NIPSNAP1	2.26	**
DNAJC16	2.26	***
PRIM2	2.26	**
THOC3	2.26	**
PSMD3	2.25	*
DNMT1	2.25	*
ATP6V1A	2.24	**
CUL2	2.24	***
PSMD10	2.24	*
TROVE2	2.22	*
TTC26	2.22	**
CHST14	2.22	**
PSMB1	2.21	***
PHLDA2	2.20	*
PPP6C	2.20	***
APOL2	2.20	**
NUDCD3	2.20	**
BAG3	2.20	**
PSMC3	2.19	*
PSMA5	2.19	**
CCDC85B	2.19	*
CYC1	2.19	*
UQCRQ	2.18	**
HPS3	2.18	**
LDHB	2.18	**

TUBB4B	2.18	***
GEMIN5	2.17	***
METTL3	2.17	*
CDC37	2.17	**
ELAC2	2.17	**
DNAJC3	2.16	**
EML3	2.16	**
IARS2	2.16	**
DDB1	2.15	***
TBCD	2.15	**
SNAP47	2.15	*
TRIP12	2.14	***
TIMM21	2.13	**
DCAF8	2.12	***
EIF2AK4	2.12	**
PSMD4	2.12	**
SMARCA4	2.11	*
TRIM32	2.11	**
PFDN4	2.10	ns
GBAS	2.10	**
SPATA5L1	2.10	***
MARCH7	2.10	**
RARS	2.09	**
MGRN1	2.08	*
ERCC2	2.08	**
EXOC5	2.08	**
RTN4	2.08	**
RFC4	2.07	*
SLC16A1	2.07	**
FAM83D	2.07	**
DUSP11	2.06	*
PSMD12	2.06	**
MMS19	2.06	**
TUBB2A	2.06	***
PYCR1	2.05	**
GNB4	2.04	**
GNA11	2.04	*
BAG1	2.04	**
SLC25A12	2.04	*
MTHFD2	2.04	*
EIF5B	2.03	*
ZMYM2	2.03	*
ALG1	2.02	**
TECR	2.02	**
FKBP4	2.02	*
LRWD1	2.02	*
CDK4	2.01	**
KDM1A	2.01	**
DMWD	2.01	***
ARHGEF1	2.00	**
SHMT2	2.00	**
HERC2	1.99	ns
DNMBP	1.99	*
ADRM1	1.97	**
NDUFA9	1.97	**
TOR4A	1.95	***
SDF2	1.95	**
PON2	1.95	*

ATR	1.94	**
C14orf80	1.94	**
NDUFA4	1.94	**
TRIP13	1.93	***
ALDH3B1	1.93	**
HK1	1.92	**
TUBB3	1.92	**
FOXRED2	1.92	**
NUP205	1.92	*
GPS1	1.92	*
CPT1A	1.92	**
PLEKHG4	1.91	***
TCEB2	1.91	**
DNAJC11	1.91	**
SFRP1	1.90	*
PRKAG1	1.90	*
ZNF687	1.90	**
PRDX4	1.89	*
GNAI2	1.89	**
FOXK1	1.89	*
UMPS	1.88	**
SEC23IP	1.88	**
AUP1	1.88	*
OXA1L	1.87	**
SEPT2	1.87	*
PRMT1	1.87	**
CYCS	1.87	*
TIMM50	1.87	**
ATXN10	1.86	**
INTS1	1.86	*
VPS13C	1.86	*
IGBP1	1.86	**
PTPN23	1.86	**
MCM8	1.85	***
ETFB	1.85	**
HERC4	1.85	**
GTF2H2C;GTF2H2	1.84	**
NUP85	1.84	**
HAX1	1.83	**
CHPF2	1.83	**
LGALS3BP	1.83	**
ECSIT	1.82	*
TUBB6	1.82	**
ACLY	1.82	**
SEC24D	1.81	**
CDC2;CDK1	1.80	*
SLC25A3	1.80	**
CAPN2	1.80	**
NCAPD2	1.80	*
IARS	1.80	**
ASPM	1.79	*
MAN1B1	1.79	*
PSMD7	1.79	*
NACA	1.79	**
PSMB7	1.79	*
LONP2	1.79	**
PNKD	1.78	**
TAF6L	1.78	**

HAUS7	1.78	**
MAP1B	1.78	**
EEF1B2	1.77	*
SLC25A11	1.77	**
FARSA	1.77	**
GTF2F2	1.75	ns
CTR9	1.75	**
ANAPC5	1.74	**
ATP5SL	1.74	**
HSPA4	1.74	**
VARS	1.74	**
ANAPC7	1.74	*
PSMB4	1.73	**
ALDOA	1.73	**
ATP5C1	1.73	**
RNF219	1.73	**
GNAI1	1.72	*
DNAJB11	1.72	*
ATAD3B	1.72	**
QTRT1	1.72	*
GNG11	1.71	*
CC2D1A	1.71	**
POLR3A	1.71	**
SMG9	1.71	**
GTF3C4	1.71	**
ASNS	1.71	*
ALDH3A2	1.70	**
RBPMS	1.70	**
USP19	1.70	**
TXNRD1	1.69	*
RNF213	1.69	**
KARS	1.69	**
ATM	1.68	ns
POLR2E	1.68	**
THEM6	1.68	*
PSMC5	1.68	**
PPP2R2A	1.68	**
SLC25A20	1.67	*
PYCR2	1.67	**
DARS2	1.67	**
TCP11L1	1.67	**
ACOT9	1.66	**
RPS19BP1	1.66	**
SFXN1	1.66	**
HAUS8	1.65	**
STOML2	1.65	**
NUP160	1.65	**
NDUFS3	1.65	*
LARS	1.65	**
NDUFS7	1.64	*
TMEM201	1.64	**
NDUFB4	1.64	**
NUBP2	1.64	**
RUVBL2	1.64	**
TAF2	1.64	*
ECD	1.63	*
GAK	1.63	*
GFPT1	1.62	**

RFC2	1.62	*
COX16;SYNJ2BP-COX16	1.62	*
ATP6V1F	1.61	*
HAUS2	1.61	*
SMG8	1.59	**
SCCPDH	1.59	*
DDOST	1.59	*
SCO2	1.59	**
UGGT1	1.58	**
MICU2	1.58	*
POLDIP2	1.58	**
WDR81	1.57	*
TIGD5	1.57	*
SMC4	1.57	*
SMC3	1.57	*
FAM96B	1.57	*
ENDOG	1.56	**
MED12;TNRC11	1.56	*
DPY30	1.56	ns
PSMD6	1.56	*
PXN	1.55	**
BRCA2	1.55	*
RANBP9	1.55	*
NTPCR	1.55	**
PSMB5	1.55	**
PBRM1	1.55	**
SMC6	1.54	ns
SEC13	1.54	*
NUF2	1.54	ns
NDUFA5	1.54	*
TUBG1;TUBG2	1.53	*
MARS	1.53	*
TUBGCP3	1.53	**
CPSF2	1.53	*
RAE1	1.52	**
CSNK2A1;CSNK2A3	1.52	*
MRFAP1	1.52	*
FNDC3B	1.52	*
OGDH	1.52	ns
IDE	1.51	*
LRRC41	1.50	ns
PLEKHA5	1.50	*
ANXA2;ANXA2P2	1.50	ns
POLR3E	1.50	ns
AIP	1.49	*
TOP2B	1.49	ns
IKBIP	1.49	*
GNB1	1.49	**
SPTLC1	1.48	*
PDCD2L	1.48	**
PRNP	1.48	ns
SMC1A	1.47	ns
GOLGA7	1.47	*
TRIM56	1.47	*
SDF2L1	1.47	**
GMPPA	1.47	*
SFXN3	1.45	*
RFC5	1.45	**

EIF2S1	1.45	*
RALB	1.44	*
ILVBL	1.44	**
SDHA	1.44	*
RBM27	1.43	*
OPA1	1.43	ns
DRG1	1.43	*
SKIV2L	1.42	**
TFB2M	1.42	*
MCM7	1.42	**
NARS	1.41	*
SEC24C	1.41	*
MARCKS	1.41	ns
SNRNP200	1.41	*
CTPS1	1.41	**
EFR3A	1.41	ns
WRNIP1	1.41	**
HDAC3	1.40	*
PCDH10	1.40	ns
AIFM1	1.40	*
MRPL32	1.40	*
DSC1	1.40	ns
SLC25A6	1.40	**
RUVBL1	1.40	**
CAPN6	1.40	ns
MOGS	1.40	*
BRIP1	1.40	*
FBXO3	1.39	*
ATAD3A	1.39	**
ACTL6A	1.39	*
STUB1	1.39	**
FAM91A1	1.38	*
AIMP2	1.38	**
BTAF1	1.37	*
RECQL4	1.37	*
PPP1R15B	1.37	ns
TYMS	1.36	*
SEC23B	1.36	*
PTGES3	1.36	*
MED17	1.36	ns
ATP5J2-PTCD1;PTCD1	1.35	*
MSTO1	1.35	*
MRPL50	1.35	*
GNAI3	1.35	*
MIIP	1.35	*
HSP90AB1	1.34	**
NOMO1	1.34	**
ST13;ST13P5;ST13P4	1.34	*
SYDE1	1.34	*
PIK3R4	1.33	*
MRPS9	1.33	ns
TCEB1	1.33	*
PSMD8	1.33	**
DLST	1.33	ns
PAAF1	1.32	*
MEF2A;MEF2C	1.32	ns
TYK2	1.32	*
ENO1	1.32	**

ZNF787	1.32	*
MCM2	1.32	ns
CLK1	1.31	ns
QSOX1	1.31	**
SLC3A2	1.31	*
AHNAK	1.30	*
PELO	1.30	ns
UBA1	1.30	**
MCMBP	1.30	*
HSP90AA1	1.29	**
PPP2CA	1.29	*
SKP1	1.29	ns
RSAD1	1.29	*
EP400	1.29	**
CEP192	1.29	ns
MAGED2	1.28	*
CXorf56	1.28	*
ACY1;ABHD14A-ACY1	1.28	ns
EMILIN1	1.27	**
WDR48	1.27	*
SEC23A	1.27	*
COX4I1	1.27	*
PSMG1	1.27	ns
GNAS	1.27	**
ZNF512	1.27	ns
DSG1	1.27	ns
RAP2B	1.26	ns
POLR1E	1.26	*
CNN2	1.25	*
GAPDH	1.25	*
SMARCB1	1.25	*
HCCS	1.25	*
PHLDA1	1.25	ns
COX6C	1.25	ns
MRPS21	1.24	*
VCP	1.24	*
WDR77	1.24	ns
ATP1A1	1.24	*
HOXC4	1.24	*
METTL13	1.24	*
FAM129A	1.23	ns
MRPS35	1.23	*
DPM1	1.23	*
WDR82	1.23	ns
PRPF8	1.23	*
GTF3C3	1.22	*
POLR2H	1.22	**
SEMA3A	1.22	*
SLC25A5	1.22	*
MTCH1	1.21	*
COPE	1.21	ns
NAE1	1.21	*
AP1S1	1.21	ns
LAS1L	1.21	**
CTSB	1.20	ns
RSPO3	1.20	ns
CHP1	1.20	ns
FNDC3A	1.20	*

AAAS	1.20	*
UTP15	1.19	ns
ATP5I	1.19	**
CACYBP	1.19	**
KEAP1	1.19	ns
FAM129B	1.19	*
MRPS12	1.19	*
ARPC1B	1.19	ns
CDK6	1.18	*
CSTF1	1.18	*
EIF2S3;EIF2S3L	1.18	*
CDK17	1.18	ns
TBX2	1.18	ns
UQCRH	1.18	*
DYNC1H1	1.18	*
SYNPO2	1.18	ns
XRCC6	1.18	*
SH3BP4	1.18	**
CDK13	1.17	*
ZNF592	1.16	ns
COPA	1.16	**
ZNF638	1.16	ns
PTCD3	1.16	*
RAP1A;RAP1B	1.16	ns
SPSB3	1.15	ns
CD109	1.15	ns
TRMT10C	1.15	ns
SNAP23	1.15	ns
SSR4	1.14	**
RHOT2	1.14	*
GDI2	1.14	ns
INTS6	1.14	*
NFXL1	1.13	ns
CDCA8	1.12	ns
PTPN14	1.12	*
RCN1	1.11	*
FOXRED1	1.11	*
FAF2	1.11	*
CHTF18	1.11	*
NDUFA13	1.11	*
EIF5	1.11	ns
PSMB2	1.11	ns
SEC31A	1.10	ns
DECR2	1.10	ns
PLOD1	1.10	*
LAMTOR1	1.09	ns
MRPL14	1.09	*
ERP44	1.09	*
LRP1	1.08	ns
RCOR1	1.08	*
MME	1.08	ns
KLHL26	1.08	ns
GNB2	1.07	ns
TRIM65	1.07	ns
EXOSC3	1.07	ns
CUL3	1.06	ns
WDR76	1.06	ns
PSMD9	1.06	*

AP1M1	1.05	*
MRPS7	1.05	*
LCMT2	1.04	ns
MRPS15	1.04	ns
NPLOC4	1.04	ns
ACP1	1.04	ns
CHAF1B	1.04	ns
ASCC1	1.04	ns
GTF3C5	1.03	ns
RP2	1.03	ns
JUP	1.03	ns
CAPNS1	1.03	ns
NUP188	1.03	*
WBSCR16	1.03	ns
RBFOX2;RBFOX1	1.02	*
TELO2	1.02	*
NCDN	1.02	ns
KIAA1429	1.01	ns
SRPRB	1.01	*
MRPL23	1.01	*
METAP2	1.01	*
TDP2	1.01	*
SF3B3	1.01	ns
HJURP	1.01	ns
PBDC1	1.01	*
RAC1;RAC3	1.01	ns
ALDH16A1	1.00	ns
TAF8	1.00	ns
NCAPD3	1.00	ns
UBA52;UBB;UBC;RPS27A	1.00	ns

ii. total-proteomics data – corresponding to section 2.1.4

Values in Table 27 (below) of total-proteomics corresponding to the volcano plot presented in Figure 15.

Table 27: total-proteomics data table

The table displays the enrichment of proteins IMR-5 cells in presence and absence of USP11 (log_2FC, count = 2) and their significance indicated as p-values (for $p<0.05$ ** for $p<0.01$, *** for $p<0.001$).*

Gene name	log_2FC	Significance
EXD2	-1.73	*
USP11	-1.40	***
COX7A2	-0.96	**
RAB30	-0.89	***
MT-ND5	-0.75	*
RBM18	-0.69	*
C3orf58	-0.66	**
CENPP	-0.65	*
NDUFB4	-0.64	*
KIAA0391	-0.62	*
KDM4A	-0.59	**
NQO1	-0.59	*
ERLIN2	-0.58	**
POLR2H	-0.57	*

NDUFB9	-0.56	*
SH3BGRL2	-0.52	*
NDUFAF1	-0.52	*
SLAIN1	-0.51	*
NDUFA12	-0.50	*
YPEL5	-0.50	*
HMGCS1	-0.49	*
MT-ND4	-0.48	*
FASTKD1	-0.47	*
NDUFS6	-0.46	*
SPHK2	-0.45	*
IQSEC1	-0.45	*
TBL1XR1	-0.43	*
WDR41	-0.42	*
STAU2	-0.42	*
POLR3F	-0.42	*
AFAP1	-0.42	*
HSPA12A	-0.41	*
NDUFA7	-0.41	*
MT-ND1	-0.41	*
PRC1	-0.40	*
NDUFS1	-0.39	*
SAMD4B	-0.39	*
RAN	-0.39	*
GCLM	-0.38	*
NDUFV1	-0.38	*
FDFT1	-0.38	*
HDAC3	-0.38	*
PKIB	-0.38	*
PBXIP1	0.37	*
NDE1	0.38	*
PRKAA1	0.38	*
PKM	0.39	*
QPRT	0.39	*
C18orf25	0.39	*
RLN3	0.39	*
ELP6	0.40	*
CCDC132	0.41	*
LEMD3	0.41	*
IRF2BPL	0.41	*
POMGNT2	0.41	*
SLC1A4	0.42	*
EGFR	0.42	*
APP	0.42	*
SNCA	0.43	*
DTD2	0.43	*
SIGMAR1	0.43	*
AGPAT4	0.44	*
PPP1R21	0.44	*
AGO2	0.44	*
SGSH	0.45	*

BCL9	0.45	*
PNMAL1	0.46	*
OTUD4	0.46	*
TMEFF1	0.50	*
TMEM222	0.51	*
CD276	0.51	*
MAPT	0.52	*
ITGA2	0.52	*
DLG1	0.53	*
ERC1	0.55	*
C12orf57	0.63	*
ATG9A	0.67	**
STXBP4	0.70	**
CMC1	0.71	*
SERPINB12	0.74	*
PNISR	0.80	*
DNTTIP1	0.84	**
DIS3L2	0.94	**
S100A9	1.47	**
PDLIM3	1.63	***
LYZ	1.79	***

iii. diGLY SILAC data – corresponding to section 2.1.4

Hits in Table 28 (below) of diGLY SILAC-based ubiquitin remnant profiling analysis are presented in the plot in Figure 17.

Table 28: diGLY-SILAC data table

The table displays the enrichment of proteins IMR-5 cells in presence and absence of USP11 (log_2FC, count = 2) and their significance indicated as p-values (for $p<0.05$ ** for $p<0.01$, *** for $p<0.001$) of diGLY SILAC-based proteomics. The sequence window shows the sequence of amino acids corresponding or containing the GlyGly peptide.*

Gene name	Sequence window	log_2FC	Significance
TCEAL4	KRKTNKGLAHYLKEYKEAIHDMNFSNEDMIR	-2.96	***
THAP9	LFDIFNSRNCYGKGLKGPLLPETYSKINHVL	-2.58	*
DNMT1	GSNLDAPEPYRIGRIKEIFCPKKSNGRPNET	-1.42	*
UPF1	YLNRTEAANVEKITTKLLKAGAKPDQIGIIT	-1.26	*
WBP5	KGTFRERLIQSLQEFKEDIHNRHLSNEDMFR	-1.20	**
PTBP1	EEDLKVLFSSNGGVVKGFKFFQKDRKMALIQ	-1.10	*
DHX29	LVAGLYDNVGKIIYTKSVDVTEKLACIVETA	-0.92	**
NUDT16L1	GLEVLGLVRVPLYTQKDRVGGFPNFLSNAFV	-0.89	*
SLC4A7	KVTRSNMSPDKPVSVKISFEDEPRKKYVDAE	-0.79	*
EIF4G1	TAADKDRGEEDADGSKTQDLFRRVRSILNKL	-0.79	*
ISL1	KQPEKTTRVRTVLNEKQLHTLRTCYAANPRP	-0.76	*
RNF31	HAPRPYASSLEKGPPKPGPPRRLSAPLPSSC	-0.74	*
CHRNA1	PPMGFHSPLIKHPEVKSAIEGIKYIAETMKS	-0.73	*
SESN3	LVNRLYSDIGHLLDEKFRMVYNLTYNTMATH	-0.73	*
ARHGAP36	FIRRRNLRKIQSARIKMEEDALLSDPVETSA	-0.72	*
ATP1A1	ERYAKIVEIPFNSTNKYQLSIHKNPNTSEPQ	-0.69	*
PRKACA	RNLLQVDLTKRFGNLKNGVNDIKNHKWFATT	-0.68	*
SQLE	MTVAFKDIKLWRKLLKGIPDLYDDAAIFEAK	-0.64	*

NIP7	YCFRLHNDRVYYVSEKIMKLAANISGDKLVS	-0.61	*
CS	DEGIRFRGFSIPECQKLLPKAKGGEEPLPEG	0.64	*
RPS14	TALHIKLRATGGNRTKTPGPGAQSALRALAR	0.66	*
UIMC1	_____MPRRKKKVKEVSESRNLEKKDVET	0.70	*
TKT	ITVTHLAVNRVPRSGKPAELLKMFGIDRDAI	0.72	*
ADAM9	SYFRKKRSQTYESDGKNQANPSRQPGSVPRH	0.76	*
FGFR1	KKSDFHSQMAVHKLAKSIPLRRQVTVSADSS	0.81	*
PTPRF	RTHSPSSKDEQSIGLKDSLLAHSSDPVEMRR	1.18	*
DYNLRB1	_____MAEVEETLKRLQSQKGVQGIIVVN	1.29	*
ELP3	IGDVIKQLIEAHEQGKDIDLNKVKTKTAAKY	1.30	*
OTUD7B	DRDLMLRKALYALMEKGVEKEALKRRWRWQQ	1.34	**
PDCD6IP	QLKKTSEVDLAKPLVKFIQQTYPSGGEEQAQ	1.47	*
EPB41	TISDNANAVKSEIPTKDVPIVHTETKTITYE	1.59	*
DCBLD2	DRAGWWKGMKQFLPAKAVDHEETPVRYSSSE	1.88	*

iv. TCEAL1 sequence similarity analysis – corresponding to section 2.3.1

TCEAL1 shares several amino acids with the its C-terminal domain with TCEAL9, TCEAL8, TCEAL7, and TCEA1. The parameter details of the blastn analysis are displayed in Table 29.

Table 29: Sequence similarity analysis of TCEAL1

The table displays the sequence similarity of TCEAL1 with other members of the Transcription elongation factor A protein-like protein family and TCEA1. The data was generated by using blastn algorithm (available online at NIH). Statistical significance and sequence ID are indicated.

Genomic locus	Query bp	Overlapping Gene	Score	E-value	% ID	Length
X:103629917-103630393	1-159	TCEAL1	217	6.40e-64	100.00	159
X:103357987-103357987	100-158	TCEAL9	78.2	1.85e-15	54.24	59
X:103253641-103253799	113-159	TCEAL8	53.9	5.71e-07	52.83	53
X:103331428-103331703	80-159	TCEAL7	50.1	1.29e-05	35.87	92
8: 53966552-54022448	116-139	TCEA1	19.6	0.037	15.00	24

Abbreviations

Abbreviation	Definition
4-OHT	4-Hydroxytamoxifen
ADRN	Adrenergic lineage
AF2	AlphaFold2 model algorithm
BCA	Bicinchoninic acid
bHLH	Basis helix-loop-helix
BSA	Bovine serum albumin
CAA	Chloroacetamide
CDK	Cycline dependent kinase
CNS	Central nervous system
CRC	Transcriptional regulatory circuitry
CTD	C-terminal domain of RPB1 (RNAPII)
DDR	DNA damage response
DSB	Double strand break
DTT	Dithiothreitol
DU	abbrev. for DUSP+UBL
DUB	deubiquitinase
DUSP	Ubiquitin-specific protease domain
EC	Elongation complex
EC*	Activated elongation complex
gb	Gene body
HR	Homologous recombination
IDRs	Intrinsic disordered regions
INGRSS	Internation Neuroblastoma Risk Group Staging System
LZ	Leucine zipper structural motif
MB	MYC box
MES	Mesenchymal lineage
ms	mouse
NGS	Next generation sequencing
NLS	Nuclear localization signal
ns	not significant
PAS	Poly-adenylation site
PBS	Phosphate-buffered saline
PEC	Paused elongation complex
PFA	Paraformaldehyde
PIC	Preinitiation complex
PLA	Proximity ligation assay
PTM	Posttranslational modification
rb	rabbit
RNAPII	RNA polymerase II
RPM	Reads per kilo base per million mapped reads
RT	Room temperature
SDM	Site directed mutagenesis
TAD	Transactivation domain
TC-NER	Transcription coupled nucleotide excision repair
TES	Transcription end site
TF	Transcription factor
TFA	Trifluracetic acid
TRC	Transcription replication conflict
TSS	Transcription start site
UBD	Ubiquitin binding domain
UBL	Ubiquitin-like
UFM	Ubiquitin-family modifier
UPS	Ubiquitin Proteasome System
USP	Ubiquitin specific protease
UV	Ultraviolet light
w/o	without
wt	wildtype

Table of figures

Table of tables

Acknowledgement

This fascinating project would not have been nicely developed and successfully completed without the encouragement and support of so many people.

First and foremost, I want to express my gratitude to Prof. Dr. Martin Eilers and Prof. Dr. Gabriele Büchel who gave me the opportunity to work in their research groups to conduct my doctoral thesis project.
Martin's support, encouragement and passion for science, has no equal and was absolutely advantageous to run this PhD project successfully.
Gabriele, I feel honored that I have been part of your nicely growing junior group. Your great guidance, supervision and wisdom helped me a lot to become the scientist that I am today.

In addition, I am really thankful that Prof. Dr. Caroline Kisker and PD Travis Stracker have been members of my thesis committee. Under your supervision I have had a constant scientific progress in my project.

I had the pleasure to collaborate with numerous working groups and institutions during my PhD. I would like extend my sincere thanks to Francesca Conte for performing diGLY-SILAC assays (Beli Group, IMB Mainz, Germany); Dr. Florian Sauer for designing USP11 deletion mutants (Kisker Group, RVZ Wuerzburg, Germany); Dr. Seychelle Vos for Cryo-EM and transcription studies with TCEAL1 and RNAPII (Vos Group, MIT, USA); Prof. Dr. Andreas Schlosser and Dr. Stephanie Lamer for performing and analyzing mass spectrometry (Schlosser Group, RVZ Wuerzburg, Germany).

Moreover, it was a great benefit for me to run my PhD project under the wings of the GSLS (Graduate School of Life Sciences) school where I could foster excellence with interdisciplinary training. Further, I want to give thanks to two research training groups where I have been associated. First, GRK2243 "Understanding Ubiquitylation: From Molecular Mechanisms To Disease" where I broaden my horizon far beyond USP11 deubiquitinase biology. Second, MSNZ ("Mildred Scheel Early Career Center") where I had the great opportunity to discuss translational views between understanding molecular mechanisms and new approaches for tumor therapy.

In particular, I am extremely grateful to underline the generously provided knowledge and support by Dr. Steffi Herold for exchanging views about my "BRCA1"-follow up story; by Prof. Dr. Peter Gallant, Dr. Carsten Ade and Dr. Raphael Vidal - our sequencing and bioinformatics heroes - for conducting and discussing high throughput sequencing experiments, by Dr. Giacomo Cossa and Dr. Dimitrios Papadopolous for inspiring and very smart discussions about transcriptional

regulation and by Dr. Ursula Eilers and Dr. Christina Schülein-Völk for helping with Operetta microscope measurements and analysis. Further, thanks to Maximilian who investigated RPB8 biology in neuroblastoma cells during his bachelor thesis project. A particular concern of mine is to thank people which were also very important to ensure such a successful and professional working atmosphere in our department – namely, Ulrike Samfaß, Barbara Bauer, Wolfgang Hädelt, Ryan Ramjan and Tobias Roth.
Thanks of course to all former and current members of the Eilers and Büchel groups for support- it's been great fun working with you all!

Last but not least I want to thank Dr. Giacomo Cossa, Dr. Steffi Herold, and Dr. Sebastian Richter for their proofreading work on this thesis.

This endeavor would not have been possible without getting to know Bikash. Your genuine and amicable character was a constant source of inspiration and motivation. My appreciation also goes out to all my friends for their encouragement and support during my PhD project.

Lastly, I want to mention my parents, my brother Christoph, Miriam, little Ben and my love Helena. None of this could have happened without you. Your belief in me has kept my spirits and motivation high throughout my studies – I love you!

Publication list

2018 Ladenburger EM, **Dehmer M**, Grünberg R, Waiblinger HU, Stoll D, Bergemann J. Highly Sensitive Matrix-Independent Quantification of Major Food Aller-gens Peanut and Soy by Competitive Real-Time PCR Targeting Mitochon-drial DNA. Journal of AOAC International. 2018. 101 (1).170-184. DOI: 10.5740/jaoacint.17-0406.

Affidavit

I hereby confirm that my thesis entitled: "A novel USP11-TCEAL1-mediated mechanism protects transcriptional elongation by RNA Polymerase II" is the result of my own work. I did not receive any help or support from commercial consultants. All sources and / or materials applied are listed and specified in the thesis.

Furthermore, I confirm that this thesis has not yet been submitted as part of another examination process neither in identical nor in similar form.

Place, Date Signature

Eidesstattliche Erklärung

Hiermit erkläre ich an Eides statt, die Dissertation „Ein neuer USP11-TCEAL1 vermittelter Mechanismus schützt die transkriptionelle Elongation der RNA Polymerase II" eigenständig, d.h. insbesondere selbstständig und ohne Hilfe eines kommerziellen Promotionsberaters, angefertigt und keine anderen als die von mir angegebenen Quellen und Hilfsmittel verwendet zu haben.

Ich erkläre außerdem, dass die Dissertation weder in gleicher noch in ähnlicher Form bereits in einem anderen Prüfungsverfahren vorgelegen hat.

Place, Date Unterschrift